EFFECTS OF EXTENSIVE AGRICULTURE ON THE HYDROLOGIC CYCLE IN TROPICAL LOWLANDS

Angélica M. Gómez

"A dissertation submitted to the faculty at the University of North Carolina at Chapel Hill in partial fulfillment of the requirements for the degree of Doctor of Philosophy in the Curriculum of Geography."

Chapel Hill
2021

Approved by:

Erika Wise

Tamlin Pavelsky

Conghe Song

Aaron Moody

Marc Serre

ABSTRACT

Angélica M. Gómez: Effects of extensive agriculture on the hydrologic cycle in tropical lowlands
(Under the direction of Erika Wise and Tamlin Pavelsky)

In the tropics, global demands for food and services accelerate land cover changes that impact water availability, modify energy and water balances, and intensify the consequences of extreme climate (e.g., droughts and flooding). Among the tools to understand the effects of these changes are regional earth system models. These models required ground data for model verification, which is often limited in tropical regions. This dissertation addresses this need by exploring avenues to improve our understanding of hydrological and energy processes in tropical regions. This work is focused on the North Colombia lowlands, where land has faced long-term disturbances due to agriculture intensification. I start by exploring how the combined use of depth to groundwater measurements collected by the community and their descriptive observations can inform depth to groundwater mapping. I show that incorporating depth to groundwater qualitative descriptions to a Bayesian Maximum Entropy geostatistical model improves model performance and spatiotemporal representation of depth to groundwater. Then, I focus on understanding the global dynamics of oil palm plantations in the context of vegetation and water interactions. Oil palm is the most important vegetable oil globally and an essential economic driver in some tropical countries. I start by identifying the state of knowledge in oil palm-hydrologic interactions across the tropics by developing a systematic literature review. Through this process, I identify major gaps, including a lack of studies in the Neotropics and

Africa, a lack of understanding of microclimatic conditions over longer timescales, and a lack of studies in alternative oil palm species that has potential for expansion. To address one of the gaps identified in the systematic literature review, I installed three microclimatic stations in Northern Colombia at three sites, where OxG interspecific hybrid is planted. I collected hourly data for a year. The data show that seasonal variability in vapor pressure deficit impacts the atmospheric water balance and potentially oil palm greenness. The energy balance partition shows the important role of evapotranspiration in these plantations. The resulting dataset, the first in oil palm OxG hybrid plantations, provide data on key variables for modeling water and energy processes in tropical regions.

To Yadira Gómez and Flor Zabaleta: my mom and grandma, who open the path and kept it open without borders.

ACKNOWLEDGEMENTS

An important number of people have contributed to this dissertation. First, I thank my graduate advisors: Dr. Erika Wise and Dr. Tamlin Palevsky, for their support, patience, and the ideas that helped shape this work. This work would not be possible without them. I thank the members of my graduate committee – Dr. Conghe Song, Dr. Marc Serre, and Dr. Aaron Moody. I appreciate their insights and dedication and their commitment to helping me drafting ideas and navigating through them. I also appreciate my collaborator's time, dedication, and ideas in Colombia, Dr. Juan Camilo Villegas Palacio. Thank you to the external collaborators, editors, and reviewers who comment on my manuscripts and help me to shape this dissertation.

This thesis could not be the same without the help of my lab mates, who never were busy to help. I thank C-TRES lab members Manuel Hernandez, Karly Schmidt-Simard, and Carl Jurkowski. I also thank UNC Global Hydrology Lab members, especially Melisa Wrzesein, Wayana Dolan, John Gardner, Arik Tashie, Chao Wang, and Xiao Yang. All my lab mates were always willing to examine a figure, a manuscript's section, go for a walk, or do a video call, particularly during the pandemic. Thanks to the members of my cohort that have been there in many ways to even take conversations beyond academia and to the graduate students in the department of Geography. They have helped me understand what it means to be a geographer and the different subfields Geography has. Thanks to Adriana Parra at the University of Reno for following my lead on writing a literature review paper and continuing with the idea it happened. I am also grateful for the undergraduates assisting in the field Haley Moser, Juan Manuel Cardona Durango, Jhan Carlos Rodriguez Cuartas. Also, I am thankful for the undergrads who

helped me preprocess data Sofia Vela Castillo and Alejandra Vela Castillo, during the pandemic. Special thanks to the Applied Ecology research group at the University of Antioquia for all the questions, contributions, and discussions. Thanks to the members of my former lab group at GIGA research group, the groundwater team, for being there, helping me to make the connections in the field, read my materials, but, more importantly, for being my friends.

I also thank the environmental agency CORPOURABA and its director, Vanessa Paredes, for opening the door and connecting with the palmers. To Bioplanta Palmera para el Desarrollo, for welcoming my project and ideas, academic discussions, and the lessons on agronomy from Oscar Castillo. Also, thanks to all the workers at each farm and the farm administrators, Luis Carlos Manjarrés, Robinson López, Don Emiro, and Andrés Cerezo, that provide the logistics to keep the stations working. I also would like to thank Santiago Correa and all the members of Sioma for providing technical and logistical support, especially to Diego Escobar, Samuel Salas, Moises Luna, and Sebastián Usma, to keep my stations working and running. Many thanks to Giovanni Ruiz for help me to turn my conceptual ideas into beautiful conceptual figures.

This work was fund in part by Minciencias-Fulbright and Faculty for the Future program. Thank you to them for opening the possibilities to study and helping increasing knowledge in tropical environments. Finally, and importantly, thanks to my family-friends, my family, my friends, and a huge chain of support for being there in many ways.

TABLE OF CONTENTS

LIST OF TABLES

LIST OF FIGURES

LIST OF ABBREVIATIONS

BME: Bayesian Maximum Entropy

DTG: Depth to Groundwater

ET: Evapotranspiration

FAOSTAT: Food and Agriculture Organization Corporate Statistical Database

IDEAM: National Institute of Hydrology, Meteorology and Environmental Studies of Colombia

ME: Mean Error

MSE: Mean Square Error

NDVI: Normalized Difference Vegetation Index

OxG Hybrid: hybrid interspecific E. oleifera x E. guineensis

P: Precipitation or Rainfall

PDF: Probabilistic Distribution Function

R^2: Pearson Coefficient of Determination

S: Spatial interpolation model

SOC: Soil Organic Carbon

ST: Spatiotemporal interpolation model

STRM: Shuttle Radar Topography Mission

STSD: Spatiotemporal interpolation model with soft data or probabilistic data

SWC: Soil Water Content

USDA: United States Department of Agriculture

VE: Variance of Error

VO: Variance of observations

VPD: Vapor Pressure Deficit

VZ: Variance of estimates

CHAPTER 1: INTRODUCTION

Tropical regions account for more than 50% of renewable water resources on Earth (State of Tropics, 2020). Population growth and the need to satisfy demands for global production of food, energy, and goods threaten this region by leading to extensive changes in land cover (biophysical attributes of the landscape) and land use (operations on land made by humans). Land transformation shifts the hydrologic cycle and results in changes to the local climate, alteration of soil properties, and frequency of wet and dry periods (DeFries & Eshleman, 2004). Land cover changes modify energy heat fluxes that impact surface temperature (Sabajo et al., 2017), alter the atmospheric water balance by shifting available moisture storage and transport (Yuan et al., 2019; Sheil et al., 2018), and affect surface and groundwater by influencing interception, runoff, and soil infiltration capacity (Margat & van der Gun, 2013). All these changes may constrain the resilience capacity of landscapes.

In this dissertation, agricultural intensification in tropical lowlands is studied through a variety of novel approaches that aim to improve our understanding of hydrological and energy processes in tropical regions. This research shows how working with local populations, whether through community science or direct engagement with plantation owners, can lead to improved models and opportunities for long-term monitoring. This dissertation focuses on the North Colombia lowlands, where land has faced long-term disturbances and agriculture is a fundamental component of the national economy.

Chapter 2

Research Questions:

- How can descriptive information be incorporated into depth to groundwater mapping?
- Does the inclusion of this information improve model performance?

Main Finding:

- Incorporating descriptive knowledge from the community with Bayesian Maximum Entropy geostatistics improved the representation of depth to groundwater, while allowing the design of mechanisms to involve the community in different stages of the model construction.

In chapter 2, I focused on how to incorporate knowledge with different levels of uncertainty in hydrologic mapping. In particular, I combined data and knowledge collected in a community science project in a remote rural region in Colombia, the Man River watershed. The community provided depth to groundwater measurements and descriptive observations of the wetland water level during the wet season. The groundwater system represents a primary source of water supply for this region. However, as happens in many cases, continuous depth to groundwater measurements are challenging to obtain, although they are essential for understanding groundwater recharge and surface-groundwater connectivity. This challenge constrains informed decision-making processes in water and land management. In this chapter, I showed how geostatistical techniques (i.e., Bayesian Maximum Entropy geostatistics) that include qualitative local knowledge helped characterize the spatiotemporal distribution of depth to groundwater and identified depth to groundwater dynamics in response to extreme precipitation events. This study's results provide insights concerning how land use activities may impact watersheds that are highly affected by agricultural and mining practices, opening new avenues to link land changes with hydrologic processes.

Chapter 3

Research Questions:

- What are the effects of oil palm on surface energy and water balances, fluvial and subsurface processes?
- How do ecohydrological processes vary under different types of land use and land cover transitions and to what extent have these variations been studied?
- How have the major impacts on water resources have been perceived by local communities?

Main Finding:

- Oil palm ecohydrological processes have been mostly studied in the transition from humid forest to oil palm, in which the predominant spatial scales range from plot to regional and temporal scales from days to a few months. The main focus of the studies are related to surface air temperature and moisture, runoff, sediment yield and soil organic carbon. The effects of oil palm plantations vary with the land transition, but there are limited studies in understanding land transitions other than humid forest to oil palm. Few examples of community perceptions associated with biogeophysical processes were found.

In Chapter 3, I synthesized the advances on understanding ecohydrological processes in oil palm plantations by doing a systematic literature review. Current literature reviews in related topics have concentrated on summarizing the work done in the transition from forest (mainly rainforest that grow over mineral and peat soils) to oil palm. I focused my search on different scenarios of land transition looking at the three main components of the hydrologic cycle (land-atmosphere, streams and landscape, and subsurface) and different oil palm species. I also included sociopolitical literature of community perceptions of water to help to identify to what extent community knowledge and perceptions have been included in biogeophysical oil palm

research. Finally, I included spatial and temporal scale of the studies and their geographical distribution into the analysis. I found an increase in scientific literature in ecohydrology of oil palm has been happening since 2011. Although these efforts have identified plant transpiration, shifts in air temperature, and moisture within the crops and at different land covers, as well as runoff and sediment yield, this progress has been made mainly at plot and regional scales and under short periods of time (days to months). These limitations make it difficult to detect trends and thresholds in the limits to oil palm expansion. There are similar limits to our understanding of the impacts of oil palm on subsurface processes. Important gaps were also detected in addressing land transitions. Most of the work has been done in the transition from forest to oil palm and less in addressing other patterns or expansion (i.e., transitions from pastures or croplands). These gaps limit the identification of constraining factors on oil palm development in other regions. More work is needed in oil palm hybrids and alternative varieties of oil palm cultivars given the high tolerance of these species to extremes (i.e., drought, flooding, and plant diseases) and the commercial attention in cultivating these species. Examples were found in which community perceptions have been included in addressing scientific questions focusing on community concerns. However, these studies were limited and focused in a few geographical areas. The synthesis built in this chapter helped to identify key areas of needed research and to move towards the characterization of important thresholds in water requirements at water-limited as well as water-abundant systems.

Chapter 4

Research Questions:

- How do microclimatic conditions in oil palm plantations vary through the dry and wet season during a year in northwestern Colombia?

- How can those differences be explained?
- What is the diurnal energy balance partition in plantations growing the E. Guineensis x E. Oleifera variety of oil palm?

Main Finding:

- Average microclimatic conditions were similar across the stations. However, seasonal variations in temperature and vapor pressure deficit were detected in the wet vs the dry seasons. These changes might be explained by environmental conditions in the sites (winds that are moving faster and stronger and carrying moisture from the Andes cordillera during the dry season vs. the wet season). The environmental conditions seem to have an impact on the photosynthetic activity reflected in a lower vegetation index. Results of the energy balance partition showed similarities across the stations, probably due to the similar environmental conditions during the dry season, and were similar to existing studies in Indonesia.

In Chapter 4, I worked to fill some of the knowledge gaps found in Chapter 2 (i.e., the lack of studies in oil palm hybrids and under the conversion from pastures and croplands to oil palm). For that purpose, I installed three microclimatic stations in Northwest Colombia measuring environmental microclimatic conditions (i.e., temperature, radiation, relative humidity, wind speed and direction, spectral reflectance, soil matric potential and soil temperature) across the vertical profile from 0.65 m below the surface to 11 m above, which covers the active root depth, under canopy, and over the canopy of the palms. The collected dataset was preprocessed to filter out inconsistent data. This chapter explains how the data was used to derive Normalized Difference Vegetation Index (NDVI) from a 7-band spectrometer, vapor pressure deficit (VPD), for the dry and the wet season, and the four components of the energy balance (i.e., latent,

sensible, and ground heat, and net radiation) during the wet season based on the Bowen ratio method. I found NDVI coincide with low VPD across the stations, suggesting a variation in photosynthetic activity that requires further explore using more direct techniques. Chapter 4 also discussed how Bowen ratio results are similar to those obtained in Indonesia when net radiation is taken into account. The collected dataset is unique to the region, and unique for the type of species and land transitions. This chapter also explored how the collaborative efforts with the local institutions (environmental agency, farmers, and university) helped to maintain the stations remotely, and the challenges faced in data acquisition.

Overall, this dissertation shows how the difficulties of working in rural tropical lowlands have led to a lack of long-term studies of appropriate species in the Neotropics in Chapter 3, while also providing clear examples of how these challenges can be addressed through direct engagement with communities and plantation workers in Chapters 2 & 4. Given the accelerated transformation of tropical regions, more tools are needed to understand landscapes under disturbance. In this dissertation, I demonstrate paths towards building that understanding from a collaborative perspective, first by engaging local community in scientific research and included their insights in the model construction, second by including perspectives of the community in my systematic literature review, and third by collaborating with a variety of stakeholders to developing a monitoring system to gain understanding of local environmental conditions.

CHAPTER 2: INTEGRATING COMMUNITY SCIENCE RESEARCH AND SPACE-TIME MAPPING TO DETERMINE DEPTH TO GROUNDWATER IN A REMOTE RURAL REGION[1]

Plain Language Summary

Groundwater is a key source of water supply in many regions, supporting crop yields and maintaining water levels in rivers and wetlands. In unconfined aquifers, groundwater may reach the surface during wet periods, contributing to overland flow and intensifying erosion. Identifying groundwater level changes helps to establish water and land management activities. However, continuous depth to groundwater data collection, essential for identifying groundwater level changes, is challenging in remote rural areas. We show how Community Science Research, an approach involving active community participation, added crucial information to a statistical model to represent shallow aquifer's groundwater levels in Colombia. The community collected depth to groundwater during an extreme wet year and an average year in a middle-low-elevation watershed. We created depth to groundwater maps using three statistical models. Depth to groundwater is better represented by the model that combines descriptive observations with depth to groundwater measurements. We also created a map with the probability that the groundwater is near the surface and showed that the area was much larger in the wet year than

[1] This chapter previously appeared in the *Water Resources Research* journal. The original citation is as follows:

Gómez, A. M., Serre, M., Wise, E., & Pavelsky, T. (2021). Integrating Community Science Research and Space-Time Mapping to Determine Depth to Groundwater in a Remote Rural Region. *Water Resources Research*, *57*(6). https://doi.org/10.1029/2020WR029519

during the average year. This difference implies that after the watershed receives a lot of precipitation, its flow regulation capacity decreases, which is threatened by land-use activities.

Introduction

Depth to groundwater (DTG), the depth measured from the terrain surface to the groundwater table, is essential to identify groundwater availability and groundwater-surface water interactions (Fan et al., 2013). Groundwater can influence the landscape, acting as a discharge system feeding the tributaries that support streams (Margat & van der Gun, 2013), creating water-logged soil conditions that define wetland ecosystems, and supplying water to the root zone to maintain plant photosynthetic activity (Lewandowski et al., 2019). The landscape also influences groundwater as groundwater flow is often related to topography. Surface waters and areas where deep infiltration occurs can recharge aquifers (Sophocleous, 2002; Winter et al., 1998). In addition to its ecosystem function, groundwater is the primary water supply in many regions, sometimes acting as the only source (UNESCO & UN-Water, 2017). In the absence of regulation, land use activities may substantially change shallow groundwater systems' capacity to regulate flow or attenuate groundwater pollution (Gleeson et al., 2016). In precipitation-driven groundwater systems, extreme rainfall changes can cause groundwater table subsidence or flooding (Marchetti & Carrillo-Rivera, 2014), influencing erosion. These effects can subsequently impact ecosystem function and services. Although continuous data collection is challenging, these data are needed to understand the links of shallow groundwater to the landscape, estimate groundwater storage, and establish limits of extraction. Large, long-term DTG datasets are mostly limited to developed countries (Fan et al., 2013), constraining the understanding of groundwater function and services and limiting land and water management decision-making in these regions.

Community participation in scientific projects provides a way to address environmental questions with a meaningful social impact and to reduce information gaps (Arias et al., 2016; Sandoval, 2004; Wiggins & Crowston, 2011). Approaches to community participation in scientific projects can be defined as a function of the type of relations, the strategies implemented, and the level of engagement developed between the public and the researchers (e.g., citizen science, participatory action, community-based, social monitoring, etc.). In this paper, we use the term Community Science Research (Cooper et al., 2007) to describe research projects in which the public participates in significant ways. Significant participation can take place at different stages where the participants engage in activities that may last beyond the projects (Wijnen et al., 2012), influence local governance decision-making processes (Arias et al., 2016), and help solve scientific questions that increase the system's knowledge (Baldwin et al., 2012; Le Coz et al., 2016).

Community science projects have a long history in data collection in several biogeoscience disciplines. In hydrology, the participation of the public and explicit design of community science projects has been increasing (Buytaert et al., 2014). There are several existing examples of community participation in water level and precipitation data collection (Piragua project, Colombia, http://www.piraguacorantioquia.com.co/piragua/; Pluviometros Cuidadanos, Chile, http://milluvia.dga.cl/index.php; CoCoRaHS, USA, https://www.cocorahs.org/; Little et al., 2016; Lowry et al., 2019; Weeser et al., 2018); its use in modeling river discharge (Starkey et al., 2017); and on identifying lake water storage changes (Little et al., 2021). Most projects concentrate on data collection, leaving data analysis and modeling to the scientist (Assumpção et al., 2018; Njue et al., 2019). Beyond data collected by the local population, their knowledge of the landscape also encompasses local environmental conditions that help to define the logistics to

access or install measurement devices and provide a qualitative understanding of hydrologic systems. This type of information is not always formally collected or included in the analysis and model implementation process. Therefore, high levels of active participant engagement and valuable qualitative descriptions are left out of the quantitative data analysis. The qualitative nature and the potential high levels of uncertainty of the descriptions made by local inhabitants make it challenging to incorporate into the model construction. Overcoming this challenge will be key in integrating community knowledge into models and data analysis.

One potential solution to add local knowledge to models is through the creation of a probabilistic representation using Bayesian Maximum Entropy (BME). BME incorporates general information about the salient variable (spatial dependencies, conceptual assumptions, etc.) by maximizing an entropy function (Christakos, 1990; He & Kolovos, 2018; Serre & Christakos, 1999). BME is an extension of linear geostatistical approaches (kriging-based methods). It can combine data that carry higher levels of uncertainty, known as soft data, with spatiotemporal measurements that have lower uncertainty, known as hard data. In groundwater hydrology, BME has been used to effectively map groundwater flow direction using water table data (Serre & Christakos, 1999). In this study, each measurement had a source of error reported during the monitoring campaigns. Those water table measurements with an identified source of randomized errors or errors manually flagged by experts were defined as soft data. Hard data were defined as water table measurements with no recorded random errors and no errors manually flagged by experts after data collection. Another example of applied BME estimates aquifer hydraulic conductivity (Serre et al., 2003), soft data correspond to hydraulic conductivity derived from porous media analysis at different sites and hard data are hydraulic conductivity measurements performed at specific locations. These combinations of soft and hard data

minimized estimation errors of the hydraulic subsurface properties in saturated media. BME has also been applied to assess water quality by combining space-time variability of the water quality within the river network (Akita et al., 2007). In this study, soft data included detected nitrate concentrations in water, using concentrations under the detection limit, while hard data included nitrate concentrations over the detection limit (Messier et al., 2014). Also, BME served to combine different temporal scales of arsenic concentrations, with soft data defined as arsenic concentrations at coarser temporal scales and private wells, and hard data as the concentrations officially provided by the local authorities (Sanders et al., 2012). In all these cases, the use of BME approaches led to an improvement in the detection of water quality levels. BME has also been used to design monitoring networks (Hosseini & Kerachian, 2017) by incorporating the uncertainty of having areas with no monitoring stations and different start monitoring dates in the modeling design. These examples show the potential of BME to include ancillary information with high levels of uncertainty in data-driven models.

To our knowledge, BME has not previously been used to model DTG. In the absence of continuous measurements, the shallow groundwater table is often assumed to be a function of the topography and simulated using classic geostatistical interpolation methods, which require high resolution elevation maps. However, topographic information is often only available at coarse resolution in remote rural regions. Therefore, modeling DTG as a function of the topography may hide shallow DTG in lowlands, close to depressions, that may impact identification and mapping of near-saturated areas that affect discharge (Snyder, 2008).

The central research questions of this study are: How can descriptive information be incorporated into DTG mapping? Does the inclusion of this information improve model performance? We show the potential for combining DTG quantitative and qualitative data

collected in a community science project in the 481 km^2 Man River middle-low elevation watershed (Bajo Cauca region, Colombia). The data collected by the community previously helped to generate monthly groundwater table maps using classic kriging interpolation (Palacio, 2014). This interpolation used the elevation from the Shuttle Radar Topography Mission dataset (http://srtm.csi.cgiar.org/), with a 30 m spatial resolution, SRTM-30. The resulting maps were useful to identify potential flow direction in the shallow aquifer. However, monthly average groundwater table estimates may hide peaks, missing potential high and low values and making it difficult to identify rapid water table responses to precipitation. We present a different approach to obtain weekly depth to groundwater. The regular flooding in the region during extreme wet seasons (Betancur-Vargas et al., 2017) motivated us to apply our results to address how extreme precipitation influences changes in DTG.

Materials and Methods

Study area

The 481 km^2 Man River middle-low watershed drains the foothills between the Western and the Central Andes Cordillera in Colombia (Figure 2.1). The relief is low with a landscape characterized by extensive valleys and rolling hills. The middle-low watershed's elevation ranges between 12 and 148 m.a.s.l.. The Man River, originating at 1,050 m.a.s.l., is a tributary of the Cauca River, a main river in Colombia. Its most important tributaries are the Quebradona and the Ciénaga Colombia creeks (Figure 2.1a). The Ciénaga Colombia, a wetland to the north-east, regulates flow during the wet season and provides ecological and cultural services to the region's socio-economic development (Santa-Arango et al., 2010). The climate is humid (average relative humidity 78%) and warm (average temperatures between 25 and 30 °C). The average precipitation is 2,800 mm/year, with a dry period between December and March and a wet

period between April and November. The region's geology is primarily composed of Tertiary clastic sedimentary rocks of continental origin, represented by the Cerrito Formation (Ngc), which occupy 404.3 km^2 of the watershed; Sincelejo Group sedimentary rocks (NgQs), 17.5 km^2; and recent Quaternary alluvial deposits (Qal), 57.4 km^2 (Figure 2.1c). These features form three hydrogeological units: a shallow aquifer, an aquitard, and a confined aquifer (Betancur et al., 2012). Our work centers on the shallow aquifer, formed by Man River alluvial deposits and non-consolidated saprolite from the Cerrito Formation, with depths ranging between 13 and 65 m (Palacio et al., 2013). Previous studies in this region identified groundwater and surface water connections (Santa-Arango et al., 2010), and groundwater recharge occurring directly from precipitation (Palacio & Betancur, 2007).

A 2003 water well inventory indicated 147 dug and five drilled wells in this area; 86% are for domestic use (CORANTIOQUIA & Universidad de Antioquia, 2003). At the time of this project, no water supply treatment system was operational in the area. In 2011, 66.8% of the population from the municipalities where the watershed is located lived in poverty (Departamento Administrativo Nacional de Estadística, 2012). A few people engage in small-scale agriculture and fishing, but the main economic activity is cattle raising (Instituto Geográfico Agustín Codazzi, 2007a). Cattle ranching occupies around 80% of the watershed (Instituto Geográfico Agustín Codazzi, 2007b) and along with strip mining, land conflicts, and illicit crops, leads to population displacement (Cuartas et al., 2000).

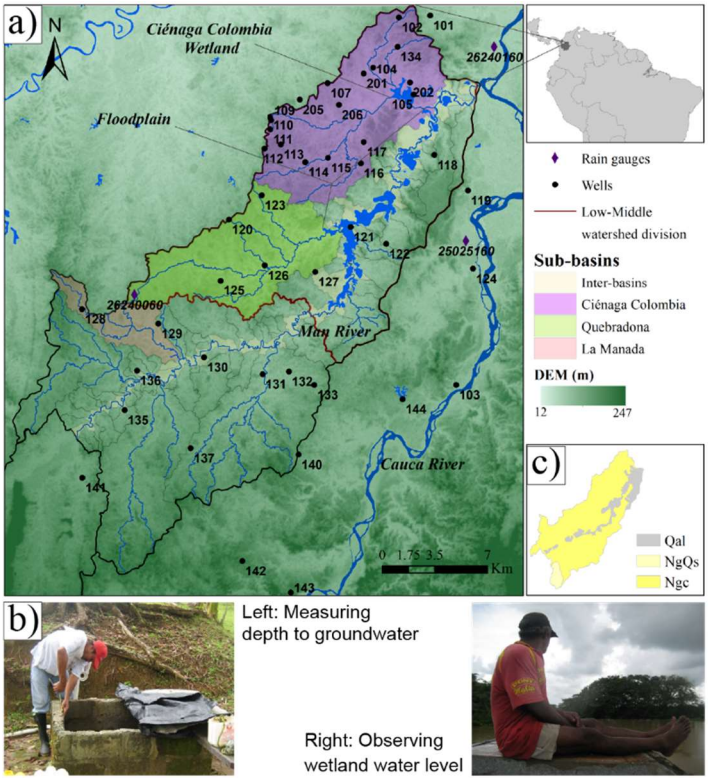

Figure 2.1. Study area and community science activities. (a) Wells used as monitoring stations. (b) Activities developed by the community (source: Grupo GIGA, Universidad de Antioquia). (c) Geology of the region describing the shallow aquifer: Qal, recent Quaternary alluvial deposits (12% of the watershed); Ngc, Cerrito Formation (84%); and NgQs, Sincelejo Group (3%).

Community science data collection

The DTG monitoring network started with the analysis of a conceptual hydrogeological model for the Bajo Cauca region (Betancur, 2008), that estimates groundwater flow directions at a regional scale and identifies aquifer units and their thickness. The potential wells and associated collaborators were obtained from the 2003 well inventory (CORANTIOQUIA & Universidad de Antioquia, 2003) based on three criteria: 1) spatial distribution across the watershed, 2) accessibility, and 3) well depth. The wells' spatial distribution was selected based on areas where groundwater-surface water interactions were and were not expected. These decisions were based on expert knowledge of the region and the conceptual hydrogeological model. The accessibility conditions aimed to facilitate visits to the sites and access to a good

cellphone signal to receive data from the collaborators. Finally, the wells' depth helped to identify the hydrogeological unit from which water is extracted. With this selection, six field campaigns were conducted. In the first reconnaissance campaign, each household's well location and contact information registered in the well inventory was confirmed with the collaborators at each house and farm where the wells are located. The rest of the sampling campaigns were designed to reinforce data collection procedures, collect hydrogeochemical data, share guidance, and follow up on the maintenance of each well's sanitary condition.

The campaigns were designed to facilitate data collection with limited resources. Potential collaborators were introduced to the project, and characteristics of water wells, pumps, and pumping times were identified. Collaborators were trained in water depth measurements at each site and provided with a tape measure and forms to register measurements. Each collaborator was trained individually. The distance was measured from the top of the well to the water table weekly before pumping. The height from the top of the well to the ground was subtracted later to obtain the DTG (Figure 2.1b). Weekly phone calls gathered information and verified anomalous values, representing extremely low or high DTG. The verification followed a 2-step process. The first step was to verify by phone the time of the day and how the collaborator was measuring. The second step was during the sampling campaign. In most cases, phone call verification was enough to improve data collection. Some collaborators moved during the study, which is common in this area; data were either no longer collected or the collaborator trained a new person to monitor their well. This practice of knowledge transfer was identified in highly engaged participants. In addition to obtaining DTG, collaborators located close to the wetland area or the Man River described weather conditions and observed surface water levels. These descriptions were not systematically collected among collaborators but were mostly provided

during the phone calls to collect the data or during the sampling campaigns. After the third campaign, the monitoring network was updated to include additional wells, following the same procedure established with the first group of wells. Ultimately, we managed to collect a total of 2,397 high-quality noncontinuous data at 44 wells between 2008 and 2009. These data would have been challenging and expensive to acquire with a traditional approach.

Although the project did not provide monetary compensation to the collaborators, hydrogeochemical data collected to identify groundwater sources and surface-groundwater interactions (Santa-Arango et al., 2010) were reinterpreted in terms of their sanitary meaning, and the results were provided to the collaborators. Those data were for the benefit of the collaborators and are not part of this research study. In addition, after finding poor sanitary conditions at some of the wells, recommendations were provided, such as covering wells to prevent animal and debris access and simple disinfection techniques (Organization World Health, 1999). The data collection team followed up with each household regarding these recommendations. Some households shared advice with other relatives or friends not included in the monitoring network. We did not measure or collect information on how much of this information transfer occurred among households.

Model framework and implementation

In this work, we built three model combinations using the BME framework: spatial interpolation with only observed DTG at each monitoring wells, i.e., hard data (S), space-time with only hard data (ST), and space-time with probabilistic or soft data, i.e., data corresponding to expected low DTG at the wetland locations (STSD). In the spatial interpolation, S, we interpolated each week independently, assuming no correlation in time, a common approach in

classic geostatistical analysis. For the space-time interpolations (ST and STSD) we hypothesized high correlations of DTG in time would improve DTG estimates (Figure 2.2).

The summary of the BME framework provided below is adapted from previous work; the reader is referred to these papers for more details on the mathematical underpinnings of the BME framework (Christakos et al., 2001; Serre & Christakos, 1999). The BME framework is a nonlinear extension of the classical kriging methods of linear geostatistics. BME has the capacity to use only the knowledge base kriging can process. In that case, the BME equation reduces to a linear kriging estimator with a Gaussian posterior probability distribution function, PDF. However, using information processing principles such as information entropy maximization and epistemic Bayesian principles, the knowledge base that BME considers can extend beyond those used in kriging.

Let $X(p)$ be a space-time random field (S/TRF) representing the variation of DTG across space-time coordinate $\boldsymbol{p}$=($\boldsymbol{s}$,t), where $\boldsymbol{s}$ is a geographical location, and t is time. We denote as $G = \{m_X(p), c_X(p,p')\}$ the general knowledge characterizing $X(p)$, where $m_X(p)$ and $c_X(p,p')$ are the mean and covariance of $X(p)$, respectively. We denote $S = \{x_h, f_S(x_s)\}$ the site-specific knowledge characterizing the data at hand, where x_h are the space-time hard data DTG values observed at each monitoring wells, x_s are space-time soft data DTG values corresponding to where we know the DTG is low, and $f_S(x_s)$ are the density functions characterizing the shallow DTG and its uncertainty.

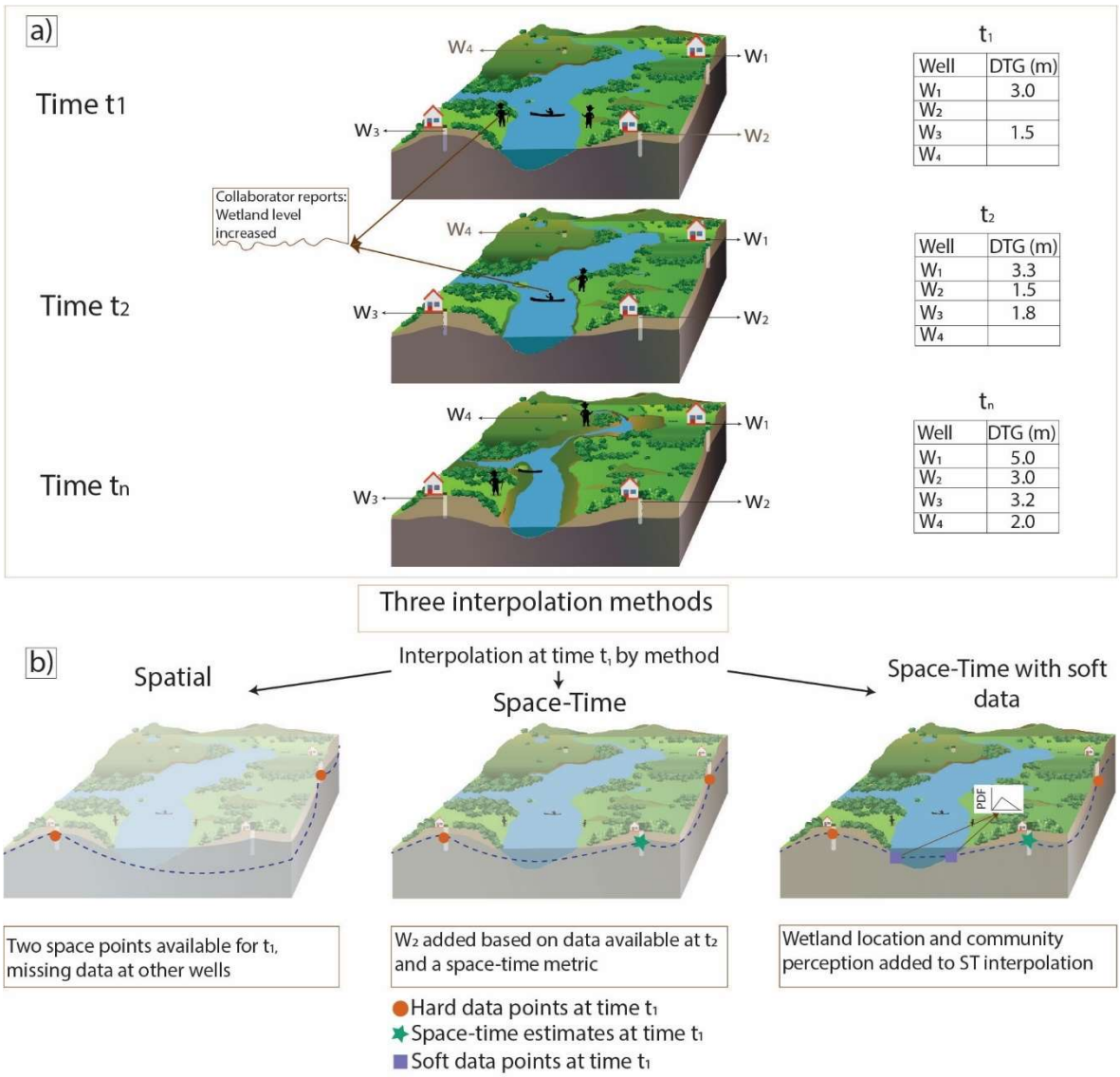

Figure 2.2 Schematic differences in the interpolation methods. A) Shows a watershed conceptual block-diagram closed to the wetland location at three different times: t_1 and t_2 correspond to the wet season and t_n to the dry season. Tables t_1, t_2, and t_n show examples of the data collected. Collaborators qualitatively reported the wetland stage, mainly during the wet season. B) DTG interpolation example at time t_1(dashed line). Spatial interpolation (S) interpolates only data collected at t_1; space-time interpolation (ST) incorporates correlations in time of DTG to improve interpolation results; in the space-time with soft data (STSD) interpolation, descriptions from collaborators are incorporated to further improve results.

BME can be summarized in three stages: Prior, Posterior, and Interpretive. At the prior stage, we use the *Maximum Entropy* principle of information theory to create a prior PDF $f_G(x_{map})$ that integrates the general knowledge G, where $x_{map} = (x_k, x_h, x_s)$ is the value of $X(p)$ at points $p_{map} = (p_k, p_h, p_s)$ and where p_k is an estimation point of interest. The PDF statistical

properties are consistent with *G*, and maximize the amount of choice in the value DTG can take. *G* consists of the knowledge of the mean and covariance of $X(p)$, which are statistical moments up to order two only. As a result, f_G is the multivariable Gaussian PDF with means and covariance specified in G.

At the posterior stage, we integrate the site-specific knowledge *S* using an epistemic *Bayesian* conditionalization equation 1.

$$f_K(x_k) = A^{-1} \int dx_s f_S(x_s) f_G(x_k, x_h, x_s) \quad (1)$$

In Equation 1, A is a normalization constant. This equation creates the BME posterior PDF, $f_K(x_k)$, providing a full stochastic representation of $X(p_k)$, the DTG at the estimation point p_k.When we restrict the analysis by not using the soft data, equation 1 reduces to equation 2:

$$f_K(x_k) = f_G(x_k, x_h) / \int dx_k f_G(x_k, x_h) = f_G(x_k | x_h) \quad (2)$$

which is the conditional PDF x_k gives x_h under the general knowledge base *G*. Since $f_G(x_k, x_h)$ is Gaussian, the conditional PDF in equation 2 is also Gaussian, which means the PDF is a linear combination of observed values that correspond to the kriging approach. Since the mean is assumed constant and calculated within a local estimation neighborhood, BME reduces to moving window ordinary kriging when only household well observation data are used. This is the case of the S and ST approaches. This kriging limiting case makes BME attractive since it means that BME reduces to a linear kriging estimator whenever the analysis is restricted to hard data, but it extends to a nonlinear and non-Gaussian estimator when soft data is used. Finally, at the interpretive stage, we calculate the BME mean $\tilde{x}_k$ and corresponding posterior BME variance $\tilde{v}_k$ of the BME posterior PDF at estimation points p_k on an estimation grid to obtain BME estimation maps and the corresponding uncertainty of DTG.

Prior to model implementation, we examined the general spatial and temporal distribution of the raw data. Because of its high right skewness (most of DTG are close to 0), we normalized the data by transforming DTG using natural logarithm, and used it in all the interpolation methods expressed in ln(depth (m)) units, here denoted as ln-depth. This decision was made to have comparable results across the models since BME reduces to a linear Gaussian estimation when only wells measurements are included. We defined x_h as all the 2,395 space-time hard data DTG values observed at the 44 household monitoring wells, x_s as the 2,600 space-time soft data DTG values corresponding to where we know the DTG is low (i.e., these points are geographically located at 50 nodes uniformly distributed across the wetland area and during the wet season, April-November), and $f_S(x_s)$ were the corresponding 2,600 triangular probability density functions characterizing the shallow DTG and its uncertainty.

For STSD, the triangular PDF was based on precipitation records combined with community members' descriptions of the water levels in the wetland and floodplains during wet months (end of April to November). The collaborators reported increasing wetland surface levels and shallow DTG in nearby wells. These observations, while not quantitative, gave us tools to hypothesize the aquifer connections to the wetland. Using collaborators' qualitative statements, we defined a probability function of shallow DTG in the wetland during the wet season. First, we used the piezometers 201 and 206 installed in the Ciénaga Colombia sub-catchment (Figure 2.1a) to identify the relation between the intra-annual precipitation pattern and groundwater level change. These piezometers have complete DTG records and are at 500 and 860 m distance to the nearer stream. We built a Cumulative Deviation of the Mean, CDM, to identify rainfall changes that reflect DTG changes. The shift from negative to positive slope in the CDM curve marked the beginning of the wet conditions (Custodio & Llamas, 1996). Second, we defined uniformly and

randomly distributed points in the wetland as representative wetland data locations, i.e., soft data, using the wetland and inundated areas dataset (Lasso et al., 2014). For each, we defined a triangular PDF with the lower, middle, and upper bound parameters obtained from well 121, the only one in the Man River floodplains. The lower bound was set to 0 m (minimum depth expected), the middle to the minimum of non-zero (0.01 m), and the upper to the maximum (0.8 m) DTG during the wet season. A descriptive report of low shallow DTG in well 121, coincided with a report of shallow depths in the north of Ciénaga Colombia wetland, and the confluence of the wetland with the Man River. Based on the qualitative descriptions made by the community about the low topographic locations close to the wetland, we expect DTG at those locations will follow a similar pattern to that observed in well 121 during the wet season. However, heterogeneity is expected to alter the parameters of the PDF function. To limit the assumption of equal behavior, we limited the PDF function to the wet months in the wetland area.

In this work, the BME framework was implemented using MATLAB functions from BMElib version 2.0c (available at https://mserre.sph.unc.edu/BMElib_web/). The BME implementation parameters chosen for this work varied according to the model approach. In the spatial approach, S, we used six hard data points in the estimation neighborhood, with a maximum spatial radius covering the study area extent (36.5 km) and a maximum temporal radius of zero weeks. In S and ST approaches, we considered 300 hard data points in the estimation neighborhood, with the same spatial radius as in the spatial approach and four weeks as the maximum temporal radius. For space-time with soft data approach (STSD), we used two soft data points as the maximum soft data estimation neighborhood. We used an estimation grid of 250 by 200 estimation points and included the hard data points as the Voronoi points. The mean within the estimation neighborhood was assumed to be constant and equal to the mean of the observational data within

that neighborhood (i.e., the average of the closest hard data points). The estimation grid was expanded outside the middle-low watershed domain to avoid edge effects.

We only considered the mean and covariance of DTG observations at the prior stage for all the modeling approaches. As a result, the prior stage is multivariate Gaussian. Although, higher statistical moments up to an even order can also be considered, though we did not attempt that. In the STSD approach, we considered both hard and soft data at the posterior stage, which leads to a non-Gaussian posterior pdf and a nonlinear combination of the observations. This BME posterior PDF is particularly adept at integrating the knowledge of the triangular PDFs at the wetland soft data points. The integration allows us to incorporate soft data derived from knowing the location of wetlands and from household knowledge of wetland flooding during the wet season. This unique feature of BME makes it an ideal framework to process data from a community science project.

Model evaluation

To quantify each model performance, we used leave-one-out cross-validation over the entire space-time domain, using 4,397 validation values in total, consisting of 2,397 well observations and 2,600 wetland values obtained by taking the expected value of the probability density function at each soft data point. We quantified the total error (estimate minus validation value) in terms of systematic error (i.e., error that is consistent and can be removed through bias correction), and random error (i.e., residual error after systematic errors are removed), which indicate the degree of precision (Reyes et al., 2017). For the statistical metrics, we used the following notation. The first letter designates the statistical operator: M = mean, V = variance, S = Standard Deviation, MS = Mean Square, Cov = Covariance. The last letter represents the values to which each statistic is applied. Z = ln-depth estimations, O = ln-depth validation value

observed at the well or wetland points, and E = Z-O = ln-depth errors. Let $e_i = z_i - o_i$ be the error at the space-time i, and n be the number of space-time validation values. Positive errors mean overestimation and negative errors mean underestimation.

The Mean Error, ME; (Equation 3) and the Variance of Error, VE, (Equation 4) quantify the systematic and random errors, respectively. The systematic errors explain the bias of the method, while the random error describes the precision. These two errors are quantified in the total error or Mean Square Error (Equation 5) (Reyes et al., 2017).

$$ME = \sum_{i=1}^{n} e_i / n \quad (3)$$

$$VE = \sum_{i=1}^{n} (e_i - ME)^2 / n \quad (4)$$

$$MSE = \sum_{i=1}^{n} e_i^2 / n = ME^2 + VE \quad (5)$$

Finally, we used the Pearson coefficient of determination R^2 (Equation 6) to quantify the fraction of the variance explained by the estimates.

$$R = cov(O, Z) / (SO \times SZ) \quad (6)$$

Where cov(O, Z) is the covariance between O and Z. Knowing that VE = V(O,Z), VE can be written as in equation 7.

$$VE = SO^2 + SZ^2 - 2 \times cov(O, Z) \quad (7)$$

Combining equations 6 and 7, R^2 can also be expressed as:

$$R^2 = (VZ + VO - VE)^2 / (4 \times VZ \times VO) \quad (8)$$

which allows interpreting the influence of the random errors over the variance of the estimates.

Areas impacted by shallow depths

Mapping DTG helps to reveal groundwater-surface water connectivity and quantify seasonal fluctuation in groundwater level and flooding (Fan et al., 2013). With the STSD model, we established the areas more susceptible to shallow groundwater in response to precipitation, given that 2008 was a wet year in which the middle-low watershed experienced flooding. To accomplish this goal, we used BME mean and variance and calculated the probability that DTG is less than a cutoff value of interest at each estimation point, i.e., Prob[DTG < 0.1 m]. Values smaller than the cutoff value of 0.1 m are interpreted as shallow DTG which are more likely to maintain flow in surface streams, connect to the wetland, and increase the probability of flooding during extreme precipitation periods. We used the BME posterior Probabilistic Distribution Function (PDF) to calculate for each space-time estimation point the probability that DTG is less than 0.1 m, Prob[depth < 0.1]. The probabilities were classified as high = [0.8 - 1.0], moderate = [0.6 – 0.8), low= [0.4 – 0.6), and very low = [0.0 – 0.4).

With the probability maps, we accounted for areas of a high probability of shallow groundwater. We built a time series of the area and compared it with the cumulative average weekly precipitation. The precipitation records were obtained from the three closest weather stations managed by the National Institute of Hydrology, Meteorology and Environmental Studies of Colombia, IDEAM, (http://dhime.ideam.gov.co/atencionciudadano/). Two stations (i.e., Guarumo-La Lucha, National ID: 25025160 and La Coquera, National ID: 26240160) are located outside the middle-low watershed, around 3 km from the catchment to the Northeast. The third station is situated at the upper side of the Quebradona sub-catchment (i.e., Manizales, National ID: 26240060) (Figure 2.1). We used this information to analyze the influence of intensity, amount of precipitation per week, and frequency, days of continuous precipitation, in the shallow DTG area.

Results and Discussion

Monitoring network results

The monitoring period overlapped with the 2008 La Niña year, with 3,375 mm of precipita1tion (700 mm above average); 2009 was relatively dry and received 1,119 mm less rainfall than 2008 (2,255 mm) (data obtained from the IDEAM). The decrease in precipitation in 2009 compared to 2008 was reflected in the DTG. During the wet season, average DTG ranged between 0.9 and 1.3 m in 2009, whereas in 2008, it ranged between 0.5 and 1.1 m (Figure 2.3). During the 2009 dry season, average DTG was 2.4 m, while in 2008, DTG reached 3.3 m in March (Figure 2.3b). DTG ranged from 0 to 20 m; for 75% of the data points DTG was less than 6 m (Figure 2.3b). Wells with DTG greater than 6 m were located to the North (wells 120 and 123), and to the South, outside the middle-low watershed (well 140).

The closest monitoring stations to Ciénaga Colombia wetland were piezometer 202 and well 105 (Figure 2.1 and Figure 2.3). During the 2008 wet season, DTG in piezometer 202 reached the surface in June, while for well 105 the minimum DTG was 1 m. These differences are explained by the fact that well 105 is topographically higher (55 m.a.s.l) than piezometer 202 (47 m.a.s.l). Well 121 was the only one located in the Man River floodplain (Figure 2.3). In this well, groundwater reached the surface during the two wet seasons, fluctuating from 0 to 0.8 m, and had a maximum DTG (3.29 m) during the dry period of 2008 (Figure 2.3).

DTG varied with the season and well's location (Figure 2.1 and Figure 2.3). For wells located at a high topographic location, at the catchment boundary or between two tributaries (e.g., wells 120, 127, 128, and 140), the water table was deeper during the entire period compared to wells located in topographic depressions. Consistently shallower depths were found close to the springs of the Ciénaga Colombia creek sub-catchment, especially during the wet season, at

Quebradona Creek (well 126), and at La Manada Creek (well 129). Difficulty accessing wells located close to the wetland impeded measurement of DTG in these areas.

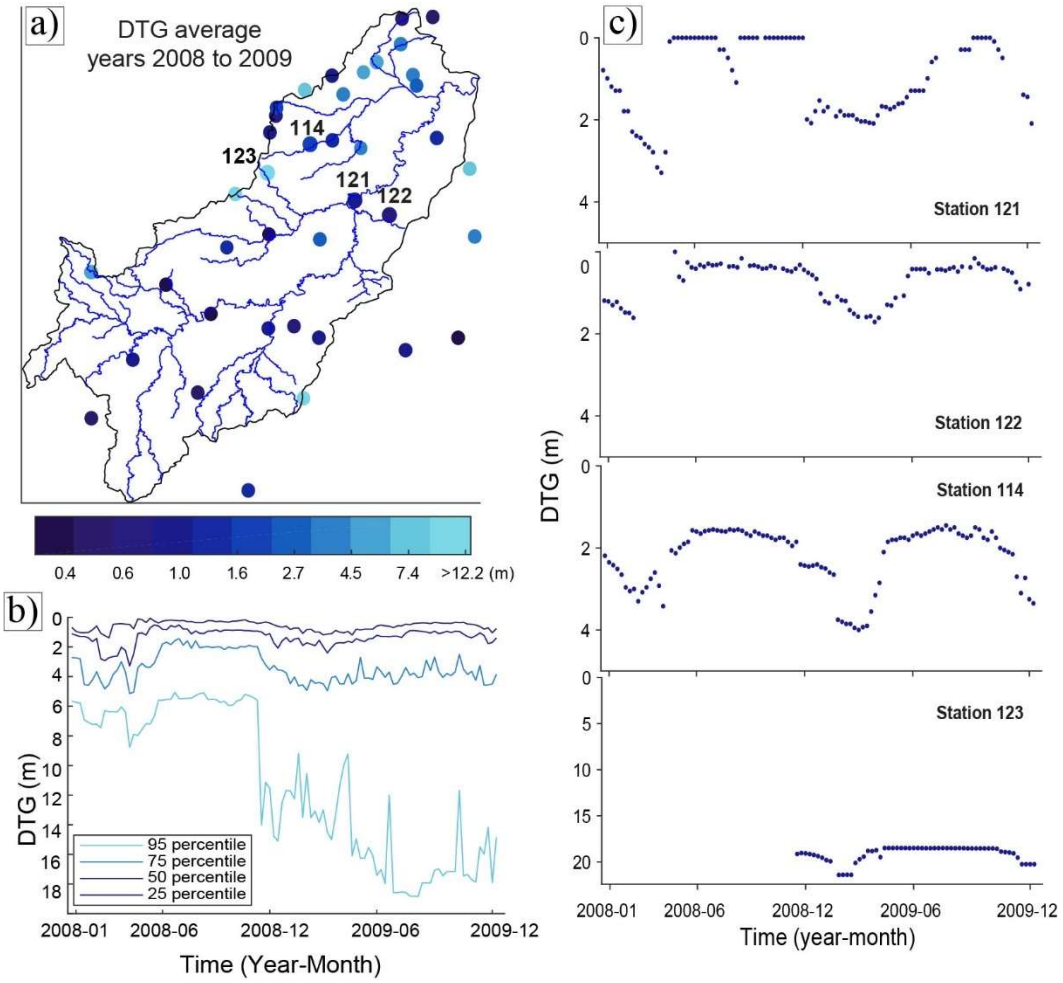

Figure 2.3. Summary of data collected in the watershed. a) annual average distribution of DTG during 2008 and 2009. b) weekly DTG percentiles in all wells. c) examples of DTG time series chosen based on depth range.

Cross-validation and method selection

The cross-validation MSE metric, calculated by combining well and wetland validation data, showed a reduction in the overall error (MSE) when using space-time models compared to spatial interpolation (Table 2.1). The MSE dropped from 9.41 $(\text{ln-depth})^2$ in the S model to 7.21 $(\text{ln-depth})^2$ in the ST model. This reduction is explained by an improvement in precision (VE), but not in bias (ME), as depths to groundwater are consistently overestimated due to lack of hard

data collected near the wetland. Adding soft data generated by knowledge of low DTG at the wetland locations and wet weeks (i.e., weeks in which the water table rose to the ground in the vicinity of wetland areas) resulted in further reduction of the MSE from 7.21 (ln-depth)^2 in ST to 0.61 (ln-depth)^2 in STSD. This change resulted from the addition of soft data, which caused a decrease in VE, from 3.81 to 0.41 (ln-depth)^2, and ME, from 1.84 to 0.44 (ln-depth). Therefore, the STSD model reduced the overestimation of DTG, and the total error by a factor of 15 (MSE_S/MSE_{STSD}) when S is compared to STSD. Consistent DTG overestimation could be due to the lack of well observations in the wetland. Although further reductions could be reached with more well observations in the wetland area, our wetland space-time data contribute to a better representation of the DTG in the floodplain. Cross-validation results using only the well and wetland validation data, data agree with these results and are included in the supporting information (Table A.1).

Table 2.1 Cross-validation model results for the hard and soft data points

Model	**MSE (ln-depth)^2**	**VE (ln-depth)^2**	**ME (ln-depth)**	**R2 unitless**	**VZ (ln-depth)**
S	9.41	5.97	1.86	0.004	1.23
ST	7.21	3.81	1.84	0.268	2.23
STSD	0.61	0.41	0.44	0.930	3.71

Note: For each cross-validation evaluation, MO is -1.93 (ln-depth), and VO is 5.06 (ln-depth)^2.

The Pearson regression coefficient, R^2, increased from 0.004 for the S model to 0.268 for the ST model. Since VO is the same for S and ST, an increase in R^2 may be due to a decrease in VE or an increase in VZ. Here, the increase in R^2 is due to an effect on both VE and VZ. VE decreased from 5.97 (ln-depth)^2 for the S model to 3.81 (ln-depth)^2 in the ST model (i.e., the ST

model produces smaller error estimates), while VZ simultaneously increased from 1.23 (ln-depth)^2 in S to 2.23 (ln-depth)^2 (i.e., the ST model provides a stronger contrast between small versus large DTG values). These results reveal the benefits of building a space-time interpolation over a pure spatial analysis. For the ST model, high temporal correlation of DTG informed the model in areas where DTG were missing for a particular date. R^2 increased further, to 0.930, in the STSD model due to an increase in VZ from 2.23 (ln-depth)^2 in ST to 3.71 (ln-depth)^2 in STSD, and a decrease in VE from 3.81 (ln-depth)^2 to 0.41 (ln-depth)^2. The dual-action on VE and VZ reflects the positive impact of adding soft data describing the expected low DTG in the wetland and floodplains during wet periods.

Inclusion of wetland space-time data improved DTG estimates (Figures A.3-A.4 in the supplemental information). The models showed shallow DTG in the northwest of the middle-low watershed, close to springs and depressions, especially in the wet season. However, models without soft data (S and ST) failed to represent the expected small depths near wetland and floodplains (DTG estimation resulted in larger values) due to the lack of observations in the topographic low-elevation sectors of the catchment.

The collaborators reported increases in flooded areas and wetland open water during the wet season. Our results can spatially represent these findings and observations at a weekly temporal scale. Moreover, our findings are consistent with previous studies in the region that used hydrogeochemistry and isotopic techniques to identify groundwater recharge sources (Palacio & Betancur, 2007), and surface-groundwater interactions in the Man River middle-low watershed (Palacio et al., 2013) and the Ciénaga Colombia wetland (Santa-Arango et al., 2010). According to these studies, in the Quebradona and Ciénaga Colombia sub-catchment, evaporation from the aquifer occurs in the upper left side of each of the sub-catchments (Palacio et al., 2013).

Moreover, direct recharge takes place across the watershed. This pattern was identified by detecting similar isotopic composition in the rainwater and the shallow groundwater, which suggested recent groundwater in the aquifer with potential short resident time (Palacio & Betancur, 2007). These water composition similarities were consistent during the wet and dry seasons, implying a high dependency of the aquifer on precipitation, which also may explain some of the shallow depths obtained during the wet year.

BME total error reduction is consistent with BME applications in water quality (Akita et al., 2007; Messier et al., 2014), highlighting that accounting for temporal correlation results in significant decrease in the total error. Our approach allowed us to partition the total error into systematic and random error to analyze them separately. We found that the main contribution in the STSD model is that it increases the precision (i.e., reduce the random errors) more than it reduces the bias, although the bias is also reduced (i.e., systematic error decrease). All methods overestimated DTG. This may be explained by the lack of hard DTG data in the low-elevation locations. Nevertheless, STSD overestimated DTG the least compared with the S and ST model. This consistent overestimation implies more contrast between deep and shallow DTG is expected in the area and predictions can be improved by adding new hard data measurements at the depression locations.

Areas impacted by shallow DTG

The probability of shallow groundwater (DTG<0.1 m) increased as precipitation increased. The area of high probability of shallow DTG expanded during April–November, and decreased between December–March (Figure 2.4a). After the middle-low watershed received six or more continuous days of precipitation in a week, the area with shallow DTG increased, reaching its maximum (56%) the second week of May 2008 (Figure 2.4a). We saw a bigger increase in the

area in 2008, the wetter year, suggesting a relationship between days with continuous precipitation, rainfall intensity, and shallow DTG (Figure 2.5). Conversely, shallow DTG area decreased two weeks after reaching its peak when precipitation also decreased, suggesting that soil moisture's antecedent and posterior conditions influence shallow DTG area changes. Our results suggest a nonlinear relationship may be occurring between precipitation intensity and frequency, and the fluctuation of shallow DTG areas (Figure 5). We found a relationship between the aquifer response to precipitation and the intensity and duration of the rain. Longer DTG records are necessary to define the threshold in precipitation after which groundwater contributes to overland flow and subsequent flooding, and the nature of the nonlinear relationship defining this threshold.

The distribution of the high probability of shallow DTG areas indicates the aquifer's potential exchange of groundwater and surface water. Zones with consistently shallow DTG included the Ciénaga Colombia wetland and the Man River floodplains in the low watershed, i.e., topographic depressions, and the up-stream La Manada and Quebradona sub-catchments, where the headwaters are located (Figure 2.6 & Figure 2.7). Shallow DTG areas up-stream of the main sub-catchments may explain the permanent streamflow of the Man tributaries throughout the year. Low probabilities of shallow DTG, situated to the North in the watershed's upper margin (Figure 2.4b), are consistent throughout the two-year period (Figure 2.6 & Figure 2.7).

Previous studies suggested a dominant contribution of the aquifer to the surface water, and evaporation from the upper La Manada and Quebradona sub-catchments (Betancur, 2008; Palacio et al., 2013). Evaporation may explain the rapid decrease in the shallow DTG area after it reaches its peak (Figure 2.4a). Another explanation of this rapid decline of shallow DTG area could be associated with the soil characteristics and the sparse vegetation. 80% of the watershed

is associated with sandy clay and loam soils derived from poorly consolidate sandstones with a hydraulic conductivity of about 0.2 cm/h (Instituto Geográfico Agustín Codazzi, 2007a). These soil characteristics allow the soils to reach saturation quickly. Therefore, DTG increases during continuous and intense rainy days.

Land use activities may play an essential role in shaping the aquifer response to precipitation in the watershed. The region has alluvial mining exploitation and grazing since the 16th century (Cuartas et al., 2000). Mining activities in the Man River floodplains and other tributaries have affected the watershed's capacity to control erosion in the riverbanks. Additionally, around 80% of the middle-low watershed is used for grazing, in which a common practice is to create artificial open water ponds to provide water for the animals (Instituto Geográfico Agustín Codazzi, 2007a). These activities have reshaped creeks and channels, disrupting the surface flow (Betancur, 2008, 2014) and threatening wetland ecosystem services such as flow control, groundwater replenishment, erosion control, and food provision (Betancur-Vargas et al., 2017). This practice and the favorable atmospheric moisture conditions for evaporation may be drivers for rapid water loss after precipitation days cease. Evidence of an increase in intensity and frequency of La Niña events (Wang et al., 2019) is cause for concern, as an intensification of wet events would increase the probability of flooding in agricultural areas, promoting sediment deposition and erosion that may cause soil compaction and reduce the infiltration capacity.

Impact of community knowledge added to model implementation

Our approach allowed us to identify the combined action of intensity and frequency of precipitation over DTG response. This identification was possible due to the community knowledge that allowed to add detailed temporal data to the model. Previous studies used the classic kriging spatial interpolation to model monthly groundwater table in the River Man

middle-low watershed using SRTM-30 (Palacio, 2014). While SRTM-30 was the best-known elevation model for the area, heterogeneity is missing in a relatively flat landscape (i.e., the elevation of a well located in high topography can appear lower than expected). Although we cannot compare both studies' results numerically, both studies revealed the groundwater table fluctuation in response to precipitation changes. In addition, our results provide insights about how DTG may respond to precipitation.

The fact that STSD is the best representation of DTG suggests that community knowledge added vital information to improve DTG mapping, even though incorporating this knowledge into the model implementation was not planned from the beginning of the community science project. A more systematic qualitative knowledge collection with the community (e.g., interviews or surveys, storytelling, knowledge dialog) would enhance community perceptions into the model. These systematic qualitative methods require design strategies for sustaining community engagement (Haklay, 2013). For future projects we suggest, regardless of the knowledge collection strategy, to include the community as part of the model validation. Further feedback from the community will help confirm and validate model results collectively. A technique that can be adapted for this model validation purpose is social cartography (Liebman & Paulston, 1994). This technique has proven effective in identifying relevant monitoring sites while also helps to identify environmental risk (Arias et al., 2016).

Participatory approaches are effective mechanisms to increase the knowledge about the groundwater system while involving the community in the process at different levels (Grieef & Hayashi, 2007; Little et al., 2016; Re, 2015). Our approach can be used in systems with no data for exploratory purposes (e.g., monitoring network design or seasonal groundwater-surface water connectivity detection, and aquifer characterization). Additionally, our approach is helpful for

incorporating continuous groundwater monitoring because locals can be involved in different project stages, from data collection to data analysis to model validation. Building collaborative links between scientists and the community also help address research questions with a meaningful social impact (Arias et al., 2016; Haklay, 2013).

Constant communication and knowledge sharing are effective engagement mechanisms in community science projects (Assumpção et al., 2018; Cooper et al., 2007). One of the tasks that made the communication effective was to have short informal conversations with each household before discussing the data collection. Communication and trust-building are key in community science projects (Baldwin et al., 2012; Little et al., 2016). Fieldwork campaigns were also designed to build trust and establish collaborations with the households. Providing recommendations for the wells' maintenance, sharing water quality analysis results, and having a conversation with the households about activities not necessarily related to data collection were effective mechanisms to build trust, and at the same time, help to solve issues affecting water quality at the household level. These ways of communication helped to maintain the monitoring network remotely and to learn from the locals. We believe that our approach allows us to include the community knowledge in the data analysis.

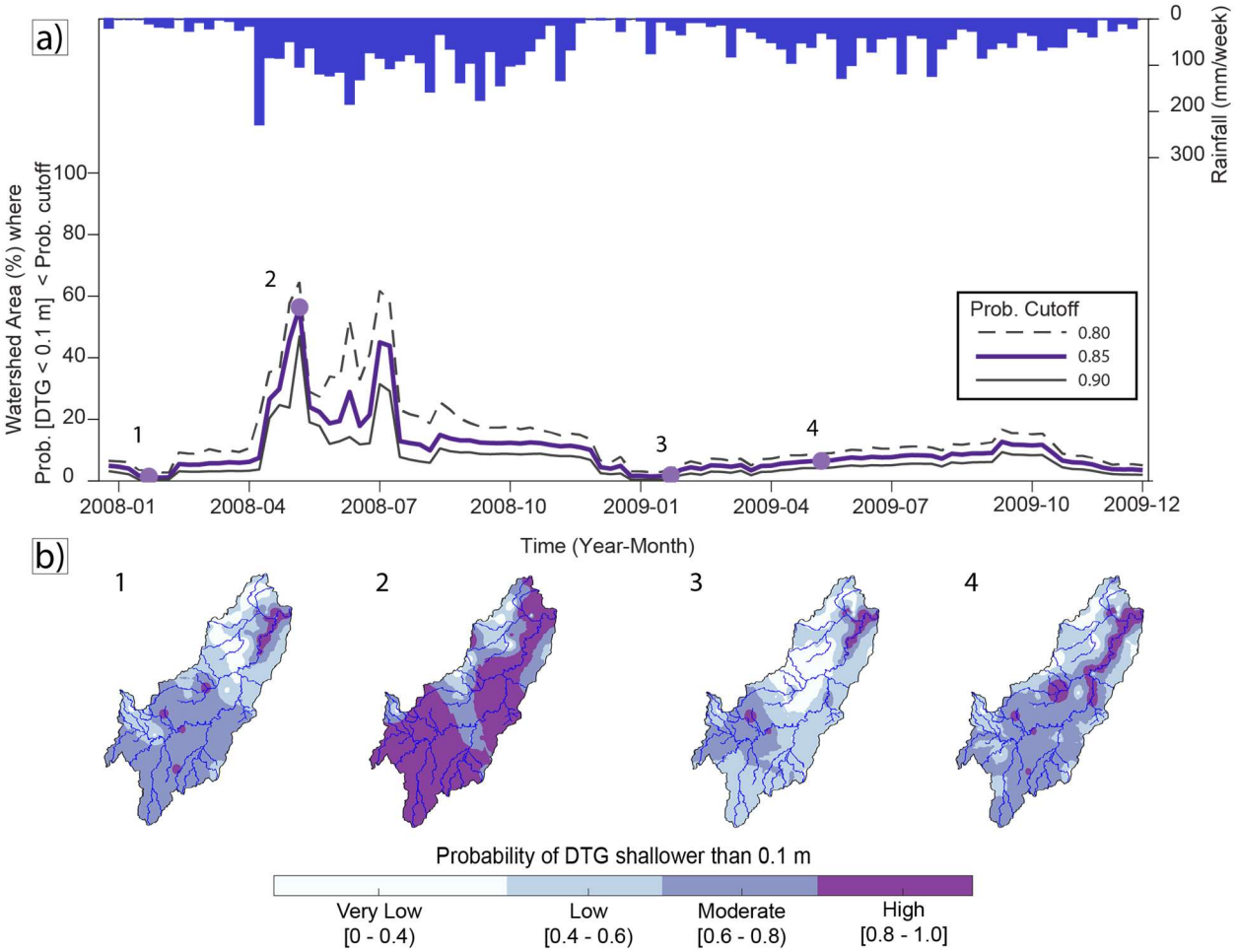

Figure 2.4. Temporal and spatial distribution of Prob[DTG < 0.1 m]. a) Weekly precipitation compared to weekly area of high Prob[DTG < 0.1 m] expected at 0.8, 0.85, and 0.9 cutoffs. Values at each probability cutoff are expressed as a percentage of the total watershed area (481.3 km2), including wetlands (11.1 km2). Precipitation is the average of the three closest national weather stations. b) Example weekly maps of the spatial distribution of Prob [DTG < 0.1 m] for time points 1,2,3, and 4 (see a), illustrating dry and wet months.

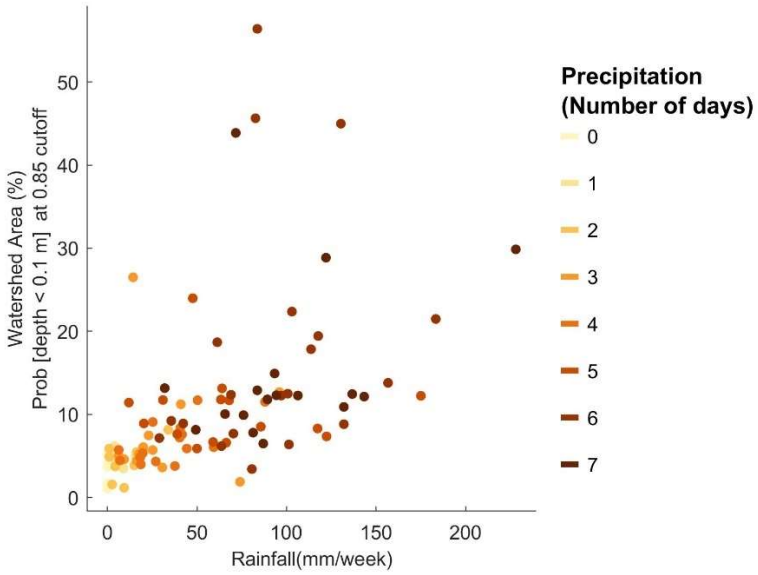

Figure 2.5. Relation between precipitation of the previous week and the high probability of shallow DTG area. The combined precipitation intensity (i.e., mm per week of rainfall) and duration (i.e., number of rainy days) have an effect on the area of shallow DTG.

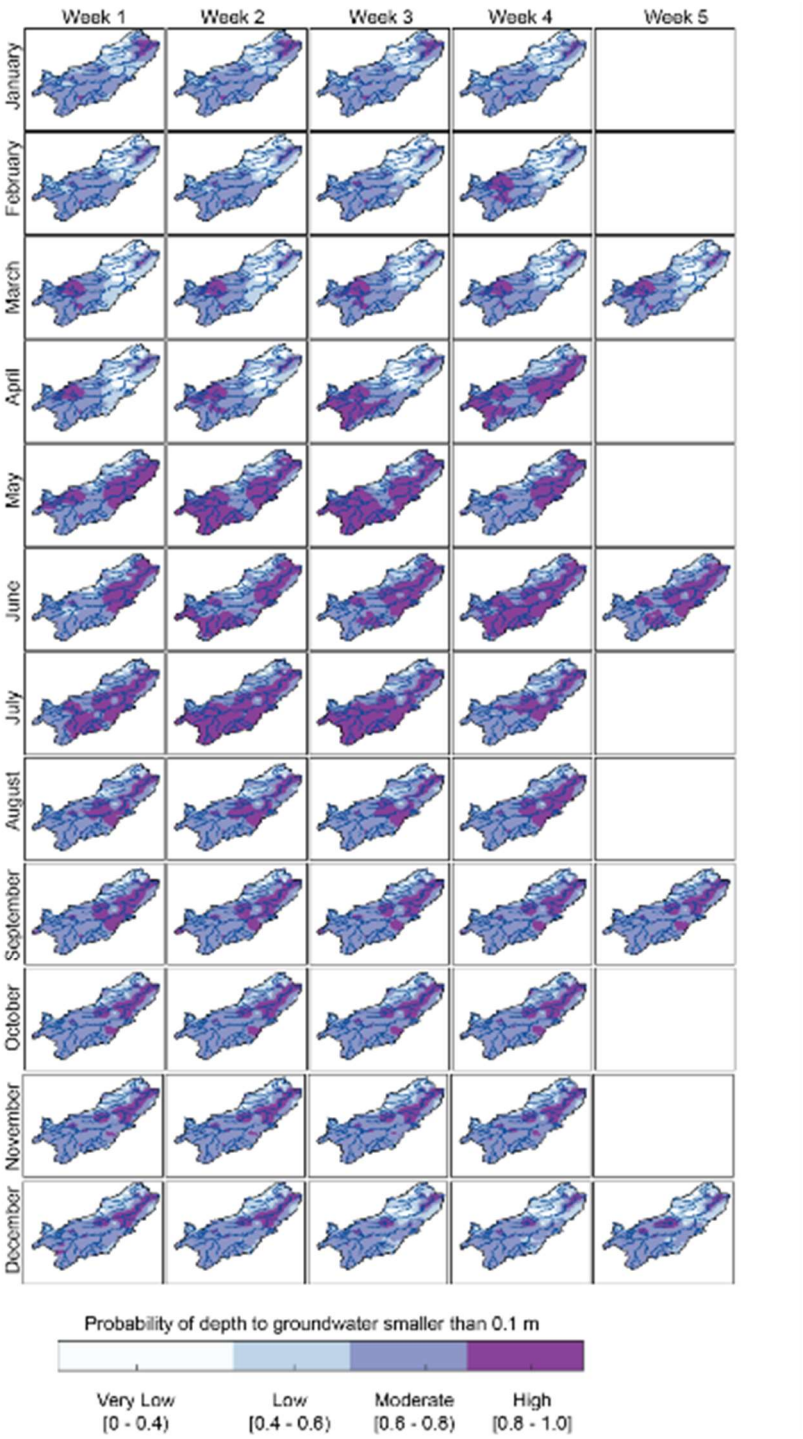

Figure 2.6. Spatial distribution of the probability that the weekly average of DTG is smaller than 0.1 m (Prob. [DTG<0.1m]) for each week in 2008. The first week of the year is considered to start on 12/31/2007.

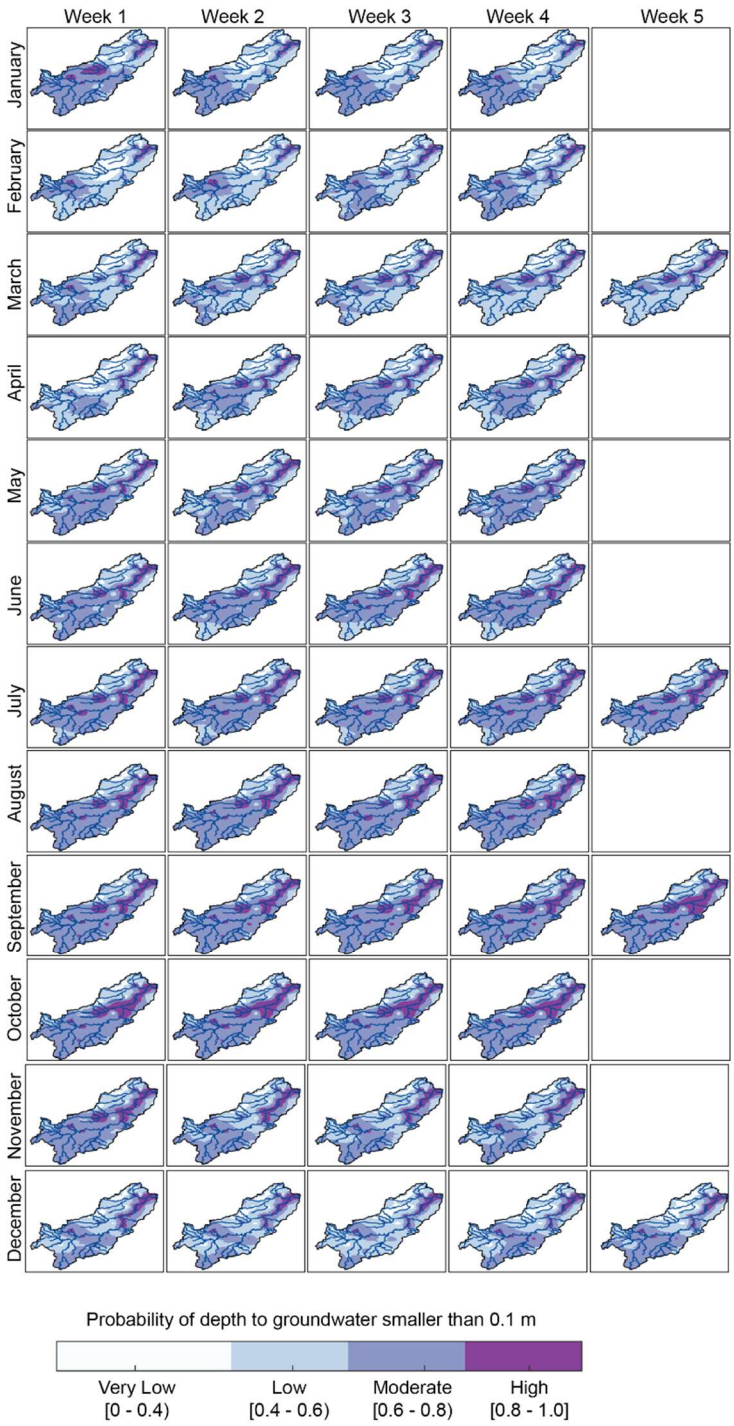

Figure 2.7. Spatial distribution of the probability that the weekly average of DTG is smaller than 0.1 m (Prob. [DTG<0.1m]) for each week in 2009. The first week of the year is considered to start on 01/05/2009.

Conclusions

Community participation in scientific hydrologic studies provides benefits through both community engagement (e.g., knowledge transfer, community self-training, education outreach, and informed decision making) and the understanding of hydrologic systems. In groundwater-dependent regions with limited or no DTG information, our results suggest that the combination of Community Science Research and BME modeling can contribute to a better understanding of groundwater dynamics. We used community descriptions, locations of wetlands, and precipitation records to define a probabilistic function that informs us about shallow DTG in the floodplains and wetland areas and complements the data collected by the community. The community helped create a dataset that would have been challenging to acquire with conventional data collection methods and provided local descriptive knowledge essential to improving DTG representation. BME's capabilities make it suitable to incorporate both qualitative and quantitative data into a model. Our results show how this combination contributed to the modeling effort, specifically:

1. The reduction of the total error occurred progressively from space (S), to the space-time (ST), to the space-time with soft data model (STSD). The high temporal correlation characteristic of DTG allowed improved space-time (ST) interpolations compared to spatial interpolation (S). MSE further reduced from ST to STSD by adding soft probabilistic DTG in the wetland and floodplain areas, resulting in the combined improvement in precision and a reduction in DTG overestimation and bias. Also, STSD incorporated information where DTG values were missing, increasing the variability in DTG values.
2. The spatial and weekly temporal distribution of the groundwater and surface water connections showed consistency with previous studies using hydrogeochemistry and isotopic

approaches. In those studies, evaporation from the aquifer was identified to occur in areas of the main sub-catchments (Palacio & Betancur, 2007), which may explain why the area of shallow DTG decreased around two weeks after reaching its peak. Similar isotopic composition between groundwater and surface water during the wet and dry periods in topographic depressions (Palacio et al., 2013; Santa-Arango et al., 2010) explains the consistent shallow DTG in our maps. By incorporating the wetland locations and their most likely DTG during the wet season, we delineated shallow DTG in these topographic depressions.

3. Our results suggest a nonlinear relationship between precipitation intensity and frequency and the shallow groundwater area. The rapid increase in shallow DTG area in the extreme wet year compared to the average year may be related to high antecedent soil moisture conditions due to continuous rainfall, raising the groundwater table. In contrast, middle-low watershed topographic features, atmospheric conditions, and land-use practices create favorable conditions for high evaporation, contributing to decreasing the shallow DTG area over the year when precipitation ceases. Additional data will be required to investigate further specific threshold values after which shallow DTG area increases.

From a modeling perspective, one limitation of our approach is that the lack of observations in the wetland areas constrains the reduction of DTG overestimation. That said, recognizing the value of using BME in Community Science projects may contribute to the design of monitoring networks or to model use for exploration purposes. The combined use of BME and Community Science may allow for closer interactions with the collaborators, contributing to the formulation of new hypotheses and further identification of critical environmental concerns. Our results suggest that both quantitative and, crucially, qualitative information from community members

can result in substantially better spatial and temporal understanding of DTG, which may be of use in many similar environments around the world. Including the community in the model validation would be a further step towards fully integrating community science projects in the broader scientific enterprise.

Acknowledgments, Samples, and Data

The authors acknowledge the Grupo de Ingeniería y Gestión Ambiental, GIGA, at the Facultad de Ingeniería, Universidad de Antioquia, and the International Atomic Energy Agency (project: CRP-14031), which funded the community science research component of this paper. Data Analysis was completed with support from Minciencias-Fulbright, Colombia, and Faculty for the Future fellowships awarded to Angélica M. Gómez.

Special thanks to Teresita Betancur Vargas at Universidad de Antioquia for her essential contributions to the design and maintenance of the monitoring network as a director of the Community Science Research project, and her mentorship of the first author's M.S.thesis. Thanks to all the collaborators of the Man River middle-low watershed (Complete list of names in the supplemental material), and to Paola A. Palacio, Diana Montoya-Velilla, and Diana Santa-Arango. Thanks to Jhon C. Duque and Arik Tashie for their time to discuss data analysis results and to Giovanny Ruiz for his contributions to the design of figure 2.2.

We would also like to thank the editors and the anonymous reviewers for their valuable comments and feedback.

All the Depth to Groundwater data used in this paper are available in the repository DOI: 10.5281/zenodo.3923896 [License Creative Commons Attribution 4.0 International]

Wetlands and inundated areas dataset are available in Lasso et al., (2014).

All maps of the STSD model results used in this paper are available in the repository DOI: 10.5281/zenodo.3928587 [License Creative Commons Attribution 4.0 International]

CHAPTER 3: ECOHYDROLOGICAL IMPACTS OF OIL PALM EXPANSION UNDER DIFFERENT SCENARIOS OF LAND TRANSITION[2]

Introduction

The extensive use of palm oil in consumable goods and biodiesel has resulted in widespread global demand of this vegetable oil, resulting in accelerated land-use change across tropical countries towards oil palm crop establishment and expansion (Bessou et al., 2017a; Pirker et al., 2016). According to the FAO statistics database (FAOSTAT, 2020), the total harvested oil palm area increased by over 400% between 1961 and 2018, from 3,621,037 ha to 18,969,417 ha. Moreover, Meijaard et al. (2018) estimate that about half of oil palm development expanded into forested lands between 1972 and 2015, while the other half replaced other land uses. These findings indicate that, in tropical countries, oil palm is a direct driver of deforestation. Additionally, oil palm cultivation indirectly causes further land-use change by displacing other crops onto non-cultivated land (Fitzherbert et al., 2008; Koh & Wilcove, 2008). The expansion of oil palm cultivation is expected to continue based on the current palm oil market demands (Bessou et al., 2017b; von Geibler, 2013). National governments promote the crop as a driver of economic growth by establishing tax exemptions, subsidy programs, and other policies (Castiblanco et al., 2013; Dislich et al., 2017; Furumo & Aide, 2017). Currently, the mean annual oil palm production is greatest in Asia (85.9% of global production), where Indonesia and Malaysia hold the first and second place in the world production, and Thailand is fourth;

[2] The outline of this work has been accepted for submission at *Environmental Research Letters Review*
As co-authors:Gomez A.M., Parra A, Pavelsky T. M, Wise, E. Villegas-Palacio, J. C, Meijide A.

followed by Africa (7.8%), where Nigeria is third in global production; America (5.4%), where Colombia occupies the fifth place; and finally, Oceania (0.8%) where Papua New Guinea holds the seventh position (FAOSTAT, 2020).

The establishment of oil palm plantations in previously forested land typically involves terrain clearing, which sometimes is done by slashing and burning, drainage of waterlogged soils, terracing in areas with high slopes, and construction of drainage channels and access roads (Dislich et al., 2017). This process results in removing organic material, carbon loss, soil degradation and compaction, and biodiversity loss, among other negative impacts (Dislich et al., 2017; Meijaard et al., 2018). Planted areas generally constitute large-scale monocrops with homogeneous canopy vertical structure, as plants are of uniform age, and understory vegetation is commonly cleared (Meijaard et al., 2018). With the continued expansion of oil palm planted areas in countries outside Southeast Asia, new trends in land cover transition are being reported, particularly crop establishment in land previously used for pasture and agriculture (Furumo & Aide, 2017). These trends and the need to increase oil palm adaptation to local environmental conditions motivate oil palm species to be different from the traditional commercial *Elaeis guineensis Jacq.* or African oil palm (*E. guineensis)*. An interspecific hybrid between *E. guineensis* and *E. oleifera Cortés* (American oil palm), called OxG hybrid, is getting more commercial attention (Barcelos et al., 2015). Compared to the conventional oil palm species (*E. guineensis*) that has a rotation of around 25 years (i.e., palms become too tall to be harvested) (Corley and Tinker, 2003), the OxG hybrid has slower growth that increases its life cycle. This hybrid is also tolerant to butt rot disease, an infection that attacks oil palm plantations, and its oil has improved nutritional properties (Mozzon et al., 2020). Understanding how different environmental processes shift under different transition scenarios and different plant species

contributes to identifying ecohydrological impacts in water availability and ecological function. However, to our knowledge there has not yet been a review that systematically examines ecohydrologic impacts in different land transitions and incorporates oil palm varieties in addition to *E. guineensis*.

The growing heterogeneity in oil palm expansion patterns and the variety of species planted make it challenging to generalize the environmental implications of oil palm development. Land conversion to monocrops shifts vegetation structure and composition, causing ecohydrological impacts in water availability and ecological function. In humid tropical forests, deforestation can increase runoff and decrease infiltration (Sun et al., 2017; Wright et al., 2018). These changes affect soil retention capacity, soil structure, and erosion, increasing sediment transport and nutrient loss into streams (Hunter & Walton, 2008). Land cover changes can modify local-to-regional precipitation patterns and ultimately alter the regional climate in humid and semi-arid environments (Spracklen et al., 2018; Hoyos et al., 2018). Land conversion also alters the energy balance partitioning (Spracklen et al., 2018). Sensible heat may increase in recently deforested areas due to an increase in albedo and surface temperature (Bonan, 2008). Similarly, latent heat may vary in distinct ways when crops replace natural vegetation due to differences in stomatal conductance, which impact transpiration (Pongratz et al., 2006). Existing reviews (Carr, 2011; Comte et al., 2012; Pardon et al., 2016) demonstrate that environmental effects of oil palm intensification, its impacts on water, and plant-water relations have been studied in oil palm plantations, but mostly in regard to forest conversion.

Although publications regarding different land transition scenarios and plant species and research focused on oil palm outside of Southeast Asia have been growing in the last decades, a systematic review that includes those topics has not been produced. Available reviews that

specifically evaluate the effects of oil palm crops on water resources explore the relationship between *Elaeis guineensis* plant water requirements and irrigation (Carr, 2011), the impacts of agricultural practices in nutrient cycling (Pardon et al., 2016) and hydrologic fluxes (Comte et al., 2012), and the application of remote sensing analysis to oil palm studies (Chong et al., 2013). Additional works investigate oil palm impacts on both biodiversity (Meijaard et al., 2018) and changing ecosystem functions under scenarios of forest conversion (Dislich et al., 2017). Carr (2011) summarizes the connections between stomatal opening, transpiration, and gas exchange across seasons and how these three aspects relate to soil moisture. In doing so, Carr (2011) highlights the lack of information regarding both, the maximum water table depths palm oil plants can tolerate and the different water management strategies in oil palm productivity. Comte et al. (2012) remark on gaps in the understanding of the water balance partition when reviewing the impact on hydrological fluxes of oil palm conversion from forests and its relations to nutrient assimilation and excess. In particular, they identify throughfall and rainfall interception changes across different oil palm ages, evapotranspiration at immature oil palm stages, and long-term runoff changes. The impacts of oil palm on ecosystem functions under forest conversion scenarios are reviewed by Dislich et al. (2017). In this review, the authors highlight the tendency of the regulation ecosystem function to decrease in oil palm plantations and the influence of plant age, local environmental conditions, and crop management in the ecosystem function response. All the existing reviews describe the gaps and opportunities for understanding oil palm processes. However, a common aspect of all the cited publications is that they limit their scope to *Elaeis guineensis* and to the transition from forest to oil palm crop. Moreover, the cited publications in these reviews limit their geographical scope mostly to Indonesia and Malaysia,

the largest palm oil producers (Fitzherbert et al., 2008; Wilcove and Koh, 2010; FAOSTAT, 2020).

Here, we review the state of the field and highlight emerging knowledge gaps and research challenges associated with the effects of oil palm cultivation on water resources in the tropics and associated ecological processes. We looked at the gaps and advances synthesized by existent reviews as a baseline and expanded our search to other regions, land transition types, and oil palm species. We summarized the work done by exploring different land transitions to oil palm across the tropics at different spatial scales, focusing on understanding the linkages between oil palm plantations and hydrologic processes. Available information at the global and regional scale is evaluated and synthesized to 1) determine the extent of oil palm research on ecohydrological processes, in particular, land-atmosphere interactions, fluvial processes, and soil and groundwater dynamics, 2) summarize the effects of oil palm on the water budget and how these effects link to other ecosystem processes and to other scenarios of land transition (we considered tropical forests, croplands, and pastureland or grasslands), and 3) describe areas of future research associated to ecohydrological fluxes that have not been addressed.

Material and Methods

Literature search and selection

We conducted a literature search across nine databases and one search engine: Redalyc, Scielo, Dialnet, IEEE, Springer Link, Scopus, Science Direct, Web of Science, PubMed, and Google Scholar. Considering the expansion of oil palm cultivation into Latin America (Furumo and Aide, 2017), we decided to include literature written in Spanish and Portuguese to ensure that relevant research from Latin American countries was not filtered out due to a language barrier. Redalyc, Scielo, and Dialnet databases were used mainly to find literature written in

these languages. Literature in oil palm research that explicitly included the term 'ecohydrology' is not very common. Therefore, the search query across the different platforms was done using combinations of search terms associated with ecohydrology. These terms are presented in the supplemental material (Table B.1). Given the variety of databases used in this review, we discarded non-peer-reviewed papers. Our search was performed between November 2018 and February 2019. During the preparation of the manuscript, we included relevant and more recent literature that was not systematically collected. We did not limit the search to any year or period.

The resulting publications were filtered in three primary stages: 1) select by title, 2) select by abstract and categorize, and 3) detailed reading. In the first stage, we screened the search results by title and abstract (Figure 3.1). We excluded papers referring to the industrial aspects of palm oil production, detailed agronomic studies or food industry studies (including topics such as waste and yield management, pest control, and nutritional analysis of oil palm), and articles that did not include any explicit mention of oil palm. In the second stage, we classified the documents that were retained from the first filter into three categories according to the information included in the title and abstract (categories described below). In the third stage, we made a detailed reading of papers from each category. We subcategorized those papers based on their specific topic, i.e., oil palm distribution and expansion, land-atmosphere, fluvial processes, and soil and groundwater. We excluded documents that did not match any of the category's criteria or fall into the research subquestions. During this process, we reclassified papers into a different category if necessary.

We defined categories to facilitate the systematic revision, as we wanted to focus on papers related to ecohydrological processes, land-use change, and the perceptions that socio-political literature presents on water availability and water quality. These categories were then distributed

into subcategories during the data extraction and analysis. The categories were defined as follows:

Category A: hydrological papers, including work examining current or expected oil palm transformation scenarios and their hydrologic effects. The articles could address one or several processes in the hydrologic cycle or water budget at one or more scales. Guiding questions: How do studies consider coupled hydrologic-vegetation function? What are the effects of oil palm on surface energy and water balances? Which type of land use and land cover transitions have been studied?

Category B: research on oil palm extension and expansion patterns including papers quantifying and mapping oil palm biophysical characteristics, such as leaf area index and canopy related metrics, and water use efficiency. Guiding questions: What is the geographical distribution and expansion of oil palm? Which type of land use and land cover transitions have been studied?

Category C: research on political, economic, sustainability, and social aspects related to oil palm cultivation and water resources; e.g., conflicts in water use and communities' perceptions of water availability and water quality. Guiding questions: What are the major impacts on water resources? What changes in water availability and quality are perceived by communities?

After the categorization, additional topic-specific classification was made to identify connections among the studies. Relevant material for this review included existing review papers associated with different ecosystem functions in oil palm plantations and research papers addressing any of the guiding questions.

Data extraction and analysis

We collected general (e.g., year, authors, study area, and temporal and spatial scale of the analysis) and specific information (i.e., topic-specific information) from each paper (Figure 3.1). Given the variety of definitions of spatial scale, we classified papers using the scheme developed by Becker and Nemec (1987), who define spatial scale as plant (at a specific part of the plant), plot (1 m^2 to 1 km^2), regional (small mesoscale >1 km^2 to 100 km^2), mesoscale (large mesoscale >100 km^2 to 10000 km^2), and macroscale (continental scale >10000 km^2). Papers with study areas covering the entire tropics were considered macroscale. We based the selection of specific information variables for categories A and B on Bonan (2008), who described biogeophysical ecosystem processes and how they are integrated to treat the biosphere as a couple system, and D'Odorico et al. (2010), who described land ecohydrological processes. Following the components of the water cycle and their interactions with vegetation, we distributed type A, B, and C papers in subcategories defined as (i) oil palm distribution and expansion, which bring insights to understanding patterns of land transition and distribution of oil palm species; (ii) land-atmosphere, which describes microclimatic variables, energy balance partition, and evapotranspiration; (iii) fluvial processes, indicating the hydrologic connectivity of the landscape through sediment transport and surface runoff, including streamflow; and (iv) soils and groundwater processes, which includes soil properties given its a critical role regulating the water balance (Rodriguez-Iturbe, 2000), and water table fluctuation in groundwater systems. The list of specific information extracted appears in the supplemental material. (Figure B.1).

To identify the differences in ecohydrological processes under different scenarios of land transition into oil palm plantations, we designed a coding system that differentiates direction of change (i.e., increase, decrease, no change, inconclusive), type of land transition, oil palm species, oil palm age, and the scale of the analysis. We identified the transition types as forest,

grassland or pastureland, and cropland. Oil palm species included *E. guineensis*, the hybrid interspecific *E. oleifera* x *E. guineensis*, other species, and non-specified species. Regarding oil palm age, we classified processes happening at the nursing stage of oil palm (less than two years old), the young stages (2- 6 years), and the mature stage (>6 years), where oil palm dominated the canopy cover. When papers compared processes associated with oil palm crops and other land covers, we identified three types of analysis: pair-comparison, time series of land use-land cover transition, and building of land use-land cover change scenarios. We also extracted the type of approach the study followed, separating fieldwork and experimental studies from modeling approaches and statistical from physically-based approaches.

We included the mean values of each of the variables analyzed for each of the relevant papers, the type of land transition analysis, and the direction of change (Table B.2). We also include the summary of papers that do not include land transition. Given the differences in approaches, units, and ways to present error metrics, values from different studies were not averaged. For papers that do not include data results in tables but only in figures, we relied on the figures to extract maximum, average, and minimum values for the variable(s) analyzed.

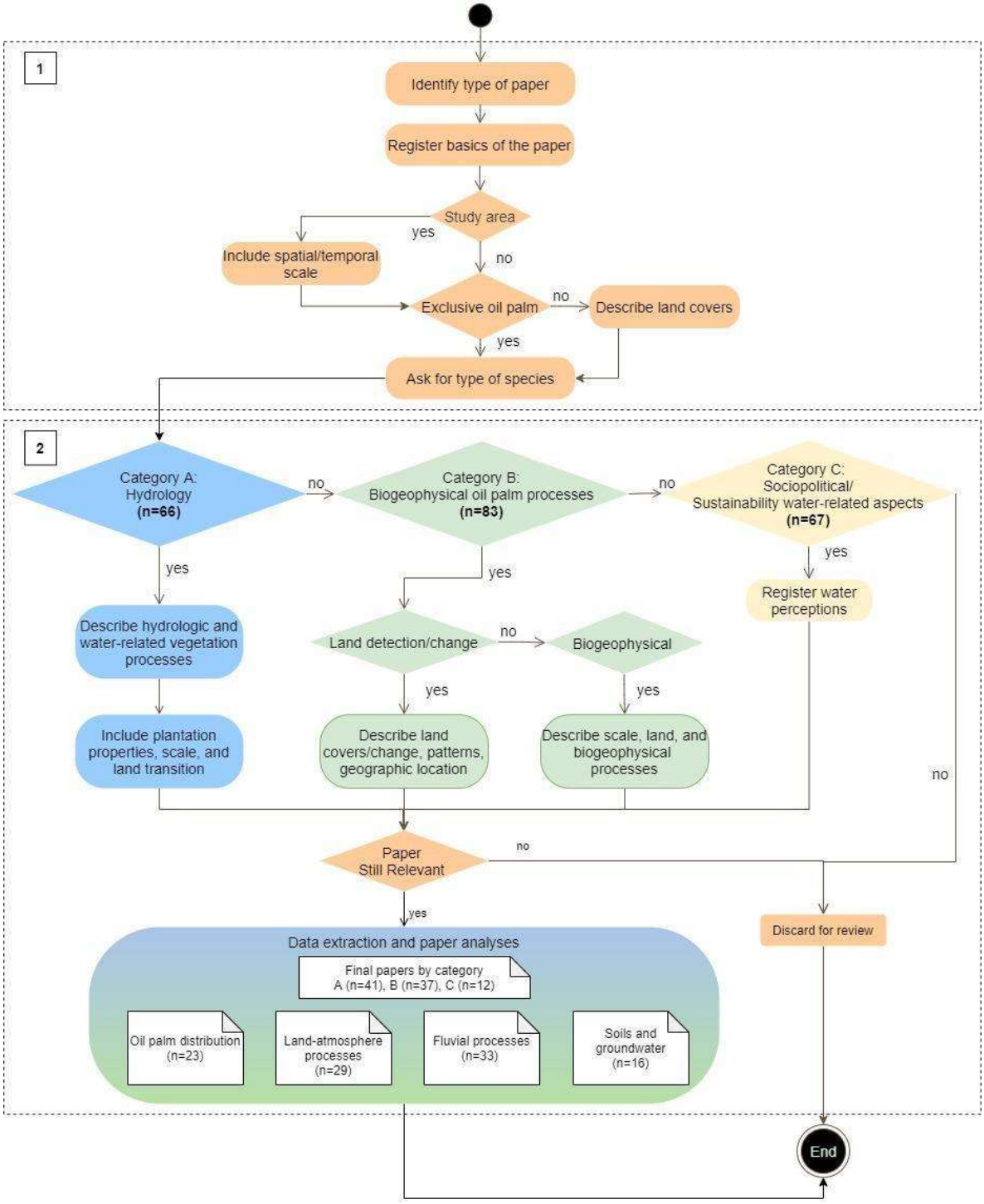

Figure 3.1. Information extraction process applied to relevant literature. 1. General descriptive information obtained at the beginning of reading each paper. 2. Specific information by category and subcategory. Blue shapes are associated with category A: Hydrologic processes; green shapes with category B: Biogeophysical processes; and yellow shapes refer to category C, which includes sustainability and sociopolitical aspects of oil palm development. Once all the literature was selected, papers were distributed into subcategories (blue-green shapes), and their results and approaches were analyzed based on four components: oil palm distribution, land-atmosphere, fluvial, and soil and

groundwater processes. The final relevant papers for each subcategory are presented in the figure, with some papers overlapping subcategories.

Results

A total of 90 relevant articles remained in the analysis after the filtering stages: the hydrology category (A) included a total of 41 papers, the biogeophysical oil palm processes category (B) included 37, and the sociopolitical and sustainability category (C) included 12 papers (Figure 3.1). Three studies cover the continental scale for the entire tropics, addressing land suitability for oil palm expansion (Pirker et al., 2016; Paterson et al., 2016, Vijay et al., 2016). Unsurprisingly, of the 90 publications, 59 (65%) correspond to studies taking place in Indonesia and Malaysia, the major palm oil producers (Figure 3.3). An important percentage of the rest of the studies (28 papers, 31%) focus on countries in the American continent, a region that has had an increase in publications since 2008. A smaller number of studies on Africa (5 papers) focus on land-atmosphere processes (Burton et al., 2017; Radersma and de Ridder, 1996; Dufrene et al., 1992), land suitability in Gabon (Paterson et al., 2016), and a review of plant-water interactions for irrigation purposes (Carr, 2011), which is the only reference on Nigeria found in the literature, even though Nigeria is the world's third-largest oil palm producer. The oldest relevant study identified in this analysis was from 1992 (Dufrene et al., 1992). After that year, research only started being published consistently after 2005, and there was a sharp increase in research after 2010. Most of the selected literature was written in English; we found two relevant papers written in Spanish and one in Portuguese.

We found high variability in the temporal scale of the studies, ranging from a few days to three years in experimental and field sites, to multiple years using modeling approaches. Notably, most of the work with experimental and field data has short-term data collection (days to months that sum less than a year). In terms of the spatial scale, the highest number of studies

have been at plot scale followed by regional and mesoscale. Most of the studies identifying oil palm distribution use mainly remote sensing techniques (Figure 3.4). We found four studies that center on identifying how different management practices impact hydrological fluxes, specifically the reduction of runoff (Tarigan et al., 2016), and the benefits of riparian zones (Chellaiah et al., 2018; Luke et al., 2017; Horton et al., 2018). Typically, the oil palm species analyzed is *Elaeis guineensis* (44% of studies). However, the species is not explicitly specified in 38% of the studies. Only 2% of the studies cover the interspecific *OxG* hybrid (Figure 3.2). Land conversion or implications of land conversion to oil palm appeared in 31 publications, of which 13 studies performed pair comparisons among different land covers, 11 evaluated the changes in time, and seven corresponded to analyses of land conversion scenarios. The specific forest type is not often specified in the literature, i.e., rainforest, mangrove forest, peatland forest, etc.

Within the literature comprising sociopolitical and sustainability aspects of oil palm, we found few examples that conduct a comprehensive analysis of community perceptions on water-related issues related to oil palm cultivation, though some studies include anecdotal information from local residents. Merten et al. (2016) evaluate local perceptions on water dynamics along with environmental data to assess local knowledge in Indonesia. Using semi-structured interviews conducted in the Jambi province, Indonesia, along with eddy covariance, sap flux, and streamflow measurements, Merten et al. (2016) concluded that the villagers' perceptions of increased water scarcity can be related to changes in ecohydrological processes derived from land cover changes to oil palm. In another study, Larsen et al. (2014) used interviews and focus groups among different actors (e.g, farmers, government officials, managers, residents, researchers) to collect perceptions related to hydrologic processes in Indonesia. They found that actors had different perspectives on water contamination due to erosion and runoff from oil palm

plantations and mills, toxins from pesticides, and reduced surface water in rivers during the dry season and in the water table in land adjacent to the plantation. In addition, actors noticed floods from deforestation with an increased peak flow and flashy floods in the rainy season as well as a reduction in the fishing capacity. In general, local perceptions point towards water scarcity or loss of flow regulation capacity of watersheds with extended oil palm plantations (Merten et al., 2016; Tarigan et al., 2016). Other studies also indicate that social conflicts are related to the reduction in water availability resulting from the high-water demand for oil palm production and water pollution due to the use of fertilizers (Tittor, 2017; Saadun et al., 2018; Larsen et al., 2014). These studies were done in Nicaragua (Tittor, 2017), Malaysia (Saadun et al., 2018), and Indonesia (Larsen et al., 2014).

The following subsections summarize the geographic distribution of relevant studies and the main findings related to ecohydrological processes in oil palm crops and changes in these processes due to land cover transitions. The land-atmosphere section describes the progress made in understanding energy balance partition, evapotranspiration, and environmental variables that determine water use efficiency in the crops. The fluvial processes section describes runoff, streamflow, sediment generation, and transport due to oil palm conversion and in oil palm crops, as well as nutrient leaching. The soil and groundwater section describes the changes in soil physical structure associated with texture and soil organic carbon composition. The final section summarizes the research addressing how different management practices impact changes in hydrological fluxes in oil palm plantations.

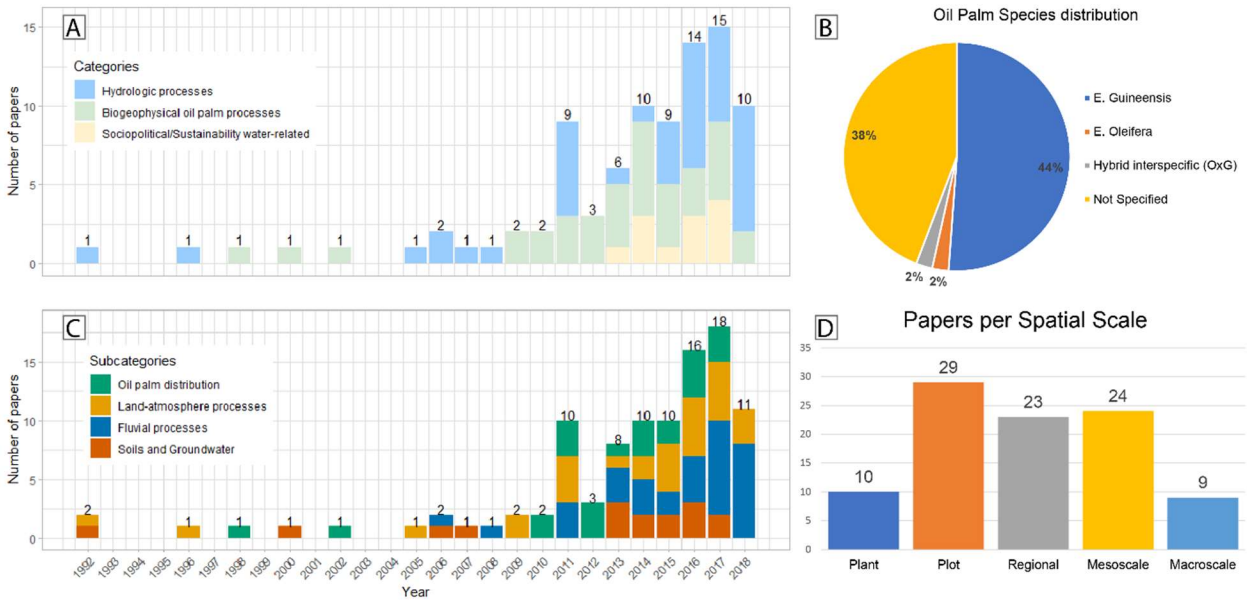

Figure 3.2 Distribution of papers by year, species, and spatial scale. (A) Total number of relevant papers by category and year. (B) Distribution of papers per oil palm species. (C) Distribution of papers per subcategory (papers can be in more than one subcategory.) (D) Distribution of papers per spatial scale (papers can include more than one scale).

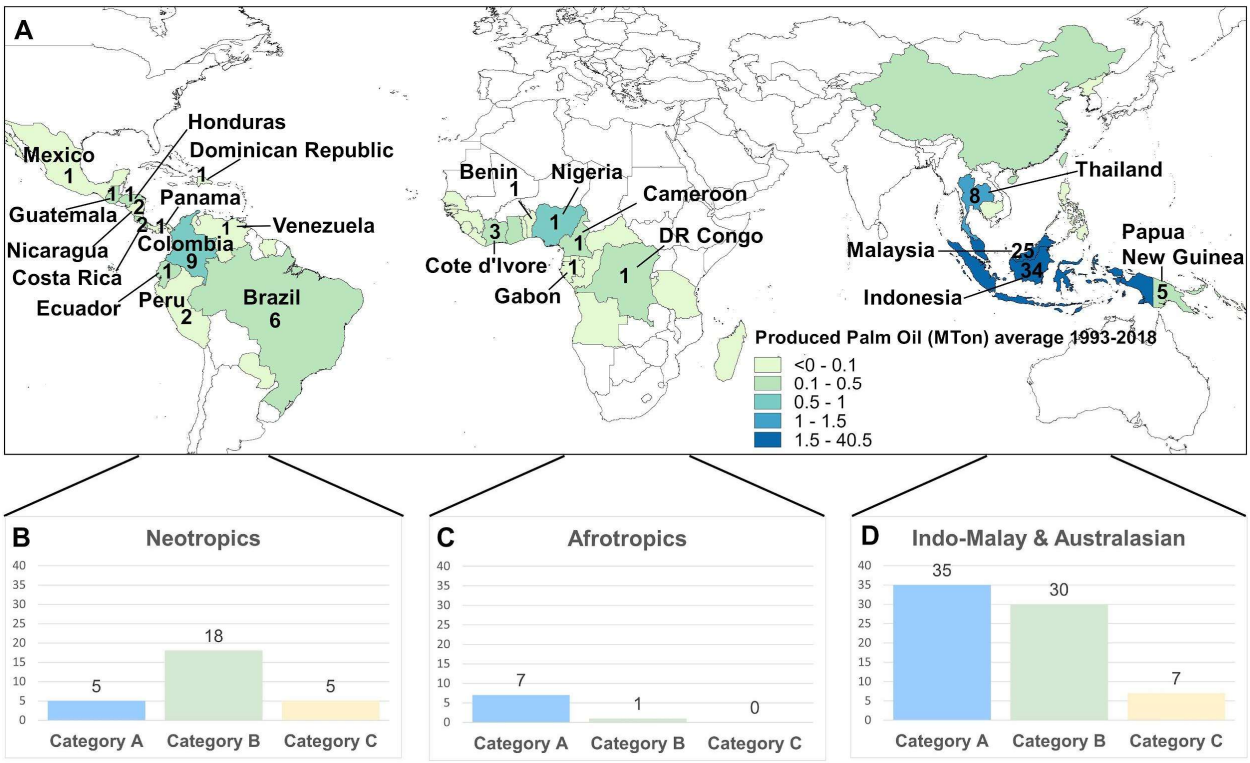

Figure 3.3. Relevant studies by country, type of paper, and biogeographical regions. A study can include more than one country. (A) Total number of relevant studies per country compared to oil palm production. (Source of oil palm production FAOSTAT, 2018). (B) Number of studies per category for the Neotropics region. (C) Number of studies per category for the Afrotropics region. (D) Number of studies per category for the Indo-Malay and Australasian regions. Studies grouping more than one country are distributed among the locations they cover.

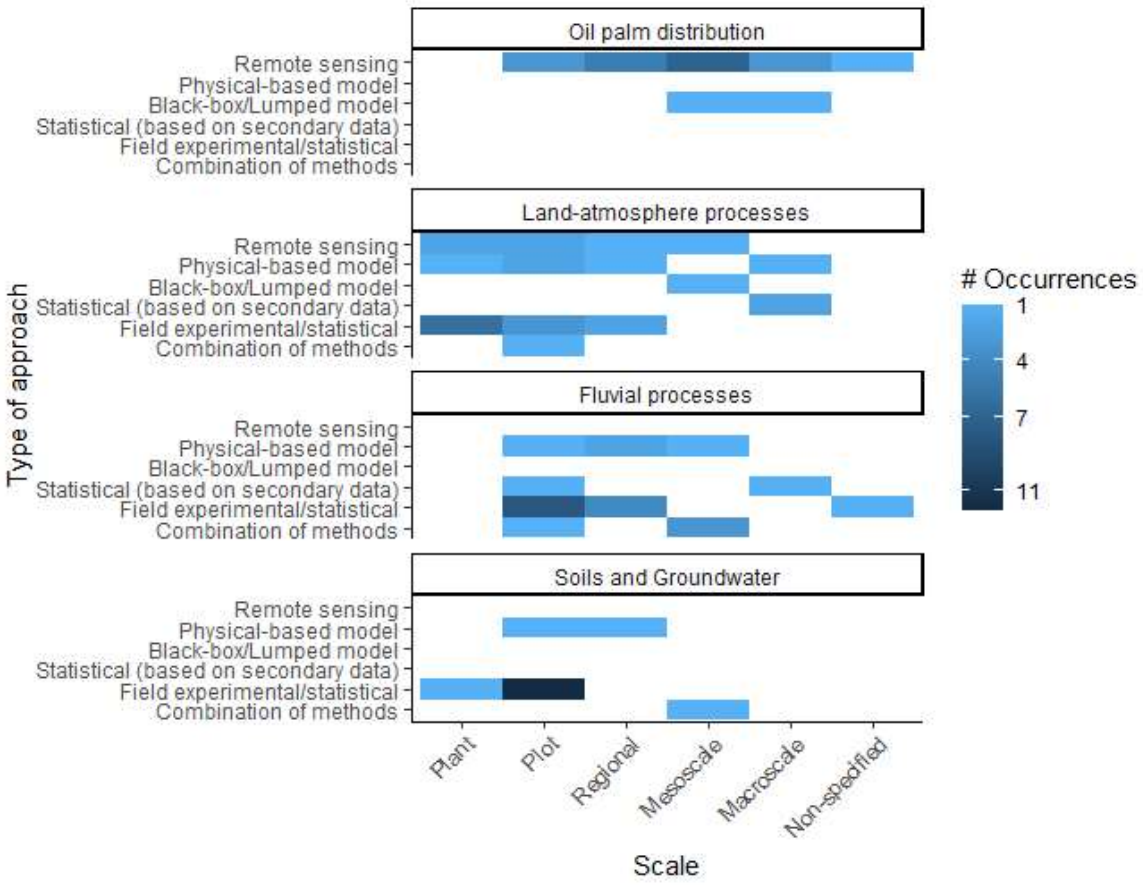

Figure 3.4. Summary of main approach and spatial scale in papers covering hydrologic (A) and biogeophysical processes (B) categories. Method approaches were summarized based on the main method used.

Global expansion of oil palm crop

According to the Food and Agriculture Organization, FAO, statistical database (FAOSTAT, 2020), the global extent of oil palm harvested area was over 189,000 km^2 in 2018. Approximately 69% of the harvested area is located in the Indo-Malay and Australasia biogeographical regions, with Indonesia and Malaysia accounting for 63% of the total area. The Afrotropical region covers approximately 24% of the area, with Nigeria accounting for 16% of the total harvested area. Finally, 7% of the area is located in the neotropical region, with Colombia accounting for approximately 1.5% of the harvested area.

According to the literature available for Southeast Asia, oil palm expansion has resulted in severe deforestation processes, with a large portion of crop area replacing primary and secondary peatswamp forest and rainforest (Miettinen et al., 2016; Tsujino et al., 2016; Austin et al., 2017). About half of oil palm development expanded into forested lands between 1972 and 2015 (Meijaard et al., 2018). Koh et al. (2011) estimate that for the early 2000s in Peninsular Malaysia, Borneo, and Sumatra, approximately 880,000 ha (6% of total plantations) were previously peatland forest areas. However, some studies found deforestation is also due to other factors Abood et al. (2015) estimate approximately 6.6 Mha (11%) of forest conversion to oil palm in Indonesia between 2000 and 2010. In this study, they show how forest loss is also associated with logging (12,5%) and fiber (12.8%) concessions. While deforestation is the dominant land cover pattern in Southeast Asia, oil palm plantations have also replaced agricultural land, with Austin et al. (2017) estimating a proportion of 37.9% replacement between 2010 and 2015 in Indonesia. It is not clear if current oil palm expansion follows a similar pattern in the Afrotropics as in Southeast Asia, but some studies indicate that similar trends might take place in the future (Amigun et al., 2011; Burton et al., 2017). In the eastern region of Ghana, a land use land cover change analysis showed that between 1986 and 2015, 11.9 of semi-deciduous forest was lost, followed by 10.7% in food crop losses, while oil palm and cacao gained 11.2% and 8.9%, respectively (Asubonteng et al., 2018). By doing a swap analysis in which partial gain and losses are estimated, Asubonteng et al (2018) found that oil palm has been replacing food-crop land (7.20%), closely followed by cacao (7.02%) and forest (5.98%). In Latin America, oil palm expansion has mostly replaced non-forested land. Furumo & Aide (2017) estimated that between 2001 and 2014, 79% of crop expansion occurred in already intervened lands, mainly in cattle pastures, with the remaining 21% occurring in areas with

woody vegetation. The available literature indicates that deforestation is more common in countries like Peru and Brazil, while in Colombia, the main land cover change is from pastures and cropland (Gutierrez-Velez et al., 2011; Furumo and Aide, 2017; Bicalho et al.,2016; Romero-Ruiz et al., 2012). Most of the studies above focused on large-scale industrial oil palm, but there are some local examples of oil palm distribution and patterns of change among smallholders and small-scale plantations. In Indonesia, Erniwati et al. (2017) found that 53% of the smallholder plantations planted between 1990 and 2002 come from degraded land and not from rainforests. Another example shows the differences between land suitability and actual land occupation by oil palm smallholders in Brazil, where oil palm has occupied less area than expected (Benami et al., 2018). Finally, in Mexico, it was found that smallholders displaced natural vegetation to plant oil palm following a different pattern than industrial plantations, mostly planting in pastures and previous cropland (Hernandez-Rojas et al., 2018).

The continued demand for palm oil and the interest of local governments in establishing oil palm plantations for economic development have led to research into future scenarios of oil palm expansion and of identification of suitable areas for crop establishment. In general, these studies evaluate biophysical conditions that allow for oil palm establishment by overlapping suitable areas with boundaries of protected or restricted zones, areas of forest cover, or another environmental relevant zoning. After overlapping, they calculate the final available areas that guarantee zero-deforestation or minimal negative impacts (Smit et al., 2013; Austin et al., 2017; Castiblanco et al., 2013; Rhebergen et al., 2016). The effects of climate change on the distribution of suitable land for oil palm establishment have also been evaluated in the literature. Paterson et al. (2016) used climate projections to 2050 and 2100 to determine how unsuitable and highly suitable land for oil palm cultivation might change worldwide in the future. One of

their main findings is that current large producers of oil palm (Malaysia, Indonesia, Nigeria, and Colombia) might have a large reduction in suitable land with climate change projections. At the local level, in the state of Maranhão, part of the Brazilian Amazon, the oil palm potential expansion was estimated based on the hydric conditions determined in terms of water deficit (Martorano et al., 2017). In this study, the authors estimated a water deficit of 125 mmy^{-1} which indicates the low suitability of oil palm establishment under no irrigation conditions. The studies in land suitability or land use land cover change typically considered *Elaeis guineensis* or do not specify the oil palm species. We did not find studies mapping or estimating the distribution of different oil palm species across the tropics. However, Barcelos et al. (2015) evaluate the benefits and shortcomings of cultivating different species and hybrids of oil palm in relation to productivity and disease resistance and indicate that interspecific hybrids (e.g. OxG) are becoming more commonly cultivated.

Land-atmosphere processes

Land-atmosphere processes are driven by microclimatic conditions that vary across oil palm stages of growth (Figure 3.5) and from the previous land covers that transition to oil palm (Figure 3.6). Studies comparing or evaluating land cover transition impacts on land-atmosphere processes were found in forests and croplands. The changes in surface temperature, albedo, latent heat, and sensible heat fluxes have been mainly studied in Asia (Roll et al., 2015; Meijide et al., 2017; Manoli et al., 2018; Sabajo et al., 2017). In the early stages of crop establishment after replacing rainforest, open canopies cause the surface temperature in oil palm crops to increase by up to 4 °C (Sabajo et al., 2017). As oil palm grows, temperature decreases as a response to canopy closure. This decreased temperature has been reported to be close to that seen in forests but slightly higher (Figure 3.6). Meijide et al. (2017) report differences of about 1 °C between 1-

and 12-year old plantations using Eddy covariance techniques. By modeling the ecohydrology of oil palm at plot scale using the Tethys and Chloris model, Manoli et al. (2018) found that temperature in young oil palms ranges between 23-26 °C, while temperature decreases to 22-23 °C when oil palm is mature (i.e., dominates the canopy cover). In another study, temperatures in oil palm plantations with a closed canopy range between 22 and 30 °C (Meijide et al., 2018). Changes in temperature also relate to changes in relative humidity, which is lower in closed-canopy oil palm plantations (91.3 ± 0.8 %) than in forests (95.6 ± 1.0%) (Meijide et al., 2018). These studies conclude that oil palm creates drier and warmer microclimatic conditions when compared to rainforests. Changes in land surface temperature and its relation to foliage cover have been identified at the regional scale (Ramdani et al., 2014) and macroscale (Sabajo et al., 2017) using remote sensing images. In these studies, land surface temperature increases between 0.2 and 1.05 °C after the foliage is lost as a result of oil palm establishment, showing forest cover has a lower temperature (Figure 3.4). In terms of land transition, most of the studies developed in Asia evaluate the response in microclimatic conditions of replacing rain forests with oil palm plantations (Sabajo et al., 2017; Ramdani et al., 2014; Meijide et al., 2018; Manoli et al., 2018), with few examples that compare annual cropland (Radersma et al., 1996) and permanent croplands (Merten et al., 2016; Meijide et al., 2018; Radersma et al., 1996).

Air temperature highly correlate to vapor pressure deficit (VPD). One-year old oil palm in Indonesia experienced a maximum VPD of around 16 hPa while 12-year old oil palm VPD was around 14 hPa, according to Meijide et al. (2017). Roll et al. (2015) found VPD in oil palms between 2 and 9 years old to be around 15.3 ± 0.95 hPa, and a high VPD variability in palms older than 10-years old (15.4 ± 3.35 hPa). In a 12-day experiment during a wet season for a 5-year old *E. guineensis* plantation in Colombia, the average VPD was 26 ± 8.3 hPa (Bayona-

Rodriguez & Romero, 2016). These results were similar to those found in a 12-years old oil palm plantation in Indonesia during the wet season by Niu et al., (2015). In all plot and plant studies the measurement period is from days to less than a year. Although these short periods are explained by the complexities of running long-term field campaigns in the plantations (e.g., difficult access to continuous monitoring, sensor failure, high operational costs), it does not allow the evaluation of the conditions at continuous growth or at different seasonal variations. At the plot scale within the crops, few studies have estimated albedo. Despite the observed changes in temperature, albedo did not show significant changes between 1- and 12-year old oil palms (0.16±0.02 and 0.14±0.01 respectively) (Meijide et al., 2017). Similarly, albedo showed a weak influence on the land surface temperature and very small differences between forest and oil palm plantations (Sabajo et al 2017). Studies suggest canopy closure is one important condition influencing variation in microclimatic conditions given the variation in surface roughness and temperature distribution across the vertical profile (Meijide et al., 2018; Sabajo et al., 2017; Ramdani et al., 2014).

Differences in the energy balance have been reported at different stages of oil palm growth. Sensible heat appears to be higher when oil palm is young, while latent heat significantly increases in mature *E. guineensis*. Derived from field observations in Indonesia, maximum sensible heat ranges from 140 Wm^{-2} in 1-year old oil palm to 50 Wm^{-2} in 12-year old oil palm (Meijide et al., 2018). Modeled values of sensible heat in oil palm range from 180 Wm^{-2} in young oil palm to 30 Wm^{-2} in adult oil palm (Manoli et al., 2018). Fowler et al. (2011), reported daily sensible heat values in mature plantations of around 100 Wm^{-2}. Latent heat, based on data derived from field observations, is dominant in the energy balance, with maximum values that fluctuate between 220 Wm^{-2} in a 1-year old palm to nearly 410 Wm^{-2} in a 12-year old palm

(Meijide et al., 2018), and model values that rank between 300 Wm^{-2} for young plantations to 400 Wm^{-2} in mature plantations (Manoli et al., 2018). Fowler et al. (2011) obtained latent heat values in mature oil palm plantations of nearly 400 Wm^{-2}.

Environmental conditions influence oil palm water use, gas exchanges, and subsequently evapotranspiration (ET). Stomatal openness, which regulates water and gas exchanges, is limited by VPD and temperature (Dufrene et al., 1992, Carr 2011, Roll et al., 2015, Rivera-Mendes et al., 2016). In a study at nursing stages of *E. guineensis* under laboratory-controlled conditions, Rivera-Mendes et al. (2016) found that plants at different soil moisture conditions did not alter stomatal conductance, photosynthesis, or transpiration, which suggests effects on stomatal conductance may be more influenced by atmospheric environmental conditions at that stage of maturity. In relation to plant age, Roll et al. (2015) found that stand-level water conductance increased with stand age. This plot study obtained experimental sap flow measurements and stand flow and found sap flux transpiration to be 8% of ET in a 2-years old oil palm and 53% in a 12-year-old oil palm. ET was 2.8 mm day^{-1} and 4.7 mm day^{-1}, respectively. Using modeling techniques at the plot scale, evapotranspiration ranges between 1000 to 1600 mmy^{-1} in young plantations and 1200 to 1800 mmy^{-1} in mature plantations (Manoli et al 2018). Using Penman-Montieth equation ET values resulted in 918+-46 mmy^{-1} (Meijide et al., 2018). Although these studies provide a valuable contribution to understanding water-vegetation interactions in the atmosphere, they correspond to the same region (Southeast Asia) and are done at a plot scale with no intra-seasonal variation. Compared to rainforests, mature oil palms do not show a clear increase or decrease in evapotranspiration. While Manoli et al. (2018) and Kurniawan et al. (2018) found an increase in evapotranspiration in mature plantations, Sabajo et al. (2017) found comparable evapotranspiration rates in oil palm when compared to forests at a regional scale.

Radersma et al. (1996) tested different water supply conditions in a closed canopy oil palm plantation, but age of the plantation was not specified. They found that under suboptimal or drier conditions of water supply during the dry and wet season, evapotranspiration is higher in oil palm plantations than in cocoa, rice, and maize, except for cocoa in the dry season. Existing literature rarely addresses variations in local precipitation due to oil palm plantations. However, efforts have been made to partition the precipitation into interception (Tarigan et al., 2018; Kurniawan et al., 2018; Merten et al., 2016) and throughfall (Dufrene et al., 1992; Banabas et al., 2008). Studies of precipitation identify short-term precipitation events, but we did not find studies addressing changes in regional precipitation due to oil palm plantations.

Fluvial processes

Fluvial processes associated with sediment yield, transport, runoff and streamflow generation, and nutrient leaching typically contrasted early stages of oil palm establishment coming from rain forest land to mature oil palm stages (Carlson et al., 2015; Adnan & Atkinson, 2011; Babel et al., 2015; Nainar et al., 2019). Compared to rainforest, sediment yield and transport increased in oil palm plantations regardless of the stage of growth of the crop, with differences between 19,000 ± 3,400 mg h^{-1} ha^{-1} in young plantations and 8,000 ± 2,000 mg h^{-1} ha^{-1} in mature plantations (Carlson et al., 2015). In another study, annual suspended sediment concentration discharge in an oil palm catchment was estimated to be 4 to 12 times greater than primary and multiple logged forest catchments (Nainar et al., 2017). High sediment transport was also reported after forest clearing and plantation establishment (Gharibreza et al., 2013). This increase in sediment concentration was attributed to bench-terraced slopes with little to no vegetation (Nainar et al., 2018), the construction of roads, and the absence of vegetated riparian zones (Carlson et al., 2014, 2015), which increase the chances of erosion. Although sediment

yield tended to decrease as canopy increased in oil palm plantations (i.e., oil palm growth), values reported in the literature were higher than in forests, which was associated with loss of understory vegetation, oil palm planting in steep terrain, which increases erosion (Satriawan et al., 2016), and the construction of infrastructure (e.g., roads, harvesting paths) to facilitate crop's management (Carlson et al., 2014). When oil palm was compared to land cover other than rainforests, studies have shown similar trends but different results depending on the land cover. In a scenario-based analysis with oil palm and other biofuels, sediment transport was higher in oil palm compared to cassava and soybeans (Babel et al., 2012). Similarly, sediment yield was greater in oil palm plantations younger than three years old and plantations older than 10 compared to mixed logged agroforest (Carlson et al., 2014). Guillaime et al. (2015) evaluated soil erosion at the plot scale in three land-use types, including jungle with rubber trees, rubber plantation, and oil palm plantation. They found that the oil palm and rubber plantations presented higher erosion (with a maximum of 35 ± 8, and 33 ± 10 cm respectively) than jungle (14± 14 cm). The fact that the jungle with rubber land use did not require land preparation, makes this land use less susceptible to an alteration in the soil conditions. We have not found studies that contrast sediment concentration in streams draining pasturelands with oil palm plantations (Figure 3.5).

Runoff, baseflow, and streamflow generation responses in oil palm plantations vary as a function of previous land cover and topographic conditions. Tarigan et al., (2018) compared watersheds to identify how the baseflow index and the runoff coefficient vary under different dominant land covers and to what extent changes in the land cover can affect these variables. They suggest a percentage of area threshold (minimum 30% forest and maximum 40% oil palm) after which catchments can lose streamflow regulation capacity. This is one of the few studies

that included shrubland in the analysis and found no significant differences between runoff coefficients of shrubland and oil palm plantations. Nainar et al. (2018) analyzed three types of land cover: primary forest, logged forest, and mature oil palm. They found total discharge and baseflow were lower in oil palm plantations (baseflow was 34% of total discharge). However, oil palm showed the highest runoff response (runoff coefficient 32.6%), twice the mean of grassland (runoff coefficient 15.3%), which was attributed to the compacted layer of soils resulted from oil palm and former grazing management (Algeet-Abarquero et al., 2015). Runoff increased in oil palm plantations when compared to the forest in loam and clay acrisols (Kurniawan et al., 2018). By simulating oil palm expansion and continuous drainage of a peatland region in Indonesia, a hydrologic and economic analysis showed a flood-risk increase after 100 years, in which near 46% of the peat area will be subject to constant inundation (Sumarga et al., 2016). In addition, higher runoff coefficients were found in topsoil of oil palm plantations (60%) compared to grassland in an overgrazed area (40%), forest (12%), and forest plantation (33%) in Costa Rica (Algeet-Abarquero et al., 2015).

Some studies have analyzed different mitigation strategies for runoff generation (e.g., frond piles, silt pits) and water retention during the dry season, as well as the influence of riparian zones in controlling stream properties. The runoff coefficient decreased from 63% to 50% when a combination of frond piles and silt pits were used as a mitigation strategy in oil palm plantations (Tarigan et al., 2016). Different understory vegetation can be planted to prevent changes in infiltration and runoff and losses of fertile soils that are rich in organic matter. In a 1 to 2-year old plantation, different vegetation communities including oil palm were tested, and the effect on infiltration and erosion was analyzed (Satriawan et al., 2016). They found that understory vegetation and tree cover decreased runoff generation, with a positive effect in

decreasing soil erosion and nutrient loss. This is important given that Indonesian oil palm is mostly planted on sloped areas (Satriawan et al., 2016). Preserving or planting riparian zones contribute to mitigating the negative impacts in oil palm plantations by decreasing stream temperature (Chelliah and Yule, 2018a; Luke et al., 2017) and bank erosion (Horton et al 2018). Riparian zones also contribute to maintaining the quality of the streams, decreasing nutrient leaching, and contributing to the microbial activity that is enhanced by litter decomposition (Chelliah and Yule, 2018b). Most of the studies that identify the effect of riparian zones are local to the area surrounding the plantations. An attempt to map and characterize riparian vegetation and its changes in Papua New Guinea showed how oil palm encroachment into the riparian zones has degraded and displaced most of the natural riparian areas, reducing dense riparian zones mostly to areas upstream of oil palm (Sheaves et al 2018).

Soils and Groundwater

Changes in soil properties during the establishment and development of oil palm plantations depend on the previous land cover, the soil type, and the management practices. Soil properties have been studied in peatland soils retained from previous forest cover (Nurulita et al 2015; Tonks et al 2017), cropland (Couwenberg & Hoojier, 2013), and different types of mineral soils from well-drained (Bruun et al 2013) to moderately drained (Goodrick et al 2015, Nelson et al 2014). In particular, mechanical soil compaction due to the introduction of machinery for harvesting and establishment purposes increased bulk density, especially in the traffic zone (i.e., the zone in which oil palm bunches are collected) (Matysek et al., 2018; Da Sato et al., 2017). In contrast, an increase in bulk density was detected when oil palm replaced a swidden system (Bruun et al., 2013) in a 3-year old plantation, and when compared samples taken under the swidden system with a 15-year old plantation. Similar results were presented by Marwanto et al

(2014), who analyzed peatland soils. In the land conversion of grassland to oil palm in Papua New Guinea, significant changes were found in soil pH and exchangeable Magnesium, but no statistically significant variations were detected in bulk density, soil carbon, or nitrogen content, although an increase in those aspects was detected (Nelson et al 2014).

Another measure characterized in oil palm plantation soils is soil organic carbon (SOC). Frazao et al (2014), working in Brazil, measured SOC in mineral Oxisol soils (using the USDA classification) under rainforests, mixed forests, and oil palm. They found that mixed forest has the lowest SOC among the land covers. However, within two different oil palm ages (23 and 34 years old), they found the younger plantation has lower SOC across all the depths and the older plantation has higher values across all the depths. Couwenberg & Hoojier (2013) compare carbon losses and subsidence in Acacia and oil palm plantations. Annual carbon losses are similar in Acacia plantations and oil palm plantations of 5 and 19 years old when comparing the rate of carbon loss to the subsidence rate. SOC losses are also detected in repetitive plantation cycles after replanting (Matysek et al., 2018) (Figure 3.5). However, the combined analysis of SOC and bulk density indicated that while SOC decreases in oil palm plantations when compared to swidden systems, an increase in bulk density does not allow conclusions about SOC losses (Bruun et al., 2013).

Infiltration capacity and infiltration rate have been measured for different land uses and land covers and oil palm mitigation techniques to prevent erosion and overland flow (Tarigan et al 2016; Satriawan et al 2016). In Indonesia, field measurements using double-ring infiltrometers found low infiltration rates in oil palm plantations with no management treatment (around 10 cmh^{-1}) and rubber plantations (around 20 cmh^{-1}), while high infiltration rates were obtained in secondary forest (90 cmh-1) (Tarigan et al 2016). This study also measured infiltration rates in

oil palm plantations with a front pile management technique finding that this treatment increased infiltration by around 40 cmh^{-1}. Satriawan et al (2016) measure infiltration volume and estimate infiltration capacity at plots between 5 months and 2 years old, and under different understory vegetation used as a soil conservation technique to prevent erosion. They found that soil conservation techniques did not affect infiltration capacity significantly, while the infiltration volume was significantly impacted (soil conservation treatment leaded to high infiltration volume). Related to water storage in the soils, a study in Malaysia reported higher soil water content in peat swamp forest compared to mature oil palm (defined as trees more than 25 m high and canopy coverage greater than 80%) (Tonks et al., 2017) (Figure 3.6).

Less studied in the literature are processes associated with groundwater dynamics in oil palm plantations. Typically, studies looked at the first 60 cm of soil depth. However, analysis of water table variation and subsidence has been done in peatland soils (Wösten et al., 2006). By using the hydrological model SIMGRO and 15 months of data from piezometers located in a watershed in Indonesia, Wösten et al. (2006) analyzed different scenarios of peatland drainage due to oil palm conversion. They found subsidence between 2 and 3 m can occur in the catchment. This subsidence reduced the water table and the catchment discharge. Another study found that constant water drainage in oil palm plantations leaded to water table subsidence (between 3.7 and 3.9 cmy^{-1}) (Couwenberg & Hoojier, 2013).

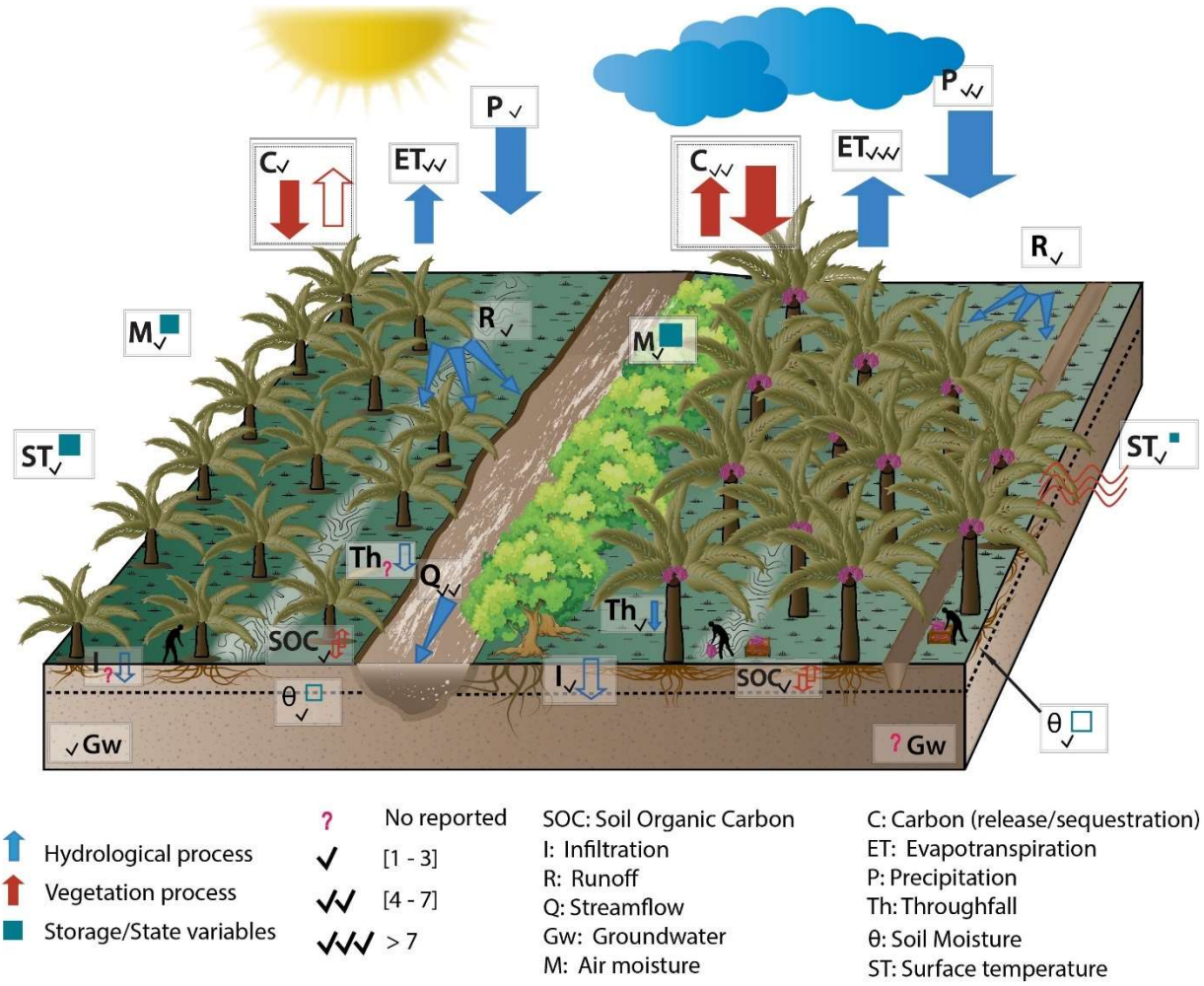

Figure 3.5. Degree of knowledge of vegetation and hydrological processes in an oil palm plantation. Left: oil palm plantation before production (young). Right: active oil palm production (mature). The width and height of the arrows and boxes indicate the difference in the fluxes between the young and mature plantations. Hollow boxes and arrows indicate no agreement was found among the studies. Checkmarks and question marks define the number of papers studying a particular process.

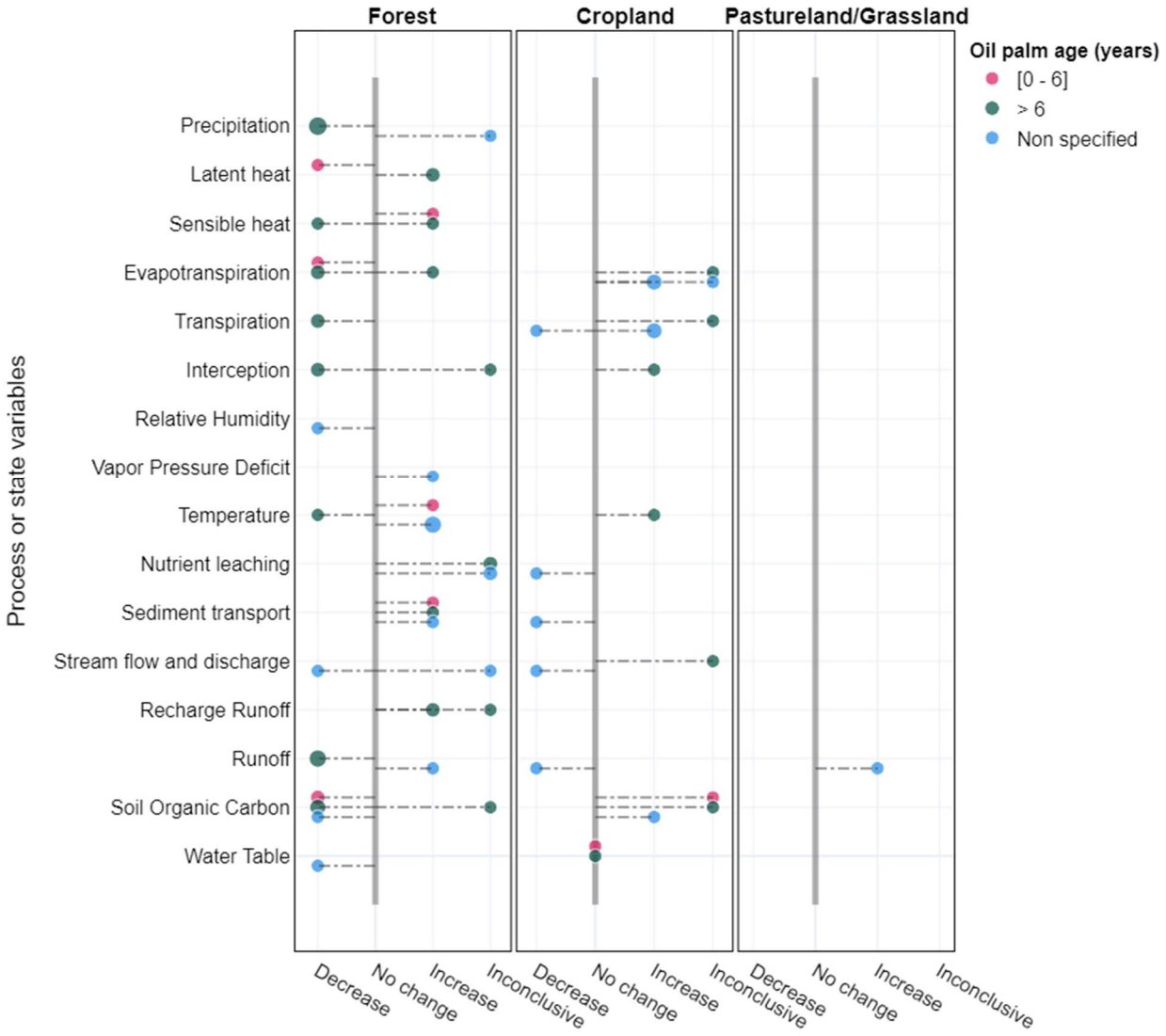

Figure 3.6. Change in hydrologic fluxes and state variables in land cover transition from rainforest (left), cropland (center), pastures or grassland (right) to oil palm. Circle sizes represent the number of papers. Given different reporting units, time and spatial scales, and environmental conditions, papers were summarized individually.

Discussion

Our review provides a description and summarizes relevant findings in oil palm research associated with hydrology-oil palm plantation interactions in the three main components of the hydrologic cycle (i.e., interphase land-atmosphere, which covers processes within the

troposphere; streams and landscape, and subsurface). While we recognize the progress in identifying oil palm establishment, development, and expansion, we found an imbalance between the number of scientific publications written in English and oil palm production in the Afrotropics, despite the relevant contributions of Dufrene et al. (1992), and the review in plant-water relations of Carr (2011). We also found a lack of replication, especially in the Neotropics at different environmental conditions and at all types of land transition. Research has been mainly focused on industrial plantations based in Asia and is gradually expanding to smallholder plantations. However, the spatial scale of the majority of ecohydrological studies is still done at plot or regional spatial scale, and short temporal scales (i.e., between days and less than a year). These findings might be explained by the complexities and high costs of long-term monitoring systems. Plant-water relations have been traditionally oriented to identify water requirements to improve oil palm yield, but we found this orientation has gradually shifted to identifying changes in the hydrological response in oil palm plantation. Still, research is needed to improve the spatiotemporal scope and geographical representation of those analyses, especially to characterize the difference in more humid vs. semi-arid tropical environments in which oil palm has been planted. Although we found examples that integrate community knowledge to improve the understanding of ecohydrological processes, more recognition of communities' perceptions as a mechanism to build hypotheses, acknowledging local knowledge, and including active participation in management practices is still needed. Due to logistical constraints, we could not address scientific literature written in all the languages of tropical regions, which may have hidden progress that has been made in some of the regions (e.g., Africa), though the inclusion of literature in Spanish and Portuguese makes visible other academic productions made in the Neotropics in different soil types and environmental conditions. We recognize that including all

the scientific literature produced in the field would require a multi-language search wider than the one we performed.

Current knowledge in ecohydrological process in oil palm research and oil palm distribution

Oil palm distribution and land use land cover transition is the main focus of 23% of the literature, especially since 2010. Most of the studies characterizing oil palm distribution and change are located in the Indo-Malay biogeographical region, where most palm oil production occurs, targeting forest conversion. Recent literature explores other land cover transitions, especially in marginal lands revealing agricultural and pastureland replacement (79% of the land in the Neotropics between 2001 and 2014 (Furumo & Aide, 2017) and 39% between 2010 and 2015 in Indonesia (Austin et al., 2017)). In terms of methods to identify oil palm distribution and land cover change, we found extensive use of remote sensing techniques and an increase in the resolution of the analysis, especially at the regional scale (1 km^2 to 100 km^2), potentially motivated by the recent availability of satellite imagery as well as robust algorithms that deal with computational constraints. Still, the majority of the remote sensing techniques have been applied at the mesoscale (Figure 3.4). Although this review does not focus on specific remote sensing analysis or classification techniques, we recognize that the use of these tools helps to advance the field.

Expansion of oil palm in pastureland allows examination of different hydrologic responses of oil palm establishments depending on the antecedent land cover type. One of the arguments behind the incentives of oil palm establishment in marginalized lands is reducing carbon emission (Garcia-Ulloa et al., 2012). However, in these lands, water availability may be an essential factor in oil palm expansion. Effects on ecohydrological fluxes from *E. Guineensis* crop establishment in previously forested areas (especially rainforest in peatland soils) are more

documented than in cropland, grassland, and pastures (Figure 3.6). These studies, mostly done at the plot scale, reveal the dominant role of evapotranspiration across the oil palm life cycle and stress the importance of vapor pressure deficit and air temperature in regulating stomata closure and therefore evapotranspiration rates. Closed canopy oil palm evapotranspiration can be higher than forest and other permanent cropland plantations. However, the trends in perennial croplands are not the same for all types of crops. Besides the type of crop, having similar trends may be conditioned by soil properties and intra-seasonal variations. Studies have shown that a rise in air temperature during the day causes stomatal closure and reduces evapotranspiration (Roll, et al., 2015). However, there are not enough studies to generalize a specific threshold in which stomatal closure happens and the daily or intra-annual variability of this process.

Based on the studies found, trends in sediment transport and production among different land uses show an increase after the transition from forest and a decrease after transitioning from pastures. However, the studies are done at short temporal scale, thus conclusions around these trends have to be treated carefully. Studies comparing sites of forest and oil palm show an agreement in the increment of sediment production. It has been observed that oil palm increases runoff during the rainy seasons in the early stages of forest conversion and decreases when oil palm canopy is dominant in the landscape. However, not enough empirical evidence is found in cropland or pasture lands (i.e., only one analysis that models oil palm conversion to cropland using scenarios (Babel et al., 2015)). This set of findings persists in the analysis of runoff. At the watershed scale, we typically found modeling involving other land use and land covers in addition to oil palm, therefore the observed trends in runoff generation include heterogeneous characteristics of the catchment. In the case of sediment transport data, the temporal scale of the data collected in the field ranges from episodic to a few months, which makes it challenging to

compare variations in time. None the less, the literature reviewed here does provide some consistent information about methods for reducing runoff and sediment flux. The use of front piles, silt splits, and the conservation of riparian zones are proven mechanisms to prevent the negative impacts of runoff and sediment generation. Riparian zones also contribute to regulating stream temperature, which in turn helps to preserve stream biological activities. Other mitigation strategies that have been useful to reduce runoff and mitigate erosion are the use of understory vegetation, conventionally used to contribute to nitrogen fixation.

In terms of the soil content and structure, oil palm plantations reduce soil organic carbon and elevated bulk density when compared to rainforest soils. When compared to other cropland and grassland, the effect of oil palm plantations in soils is less conclusive and depends on the land cover and soil composition. Studies center in the soils has been done in the first 60 cm of soils which is the region considered active in terms of root activity. Few studies discuss how variations in soil organic content impact soil water content. However, this impact has proven to be less significant for other soil types (Minasny & Mcbratney, 2018). Other than a few examples in peatland soils, water table variation has been less addressed in the literature revealing a need for future research.

Major challenges and future research needs

The information gap on oil palm distribution impedes having a clear global picture of land cover change processes driven by oil palm cultivation. Based on the reported statistics and in the number of relevant papers by country, it is clear that there is a lack of information on crop establishment and expansion processes in the Afrotropical countries (only three relevant papers) despite this region accounting for a considerable proportion of global harvested area (16%). Studies on suitable land for oil palm establishment and expansion allow exploration of possible

future changes in the crop's global distribution; however, they are either centered on *E. guineensis* or do not specify the oil palm species. Since hybrid oil palms have proven to be more tolerant of extreme environmental conditions and more resistant to diseases, it is necessary to address the distribution and potential implications on land suitability for different species and hybrids of oil palm. The lack of research in the interspecific oil palm is also evident in addressing ecohydrological questions. We did not find a dataset or information about the distribution of the different types of oil palms across the tropics despite the fact that a global dataset has been recently released at a smallholder scale. We identified the following research needs in oil palm ecohydrological processes:

1. More studies are necessary to measure the microclimatic conditions under different air moisture conditions and soil types at longer temporal scales. This would help to identify differences in evapotranspiration rates and to relate those differences with surrounding land covers. We recognize the logistical and economic complexities of installing Eddy covariance flux-towers; however, we also have found in the literature more affordable and easier to maintain examples that will potentially contribute to more widespread data collection (Villegas et al., 2017; Meijide et al., 2018). A more robust dataset would also provide the necessary inputs for regional to mesoscale oil palm ecohydrological modeling.
2. In terms of contrasting changes in fluvial process and runoff generation, more analyses in non-forested areas are still required. In particular, those analyses should include an assessment of the differences in water availability in humid vs semi-arid environments. These contrasts should also account for differences in patterns of transition. Given the high water requirements of adult oil palms and their presence in areas where other crops exist,

increased understanding on the pressure that irrigation places on community water supply is needed.

3. We found a gap in long-term oil palm eco-hydrological processes in all the components of the hydrologic cycle. Long-term analysis of oil palm, including oil palm rotation, would show how oil palm may alter hydrological processes over longer time scales.
4. Local knowledge and community perspectives in oil palm-producing regions remain largely absent from questions motivating the scientific literature. Given the human-dominated nature of this crop, these perspectives may help to advance the stage of knowledge in hydrological and ecological processes in oil palm research while also linking social and environmental dynamics.
5. Although there have been advances in developing global oil palm datasets, there is still work to be done to identify different transition patterns. Extended coverage to include regions with sparse oil palm plantations and those encompassed withing other land covers is needed.
6. In conducting this review, we have identified different terminology that is not always clarified or explained in the literature (e.g., forest types, agroforest, agriculture), which makes it challenging to compare scenarios and geographical locations, especially in conversion scenarios. Although progress has been made to characterize oil palm at different ages, management practices and species are not always described in the papers. Different temporal and spatial scales make it challenging to combine different datasets and contrast results from different geographical locations, suggesting that replication of approaches might be needed.

Conclusions

Our study synthesizes the progress on understanding ecohydrological processes in oil palm plantations at different temporal and spatial scales across the tropics. We focused our search on different scenarios of land transition, the three main components of the hydrologic cycle (i.e., interphase land-atmosphere; streams and landscape, and subsurface), and different oil palm species (i.e., the commercial African oil palm of *E. guineensis* Jacq and the OxG hybrid (*E. oleifera cortés* - *E. guineensis Jacq.*). We found important efforts have identified hydroclimatic processes in oil palm related to plant transpiration, shifts in air temperature, and water vapor pressure within different stages of oil palm growth and different land covers. Still, most of the progress has been a plot and regional scale, and at short-term temporal scales (i.e., days to months). Similar to fluvial processes, most of the work to understand runoff and sediment yield has been done at regional scales or smaller. Although we recognize the logistics and cost-related complexities of long-term monitoring in oil palm plantations, this lack of continuous data constitutes a gap to understand ecohydrological processes in oil palm research. While we found examples in which the community perceptions have been included in addressing scientific questions and attending community concerns, these are still limited but important given the human-dominated nature of oil palm. In addition, an important gap in oil palm patterns of transition and understanding of ecohydrological processes in the Afrotropics was detected despite the high oil palm production in this region. More studies are needed in oil palm hybrids given the potential for further expansion due to their commercial value and their resistance to extreme environmental conditions (i.e., plant disease, drought, and flooding). Important thresholds in water requirements in water-limited scenarios are still necessary to explore, especially in landscapes where oil palm is not the only cropland, crops require irrigation to gain

optimal yields, and there are plantations under pasture transitions. Further research in these types of landscapes will help to identify the limits of oil palm expansion from a hydrological perspective.

CHAPTER 4: MICROCLIMATIC CONDITIONS AND DAILY ENERGY BALANCE PARTITION FOR INTERSPECIFIC HYBRID OIL PALM PLANTATIONS IN NORTHERN COLOMBIA

Introduction

The perennial nature of oil palm and its high yield production, when compared to other vegetable oils, make this crop suitable for expansion in tropical regions (Monzzon et al., 2020). Massive oil palm expansion has been happening over the last 40 years in Asian countries, which contain 69% of the total harvested area of oil palm globally (FAOSTAT, 2020). In Indonesia and Malaysia, the main oil palm producers, expansion has replaced primarily at peat swamp forest and rainforest (Miettinen et al., 2016; Tsujino et al., 2016; Austin et al., 2017) in addition to croplands and pastures in a lower proportion (Abood et al., 2015). The massive conversion of rainforest to oil palm, and the corresponding impacts to increasing carbon emissions and greenhouse gasses, have driven the attention to the need for applying sustainable practices of oil palm development. One such strategy is to promote oil palm expansion in already degraded land, which has a lower impact on carbon emissions (Garcia-Ulloa et al., 2012; Quezada et al., 2019). In Central and South America, 79% of oil palm development has replaced non-forested land and already disturbed land between 2001 and 2014 (Furumo and Aide, 2017). Progress has been made in understanding microclimate in *E. guineensis* oil palm plantations at different spatial and temporal scales (Roll et al., 2015; Meijide et al., 2017; Hardwick et al 2015), and plant-water relations in the context of irrigation (Carr, 2011; Culman et al., 2019; Dufrêne & Saugier, 1993; Radersma & de Ridder, 1996). However, the characteristics of oil palm crops in regions where

oil palm has replaced pastures, other crops, or grasslands, and the implications of this expansion on water availability and microclimate, have been less studied.

The influence of microclimate on oil palm development has been studied to identify water irrigation requirements and optimal plant development (Dufrene et al., 1992; Carr, 2011; Corley and Tinker, 2003; Bayona-Rodriguez & Romero, 2016). Under a temperature threshold (case studies suggest temperatures between 32-36 ℃ (Carr, 2011)), oil palm stomata begin to close to avoid losses of water in the plant. However, temperature is highly correlated to vapor pressure deficit (VPD) (i.e., the difference between saturated vapor pressure and actual vapor pressure), which plays a dominant role in stomata openness (Corley and Thinker, 2003). As VPD increases, stomatal conductance also decreases (Carr, 2011; Culman et al., 2019; Dufrêne & Saugier, 1993). This relationship implies that stomatal openness, which regulates water and gas exchanges, is limited by VPD, and VPD in turn varies as a function of temperature. Rivera-Mendes et al. (2016) found that stomatal conductance, photosynthesis, and transpiration did not change significantly in oil palm less than 1-year old under different waterlogged conditions. In contrast, stomatal openness varies with plant age. Roll et al. (2015) evaluated plant stands in 2-year old and 12-year old oil palms. They found that stand-level water conductance increased with stand age. Although the mechanisms of this process are reported to be unknown, an increase in stomatal openness has implications for local moisture conditions, evapotranspiration, and subsequently in the energy balance partition, which together contribute to oil palm plantation modification of the local microclimate. Annual transpiration estimates for oil palm in 1- and 12-year old plantations were 64 ± 3 and 826 ± 34 mm, respectively (Meijide et al., 2017). Similar trends were obtained with evapotranspiration estimates using an ecohydrological model at the plot scale (Manoli et al., 2018). In this study, evapotranspiration ranged between 1000 to 1600

mmy-1 in young plantations and 1200 to 1800 mmy-1 in mature plantations (Manoli et al., 2018). Each of these studies was performed in *E. guineensis* at the plant and plot scale in plantations located in Africa (Dufrene et al., 1992; Carr, 2011), America (Bayona-Rodriguez & Romero, 2016; Rivera-Mendes et al., 2016), and Asia (Roll et al., 2015; Meijide et al., 2017; Manoli et al., 2018). At the regional scale, studies have also contrasted the influence of canopy cover in regulating temperature in oil palm and compared it to different land covers (Ramdani et al., 2014; Sabajo et al., 2017). As concluded from Chapter 2, despite the progress in understanding the interactions between oil palm and microclimate, there are not enough studies to generalize diurnal and daily variability and thresholds of air temperature and VPD after which stomatal closure happens.

Although the main oil palm species distributed in the tropics is the African Oil palm *Elaeis guineensis Jacq*, O×G interspecific hybrid, (i.e., a cross between African palm (*E. guineensis*) and the American palm (*E. oleifera* (Kunth) Cortés)), has gained popularity in the Neotropics due to its high tolerance for the bud-rot disease caused by Phytophthora palmivora and Fusarium wilt (Barcelos et al.,, 2015). In addition, the OxG hybrid is known for its slow vertical growth rate, which facilitates harvesting and prolongs the commercial cycle of the palm up to 40 years (Corley and Tinker, 2003). OxG is also known for high tolerance of environmental changes and extreme conditions (Barcelos et al 2015) and its high yield (Bayona-Rodriguez & Romero, 2019). Some of these characteristics are retained from the *E. oleifera Cortés*. *E. oleifera* naturally grows on riverbanks, which makes it more tolerant of high water tables and high moisture conditions than *E. guineensis*. It has a growth rate of 5 to 10 cm y^{-1}, reaching heights up to around 8 m, preserving the bunches at around 3 m height (Corley and Tinker, 2003). In contrast, African Oil Palm trees can grow up to 20 m, which causes replanting after 25-30 years when

palms become high enough that harvesting becomes unsustainable (Basiron, 2007). The differences among these palms suggest potential differences in microclimatic conditions, water, and energy partition in oil palm plantations. Physiological and agronomical properties of OxG hybrids were reported in Bayona-Rodriguez et al. (2016), who evaluated the OxG hydric potential under drought conditions, and Bayona-Rodriguez & Romero (2019), who explored the physiological responses (in leaf water potential, photosynthetic and transpiration rate, and photosynthetic water use efficiency), oil quality, and yield of six-year-old OxG hybrids under dry and rainy environmental conditions in Colombia. They found major drought tolerant in a group of oil palms that included OxG hybrid species. However, to our knowledge, the energy balance partition, and the relation of OxG hybrids to VPD and temperature have not been explicitly studied.

Here we describe the implementation and data collection of microclimatic data at OxG Hybrid oil palm plantations to characterize daily variations in temperature, vapor pressure, radiation, and biophysical properties of oil palm crops. Using the variables measured between August 28th, 2019, and September 30th, 2020, we derive different components of the energy balance using the Bowen ratio method (explained by Shuttleworth (2011) and Monteith & Unsworth, (2013)) and describe the characteristics of the microclimate across three stations located 30 km apart in the Colombian lowlands. We proposed three research questions: How do microclimatic conditions in oil palm plantations vary through the dry and wet season during a year in northwestern Colombia? How can those differences be explained? What is the diurnal energy balance partition in plantations growing the *E. Guineensis x E. Oleifera* variety of oil palm? Knowing the microclimatic conditions that dominate the plantations will help us to understand the limiting factors in oil palm development and how those factors may be associated

with water use. This has implications for determining the thresholds of oil palm expansion from the biophysical perspective. The Bowen ratio method allows the estimation of evapotranspiration that can be used in a water balance to determine differences in water availability.

Study area, data, and methods

Study area

The study area is located in Northwest Colombia, in the Uraba region close to the Pacific (West) and Atlantic (North) oceans and the border between Colombia and Panama (Figure 4.1). This region is characterized by average precipitation of 2,510 +- 938 mm y^{-1}, based on the multiannual average cumulative precipitation of 17 National Weather Stations recorded between 1977 and 2017 (National Institute of Hydrology, Meteorology and Environmental Studies of Colombia, IDEAM, (http://dhime.ideam.gov.co/atencionciudadano/)). Based on data between 1979 and 2017 at the national agrometeorological station at Uniban, the average annual temperature in the region is 26.6 ± 0.3 ℃, and the average relative humidity is 84.3 ± 1.5 % (National ID: 12015020) (Figure 4.1). The long-term annual cycle of precipitation defines the rainfall regime as mixed in the central lowlands (i.e., a highly-defined dry season between December and March, a less dry season between August and September, and a wet season from April to July and from October to November) and unimodal close to the Northeast and the west and North coasts (i.e., a dry season from December to March and a wet season from April to November) (Urrea et al., 2019). According to the most recent Colombian official Land Use and Land Cover Map (2010-2012) (Instituto Geografico Agustin Codazzi, available in: https://www.datos.gov.co), the land is mostly dedicated to pastures and agriculture, especially bananas. Oil palm has been gradually introduced, mainly replacing pastureland across the low

elevation portions of the region. However, the area covered by oil palm plantations is not part of the official Land Use Land Cover product.

In Uraba, the first oil palm plantations (*E. guineensis*) were cultivated in the 1960s (Martinez et al., 2014). However, a crop sanitary crisis constrained oil palm development due to the bud rot disease. In the last 12 years, the OxG hybrid has been planted, becoming the oil palm variety dominant in the region. Although oil palm plantations in this region are rainfed, they are designed to have a drainage system for excess runoff as it is specified for *E. guineensis*.

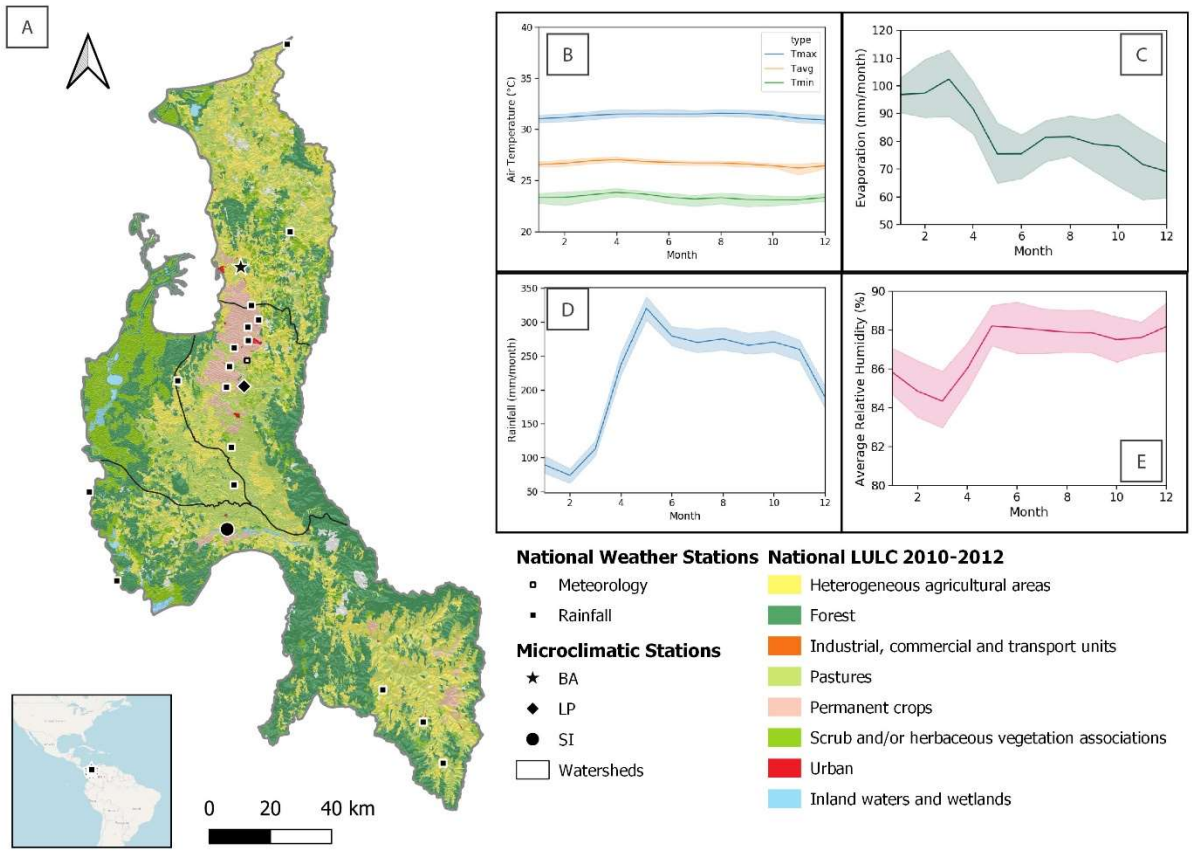

Figure 4.1. Study area and location of the stations. A. Study area region divided by watersheds, Sucio River located to the South, Leon River watershed in the center, Bajo Atrato to the West, and Mulatos River to the North. Multiannual-monthly averages of temperature (B), multiannual-cumulative evaporation (C), multiannual-cumulative rainfall (D), and multiannual-monthly averages relative humidity (E). Square symbols represent the location of the national weather stations from IDEAM. The location of the microclimatic stations designed and implemented in this work (BA, LP, and SI) are shown on the map.

Station design and implementation

Eddy covariance methods are typically used to measure microclimatic variables and derive the components of the energy balance (Monteith & Unsworth, 2013). However, their high cost and necessary maintenance make them challenging to implement and monitor. More affordable methods install fewer sensors in the vertical profile and have been implemented to identify microclimatic conditions in different land covers, including oil palm (Meijide et al., 2018), and implement a portable mobile station for rapid assessment of microclimatic conditions at different levels of forest disturbance (Villegas et al., 2017). We adapted the Villegas et al., (2017) design to implement the microclimatic stations in the Uraba region.

We performed three fieldwork campaigns to explore the region, design, install, and define the monitoring protocols necessary to maintain the microclimatic stations. The process of contacting and obtaining access to the farms started in 2018 in communication with the local environmental agency, Corporación para el Desarrollo Sostenible del Urabá, CORPOURABA. A first visit to the region took place between February 12th and 14th, 2019, to get familiar with the study area. Before the visit, we established communication with the leading oil palm company at Uraba, called Bioplanta Palmera Para el Desarrollo, Universidad de Antioquia-Sede Tulenapa, and the precision agriculture company Sioma Eco Zomac S.A.S, Sioma, that operates in the region. As a result of this visit, we defined the monitoring sites and obtained access to the farms to install the stations. At the Universidad de Antioquia, we work with Prof. Javier Lopez Sanchez, Ing. Andres Garcia, and students Juan Cardona and Jhan Cuartas. The students participated as assistants in the project while developing their undergraduate theses. Sioma supported the installation and maintenance of the stations by providing logistical and technical support. The second fieldwork campaign was dedicated to installing the stations at each site. The third fieldwork campaign was dedicated to follow-up on the stations and maintenance protocols and to

take soil samples. The details of the installation of the stations and the sampling campaigns are described in the following paragraphs.

Microclimatic stations were installed at three oil palm farms in oil palm canopy-dominated landscapes. The purpose of the stations was to measure microclimatic conditions and hourly energy balance. Each station was separated by around 30 km to account for different local environmental conditions. Station BA was located at 8°06'21.2'' N and 76°40'38.9'' W in the Sucio River watershed, in a plantation that was 6-years old at the time of installation. At station BA, oil palm heights were between 6.5 and 7 m. Station LP was located at 7°45'11.9'' N and 76°39'53.8'' W in the Leon River watershed, in an 11-year old plantation with palms 7 to 7.2 m in height at the installation time. Finally, station SI was located at 7°19'54.8'' N and 76°43'2.2'' W in the Mulatos River watershed, in a plantation that was 8 years old at the time of installation. At Station SI, palms were between 8 and 9 m in height. All heights were measured with a Nikon Forestry Pro II Laser from outside of each plot. In terms of previous land use land cover, BA and SI were at plantations that replaced pastureland, while LP was in a plantation that replaced bananas. At all the plantations the understory vegetation has naturally growth after oil palm was planted.

The station setup consisted of four sensors located above the surface at each location at 2, 9, 10.5, and 11 m in height. With this configuration, we aimed to record the conditions in the constant flow layer, just above the roughness layer, at the inertial layer, and at the canopy layer. The sensor over the canopy layer at the constant flow layer allows partitioning of the energy balance using the Bowen ratio method, while the sensors at 2 m allow identification of the times at which the lapse rate starts and stops, and vertical microclimatic profiling. The top, located 11 m above the ground (Figure 4.2), was an Arable Mark I multisensor that performs physical and

biological observations (https://www.arable.com/). The device measures 4-component radiation (i.e., 2-shortwave, one upwelling and one downwelling, and 2-longwave, one upwelling, and one downwelling radiation), reflected radiation in 7 spectral bands (bands distributed between 440 and 960 nm) that covers a surface circular region under the sensor with a diameter two times the maximum height (22 m) (the distribution of bands can be found in the supplemental material). At each spectral band, the sensor measures the upwelling and downwelling reflectance. This means that the sensor reports two reflectance values for each band (to see the band range see appendix C. Table C.1). The Arable Mark I device also measures air temperature, relative humidity, and barometric pressure. In the vertical profile, three multisensor Kestrel 5500 instruments (https://kestrelinstruments.com/) were located at 10.5, 9, and 2 m. These devices are equipped with temperature, pressure, relative humidity, wind direction, and wind speed sensors. The locations of the sensors were designed to measure both above and under the canopy. Eight sensors arranged in four pairs of soil temperature (200 TS sensors) and soil matric potential (Granular Matrix Watermark -200 SS- sensors) were installed under the ground at 0.1, 0.2, 0.35, and 0.6 m depth. (https://www.irrometer.com/). We choose these depths to account for the area where the root activity develops and where the primary ground heat flux is expected to occur. At each depth, the temperature sensor was placed 0.1 m apart from a soil water potential sensor (Figure 4.2). The 4-pair sensor arrangement at each station was connected to an Irrometer 900M Monitor Datalogger (https://www.irrometer.com/). Soil sensors were installed during the wet season when the soils were in saturated conditions. Due to sensor conditioning, the first month of readings was discarded. Prior to installation, soil matric potential sensors were submerged in clean water for 24 h, after that they were rubbed against the soil at their location's depth.

The stations were installed in mid-August 2019. To use the same period of analysis for the three stations, we selected the period of analysis August 24th, 2019, to September 30th, 2020. Data storage and temporal resolution varied according to each type of device. The temporal resolution of the Arable Mark is 1-hour, and data is transmitted using the cellular network and retrieved remotely from Amazon cloud servers. Kestrel 5500 and Irrometer 900M sensors store data locally. The Kestrel stored data at 1-hour resolution during the first six months. After that time, data frequency was updated to 20 min resolution. Irrometers were set to a 15 min resolution to allow more quality control and higher temporal resolution. After data filtering and quality control, we aggregate all data to a 1-hour resolution for further analysis (Table 4.1). Due to sensor malfunction, the Arable Mark I at station BA was replaced on August 21, 2020 with a new version of the device, Arable Mark II. This version of the device does not measure longwave downwelling radiation. However, we estimated longwave downwelling radiation using the method described by Dong (1992), following the recommendation of Arable Labs company. To verify the accuracy of these longwave downwelling estimates for the region, we verified them with longwave downwelling radiation data previously collected in the three stations using the variance, ANOVA, and non-parametric Wilcoxon analysis test. Maintenance for each station was performed once a month in close collaboration with students at the local university, Universidad de Antioquia - Sede Tulenapa, and the company Sioma.

At each station, soil samples were collected to identify soil texture profiles in the area where the soil sensors were installed. In addition, we determined soil texture by hand in the field. During the installation of the sensors, we measured percentage of Soil Water Content (SWC) and bulk density using Decagon GS3 probes and the portable handheld ProCheck reader at each depth. We took core soil samples with a core cylinder (37.7 cm^3) at each depth. The samples

were taken to the soil laboratory at Universidad de Antioquia - Sede Tulenapa to measure soil porosity. We weighed each sample, dried it in an oven at 105 ℃ for 24 hours and weighed the dry soil. After drying the soils, we weighed a portion of the soils, added 15 ml of water to the tube test (Vw), measured 15 ml of the soils (Vs) in another tube test, and finally add the water to the soils tube test until the pores were filled. We read volume displaced by the soils (Vd). Porosity was calculated as n = (Vw + Vs - Vd)/Vd.

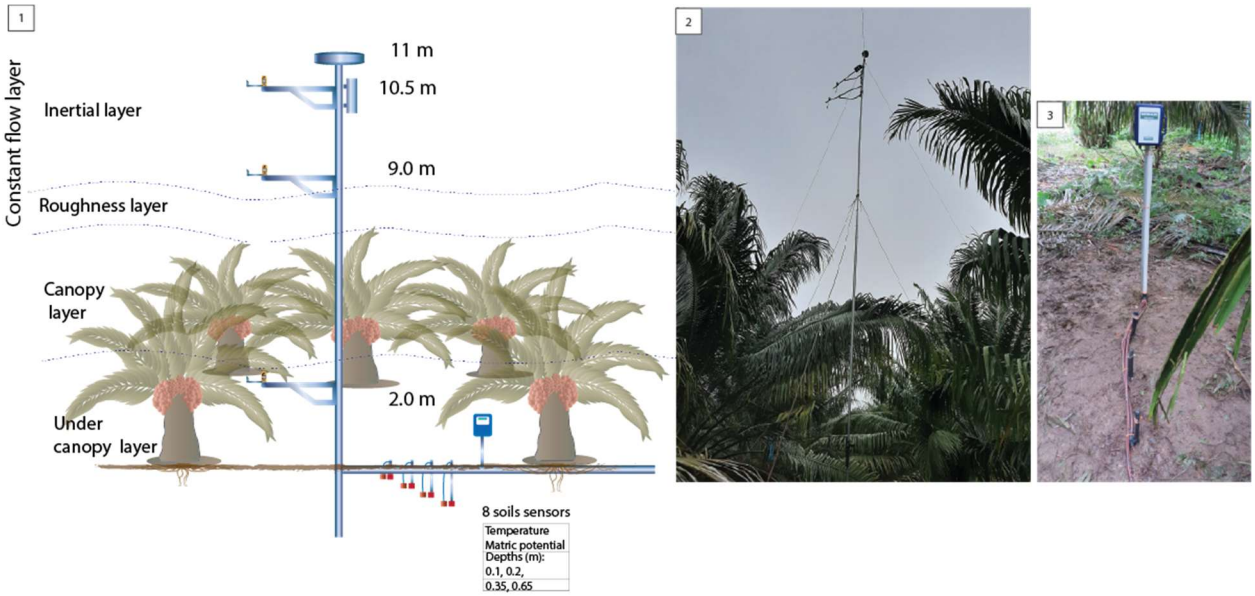

Figure 4.2. Station design and implementation. 1. Schematic of each station setup. The sensors in the vertical profile were installed oriented to the North. The distance between soil sensors and the main pole varied across stations based on conditions in the field. 2. Photo of upper part BA station. 3. Photo of soil station at SI. Sensors were arranged in a line and tagged.

Methods of analysis

Data preprocessing and filtering

Data collected by the sensors during maintenance were filtered out of the dataset. Additionally, data filtering was performed during the preparation for data analysis. Flag codes were designed to identify data out of range (10), outlier values (11), sensor failure (12), and uncalibrated sensor (13). Data out of range means that it reported data out of the measurable

range of the device. For most variables, a value was considered an outlier if it was out of the 99.9% confidence interval at the time and season for each station. For the net radiation components, the confidence interval was 90%. This was decided after detecting unrealistic values of net radiation lower than 100 W/m^2 at noon. Data out of the measurable range was detected in soil matric potential and soil temperature data. Outliers were mainly identified in the sensors in the atmosphere. We detected that Kestrel's wind direction appeared uncalibrated on a few occasions. We therefore chose to not use wind speed in such cases, but rather used the uncalibrated code to flag wind speed and wind direction. In the case of surface reflectance from the 7-band spectrometer (7 upwelling bands and 7 downwelling downwelling), only daily data (measured continuously from 7:00 - 18:00) were considered for the analysis at 1-hour resolution since the bands are in the visible spectrum. Spectral reflectance was considered in the 0 to 1 range. The reflectance, ρ_{SR}, at each band i, was calculated as the ratio between the spectrometer band upwelling (sb_{up}) and the spectrometer band downwelling (sb_{up}):

$$\rho SR = sb_{up}/sb_{dw} \quad (1)$$

Table 4.1. Summary of data used for the analysis, collected at each station by Kestrel and Arable multi-sensors by the hour for each variable from August 24th, 2019, to September 30th, 2020. Numbers correspond to raw data except for surface reflectance, which was calculated based on the spectrometer upwelling and downwelling bands (Eq 1). The number of surface reflectance records likely varies across bands due to an additional filter of the spectrometer band provided by Arable Labs when the sensor tilts, prior to calculating surface reflectance. Spectral range for each band can be found at appendix C Table C.1)

Station	Height (m)	Wind speed & direction	Relative Humidity	Air Temperature	Pressure	Radiation (4-components)	Surface Reflectance						
							Band 1	Band 2	Band 3	Band 4	Band 5	Band 6	Band 7
BA	2	7,737	8,450	8,450	8,450	-	-	-	-	-	-	-	-
	9	7,383	7,443	7,443	7,443	-	-	-	-	-	-	-	-
	10.5	5,455	7,142	7,142	7,142	-	-	-	-	-	-	-	-
	11	-	5,574	5,574	5,582	5,582	3,628	5,577	5,579	3,265	5,572	5,553	5,572
LP	2	9,646	9,646	9,646	9,646	-	-	-	-	-	-	-	-
	9	9,032	9,033	9,033	9,033	-	-	-	-	-	-	-	-
	10.5	8,533	8,639	8,639	8,639	-	-	-	-	-	-	-	-
	11	-	5,896	5,896	5,896	5,896	3,342	5,891	5,891	3,169	5,889	5,673	3,310
SI	2	7,192	7,202	7,202	7,202	-	-	-	-	-	-	-	-
	9	7,874	7,874	7,874	7,874	-	-	-	-	-	-	-	-
	10.5	6,091	6,850	6,850	6,850	-	-	-	-	-	-	-	-
	11	-	8,016	8,016	8,016	8,016	4,192	7,607	8,014	4,148	7,202	6,788	7,533

Surface reflectance out of the 0 to 1 range were flagged and excluded from further analysis but counted as data collected and were included in the final dataset (Table 4.1). We experienced several sensor issues during the monitoring campaign. At the beginning of the monitoring on September 12, 2019, the Arable Mark I installed at LP exploded. This caused loss of data at that station until mid-November 2019. After three months of operation a sensor drift was observed in the relative humidity sensor of the Kestrel device. Similarly, despite using silica gel to avoid condensation inside the data logger box, they appeared wet during the wet season in 2020. Sensor drift was also observed in the deepest matric soil potential and soil temperature sensors during the wet season 2020. We did not attempt to apply a drift correction to the data, instead, we filtered this data out of the analysis. A database structure was designed to store all the data collected by the sensors (see appendix C. Figure C.1). In addition, we created a programming class module in python to calculate all the components of the energy balance available in a bitbucket repository (https://bitbucket.org/) and at the supplemental information.

Microclimatic and vegetation conditions

To analyze daily microclimatic conditions among sites, we used air temperature, relative humidity, and radiation collected at the top of the canopy during the wet and the dry seasons. Air temperature and relative humidity were used to estimate vapor pressure deficit, VPD, and radiation components were used to obtain net radiation (NR) and albedo. Albedo, α_i, was obtained using shortwave upwelling radiation, SW_{upi}, and shortwave downwelling radiation, SW_{dwi}, at each hour i:

$$\alpha_i = -1 \times (SW_{upi} / SW_{dwi}) \qquad (2)$$

We estimated VPD as the difference between water vapor pressure and saturated vapor pressure using Arable Mark I and II records. At each site, we also explored the vertical profiles

of air temperature, wind speed, and direction for the entire period. Given that the Kestrel relative humidity sensor failed within the first three months of operation, we built the VPD vertical profile at each station only for that period of data.

We calculated the saturated vapor pressure at each height (i.e., maximum pressure of the air when saturated) using the method described by Buck (1981), who offers an enhanced correction for temperatures ranging between -80 and 50 °C. Saturated vapor pressure, at a time i, is provided by es_i,

$$es_i = 6.1121 * e^{((18.678 - Tair_i / 234.5) * Tair_i / (257.14 + Tair_i))} \quad (3)$$

where es_i is expressed in hPa, and $Tair_i$ refers to air temperature in °C at the time i.

Then we calculated the actual water vapor pressure at the time i, ea, at each height as a function of relative humidity rh_i, as a fraction, and saturated vapor pressure es_i,

$$ea_i = rh_i \times es_i \quad (4)$$

Finally, VPD at each height and time i was estimated as:

$$VPD_i = ea_i - es_i \quad (5)$$

The Normalized Difference Vegetation Index, NDVI, (Huete et al., 2002) was calculated using the bands 4 (620-690 nm Red) and 6 (780-900 nm Near-Infrared, NIR) at each hour during the day using the expression:

$$NDVI_i = (NIR_i - Red_i) / (NIR_i + Red_i) \quad (6)$$

NDVI was used as an indicator of photosynthetic activity. Gamon et al. (1995) tested NDVI at various land covers and identified NDVI as a good indicator of photosynthetic activity during the Spring for evergreen perennial conditions. Given that the conditions of temperature in the study area are similar during the year, we decided to use NDVI as an indicator for photosynthetic activity. Given the high canopy cover at each station, we expected high NDVI during the day.

We used a unimodal rainfall regime to group the data into wet and dry periods and analyze differences among the sites, using December to March as the dry period and April to November as the wet period. To test the differences among the sites, we performed the non-parametric Wilcoxon test implemented in the Python SciPy package stats. We compared air temperature, net radiation, albedo, and VPD among the stations. To identify potential conditions of temperature inversion, vertical air temperature gradients between the air temperature at the top of the canopy and under the canopy at each hour were calculated at each station.

Energy balance

The energy balance partition was approached using the Bowen ratio/energy budget method. This partition accounts for the energy distribution and storage on the surface. The Bowen ratio is the relation between the sensible heat, H, and the latent heat, λE, fluxes. It relies on the fact that the available energy, A, at any point is the sum of H and λE. (Shuttleworth, 2011).

$$A = H + \lambda E = Rn - G \quad (7)$$

Where Rn is net radiation and G is ground energy flux. The Bowen ratio method also assumes neutral stability, i.e., turbulent exchanges of water and heat are similar to each other (Monteith & Unsworth, 2013). Neutral stability implies that the change in temperature with height is equivalent to the adiabatic lapse rate (Shuttleworth, 2011). Since thermal stability is directly related to virtual potential temperature, i.e., temperature without the effect in water vapor content changes (equation 13), the rate of sensible heat between two heights is proportional to the atmospheric heat content and the Bowen ratio, at each time i, can be expressed by equation (8):

$$\beta_i = H_i/\lambda E_i = \gamma\theta_v/\Delta ea_i \quad (8)$$

Where θ_v is the potential virtual temperature, γ, is the psychrometric constant (i.e., Specific heat of the air at constant pressure). Using equations (7) and (8), energy fluxes can be expressed as

$$\lambda E = A / (1 + \beta) \quad (9)$$

$$H = \beta \times \lambda E \quad (10)$$

The Bowen ratio becomes indeterminate when Rn-G tends to 0, making it difficult to apply at night or when net radiation is small. To apply the energy balance equation, we used data collected during the wet period 2019 (October and November) to avoid using soil matric potential values before soil sensors were conditioned in the field. Given the relative humidity sensor failure in the Kestrel devices, we did not apply the energy balance to dry and wet periods. Rather, we proposed an estimate for average day energy partition using the hourly data available. To calculate the Bowen ratio, we used relative humidity and temperature measurements for the top sensors over the canopy layer. To apply equation (8), we first calculated the proportion of water vapor in the moist air, known as specific humidity, by estimating the mixing ratio at each time i, i.e., the ratio of the mass of water vapor to the mass of dry air in the moist air sample. Since water vapor is considerably lighter than dry air, specific humidity is considered equivalent to mixing ratio (Shuttleworth, 2011):

$$q = ea_i(Rd/Rv)/[\rho - e_i[1-(Rd/Rv)]] \quad (11)$$

where Rd is the gas constant of dry air (287.1 J/(kg·K)), Rv is the gas constant for water vapor (461.5 J/(kg·K), ρ is the total pressure [KPa] (i.e., barometric pressure). Simplifying the expression, equation (11) can be written as:

$$q_i = r_i = 0.622 * ea_i/\rho_i \quad (12)$$

Using q, and the fact that virtual temperature can be expressed as $Tair_i \times (1 + 0.61 \times q)$, θ_{vi} at each time can be estimated as

$$\theta_{vi} = Tair_i \times (1 + 0.61 \times q_i) \times (100/\rho_i)^{(Ra/Cp)} \quad (13)$$

where Cp is the specific heat of humid air 1,013 [J kg^{-1} $°K^{-1}$].

Soil heat depends on the exposure of the soils to solar radiation and its radiative properties. To calculate G, we used the gradient method, in which G is a direct application of Fourier's law for heat conduction. The gradient method states the ground flux is a function of the thermal conductivity and the changes in temperature

$$G_i = \lambda_{si} * (\Delta Tsoil_i / \Delta z_i) \quad (14)$$

Where λ_s is the thermal conductivity, and (ΔTsoil /Δz) is the vertical temperature gradient between z depths. The gradient method is relatively easy to apply, and its implementation does not require expensive equipment. However, the complexity relies on estimating λ_s, which can be highly variable spatially and temporally. Thermal conductivity varies considerably as a function of moisture content and temperature. The effect of the water content is due to the larger difference between the air and water thermal conduction, and the differences that latent heat transport produces in different media. We followed the implementation of Peng et al (2017) to estimate λ_s:

$$\lambda_s = \lambda_{dry} + exp(Qf_{sh} - SWC^{Cfsh}) \quad (15)$$

where λ_{dry} is the thermal conductivity of the dry soils ($Wm^{-1}K^{-1}$), SWC is soil water content, Cf_{sh} and Qf_{sh} are shape factors associated with clay fraction, fc, and quartz fraction, fq, and bulk density, ρ_b, respectively:

$$\lambda_{dry} = -0.56n + 0.51 \quad (16)$$

$$Cf_{sh} = 0.67fc + 0.24 \quad (17)$$

$$Qf_{sh} = 1.97fq + 1{,}87\rho_b - 1.36fq\,\rho_b - 0.95 \quad (18)$$

This method uses the fractions of sand and clay, as well as porosity and bulk density. Due to restrictions on access to the soil laboratory due to COVID-19, soil samples could not be analyzed during 2020. However, during the sampling campaigns we analyzed soil texture manually. With that information, we used a general soil texture classification between clay and silt, which are the dominant texture features at each station, and iterated λs within 200 randomly generated values of each main texture group (i.e., sand and clay) (Table 4.2). Given that the Watermark sensor at 0.65 m presented more data errors than the sensors at 0.1, 0.2, and 0.35, we used only 0.1, 0.2 and 0.35 depths to calculate ground energy.

Table 4.2. Properties of soils in the installation campaign. Texture description was obtained on-site, quantitative measurements taken could not be analyzed for texture due to access restrictions to the laboratories in 2020.

Station	**Texture Description**	**Depth (m)**	**Bulk density (g/cm3)**	**Initial soil water content (%)**	**Porosity**
BA	Clay-Silt	0.1	0.489	48.7	0.30
		0.2	0.344	47.1	0.43
		0.35	0.304	39.9	0.30
		0.65	0.279	42.4	0.25
LP	Clay-Silt	0.1	0.268	49.7	0.25
		0.2	0.353	51.7	0.30
		0.35	0.317	53.2	0.43
		0.65	0.22	50.7	0.30
SI	Silt-Clay	0.1	0.217	53.0	0.30
		0.2	0.237	49.0	0.36
		0.35	0.138	54.0	0.30
		0.65	0.204	48.3	0.20

Use of additional information and comparison with eddy covariance data in the neotropics

To evaluate the general hydroclimatic conditions of the region we used the available data from IDEAM. This consisted of 18 stations, 17 with rainfall data from 1977 to 2017, and one meteorological station (Uniban) with air temperature, hours of sun, relative humidity, evaporation, and rainfall from 1979 to 2017 (figure 4.1). From Uniban station, we were able to obtain relative humidity data between 2019 and 2020. None of the stations is located in an oil palm plantation.

Results

Microclimatic and environmental conditions across stations and seasons

Average values of air temperature, VPD, NDVI, albedo, soil temperature (average temperature 26 ± 1 °C) and soil water content (average 40 - 50 %) did not show differences when compared among the stations (Table 4.3). Each station had an average temperature of 28 °C during the period of analysis, which is around 1 °C higher than the maximum multiannual average (26.6 ± 3 °C) for the region. Although not significantly different, average VPD was slightly higher during the dry season at SI (1.25 ± 0.46 kPa) than during the wet season (0.89 ± 0.48 kPa). This accounts for differences between 0.38 kPa in the lower bound and 0.34 kPa in the upper bound. Average relative humidity was also similar across the stations and seasons (0.78 ± 0.09), and generally lower than the average for the same period found at Uniban meteorological station (0.86 ± 0.10). None of the mean albedo values across the stations and seasons varied significantly (Table 4.3).

Soil samples showed that the characteristics of the soils across sites are similar in terms of porosity and texture (identified qualitatively in the field) (Table 4.2). Bulk density, however, was higher at BA across all depths compared to LP and SI. In all the stations bulk density was lower

in the deep layer of soil than in the top layer. At the moment of installing the stations all soils had soil water content (measured as volumetric water content) higher than 40%. At all stations, porosity values were lower (between 0.2 and 0.3) at 0.1 and 0.65 m and higher in the intermediate layers.

When looking at the variations of NDVI during the day we found similarities in NDVI at BA (0.81 ± 0.04 for the dry season and 0.86 ± 0.02 for the wet season) and LP (0.86 ± 0.01 for the dry season and 0.84 ± 0.02 for the wet season), but hourly values of NDVI were lower at SI (0.74 ± 0.13 for the dry season and 0.75 ± 0.07 for the wet season). At each plantation, NDVI peaked between 12:00 and 14:00 (Figure 4.4), which is consistent with the hours of maximum net radiation (Figure 4.5). Although NDVI was mostly the same across seasons, mean NDVI at BA was lower at each time interval during the dry season compared to the wet season. NDVI variation is higher at the beginning and the end of the day, similarly, with albedo.

We found differences in daily variation of air temperature and VPD across the stations and seasons. Surprisingly, during the diurnal hours of maximum temperature (at 15:00), air temperature at the top of the canopy in BA was lower (28.5 ± 0.7 °C) during the dry season than during the wet season (30.0 ± 1.8 °C). At LP and SI, maximum mean diurnal temperature did not differ among seasons (29.5 ± 1.1 and 29.39 ± 1.5 for LP and 29.6 ± 1.1 and 29.4 ± 1.5 for SI). In contrast, we found differences in VPD at the hours of maximum VPD across seasons and between the stations in the North and the South. Maximum VPD typically occurred between 14:00 and 15:00 at each station and season. Maximum hourly VPD at BA (1.27 ± 0.41 kPa) was higher during the wet than during the dry season (0.95 ± 0.21 kPa). The opposite was true for SI, where VPD was higher in the dry season (1.6 ± 0.38 kPa) than in the wet season (1.25 ± 0.44 kPa). In addition, VPD had more variability within each hour during the season at SI than at BA

(Figure 4.3). However, during the dry season at BA mean VPD values were similar during the day. Hourly average values for each station, variable and season are shown in the supplemental material Table C.8 to C.14.

Table 4.3. Average meteorological and vegetation parameters at each station and season. Values were average during the daily hours (7:00 to 18:00)

Variable	Station	BA		LP		SI	
	Season	Dry	Wet	Dry	Wet	Dry	Wet
Air Temperature (C)	n	1,092	1,397	753	1,908	1,308	2,291
	Mean	28.04	28.48	28.55	28.40	28.65	28.10
	STD	1.06	2.03	1.52	1.91	1.79	2.08
Vapor Pressure Deficit (kPa)	n	1,089	1,395	751	1,907	1,305	2,286
	Mean	0.85	0.91	0.90	0.88	1.25	0.89
	STD	0.26	0.43	0.35	0.41	0.46	0.48
Relative humidity	n	1,095	1,401	754	1,911	1,310	2,292
	Mean	0.78	0.78	0.78	0.78	0.69	0.78
	STD	0.06	0.08	0.07	0.08	0.09	0.10
NDVI	n	1,114	1,428	773	1,940	1,338	2,329
	Mean	0.79	0.83	0.82	0.82	0.75	0.74
	STD	0.08	0.09	0.08	0.11	0.07	0.13
Albedo	n	1,081	1,395	751	1,891	1,304	2,265
	Mean	0.08	0.09	0.06	0.12	0.09	0.09
	STD	0.06	0.07	0.03	0.10	0.05	0.08

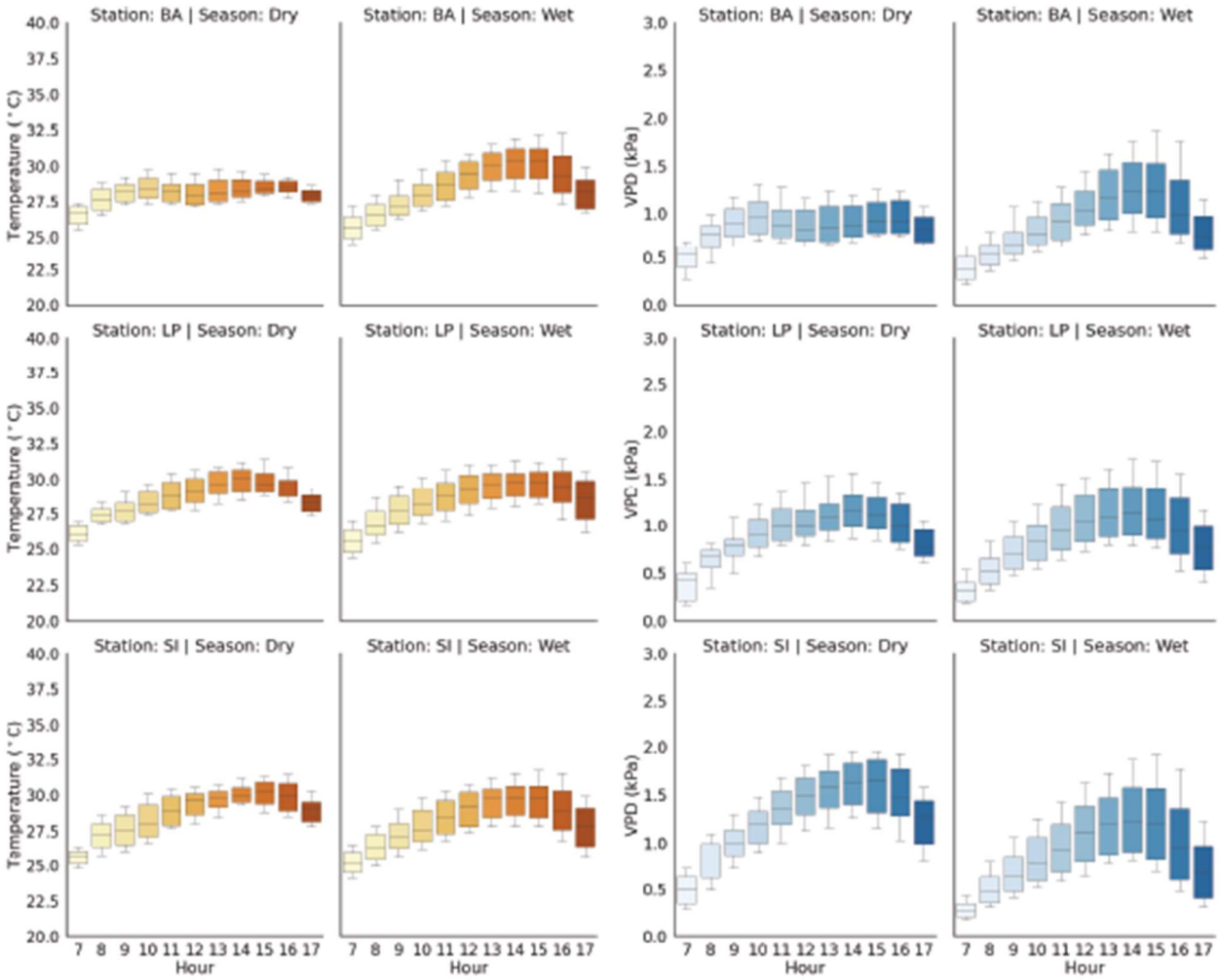

Figure 4.3. Diurnal variation of air temperature (°C) (left) and vapor pressure deficit, VPD (kPa) (right). Colors differentiate each hour. Error bars corresponding to the 10 to 90% confidence interval.

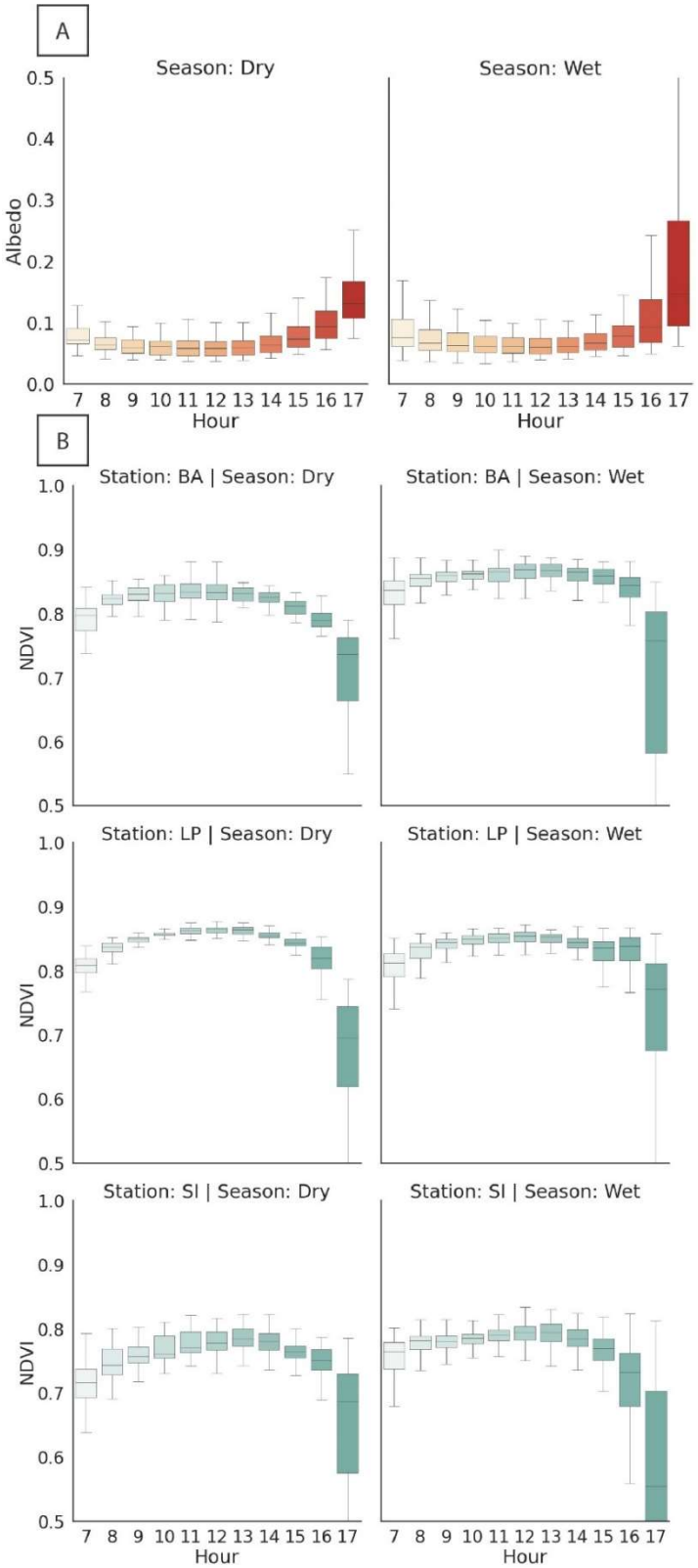

Figure 4.4. Diurnal variation of albedo and NDVI among the three stations during the dry and wet season. A) Average albedo for the three stations at the dry season (left) and the wet season (right). B) NDVI at the dry season (left) and the wet season (right) at stations BA (top), LP (middle), and SI (bottom).

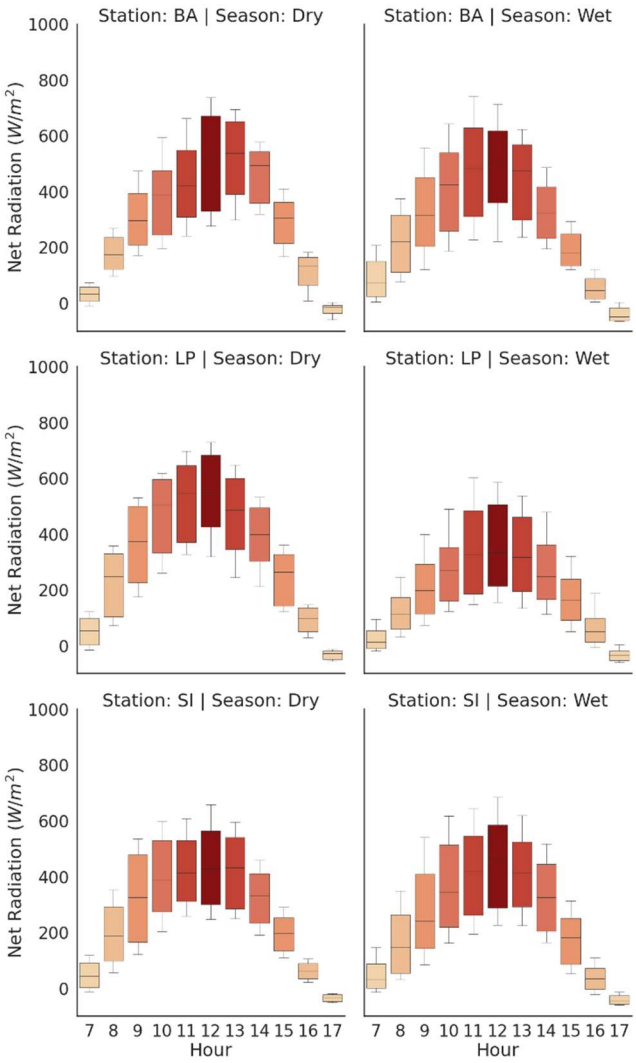

Figure 4.5. Diurnal variation in net radiation (Wm^{-2}) for each station (rows) and season (columns).

Vertical profiles at each station

Wind speed measurements were higher during the dry than the wet season at all the stations (Figure 4.6). At station BA, wind speed at the top of the canopy was higher than in the other stations, reaching values up to 7.9 mps during the wet season and up to 5.5 mps during the dry season. In terms of wind direction, we found a consistent direction of the wind coming from the Andes cordillera at each station during the dry season. However, during the wet season, wind direction was from the Pacific in the west.

At the three stations we found thermal inversion (i.e., temperature in the upper level is higher than the lower level) at different times at each station depending on the season. Thus, long periods of neutral stability conditions occurred during the dry season from 10:00 to 18:00 at BA, 12:00 to 18:00 at LP, and 10:00 to 17:00 at SI. During the wet season neutral stability occurred from 9:00 to 17:00 at BA, 12:00 to 16:00 at LP, and 13:00 to 17:00 at SI.

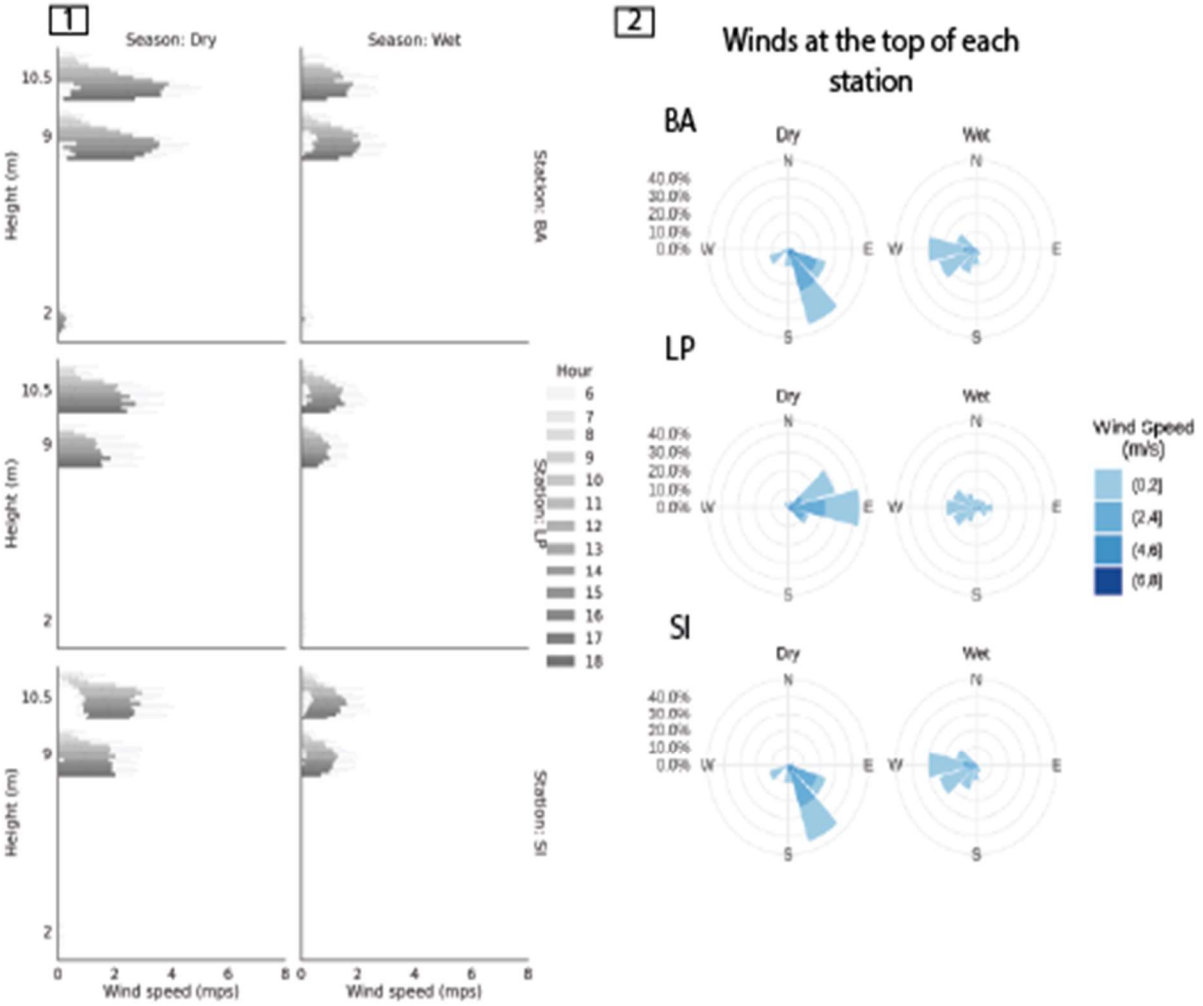

Figure 4.6. Wind speed profile and wind direction. 1) Wind speed profile at each station and season. 2) Wind direction at the top sensor.

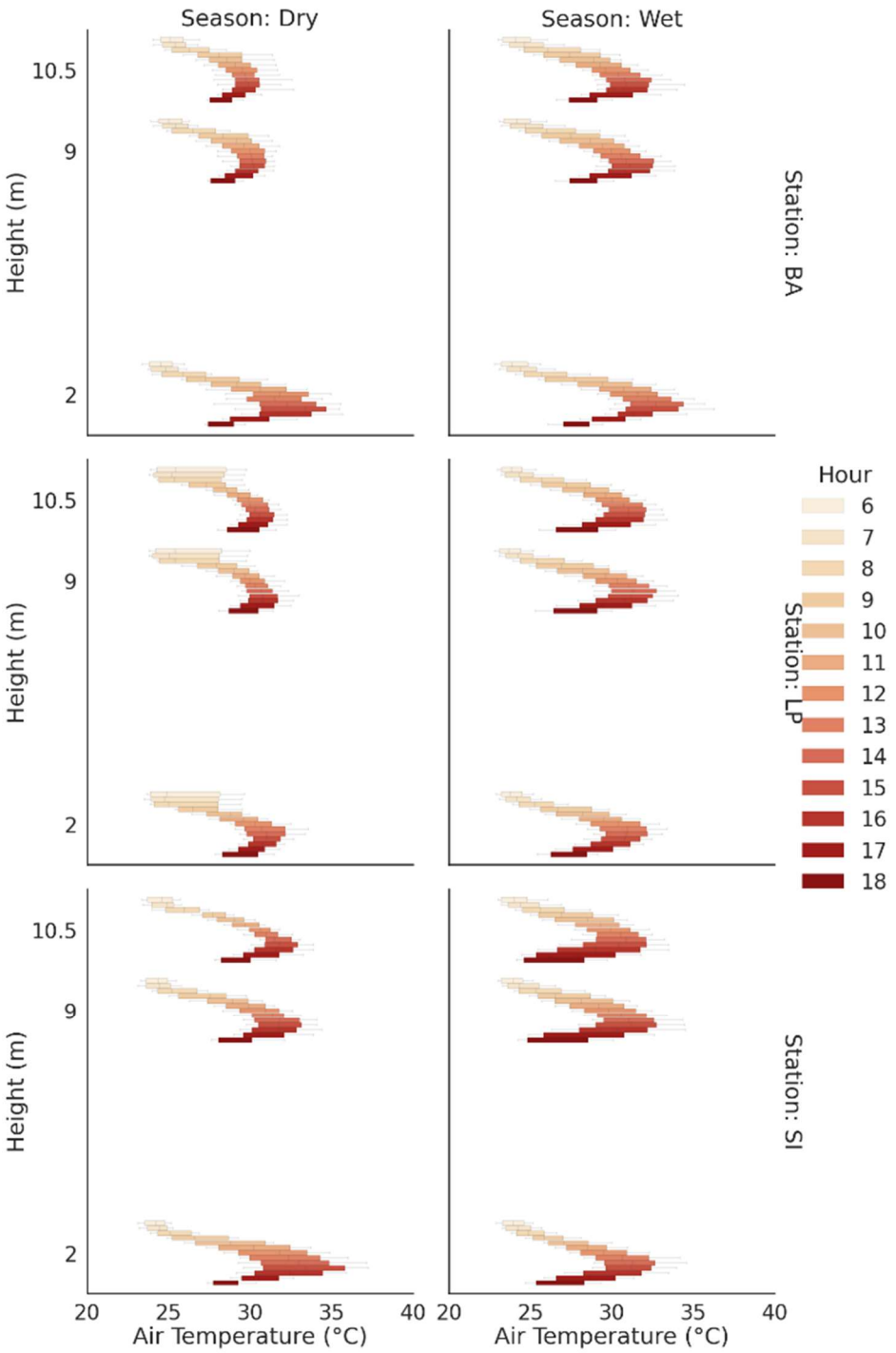

Figure 4.7. Temperature profile at each station in the three Kestrel sensors. Temperature profile at each height and station. Colors represent the different hours. Each height has the daily variation of temperature at each hour.

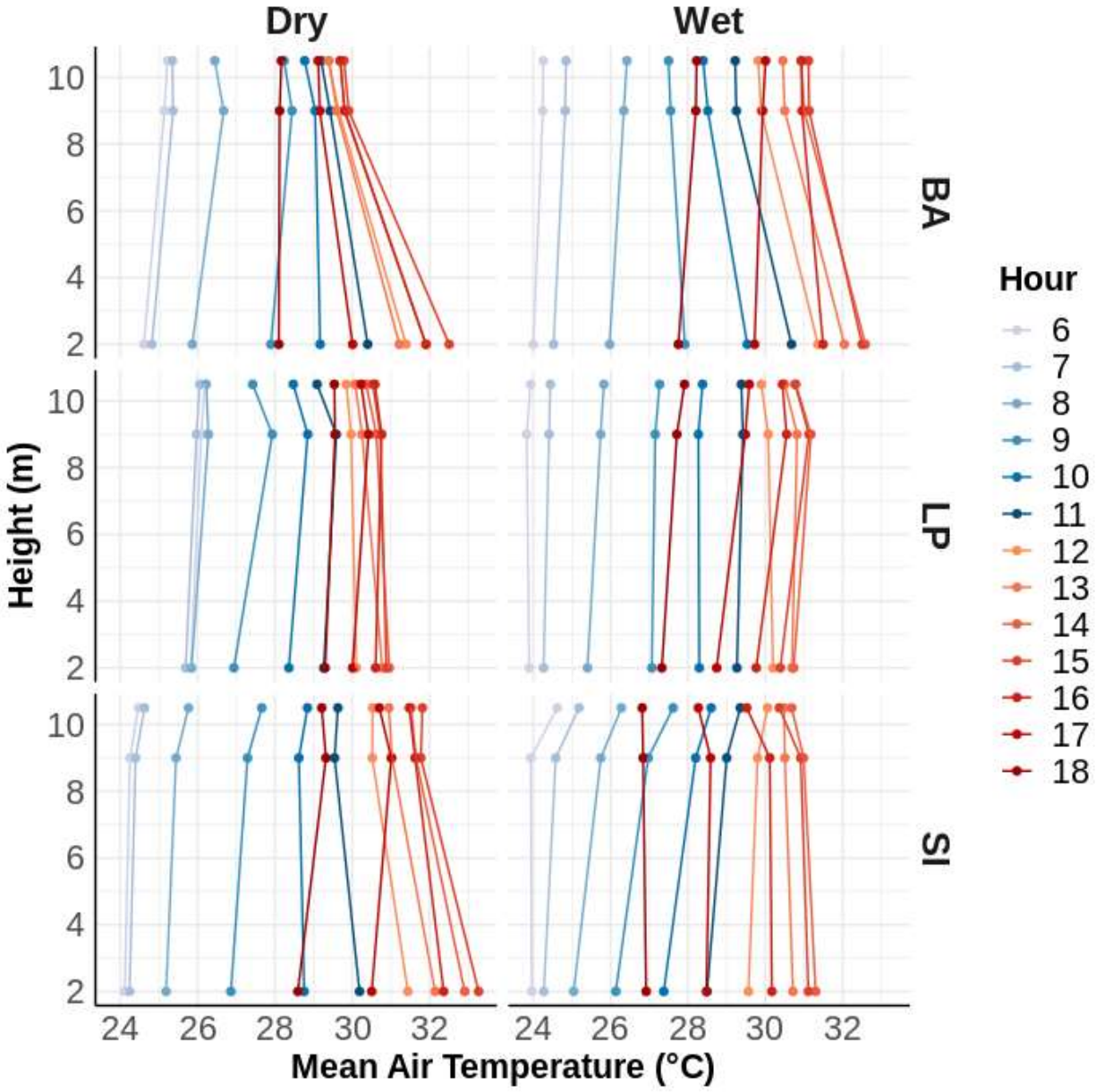

Figure 4.8. Beginning and end of lapse rate during the wet and dry season at each station.

Energy balance partition in oil palm plantations

Latent heat flux was higher than sensible and ground heat, and it constituted the dominant flux in the energy balance partition (75% of net radiation in BA and 77% in LP and SI). Sensible heat was slightly higher in BA than LP and SI (18% of net radiation in BA, 17% in LP and SI). Median, maximum, and minimum ground heat fluxes did not vary significantly at each station or

between stations (between 5% and 6% of net radiation). Maximum ground heat fluxes varied between 0 and 15 Wm^{-2}. Since G values had very little variation, we focus these results on the energy balance partition obtained with the G median. Latent heat reached its maximum at 12:00 in all three stations. Sensible heat, H, reached its maximum at 9:00 in BA and 12:00 for LP and SI. In all the stations, H remained almost the same from 9:00 to 14:00, when it started to decline. We discarded the periods of thermal inversion from the analysis because they do not follow the Bowen ratio assumptions of neutral stability (Figure 4.9). Bowen ratio did not vary significantly across the stations (0.26± 0.07 at BA, 0.25 ± 0.10 at LP, and 0.25 ± 0.10 at SI).

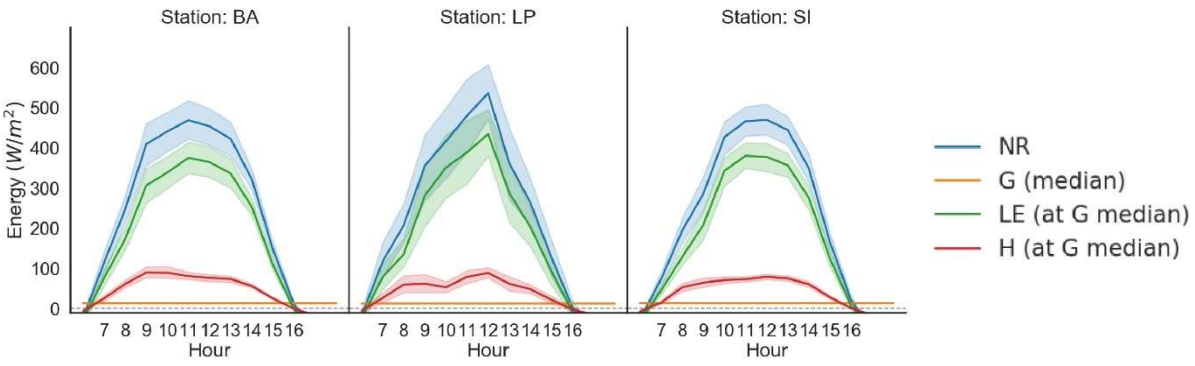

Figure 4.9. Energy balance partition at each station between October and November 2019 (wet season). Dashed line marks 0 Wm^{-2}. Shaded areas represent the distribution of the values at the same time (100% of the data is included).

Discussion

Variation of microclimatic conditions across the stations

Although average seasonal values of albedo, NDVI, air temperature, and VPD were similar across the stations and the seasons, variations were observed in the diurnal cycle across stations. VPD and temperature decreased during the dry season at two stations (BA and LP) while increased in the wet season. Especially at BA, wind speed was greater there than in the other two stations. Wind direction trends indicated the preferential path of the wind traveling from the

Andes cordillera West branch, which is located east of the study area. Lower VPD in the North compared to the South of the study area in the dry season may be due to more readily available sources of moisture. In west Colombia, local moisture recycling, the water coming from evapotranspiration in the same area where precipitation occurs, was identified at a regional scale by Hoyos et al., (2018). Specifically, they showed water vapor flux traveling from East to West between January and May.

The effect of moisture over the dry season can also be hypothesized based on the slightly lower temperatures during the dry season compared to the wet season observed in our dataset. This difference suggests a cooling effect of the winds during the dry vs. the wet season. The preferential path from the Andes cordillera might indicate that the forest cover located in that part of the Andes plays a role in driving moisture to the lowlands. However, the data collected in this work cannot test that hypothesis, nor was that the purpose of our study. We also observed a change of direction of the winds between the dry and the wet seasons. During the wet season, winds blew from the Pacific (Figure 4.6). This is likely due to the Choco low-level westerly jet, which contributes to moisture advection coming from the Pacific Ocean and produces high precipitation in western Colombia (Poveda and Mesa, 2000).

NDVI values were greater than 0.7 across the stations, which was expected given the canopy-dominated characteristics at each station and oil palm age. The similarities in NDVI values can be attributed to the degree of canopy cover: typically, OxG Hybrid covers the canopy after reaching 5-years old (Oscar Castillo, personal communication). Typically, NDVI can be used as an indicator of plant growth. However, when we compared NDVI values from each station, we did not find a strong relation between NDVI and age that would suggest a trend as a function of plant age. This is due to similarities in the canopy cover at all three plantations that cause

spectral saturation in NDVI (Chong et al., 2017). However, NDVI was lower at SI than LP and BA. This observation coincides with high temperature, and VPD observed at the same SI station, higher than the stations in the North, especially during the dry season. High VPD may inhibit stomatal conductance. Extreme values in albedo and NDVI during the first hours in the morning and after 16:00 are explained by the downwelling shortwave radiation decrease in the case of albedo; and by the saturation on the red band in case of the vegetation indices and the sun declination.

Literature on water limitation for *E. guineensis* suggests stomatal conductance decreases exponentially when VPD ranges between 1.0 and 4.5 kPa in well-watered soils (Dufrene and Saugier, 1993), although Henson (1995) found this range to be between 0.8 and 2.0 kPa. In a plot-scale study in an *E. guineensis* plantation in Brazil, VPD was a limiting factor for stomatal conductance, affecting plant transpiration in oil palm plantations (Brum, et al 2021). Although previous studies have suggested that stomatal conductance is affected by soil moisture and VPD (Carr, 2011; Culman et al., 2019; Dufrêne & Saugier, 1993), Brum et al. (2021) found VPD has a dominant role, especially under humid conditions. Zhang et al. (2016) found VPD is a strong indicator of light use efficiency in evergreen forest vegetation, showing that VPD is dominant over soil water content in determining plant stress conditions. We did not find previous studies that reported decreased stomatal conductance due to higher VPD as a limiting factor in OxG Hybrid. Though not specifically focused on oil palm, other studies have also found that higher VPD is associated with decreased vegetation productivity. In a global study (Yuan et al., 2019), multiannual changes in VPD were analyzed with changes in vegetation productivity using NDVI and other vegetative metrics. They found the influence of VPD in limiting vegetation growth changes at large temporal and spatial scales. We recognize the potential impact of NDVI

saturation due to canopy closure in all three sites. Nevertheless, we do not discard the effect of VPD in the reduction of NDVI.

Another interesting feature of the microclimatic conditions we observed is the change in the start hours of the lapse rate. Since lapse rate happens under neutral stability, high energy flux exchange would be expected during that time range. In fact, relative to the energy balance partition, we found that the dominant energy flux, latent heat, happened between the lapse rate start and end times, resulting from favorable conditions for gas exchange. Moreover, we identified a dominant effect of latent heat over sensible heat in the three stations (Figure 4.9), similar to what has been reported at other plantations in Indonesia (Meijide et al., 2017). In Indonesia, in a 12-year-old oil palm plantation, the mean maximum values of H were 12% and 78% for λE, respectively, which coincide with our results at BA (11-year old) and SI (8-year old). High λE rates are related to high transpiration rates. Our findings imply that high transpiration rates are expected during the rainy season. This aligns to what was found in an analysis of the physiological responses of oil palm species, including OxG hybrid, to environmental variables (Bayona-Rodriguez & Romero, 2019).

In a study in Indonesia Bowen ratio for a 12-year-old E. guineensis was found to be 0.14 ± 0.09 during a dry year (March 2014 to May 2015) (Meijide et al., 2017). These values are lower than the values found in our study (0.27± 0.08 at BA, 0.25 ± 0.12 at LP, and 0.26 ± 0.12 at SI). However, net radiation was lower in Uraba than in Indonesia, which compensates for the difference in Bowen ratio and suggests H/λE were almost the same. Our results were obtained for a wet season which potentially represents a contrasting scenario respect the study in Indonesia. Therefore, a closer look at soil moisture conditions and method uncertainties would need to be considered to make a strong conclusion. This is particularly important since our

method follows a different approach from the eddy covariance techniques used in Meijide et al. (2017). Our Bowen ratio was calculated between the top sensor (11 m) and the under-canopy sensor (2 m). This setup implies that the partition of the energy balance considers all the canopy as the column to transfer latent and sensible heat. This consideration can be an additional factor when comparing the differences between OxG Hybrid and E. guineensis results. Based on these results, we believe that more studies under different soil conditions are needed to draw firm conclusions and to identify the age at which each oil palm species reaches higher λE.

Limitations

Our analysis of the energy balance partition was limited to daytime hours, as our station instrumentation, especially the 7-band spectrometer, and our application of the Bowen ratio method are only valid during the daytime.

We are suggesting NDVI as indicator of photosynthetic activity. However, this index also identify characteristics associated with plant health status, which implies that local plant health can impact the plant's response to light absorption. The estimates of G are another source of uncertainty in the energy balance partition. Although the gradient heat method is a simple technique to estimate G, it requires precision in identifying the textural properties of soil. Fortunately, we did not detect high ranges of G under several combinations of soil texture fractions. However, since the sensors measure soil matric potential, the conversion to soil water content using average values can constitute an additional source of uncertainty. We believe the use of drift correction methods can help to include more of the flagged data into the estimates, thereby reducing some of these uncertainties. Given the relative humidity sensor failure in all the Kestrel devices, we could only estimate energy fluxes during the wet season. This restricted the analysis to the wet season in which the environmental conditions across the stations are more

similar. In addition, at LP average Bowen ratio was estimated with less data than the other two stations because of Arable Mark I failure during the first months. This might explain the higher variability in the results.

Conclusions

In this work, we present an analysis of the microclimatic conditions in three canopy-covered OxG hybrid plantations in Northern Colombia. We collected a series of microclimatic variables to partition the energy balance at each plantation using the Bowen ratio method. In addition to identifying the energy balance partition, we analyzed the microclimatic conditions in the region. We found the average Bowen ratio at the three plantations was around 0.25, which was similar to the one reported in E. guineensis plantations in Indonesia by Meijide et al., (2017) when net radiation in both studies is considered. By characterizing the microclimatic conditions, we found that average VPD, air temperature, and vegetation indices do not change across the stations seasonally. However, we found variations in temperature, vapor pressure deficit (VPD), and wind speed and direction at hourly temporal scale, especially during the dry season. The northernmost plantation experienced less VPD, and slightly lower temperatures compared to the station in the North. We also detected lower NDVI in the South, potentially associated with higher VPD during the dry season. Most of the year, soil moisture conditions corresponded to well-watered soils, with decreasing soil moisture during the dry season.

As discussed in Chapter 3 of this dissertation there are gaps in the understanding of the ecohydrology of oil palm. These gaps specifically relate to oil palm expansion in land covers other than forest, in different species, and in the Neotropics. Such knowledge gaps constrain informed decision-making in oil palm expansion and sustainable practices that minimize

environmental impacts in different types of landscapes. Chapter 4 contributes to minimizing the gaps mentioned above in the following ways:

1 To our knowledge, this is the first study in OxG hybrid analyzing microclimate and the energy balance partition. The data collected will advance understanding of water use efficiency and evapotranspiration in OxG hybrid, which, combined with existing studies, will enhance understanding of oil palm water-related requirements on a regional and global scale. Our dataset can be used in ecohydrological and earth system models to verify oil palm energy balance partition outputs and related them to evapotranspiration rates. Ecohydrological models have been used in Indonesia to contrast forest transition to oil palm using the data collected by Meijide et al., (2017). (Manoli et al., 2018; Fan et al., 2019). Our dataset can be implemented in a model following a similar configuration parametrization. The fact that we collected data at three sites offers the potential to model at a regional scale and verify temporally and spatially.

2 We contribute to the literature by offering a data set with a unique temporal length that allows the comparison of microclimatic conditions across seasons. The dataset produced for this study contains data representative of the rainy and dry seasons. Complexities and budget constraints of this type of research typically make it challenging to produce long-term data sets such as this one. Reflecting this reality, existing studies typically have shorter periods of data collection (days and months) (Roll et al., 2015; Meijide et al., 2017; Niu et al., 2015) than our study.

3 This work is the first of its nature in the Uraba region and thereby offers essential information for development in one of the leading agricultural regions in Colombia. Specifically, the data we have collected may inform applications that improve future

agricultural practices that minimize adverse environmental impacts or increase long-term sustainable use of resources. Our work, therefore, has potential for multiple regional applications as well.

4 Finally, the stations installed for this study continued operating after September 2020, albeit with partial functionality due to logistical difficulties associated with COVID-19. This additional data can be used in the future to contrast an average wet season in 2019 with the La Niña season of 2020, which produced extreme wet conditions in the region. This comparison would bring insights on how OxG hybrid respond to extreme events, and in general what would be the potential consequences to these extremes in the region.

CHAPTER 5: SUMMARY AND CONCLUSION

This dissertation examined critical aspects of tropical lowlands associated with regions of intensive agriculture development. Despite the extensive changes in land cover and land use occurring in this region and its importance for Earth's ecosystems and water resources, difficulties conducting long-term studies in rural regions have led to important gaps in our understanding of the interactions between ecosystems and hydrology. Through this dissertation research, I aimed to shed light on the different ways in which local communities' observations and insights can be acknowledged and included in scientific analysis.

Chapter 2 interrogated how the combined action of rural communities' data collection and knowledge and geostatistical models could be used to improve the spatiotemporal mapping of depth to groundwater. The use of Bayesian Maximum Entropy geostatistical models offered flexibility to incorporate data with high levels of uncertainty into quantitative analysis. Results showed that the use of descriptive information in model design improved the representation of depth to groundwater. At the same time, this inclusion contributed to opportunities for science and local communities to interact actively. This work represents a contribution to a broader question: How can we better acknowledge community knowledge, local legacies, and practices in scientific research? Chapter 2 reinforced the ideas of Assumpção et al. (2018); Cooper et al. (2007); and Haklay (2013) that express how constant communication and knowledge sharing are effective mechanisms to improve our understanding of environmental systems while also contributing to solving questions with a meaningful social impact. In addition, the approach

proposed in chapter 2 will hopefully help build models to explore hypotheses with the community and collaborative design strategies for data acquisition and analysis.

Regarding the specific application, the results in chapter 2 were also beneficial for improving the spatiotemporal representation of depth to groundwater in a system where groundwater is the primary source of domestic water supply. By involving community insights in the model construction, I identify a nonlinear relationship between precipitation intensity and frequency and depth to groundwater. Although further exploration of this relationship will require additional data collection, it represents progress towards understanding the responses of groundwater to precipitation. Additional research will be needed to maintain community engagement, a process that requires links between academia, the public and private sectors, and the community.

Chapters 3 & 4 explored the relations between ecological and hydrological aspects of oil palm plantations. Chapter 3 examines the progress that has occurred in global ecohydrology of oil palm research. It focuses on identifying the progress on understanding water-atmosphere, fluvial, soils, and groundwater processes, the types of land transition that have been explored, and the spatiotemporal scales of analysis and geographical distribution that are represented in research to date. By involving research published in Spanish and Portuguese, as well as in English, I worked to include a broader perspective on current knowledge.

Chapter 3 shows how the majority of the scientific production (65% of the papers analyzed) has been done in South East Asia, where the major oil palm producers are located, while in Africa, gaps in the scientific literature were found. In the Neotropics, there has been a recent increase in literature production. Most research has evaluated the African oil palm, E. guineensis, the microclimate and energy balance partition (Radersma et al., 1996; Ramdani et al., 2014;

Meijide et al., 2017; Meijide et al., 2018; Sabajo et al., 2017), their associations with evapotranspiration and water use efficiency (Roll et al., 2015; Manoli et al., 2018), sediment flux and storage, and runoff generation (Carlson et al., 2015; Adnan & Atkinson, 2011; Babel et al., 2015; Nainar et al., 2019, Gharibreza et al., 2013). Although this research has effectively advanced our understanding of the linkages between oil palm processes and shifts in local environmental conditions in the tropics, the short periods of analysis and the plot / regional spatial scales constitute a limitation to our ability to generalize trends. In addition, oil palm is expanding into areas of pastures and cropland, yet by far the main focus of study has been on conversion to oil palm from forested regions. The implications of transitions from other land cover types on ecohydrological processes remain largely unknown. Given the land heterogeneity in water-limited vs. water-abundant systems, more studies are needed under a variety of scenarios. This replication will build the necessary tools for establishing the limits of oil palm expansion. In terms of biophysical processes, studies have focused on minimizing carbon release to determine the development limit. However, that limit is unknown in areas already degraded, and water limitation needs to be considered as another strong limiting factor.

Chapter 4 builds on the findings of Chapter 3, with a specific aim of filling the gaps associated with identifying microclimate of oil palm in areas previously dedicated to grazing, the use of OxG hybrid, and the need for long-term environmental monitoring of microclimatic conditions. This work is located in northern Colombia, a region of rapid oil palm expansion. In Colombia, and countries in the neotropics, oil palm has replaced mainly pastures and grasslands (Furumo & Aide, 2017). In Chapter 4, three microclimatic stations were established to identify energy balance partition and the microclimatic conditions at plot scale. The results showed similarities in temperature, vapor pressure deficit, net radiation, and soil conditions at all

stations. However, differences in vapor pressure deficit and temperature between seasons and changes in wind direction and speed suggest an influence of moisture transport and a cooling effect during the dry season. In addition, the energy balance partition for the three plantations shows similar values across the sites and is comparable with results from Indonesia. This work ultimately contributes to advancing the understanding of oil palm in the tropics and the differences in limitations to further development.

More broadly, this dissertation advances the field of physical geography because: 1) it includes novel methods to involve communities in scientific research, methods which could be further explored in conjunction with human geographers to improve the linkages between scientists and community and the active involvement of all actors long-term; 2) it synthesizes the state of knowledge on how agricultural and hydrologic processes are integrated with land use land cover changes and ecohydrological processes, advancing the scientific knowledge while acknowledging the communities that depend on the crops; and 3) by presenting alternative techniques for the eddy covariance method, this dissertation explores the energy and biophysical relations across oil palm plantations in a region with high potential for oil palm expansion and under characteristics of species and land transitions not previously reported.

APPENDIX A: SUPPLEMENTAL INFORMATION TO CHAPTER 2

Content of this appendix

Supplemental Table A.1. Number of weekly DTG observations per month and per station.
Supplemental Table A.2. Cross-validation statistics using only the well validation values and only the wetland validation values

Introduction

This supporting information file contains details about the community science data collection and the data summary (A.1). We included how many space-time data points were collected and how we obtained weekly DTG used to perform model interpolations. Also, we have included details of the model implementation and additional cross-validation results (A.2). We specify the covariance model and its configuration for each of the geostatistical methods. We present the results of cross-validation over the hard data and the soft data domains. We include all the resulting maps for the three models: spatial (S), space-time (ST), and space-time with probabilistic or soft data (STSD) interpolations (A.3). Finally, we include the list of collaborators that contribute to the data collection in the Man River watershed (A.4).

A.1. Community science data collection

There was a total of 44 household wells (well observations) where depth to groundwater (DTG) data were recorded once a week, resulting in 2,448 daily readings. In some cases, data were not recorded every week due to several factors, including the high mobility of the collaborators, change in the weather conditions, especially during the wet season, and communication issues. In other cases, collaborators registered more data each week. When more readings were presented, the recorded readings from each week were averaged, resulting in 2,395 weekly DTG averages. DTG values ranged from 0 to about 22 meters, and the average DTG ranged from 0 to 2.5 m (Figure A.1). Data were transformed using a natural logarithm; therefore,

units are ln((m)), denoted as ln-depth. Table A.1 shows the number of weeks with DTG observations for each month of the study period. In October-November 2008, the monitoring network was updated to include more collaborators in the Southwest portion of the catchment and outside the watershed, close to the Cauca River, one of the main rivers in Colombia.

A.2. Additional explanation of model implementation and validation

Covariance model parameters for the S, ST, and STSD approaches. In a geostatistical approach, the general information is described by the process's mean and covariance model. For the spatial approach, we use the same covariance model as for the space-time approaches. However, the only difference is that we restrict estimation by using a time radius of 0 weeks around the estimation time; therefore, only data for that time is used instead of using data from the previous and following weeks. Hence it is sufficed that we describe the covariance model used for the space-time approaches (ST and STSD). That covariance model is given by the following equation, which consists of the sum of two space-time separable exponential covariance structures:

$$C(r,\tau) = VO \times (C_1 \times e^{\left(-\frac{3r}{ar_1}\right)} \times e^{\left(-\frac{3r}{at_1}\right)} + C_2 \times e^{\left(-\frac{3r}{ar_2}\right)} \times e^{\left(-\frac{3r}{at_2}\right)}) \quad \text{(S1)}$$

where r and τ are the spatial and temporal lags, respectively. The parameters of this model were obtained by fitting the covariance model to all the space-time observational data, which are as follows: VO = 3.634 ln-depth^2 is the variance of the observations in the log-transformed space; C_1 = 0.85 and C_2 = 0.15 are the percentage of the variance that can be represented by each exponential structure of the covariance model; ar^1=3 km and ar^2=30 km, are the spatial ranges of the first and second structures; and at_1 = 1,040 weeks and at_2 = 12 weeks are the corresponding temporal ranges.

The process of fitting the covariance parameters to the observational data consisted of the following steps. First, experimental covariance values were calculated for a temporal lag τ of zero and a spatial lag r, ($C(r, \tau = 0)$), varying from zero to about 9,000 m (circles in the top panel of Figure A.2), and for a spatial lag r of zero and temporal lag τ, $C(r = 0, \tau)$, varying from zero to 55 weeks (circles in the bottom panel of Figure A.2). Then covariance parameters were selected to best fit the experimental covariance values, resulting in the model shown with a plain line in Figure A.2.

Cross-validation in the soft and the hard data. The cross-validation statistics presented in Table A.1, in the main manuscript, were calculated based on the 4,996 validation data values for DTG as ln-depth, which comprises the 2,396 validation values obtained from well observations and the 2,600 validation values obtained as the expected value of the PDF for the soft data points in the wetlands. In Table A.2, we show these statistics after they are re-calculated using only the 2,396 well validation values (top rows of Table A.2) and using only the 2,600 wetland validation values (bottom rows of Table A.2).

A.3. DTG Distribution maps

All the weekly interpolation maps for each interpolation method are presented in Figures A.3 to A.8. All the results maps of the STSD model used in this paper are available in the repository DOI: 10.5281/zenodo.3928587 [License Creative Commons Attribution 4.0 International]

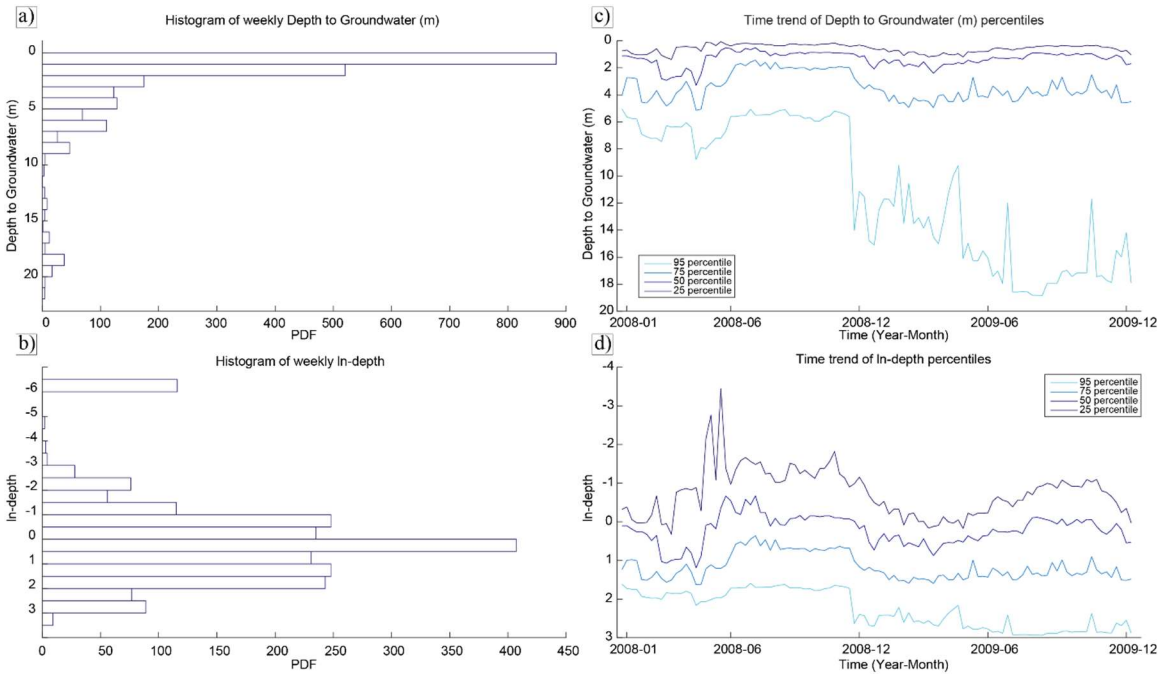

Figure A.1 Distribution of the weekly DTG and its transformed value using natural logarithm. a) DTG histogram of raw data (m); b) ln-depth DTG ln-depth; c) temporal trend percentiles of weekly DTG (m); and d) temporal trend percentiles of ln-depth.

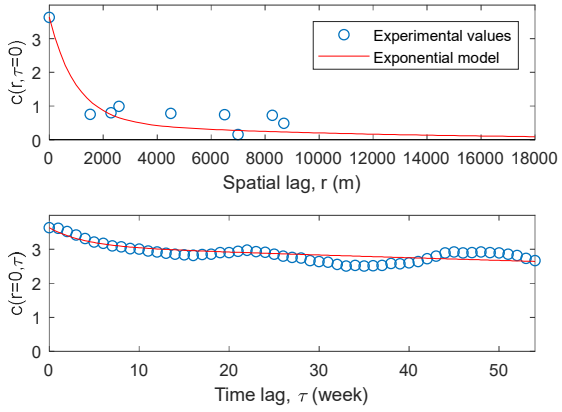

Figure A.2 Covariance models used in the space-time interpolation. Top: Spatial covariance model. Bottom: Temporal covariance model.

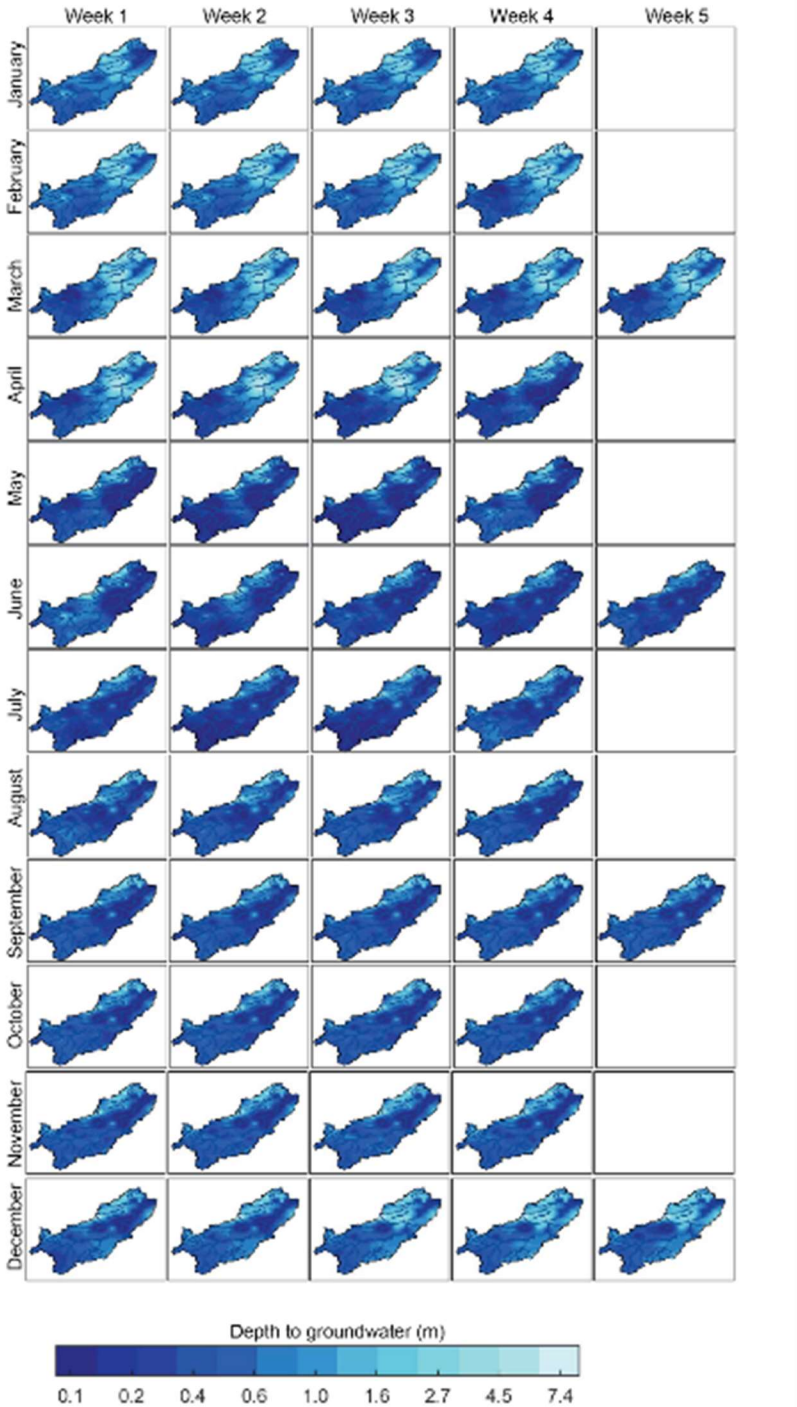

Figure A.3 Spatial distribution of the STSD estimate of the weekly average of DTG for each week in 2008. First week of the year is considered to start on 12/31/2008.

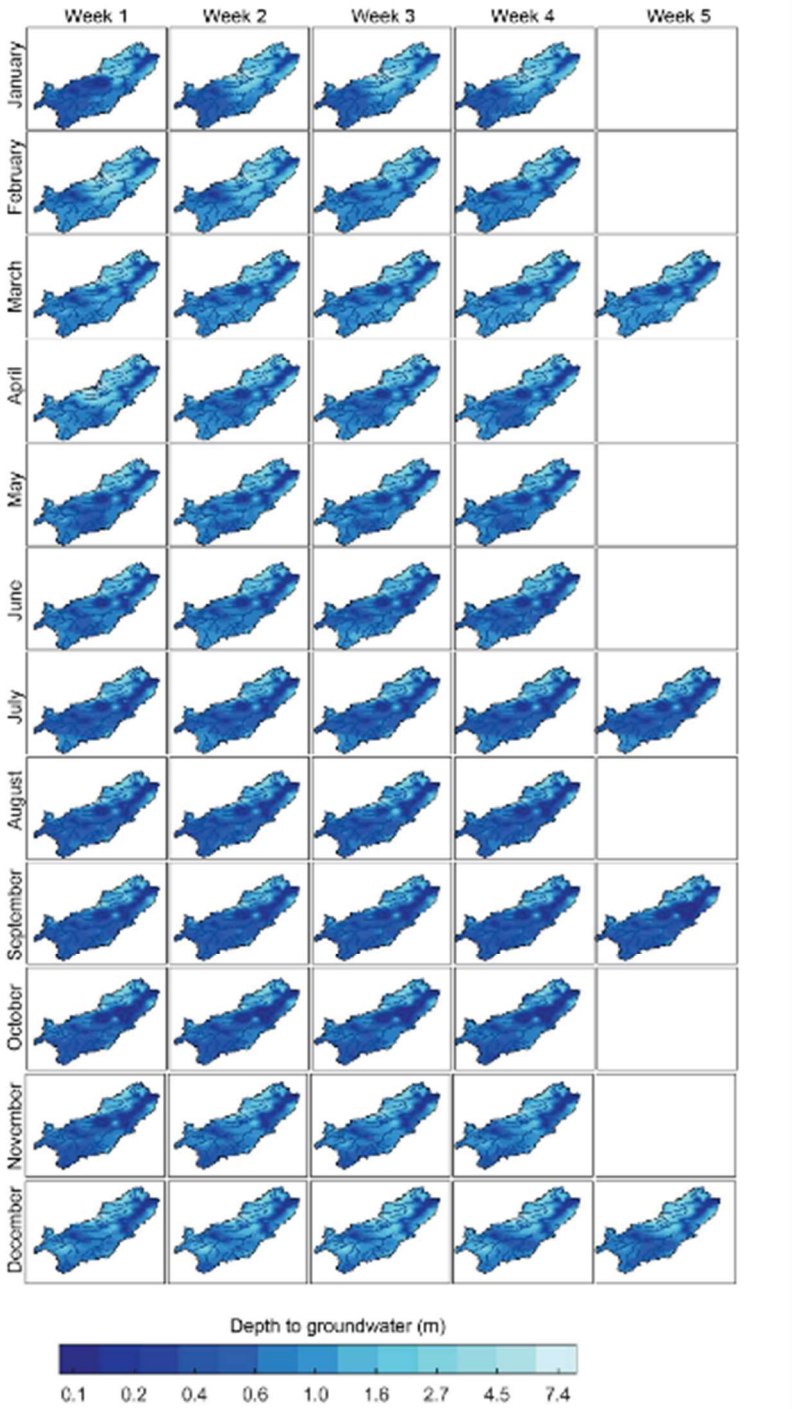

Figure A.4 Spatial distribution of the STSD estimate of the weekly average of DTG for each week in 2009. First week of the year is considered to start on 01/05/2009

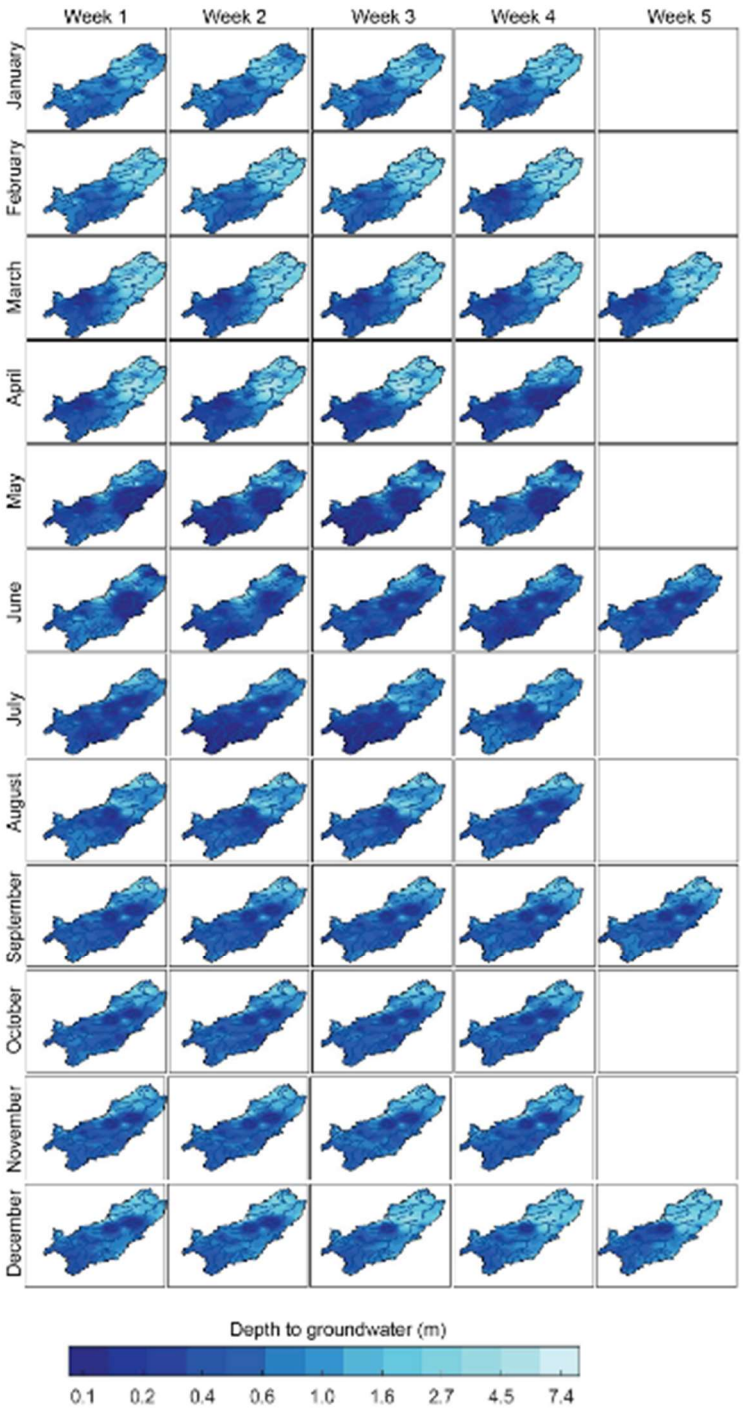

Figure A.5 Spatial distribution of the ST estimate of the weekly average of DTG for each week in 2008. First week of the year is considered to start on 12/31/2008

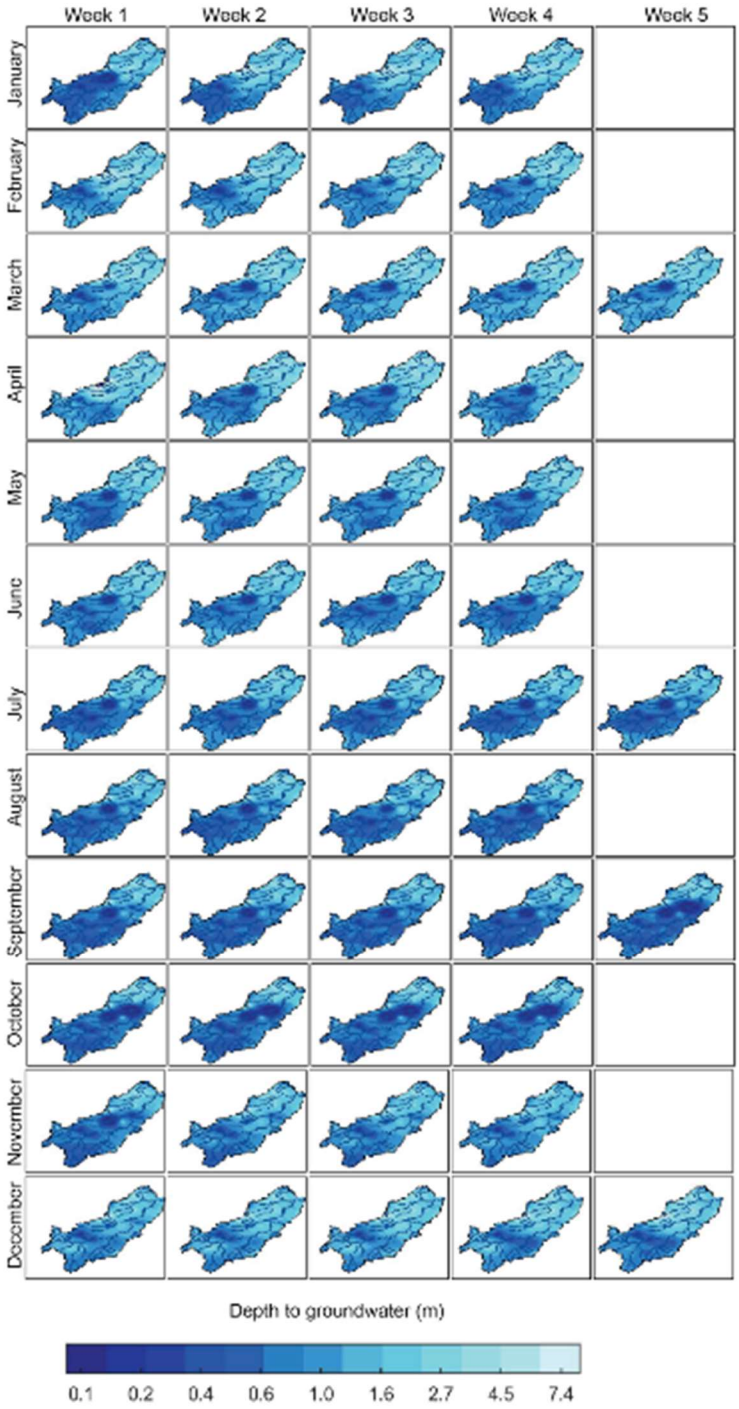

Figure A.6 Spatial distribution of the ST estimate of the weekly average of DTG for each week in 2009. First week of the year is considered to start on 01/05/2009

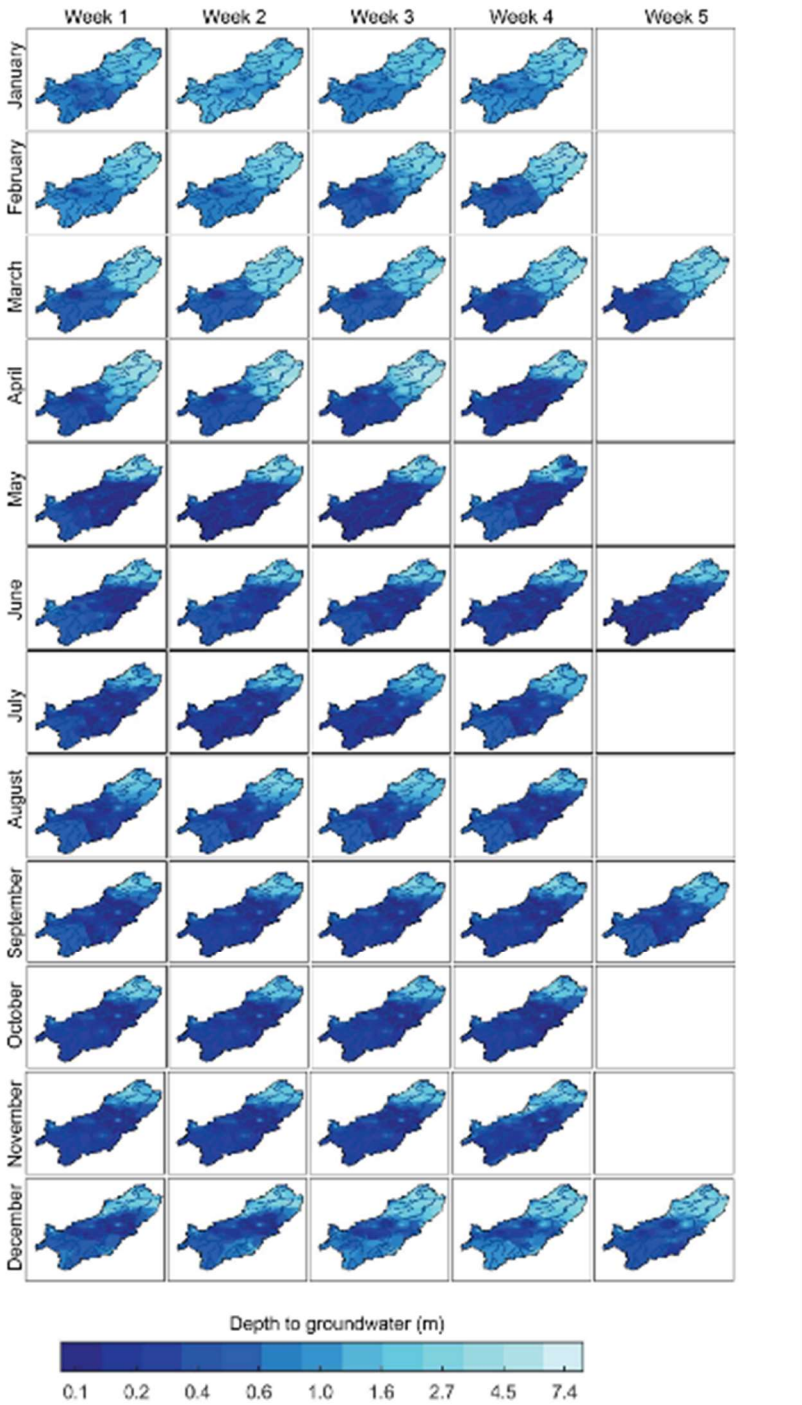

Figure A.7 Spatial distribution of the S estimate of the weekly average of DTG for each week in 2008. First week of the year is considered to start on 12/31/2008

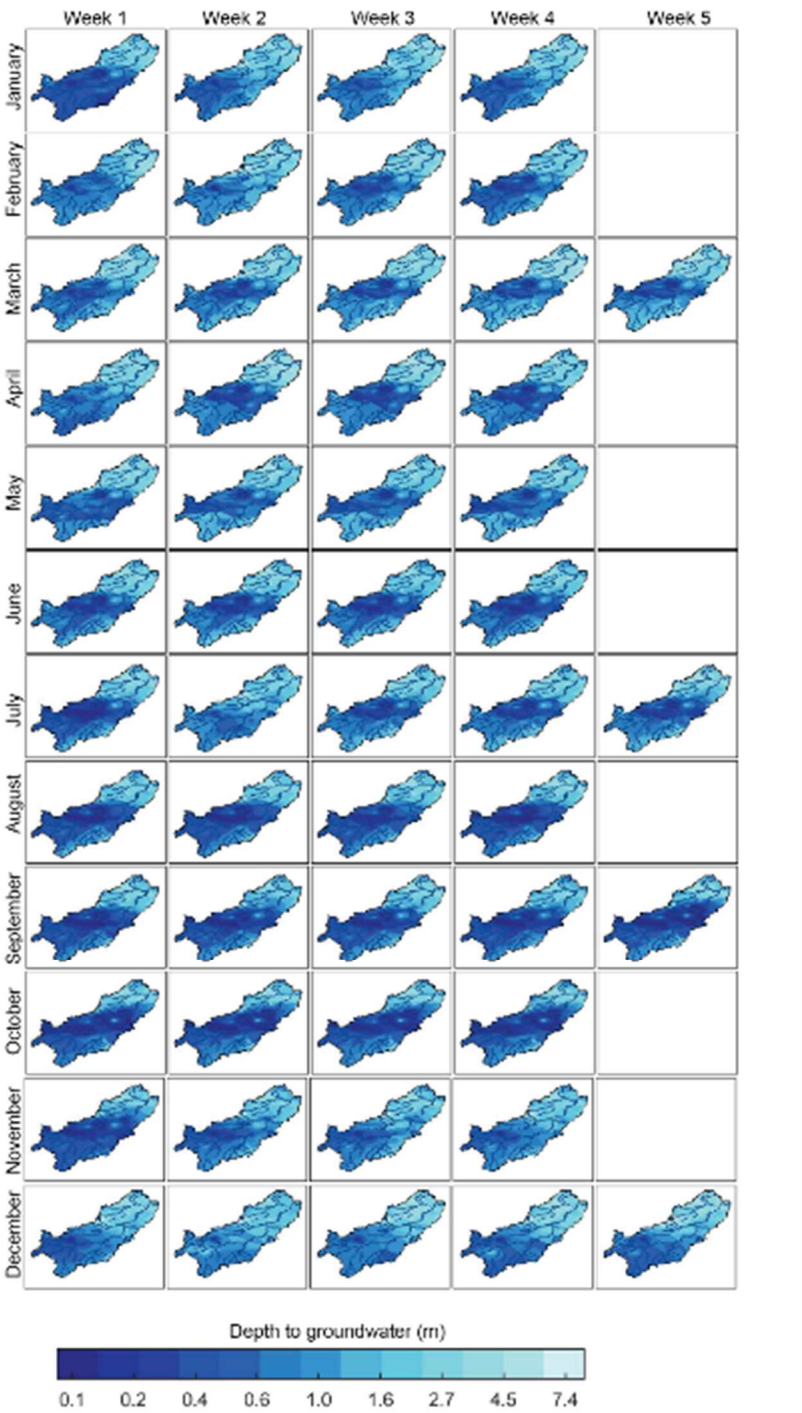

Figure A.8 Spatial distribution of the S estimate of the weekly average of DTG for each week in 2009. First week of the year is considered to start on 01/05/2009

Table A.1 Number of weekly DTG observations per month and per station. The greyscale represents the different quantities of data, where the shading helps distinguish the number of weeks with data reported each month. The darker the color, the more data collected in that station that month. The darkest gray indicates a maximum of five weeks with observations, and the lightest gray indicates a month with zero observations.

Stations	Year 2008												Year 2009												% Data 2008	% Data 2009
	Jan	Feb	Mar	Apr	May	Jun	Jul	Aug	Sep	Oct	Nov	Dec	Jan	Feb	Mar	Apr	May	Jun	Jul	Aug	Sep	Oct	Nov	Dec		
101	3	0	0	0	0	0	0	0	0	0	1	4	3	3	3	2	2	3	0	4	3	4	3	3	15.7	67.3
102	0	0	0	2	4	4	4	5	4	4	5	4	4	4	4	4	5	4	4	4	4	4	4	0	70.6	91.8
105	0	1	0	2	4	4	4	4	4	4	4	4	4	4	4	3	0	0	0	0	0	0	0	0	68.6	30.6
106	4	4	5	4	2	0	0	0	0	4	3	3	3	4	2	2	0	0	0	0	0	0	0	0	56.9	22.4
107	4	4	3	4	2	0	0	0	0	4	3	3	3	2	2	2	0	0	0	0	0	0	0	0	52.9	18.4
111	4	4	0	2	3	4	4	4	4	4	4	4	4	4	3	4	4	4	1	5	4	4	4	4	80.4	91.8
112	0	1	5	4	4	4	4	0	0	0	1	4	4	4	4	4	5	0	0	0	0	0	0	4	52.9	51.0
114	4	4	5	4	4	4	4	4	4	4	4	4	4	4	4	4	4	4	4	5	4	4	4	4	96.1	100.0
115	0	1	0	1	0	4	4	4	4	4	4	4	4	4	4	3	4	4	4	5	4	4	4	3	58.8	95.9
116	0	0	0	3	4	4	4	4	4	4	5	4	0	4	4	4	4	4	4	5	4	3	3	4	70.6	87.8
118	0	0	0	0	0	0	0	0	0	0	0	0	0	4	4	4	4	4	4	5	4	4	4	4	0.0	91.8
119	0	0	0	0	0	0	0	0	0	0	0	4	4	4	4	4	1	4	4	5	4	4	4	4	7.8	93.9
121	4	4	4	4	4	4	4	5	4	4	5	4	3	4	4	4	4	4	3	0	4	4	2	3	98.0	79.6
122	4	4	0	0	4	4	4	4	4	4	4	4	3	4	4	3	3	4	4	4	4	4	4	4	78.4	91.8
123	0	0	0	0	0	0	0	0	0	0	1	4	3	4	4	4	4	4	4	5	4	4	4	4	9.8	98.0
125	4	4	4	4	4	4	4	4	4	4	4	4	3	4	4	3	1	4	4	5	4	4	4	4	94.1	89.8
126	0	1	0	4	4	4	4	4	4	4	4	4	4	4	4	4	4	4	4	5	4	4	1	4	72.5	93.9
127	4	4	4	4	4	4	4	4	4	4	5	4	3	4	4	4	4	4	3	0	4	4	2	3	96.1	79.6
128	4	4	5	4	4	4	4	4	4	4	4	4	4	4	3	3	1	4	3	0	0	0	0	0	96.1	44.9
129	3	4	5	4	4	4	4	4	4	4	4	4	4	4	4	3	1	4	4	5	4	4	4	4	94.1	91.8
130	4	4	5	3	0	0	0	0	0	0	0	2	4	3	2	0	1	4	1	5	4	4	4	0	35.3	65.3
131	0	0	0	2	4	4	4	4	4	4	4	4	3	3	4	4	4	4	4	5	4	4	4	4	66.7	95.9
132	0	0	0	1	0	3	4	5	4	4	4	4	4	4	4	4	5	4	4	4	4	4	4	0	56.9	91.8
134	0	0	0	0	0	0	0	0	0	0	1	4	4	4	4	3	2	3	1	4	3	3	3	2	9.8	73.5
135	0	0	0	0	0	0	0	0	0	0	1	4	2	2	4	4	5	4	4	4	3	3	4	3	9.8	85.7
137	1	1	1	3	3	4	4	5	1	1	0	0	0	4	4	3	4	4	4	4	3	0	0	0	47.1	61.2
139	0	0	0	0	0	0	0	0	0	0	1	4	2	4	4	3	0	0	0	0	0	0	0	0	9.8	26.5
140	0	0	0	0	0	0	0	0	0	0	0	4	4	4	4	0	4	4	4	5	4	3	4	0	7.8	81.6
141	0	0	0	0	0	0	0	0	0	0	0	4	4	4	4	4	4	4	4	4	4	4	4	4	7.8	98.0
142	0	0	0	0	0	0	0	0	0	0	0	0	0	0	0	1	4	4	4	5	3	2	0	0	0.0	46.9
143	0	0	0	0	0	0	0	0	0	0	0	0	0	4	4	4	4	4	4	5	4	4	4	0	0.0	83.7
201	4	4	5	4	4	4	4	4	4	4	4	4	4	4	4	4	4	4	4	5	4	4	4	4	96.1	100.0
202	0	1	0	1	1	0	1	1	0	1	1	0	1	1	1	1	0	1	1	1	1	1	1	1	13.7	22.4
203	0	1	0	1	1	1	1	1	0	1	1	0	1	1	1	1	0	0	1	1	1	1	1	1	15.7	20.4
206	4	4	5	4	4	4	4	4	4	4	5	4	4	4	4	3	4	4	4	5	4	4	4	4	98.0	98.0

Table A.2 Cross-validation statistics using only the well validation values and only the wetland validation values. Well validation values are at the top portion of the table, MO= -1.93 ln-depth, VO= 5.06 (ln-depth)^2). Wetland validation are in the bottom portion of the table, MO= -1.31 ln-depth, VO= 0.0 (ln-depth)^2).

Type of validation values	**Model**	**MSE**	**VE**	**ME**	**R2**	**VZ**
		(ln(m))^2	**(ln(m))^2**	**ln(m)**	**unitless**	**ln(m)**
Wells (n= 2,396 s/t values)	S	4.05	4.05	-0.03	0.02	1.00
	ST	0.25	0.25	0.00	0.93	3.49
	STSD	0.25	0.25	0.00	0.93	3.49
Wetland (n=2,600 s/t values)	S	14.35	1.44	3.59	<0.01	1.44
	ST	13.62	1.07	3.54	<0.01	1.07
	STSD	0.94	0.21	0.86	<0.01	0.21

A.4. List of collaborators in the community science project

We thank the following collaborators in the Man River watershed for their valuable contribution to the project:

Luis Javier, Luis Osorio, Roberto Villadiego, Venegilda-Nafer, Libia Martínez, Darío Jiménez, Jaime Sánchez, Luis Carlos Chamorro, Antonio Pineda, Oscar Granados, José Heredia, Marlibia, Humberto Ramos, Antonio Navarro, Eunice, Marino Algarín, Aída Ibáñez, Elvia, Rodrigo Lambraño, Doris, Bernardo Carlos Dominguez, Emilia Vergara, Javier Casarubia, Emilsa, Fabio Escobar, José Darío, Luis Álvarez, Jorge Daniel Ameta, Ricardo Ricaute, Gabriel Pineda, Aura, Wilson Cardenas, Ernadi, Manuel Polo, Rosa, Luis Díaz, Antonio, José Vega, Rubi Guerra, Jorge Eliécer Martínez, Eliécer Martínez, Fidel Escorcia, Gumersindo Villadiego, Jessica Villadiego, Nelson Álvarez, Ana, Luis Teherán, Edilberto Masiglia, José Henao, Rafael Torres, Manuel, Maide, Jorge Acosta, Dary Luz, Hernán Usuna.

APPENDIX B: SUPPLEMENTAL INFORMATION TO CHAPTER 3

Table B.1 Search terms, filtering criteria, and the number of papers in each filtering stage

Database or Search engine	Search terms	No. of articles		
		Initial results	After first filtering	After removing duplicates and categorizing
Scielo	"palma de aceite" "oil palm" "palma do oleo" AND "hidrologia"	664	34	10
PubMed	"oil palm" AND expansion	59	59	14
Web of Science	"oil palm" AND (hydrology OR "land use" OR ecohydrology OR "land cover" OR moisture OR evapotranspiration)	404	217	84
Science Direct	"oil palm" AND ("land use" OR hydrology OR moisture OR evapotranspiration)	505	39	22
Dialnet	"oil palm"	314	30	13
IEEE	"oil palm"	166	41	13
Scopus	"oil palm" AND (hydrology OR runoff OR evapotranspiration)	81	78	37
Redalyc	"palma de aceite"	461	18	7
Springer	"oil palm" AND ("land use" OR hydrology)	238	15	4
Google Scholar	"oil palm" AND (expansion OR runoff OR evapotranspiration OR "water stress")	451	62	11
TOTALS		3343	593	215

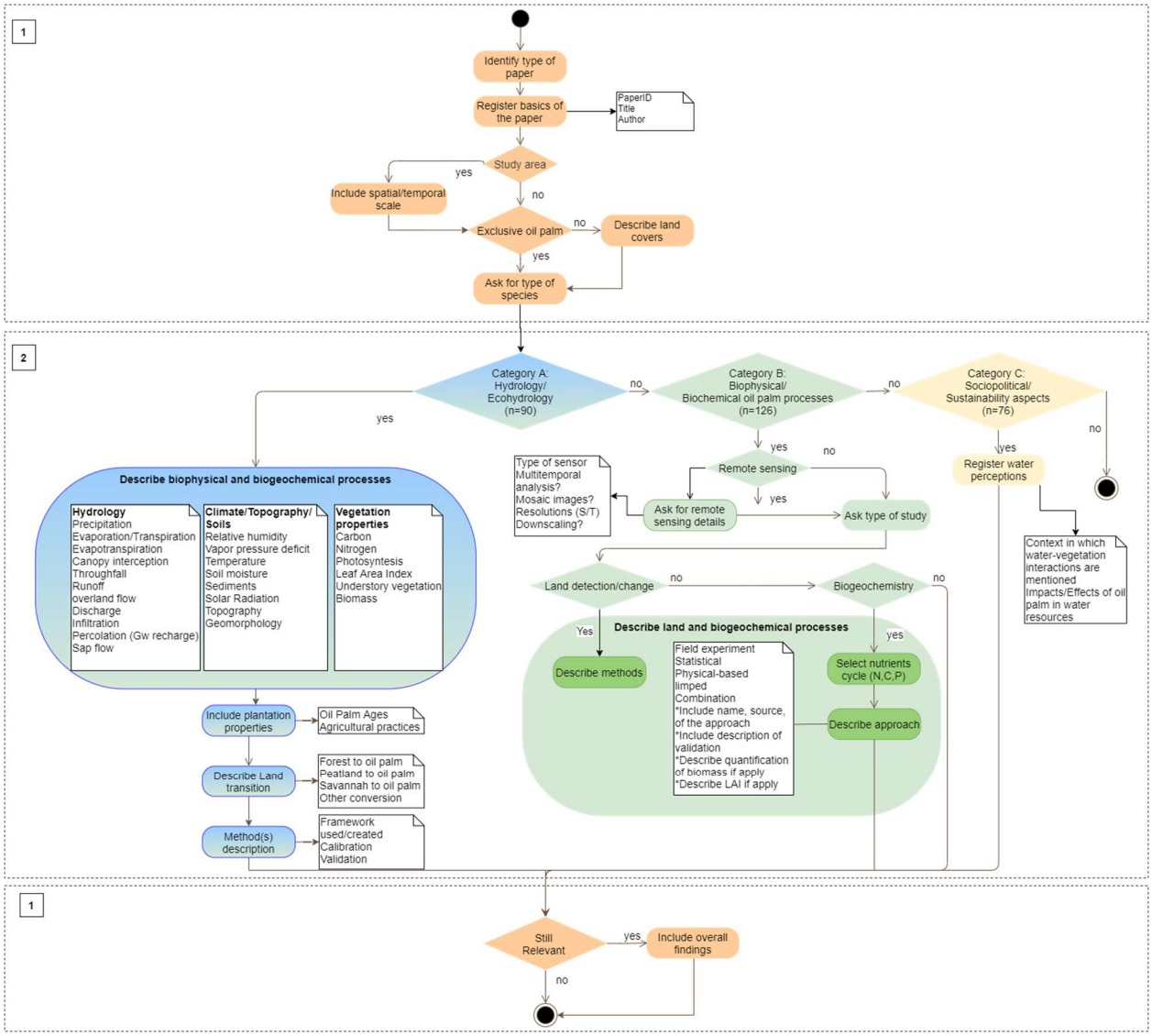

Figure B.1 Activity diagram of the complete flow process and details reading papers.

Table B.2 Coding system to summarize results in ecohydrological variables under different land transitions. Each initial was put in order 1. Change, 2. Land transition. 3, Age. 4, Scale. 5, Species for each of the fluxes and variables analyzed per each study.

1. Change	
I	Increase
D	Decrease
Q	Dont know
E	Equal
2. Land Transition	
F	Forest
C	Cropland
V	Pastures/Grazing/Husbandry
A	Savanna/Natural Grassland/Non disturbed grassland, savanna
3. Age	
N	Nursing ((0-2] years old)
Y	Young ((2-6] years old)
M	Mature (>6 years old)
Z	None/Empty/Not Specified (NS)
4. Scale	
Pl	Plant (less 1 m2)
Sm	Plot (1 m2 to 1 km2)
Re	Regional (small mesoscale >1 km2 to 100 km2)
Me	Mesoscale (large mesoscale >100 km2 to 10000 km2)
Ma	Macroscale (continental scale >10000 km2)
5. Species	
G	Guineensis
O	Oleifera
H	Interspecific Hybrid OxG
X	No specified
B	Both/ManyMore/Several

Table B.3 Data dictionary conventions of each table

Reference	**Article reference**
Value Type	Values extracted from each paper (Trend: code used to classify each article, Value OP are the values that the oil palm plantation has in each item, and Value transition are the values of the coverage with which the oil palm is compared in each variable).
Type	Paper Category (A: Hydrology, B: Biogeophysical)
Comparation or Transition	Classification if the article presents a transition comparison or other scenario with oil palm (T: Transition, C: Comparation, S: Scenario)
Season	R: rain or D: dry session according to each study.
Crop Type	Type of soil or crop according to each study.

Table B.4 Studies addressing fluxes, trends of change, and values for the variables Interception, Throughfall, Transpiration. Table conventions can be found in Table B.3

Reference	**Values type**	**Type**	**Comparation or Transition**	**Season**	**Interception**	**Units**	**Throughfall**	**Units**	**Transpiration**	**Units**
Dufrene et al., 1992	Trend	A		D	ZPlG	Interception loss/PET	ZPlG	Whole period (Throughfall/Total Rainfall)	ZPlG	Transpiration/PET
Dufrene et al., 1992	Values OP	A		D	0.07 +-0.02	mm day−1	0,82	mm	0.56+-0.08	mm day−1
Dufrene et al., 1992	Values Transiti	A		D						

Reference	Values type	Type	Comparation or Transition	Season	Interception	Units	Throughfall	Units	Transpiration	Units
	on									
Dufrene et al., 1992	Trend	A		R	ZPlG	Interception loss/PET	ZPlG	Whole period (Throughfall/Total Rainfall)	ZPlG	Transpiration/PET
Dufrene et al., 1992	Values OP	A		R	0.11 +-0.02	mm day−1	0,82	mm	0.69+-0.04	mm day−1
Dufrene et al., 1992	Values Transition	A		R						
Radersma et al., 1996	Trend	A	C	D					ICZSmX	Suboptimal to optimal water supply conditions
Radersma et al., 1996	Values OP	A	C	D					2.5-6.5	mm day−1
Radersma et al., 1996	Values Transition	A	C	D					1.9-6.1	mm day−1
Radersma et al., 1996	Trend	A	C	R					ICZSmX	Suboptimal to optimal water supply conditions
Radersma et al., 1996	Values OP	A	C	R					2.5-3.3	mm day−1
Radersma et al., 1996	Values Transition	A	C	R					1.9-3.0	mm day−1
Radersma et al., 1996	Trend	A	C	D					DCZSmX	Suboptimal to optimal water

Reference	Values type	Type	Comparation or Transition	Season	Interception	Units	Throughfall	Units	Transpiration	Units
										supply conditions
Radersma et al., 1996	Values OP	A	C	D					2.5-6.5	mm day−1
Radersma et al., 1996	Values Transition	A	C	D					4.4-5.4	mm day−1
Radersma et al., 1996	Trend	A	C	R					ICZSmX	Suboptimal to optimal water supply conditions
Radersma et al., 1996	Values OP	A	C	R					2.5-3.3	mm day−1
Radersma et al., 1996	Values Transition	A	C	R					2.2-2.7	mm day−1
Banabas et al., 2008	Trend	A			MSmG		MSmG			
Banabas et al., 2008	Values OP	A					83	%		
Banabas et al., 2008	Values Transition	A								
Röll et al., 2015	Trend	A							YPlG	
Röll et al., 2015	Values OP	A							0,224	mm day−1
Röll et al., 2015	Values Transition	A								
Röll et al.,	Trend	A							MPlG	

Reference	Values type	Type	Comparation or Transition	Season	Interception	Units	Throughfall	Units	Transpiration	Units
2015										
Röll et al., 2015	Values OP	A							2,491	mm day−1
Röll et al., 2015	Values Transition	A								
Tarigan et al., 2018	Trend	A	T		QFMMeG					
Tarigan et al., 2018	Values OP	A	T		8,4	mm				
Tarigan et al., 2018	Values Transition	A	T							
Kurniawan et al., 2018	Trend	A	C		DFMSmG				DFMSmG	
Kurniawan et al., 2018	Values OP	A	C		182	mm yr−1			437	mm yr−1
Kurniawan et al., 2018	Values Transition	A	C		196	mm yr−1			1033	mm yr−1
Kurniawan et al., 2018	Trend	A	C		DFMSmG				DFMSmG	
Kurniawan et al., 2018	Values OP	A	C		166	mm yr−1			446	mm yr−1
Kurniawan et al., 2018	Values Transition	A	C		181	mm yr−1			1284	mm yr−1
Meijide et al., 2017	Trend	A	T						NZSmG	
Meijide et al., 2017	Values OP	A	T						64 ± 3	mm yr−1
Meijide et	Values	A	T							

Reference	Values type	Type	Comparation or Transition	Season	Interception	Units	Throughfall	Units	Transpiration	Units
al., 2017	Transition									
Meijide et al., 2017	Trend	A	T						MZSmG	
Meijide et al., 2017	Values OP	A	T						826 ± 34	mm yr−1
Meijide et al., 2017	Values Transition	A	T							
Merten et al., 2016	Trend	A	C		ICMSmX				QCMSmX	
Merten et al., 2016	Values OP	A	C		28	%			1.8 ± 0.3	mm day -1
Merten et al., 2016	Values Transition	A	C		17	%			1.1 ± 0.1	mm day -1
Merten et al., 2016	Values Transition	A	C						2.0 ± 0.2	mm day -1

Table B.5 Studies addressing fluxes, trends of change, and values for the variables Surface-Runoff, Infiltration, Groundwater flow. Table conventions can be found in Table B.3

Reference	Values type	Type	Comparation or Transition	Season	Surface Runoff	Units	Infiltration	Units	Groundwaterflow	Units
Algeet-Abarquero et al., 2015	Trend	A	C		IVZSmG	Runoff coef				
Algeet-Abarquero et al., 2015	Values OP	A	C		32,6	%				
Algeet-Abarquero et al., 2015	Values Transition	A	C		15,3	%				
Algeet-Abarquero et al., 2015	Trend	A	C		IFZSmG	Runoff coef				
Algeet-Abarquero et al., 2015	Values OP	A	C		32,6	%				
Algeet-Abarquero et al., 2015	Values Transition	A	C		1,7	%				
Banabas et al., 2008	Trend	A			MSmG		MSmG			
Banabas et al., 2008	Values OP	A			6	%				
Banabas et al., 2008	Values Transition	A								
Babel et al., 2015	Trend	A	S		DCZMeG					
Babel et al., 2015	Values OP	A	S							

Reference	Values type	Type	Comparation or Transition	Season	Surface Runoff	Units	Infiltration	Units	Groundwaterflow	Units
Babel et al., 2015	Values Transition	A	S							
Nainar et al., 2018	Trend	A	T		DFMReG					
Nainar et al., 2018	Values OP	A	T		956	mm				
Nainar et al., 2018	Values Transition	A	T		2764	mm				
Nainar et al., 2018	Trend	A	T		DFMReG					
Nainar et al., 2018	Values OP	A	T		956	mm				
Nainar et al., 2018	Values Transition	A	T		1785	mm				
Nainar et al., 2018	Trend	A	T		DFMReG					
Nainar et al., 2018	Values OP	A	T		956	mm				
Nainar et al., 2018	Values Transition	A	T		1597	mm				
Nainar et al., 2018	Trend	A	T		DFMReG					
Nainar et al., 2018	Values OP	A	T		956	mm				
Nainar et al., 2018	Values Transition	A	T		1907	mm				
Sabajo et	Values	A	T							

Reference	Values type	Type	Comparation or Transition	Season	Surface Runoff	Units	Infiltration	Units	Groundwaterflow	Units
al., 2017	OP									
Sabajo et al., 2017	Values Transition	A	T							
Sabajo et al., 2017	Values Transition	A	T							
Satriawan et al., 2016	Trend	A	S		QCNSmX		QCNSmX			
Satriawan et al., 2016	Values OP	A	S		289,72	bC m3 h-1	14,68	bc mm		
Satriawan et al., 2016	Values OP	A	S		271,95	aB m3 h-1				
Satriawan et al., 2016	Values OP	A	S		262,83	aA m3 h-1				
Satriawan et al., 2016	Values OP	A	S		271,51	aC m3 h-1	17,35	c mm		
Satriawan et al., 2016	Values OP	A	S		259,42	aB m3 h-1				
Satriawan et al., 2016	Values OP	A	S		249,37	aA m3 h-1				
Satriawan et al., 2016	Values OP	A	S		403,84	cA m3 h-1	10,15	a mm		
Satriawan et al., 2016	Values OP	A	S		400,84	bA m3 h-1				
Satriawan et al., 2016	Values OP	A	S		399,84	bA m3 h-1				
Satriawan et al., 2016	Values OP	A	S		402,98	cA m3 h-1	12,34	b mm		
Satriawan et al., 2016	Values OP	A	S		400,31	bA m3 h-1				
Satriawan	Values	A	S		398,64	bA m3 h-1				

Reference	Values type	Type	Comparation or Transition	Season	Surface Runoff	Units	Infiltration	Units	Groundwaterflow	Units
et al., 2016	OP									
Satriawan et al., 2016	Values Transition	A	S				11,69	mm		
Satriawan et al., 2016	Values Transition	A	S				14,88	mm		
Satriawan et al., 2016	Values Transition	A	S				18,34	mm		
Taringan et al, 2016	Trend	A					IMSmX			
Taringan et al, 2016	Values OP	A								
Taringan et al, 2016	Values Transition	A								

Table B.6 Studies addressing fluxes, trends of change, and values for the variables Streamflow or Surface Discharge, Sediment transport, Evapotranspiration. Table conventions can be found in Table B.3

Reference	Values type	Type	Comparation or Transition	Season	Streamflow or Surface Discharge	Units	Sediment transport	Units	Evapotranspiration	Units
Manoli et al 2018	Trend	A	T						DFYPlG	
Manoli et al 2018	Values OP	A	T						1000–1600	mm yr −1
Manoli et al 2018	Values Transition	A	T						1200-2240	mm yr −1

Reference	Values type	Type	Comparation or Transition	Season	Streamflow or Surface Discharge	Units	Sediment transport	Units	Evapotranspiration	Units
Manoli et al 2018	Trend	A	T						IFMPlG	
Manoli et al 2018	Values OP	A	T						1200−1800	mm yr −1
Manoli et al 2018	Values Transition	A	T						1300+-200	mm yr −1
Carlson et al., 2015	Trend	A	C				IFYReG			
Carlson et al., 2015	Values OP	A	C				32000 ± 4800	mg h-1 ha-1		
Carlson et al., 2015	Values Transition	A	C				13000 ± 1400	mg h-1 ha-1		
Carlson et al., 2015	Trend	A	C				IFMReG			
Carlson et al., 2015	Values OP	A	C				20000 ± 3400	mg h-1 ha-1		
Carlson et al., 2015	Values Transition	A	C				13000 ± 1400	mg h-1 ha-1		
Adnan et al., 2011	Trend	A	T		QFZMaX					
Adnan et al., 2011	Values OP	A	T							
Adnan et al., 2011	Values Transition	A	T							
Dufrene et al., 1992	Trend	A		D					ZPlG	PET
Dufrene et al., 1992	Values OP	A		D					3.54+-0.16	mm day−1

Reference	Values type	Type	Comparation or Transition	Season	Streamflow or Surface Discharge	Units	Sediment transport	Units	Evapotranspiration	Units
Dufrene et al., 1992	Values Transition	A		D						
Dufrene et al., 1992	Trend	A		R					ZPlG	PET
Dufrene et al., 1992	Values OP	A		R					3.14+-0.11	mm day−1
Dufrene et al., 1992	Values Transition	A		R						
Radersma et al., 1996	Trend	A	C	D					QCZSmX	Not clear under different conditions of water suppy. Lower bound suboptimal water condition, upper bound optimal
Radersma et al., 1996	Values OP	A	C	D					395-428	mm yr−1
Radersma et al., 1996	Values Transition	A	C	D					294-490	mm yr−1
Radersma et al., 1996	Trend	A	C	R					ICZSmX	Supoptimal to optimal

Reference	Values type	Type	Comparation or Transition	Season	Streamflow or Surface Discharge	Units	Sediment transport	Units	Evapotranspiration	Units
										conditions
Radersma et al., 1996	Values OP	A	C	R					623-623	mm yr−1
Radersma et al., 1996	Values Transition	A	C	R					584-584	mm yr−1
Radersma et al., 1996	Trend	A	C	D					ICZSmX	Not clear under different conditions of water suppy. Lower bound suboptimal water condition, upper bound optimal
Radersma et al., 1996	Values OP	A	C	D					395-428	mm yr−1
Radersma et al., 1996	Values Transition	A	C	D					46-46	mm yr−1
Radersma et al., 1996	Trend	A	C	R					ICZSmX	Supoptimal to optimal conditions
Radersma et al., 1996	Values OP	A	C	R					623-623	mm yr−1
Radersma	Values	A	C	R					372-364	mm yr−1

Reference	Values type	Type	Comparation or Transition	Season	Streamflow or Surface Discharge	Units	Sediment transport	Units	Evapotranspiration	Units
et al., 1996	Transition									
Henson et al., 2007	Trend	A							MSmG	
Henson et al., 2007	Values OP	A								
Henson et al., 2007	Values Transition	A								
Banabas et al., 2008	Trend	A			MSmG	Streamflow			MSmG	
Banabas et al., 2008	Values OP	A			1100%	%				
Banabas et al., 2008	Values Transition	A								
Röll et al., 2015	Trend	A							YPlG	
Röll et al., 2015	Values OP	A							2,8	mm day−1
Röll et al., 2015	Values Transition	A								
Röll et al., 2015	Trend	A							MPlG	
Röll et al., 2015	Values OP	A							4,7	mm day−1
Röll et al., 2015	Values Transition	A								
Carlson et al., 2013	Trend	B	S							

Reference	Values type	Type	Comparation or Transition	Season	Streamflow or Surface Discharge	Units	Sediment transport	Units	Evapotranspiration	Units
Carlson et al., 2013	Values OP	B	S							
Carlson et al., 2013	Values Transition	B	S							
Wösten et al., 2006	Trend	A	S		DPZReX					
Wösten et al., 2006	Values OP	A	S							
Wösten et al., 2006	Values Transition	A	S							
Babel et al., 2015	Trend	A	S		DCZMeG		DCZMeG			
Babel et al., 2015	Values OP	A	S							
Babel et al., 2015	Values Transition	A	S							
Kurniawan et al., 2018	Trend	A	C						DFMSmG	
Kurniawan et al., 2018	Values OP	A	C						1027	mm yr−1
Kurniawan et al., 2018	Values Transition	A	C						1384	mm yr−1
Kurniawan et al., 2018	Trend	A	C						DFMSmG	
Kurniawan et al., 2018	Values OP	A	C						1071	mm yr−1
Kurniawan et al., 2018	Values Transiti	A	C						1622	mm yr−1

Reference	Values type	Type	Comparation or Transition	Season	Streamflow or Surface Discharge	Units	Sediment transport	Units	Evapotranspiration	Units
	on									
Meijide et al., 2017	Trend	A	T						NZSmG	
Meijide et al., 2017	Values OP	A	T						918 ± 46	mm yr−1
Meijide et al., 2017	Values Transition	A	T							
Meijide et al., 2017	Trend	A	T						MZSmG	
Meijide et al., 2017	Values OP	A	T						1216 ± 34	mm yr−1
Meijide et al., 2017	Values Transition	A	T							
Sabajo et al., 2017	Trend	A	T						FMMaG	
Sabajo et al., 2017	Values OP	A	T						-0.03 ± 0.03	mm h−1
Sabajo et al., 2017	Values Transition	A	T						-0.03 ± 0.04	mm h−1
Sabajo et al., 2017	Values Transition	A	T						-0.04 ± 0.03	mm h−1
Sabajo et al., 2017	Trend	A	T						FNMaG	
Sabajo et al., 2017	Values OP	A	T						-0.18 ± 0.04	mm h−1
Sabajo et al., 2017	Values Transition	A	T						-0.23 ± 0.04	mm h−1

Reference	Values type	Type	Comparation or Transition	Season	Streamflow or Surface Discharge	Units	Sediment transport	Units	Evapotranspiration	Units
Sabajo et al., 2017	Values Transition	A	T						-0.26 ± 0.06	mm h−1
Satriawan et al., 2016	Trend	A	S							
Nainar et al., 2019	Trend	A	T				IFZReX			
Nainar et al., 2019	Values OP	A	T				132 y 587	mg L – 1		
Nainar et al., 2019	Values Transition	A	T				34 y 102	mg L – 1		
Merten et al., 2016	Trend	A	C		DCMSmX				QCMSmX	
Merten et al., 2016	Values OP	A	C		21,2	l s -1 ha -1			4,7	mm day-1
Merten et al., 2016	Values Transition	A	C		36,9	l s -1 ha -1			n.d	
Merten et al., 2016	Values Transition	A	C						n.d	

Table B.7 Studies addressing fluxes, trends of change, and values for the variables Temperature, Latent Heat, Sensible Heat. Table conventions can be found in Table B.3

Reference	Values type	Type	Comparation or Transition	Season	Temperature	Units	Latent Heat	Units	Sensible Heat	Units
Fowler et al., 2011	Trend	A	C				IFMReB		IFMReB	

Reference	Values type	Type	Comparation or Transition	Season	Temperature	Units	Latent Heat	Units	Sensible Heat	Units
Fowler et al., 2011	Values OP	A	C				7,8	MJ m-2 d-1	2,1	MJ m-2 d-1
Fowler et al., 2011	Values Transition	A	C				6,7	MJ m-2 d-1	1,3	MJ m-2 d-1
Manoli et al 2018	Trend	A	T		IFYPlG		DFYPlG		IFYPlG	
Manoli et al 2018	Values OP	A	T		23-26	°C	300	W/m2	180	W/m2
Manoli et al 2018	Values Transition	A	T		21-23	°C	380	W/m2	70	W/m2
Manoli et al 2018	Trend	A	T		DFMPlG		IFMPlG		DFMPlG	
Manoli et al 2018	Values OP	A	T		22-23	°C	400	W/m2	30	W/m2
Manoli et al 2018	Values Transition	A	T		21-23	°C	380	W/m2	70	W/m2
Meijide et al., 2018	Trend	A	T		IFZSmG					
Meijide et al., 2018	Values OP	A	T		25.5 ± 0.2	°C				
Meijide et al., 2018	Values Transition	A	T		2.8 ± 0.1	°C				
Luke et al., 2017	Trend	A	T		IFZSmG					
Luke et al., 2017	Values OP	A	T		28.22 ± 0.07	°C				
Luke et al., 2017	Values Transiti	A	T		26.86 ± 0.36	°C				

Reference	Values type	Type	Comparation or Transition	Season	Temperature	Units	Latent Heat	Units	Sensible Heat	Units
	on									
Luke et al., 2017	Trend	A	T		IFZSmG					
Luke et al., 2017	Values OP	A	T		28.22 ± 0.07	°C				
Luke et al., 2017	Values Transition	A	T		25.02 ± 0.93	°C				
Luke et al., 2017	Trend	A	T		IFZSmG					
Luke et al., 2017	Values OP	A	T		28.22 ± 0.07	°C				
Luke et al., 2017	Values Transition	A	T		24.99 ± 0.67	°C				
Chellaiah and Yule., 2018	Trend	A	T		FZSmG					
Chellaiah and Yule., 2018	Values OPF	A	T		25.186 ± 0.217	(0.217b) °C				
Chellaiah and Yule., 2018	Values OPOP	A	T		27.587 ± 0.194	(0.194c) °C				
Chellaiah and Yule., 2018	Values OPNB	A	T		29.164 ± 0.194	(0.194d) °C				
Chellaiah and Yule., 2018	Values Transition NF	A	T		23.255 ± 0.166	(0.166a) °C				
Merten et al., 2016	Trend	A	C		ICMSmX					

Reference	Values type	Type	Comparation or Transition	Season	Temperature	Units	Latent Heat	Units	Sensible Heat	Units
Merten et al., 2016	Values OP	A	C		25	°C				
Merten et al., 2016	Values Transition	A	C		Similar					
Merten et al., 2016	Values Transition	A	C		Lower					

Table B.8 Studies addressing fluxes, trends of change, and values for the variables Precipitation, Relative Humidity, Vapor Pressure Deficit. Table conventions can be found in Table B.3

Reference	Values type	Type	Comparation or Transition	Season	Precipitation	Units	Relative Humidity	Units	Vapor Pressure Deficit	Units
Fowler et al., 2011	Trend	A	C		DFMReB					
Fowler et al., 2011	Values OP	A	C		2,1	mm day-1				
Fowler et al., 2011	Values Transition	A	C		13	mm day-1				
Adnan et al., 2011	Trend	A	T		QFZMaX					
Adnan et al., 2011	Values OP	A	T							
Adnan et al., 2011	Values Transition	A	T							
Radersma et al., 1996	Trend	A	C	D					ZPlX	

Reference	Values type	Type	Comparation or Transition	Season	Precipitation	Units	Relative Humidity	Units	Vapor Pressure Deficit	Units
Radersma et al., 1996	Values OP	A	C	D						
Radersma et al., 1996	Values Transition	A	C	D						
Radersma et al., 1996	Trend	A	C	R					ZSmX	
Radersma et al., 1996	Values OP	A	C	R						
Radersma et al., 1996	Values Transition	A	C	R						
Radersma et al., 1996	Trend	A	C	D					ZPlX	
Radersma et al., 1996	Values OP	A	C	D						
Radersma et al., 1996	Values Transition	A	C	D						
Radersma et al., 1996	Trend	A	C	R					ZSmX	
Radersma et al., 1996	Values OP	A	C	R						
Radersma et al., 1996	Values Transition	A	C	R						
Banabas et al., 2008	Trend	A			MSmG					
Banabas et al., 2008	Values OP	A								
Banabas et al., 2008	Values Transiti	A								

Reference	Values type	Type	Comparation or Transition	Season	Precipitation	Units	Relative Humidity	Units	Vapor Pressure Deficit	Units
	on									
Röll et al., 2015	Trend	A							YPlG	
Röll et al., 2015	Values OP	A								
Röll et al., 2015	Values Transition	A								
Röll et al., 2015	Trend	A							MPlG	
Röll et al., 2015	Values OP	A								
Röll et al., 2015	Values Transition	A								
Meijide et al., 2018	Trend	A	T				DFZSmG		IFZSmG	
Meijide et al., 2018	Values OP	A	T				91.3 ± 0.8	(0.8c) %	359 ± 38c	Pa
Meijide et al., 2018	Values Transition	A	T				95.6 ± 1.0	(1.0a) %	169 ± 39a	Pa
Nainar et al., 2018	Trend	A	T							
Nainar et al., 2018	Values OP	A	T							
Nainar et al., 2018	Values Transition	A	T							
Nainar et al., 2018	Trend	A	T							
Nainar et	Values	A	T							

Reference	Values type	Type	Comparation or Transition	Season	Precipitation	Units	Relative Humidity	Units	Vapor Pressure Deficit	Units
al., 2018	OP									
Nainar et al., 2018	Values Transition	A	T							
Nainar et al., 2018	Trend	A	T							
Nainar et al., 2018	Values OP	A	T							
Nainar et al., 2018	Values Transition	A	T							
Nainar et al., 2018	Trend	A	T							
Nainar et al., 2018	Values OP	A	T							
Nainar et al., 2018	Values Transition	A	T							
Nainar et al., 2018	Trend	A	T		DFMReG					
Nainar et al., 2018	Values OP	A	T		2680	mm				
Nainar et al., 2018	Values Transition	A	T		3504	mm				
Nainar et al., 2018	Trend	A	T		DFMReG					
Nainar et al., 2018	Values OP	A	T		2680	mm				
Nainar et al., 2018	Values Transition	A	T		2904	mm				

Reference	Values type	Type	Comparation or Transition	Season	Precipitation	Units	Relative Humidity	Units	Vapor Pressure Deficit	Units
Nainar et al., 2018	Trend	A	T		DFMReG					
Nainar et al., 2018	Values OP	A	T		2680	mm				
Nainar et al., 2018	Values Transition	A	T		2494	mm				
Nainar et al., 2018	Trend	A	T		DFMReG					
Nainar et al., 2018	Values OP	A	T		2680	mm				
Nainar et al., 2018	Values Transition	A	T		2397	mm				
Meijide et al., 2017	Trend	A	T		NZSmG					
Meijide et al., 2017	Values OP	A	T		1834	mm				
Meijide et al., 2017	Values Transition	A	T							
Meijide et al., 2017	Trend	A	T		MZSmG					
Meijide et al., 2017	Values OP	A	T		1251	mm				
Meijide et al., 2017	Values Transition	A	T							
Cock et al., 2016	Trend	A			MSmX					
Cock et al., 2016	Values OP	A								

Reference	Values type	Type	Comparation or Transition	Season	Precipitation	Units	Relative Humidity	Units	Vapor Pressure Deficit	Units
Cock et al., 2016	Values Transition	A								

Table B.9 Studies addressing fluxes, trends of change, and values for the variables Gross Primary Productivity, Carbon Secuestration. Table conventions can be found in Table B.3

Reference	Values type	Type	Comparation or Transition	Season	Gross Primary Productivity	Units	Carbon Sequestration	Units
Manoli et al 2018	Trend	A	T					
Manoli et al 2018	Values OP	A	T					
Manoli et al 2018	Values Transition	A	T					
Manoli et al 2018	Trend	A	T		IFMPlG			
Manoli et al 2018	Values OP	A	T		3000-4400	gC m-2 yr-1		
Manoli et al 2018	Values Transition	A	T		2250-3300	gC m-2 yr-1		
Sumarga et al., 2016	Trend	B					QFZReX	
Sumarga et al., 2016	Values OP	B						
Sumarga et al., 2016	Values Transition	B						

Table B.10 Studies addressing fluxes, trends of change, and values for the variables Stomatal Conductance, Carbon transport. Table conventions can be found in Table B.3

Reference	Values type	Type	Comparation or Transition	Season	Stomatal Conductance	Units	Carbon Transport	Where Carbon	Units
Koh et al., 2011	Trend	B	T				DPMMaX	AGB	
Koh et al., 2011	Values OP	B	T				5.1 ± 1.1		Mg/ha y-1
Koh et al., 2011	Values Transition	B	T				10.3 ± 2.8		Mg/ha y-1
Brunn et al., 2013	Trend	B	T				QCYSmX	SOC	
Brunn et al., 2013	Values OP	B	T						
Brunn et al., 2013	Values Transition	B	T						
Brunn et al., 2013	Trend	B	T						
Brunn et al., 2013	Values OP	B	T				QCMSmX	SOC	
Brunn et al., 2013	Values Transition	B	T						
Da Silva et al., 2016	Trend	B	C	R			ICZSmG	SOC	
Da Silva et al., 2016	Values OP	B	C	R			0.9 +- 0.07		Mg/ha yr-1
Da Silva et al., 2016	Values Transition	B	C	R			0.64 +- 0.07		Mg/ha yr-1
Da Silva et al., 2016	Trend	B		D			DCZSmG	SOC	
Da Silva et al., 2016	Values OP	B		D			0.64 +- 0.07		Mg/ha yr-1
Da Silva et	Values	B		D			0.9 +- 0.07		Mg/ha yr-1

Reference	Values type	Type	Comparation or Transition	Season	Stomatal Conductance	Units	Carbon Transport	Where Carbon	Units
al., 2016	Transition								
Sommer et al., 2000	Trend	B	C				DFZSmG	SOC	
Sommer et al., 2000	Values OP	B	C						
Sommer et al., 2000	Values Transition	B	C						
Couwenberg and Hooijer., 2013	Trend	B	C	R			ECYSmX	Carbon loss	
Couwenberg and Hooijer., 2013	Values OP	B	C	R					
Couwenberg and Hooijer., 2013	Values Transition	B	C	R					
Couwenberg and Hooijer., 2013	Trend	B	C	R			ECMSmX	Carbon loss	
Couwenberg and Hooijer., 2013	Values OP	B	C	R					
Couwenberg and Hooijer., 2013	Values Transition	B	C	R					
Marwanto	Trend	B					PMSmG		

Reference	Values type	Type	Comparation or Transition	Season	Stomatal Conductance	Units	Carbon Transport	Where Carbon	Units
and Agus., 2014									
Marwanto and Agus., 2014	Values OP	B							
Marwanto and Agus., 2014	Values Transition	B							
Frazao et al., 2014	Trend	B	C				QFMSmG	SOC	
Frazao et al., 2014	Values OP	B	C						
Frazao et al., 2014	Values Transition	B	C						
Frazao et al., 2014	Trend	B	C				QCMSmG	SOC	
Frazao et al., 2014	Values OP	B	C						
Frazao et al., 2014	Values Transition	B	C						
Dufrene et al., 1992	Trend	A		D	ZPlG				
Dufrene et al., 1992	Values OP	A		D	4.1+-1.0	mm s-1			
Dufrene et al., 1992	Values Transition	A		D					
Dufrene et al., 1992	Trend	A		R	ZPlG				
Dufrene et al., 1992	Values OP	A		R	6.6+-0.5	mm s-1			
Dufrene et al., 1992	Values Transition	A		R					

Reference	Values type	Type	Comparation or Transition	Season	Stomatal Conductance	Units	Carbon Transport	Where Carbon	Units
Frazao et al., 2014	Trend	B	T				DFYSmG	SOC	
Frazao et al., 2014	Values OP	B	T						
Frazao et al., 2014	Values Transition	B	T						
Marwanto et al., 2014	Trend	B					PSmG		
Marwanto et al., 2014	Values OP	B					46±30		Mg ha-1 yr-1
Marwanto et al., 2014	Values Transition	B							
Matysec et al., 2018	Trend	A	T				PMSmX	SOC	
Matysec et al., 2018	Values OP	A	T						
Matysec et al., 2018	Values Transition	A	T						
Allen et al., 2015	Trend	A	T				DFMSmG	SOC	
Allen et al., 2015	Values OP	A	T				1.8 ± 0.2	SOC	(kg C m-2) 4
Allen et al., 2015	Values Transition	A	T				2.6 ± 0.2	SOC	(kg C m-2) 4
Allen et al., 2015	Trend	A	T				FMSmG	SOC	
Allen et al., 2015	Values OP	A	T				3.5 ± 0.2	SOC	(kg C m-2) 4
Allen et al., 2015	Values Transition	A	T				3.3 ± 0.5	SOC	(kg C m-2) 4
Merten et al., 2016	Trend	A	C				DCMSmX		

Reference	Values type	Type	Comparation or Transition	Season	Stomatal Conductance	Units	Carbon Transport	Where Carbon	Units
Merten et al., 2016	Values OP	A	C				2,1		%
Merten et al., 2016	Values Transition	A	C				Similar		
Merten et al., 2016	Values Transition	A	C				Higher		
Tonks et al 2017	Trend	B	C				DFMSmX	SOC	
Tonks et al 2017	Values OP	B	C				497 ± 157		Mg ha−1
Tonks et al 2017	Values Transition	B	C				975 ± 151		Mg ha−1
Tonks et al 2017	Trend	B	C				IFNSmX		
Tonks et al 2017	Values OP	B	C				1050 +- 150		Mg ha−1
Tonks et al 2017	Values Transition	B	C				975 ± 151		Mg ha−1
Goodrick et al 2015	Trend	B	C				IVMSmG	SOC	
Goodrick et al 2015	Values OP	B	C						
Goodrick et al 2015	Values Transition	B	C						

Table B.11 Studies addressing fluxes, trends of change, and values for the variables Nutrient transport, Biomass, sap Flow. Table conventions can be found in Table B.3

Reference	Values type	Type	Comparation or Transition	Season	Nutrient Transport	Units	Biomass	Units	Sap Flow	Units
Koh et al., 2011	Trend	B	T				DPMMaX			
Koh et al., 2011	Values OP	B	T				24,2 ± 8,1	Mg/ha		
Koh et al., 2011	Values Transition	B	T				179,7 ± 38,2	Mg/ha		
Oktarita et al., 2017	Trend	B			SmX					
Oktarita et al., 2017	Values OP	B			20	N2O-N ha-1				
Oktarita et al., 2017	Values Transition	B								
Marwanto and Agus., 2014	Trend	B			PMSmG					
Marwanto and Agus., 2014	Values OP	B			N = 23±4, P= 0.2±0.0, K = 0.3±0.0	g Kg−1				
Marwanto and Agus., 2014	Values Transition	B								
Dufrene et al., 1992	Trend	A		D			ZPlG	Root system		
Dufrene et al., 1992	Values OP	A		D			30.5	tDM ha-1		
Dufrene et al., 1992	Values Transition	A		D						
Dufrene et al., 1992	Trend	A		R			ZPlG	Root system		

Reference	Values type	Type	Comparation or Transition	Season	Nutrient Transport	Units	Biomass	Units	Sap Flow	Units
Dufrene et al., 1992	Values OP	A		R			30.5	tDM ha-1		
Dufrene et al., 1992	Values Transition	A		R						
Banabas et al., 2008	Trend	A			MSmG					
Banabas et al., 2008	Values OP	A								
Banabas et al., 2008	Values Transition	A								
Röll et al., 2015	Trend	A							YPlG	
Röll et al., 2015	Values OP	A								
Röll et al., 2015	Values Transition	A								
Röll et al., 2015	Trend	A							MPlG	
Röll et al., 2015	Values OP	A								
Röll et al., 2015	Values Transition	A								
Bayona et al., 2016	Trend	A							YPlG	Max values
Bayona et al., 2016	Values OP	A							180 +- 40	cm3 h-1
Bayona et al., 2016	Values Transition	A								
Rivera et al., 2016	Trend	A			NPlG					
Rivera et al., 2016	Values OP	A								

Reference	Values type	Type	Comparation or Transition	Season	Nutrient Transport	Units	Biomass	Units	Sap Flow	Units
Rivera et al., 2016	Values Transition	A								
Carlson et al., 2012	Trend	B	S		QFZMeG		QFZMeG			
Carlson et al., 2012	Values OP	B	S		0,342	MtC·y −1	(5.97) A 0.62	tC·ha−1		
Carlson et al., 2012	Values Transition	B	S							
Carlson et al., 2013	Trend	B	S		QFZMeG		QFZMeG			
Carlson et al., 2013	Values OP	B	S							
Carlson et al., 2013	Values Transition	B	S							
Babel et al., 2015	Trend	A	S		DCZMeG					
Babel et al., 2015	Values OP	A	S							
Babel et al., 2015	Values Transition	A	S							
Frazao et al., 2014	Trend	B	T		DFYSmG					
Frazao et al., 2014	Values OP	B	T							
Frazao et al., 2014	Values Transition	B	T							
Kurniawan et al., 2018	Trend	A	C		QFMSmG					
Kurniawan et al., 2018	Values OP	A	C		0.995 (0.001)	mg N m−2 d −1 / mg N m−2 d −1				
Kurniawan	Values	A	C		0.997	mg N m−2 d				

Reference	Values type	Type	Comparation or Transition	Season	Nutrient Transport	Units	Biomass	Units	Sap Flow	Units
et al., 2018	Transition				(0.000)	−1 / mg N m−2 d −1				
Kurniawan et al., 2018	Trend	A	C		QFMSmG					
Kurniawan et al., 2018	Values OP	A	C		0.998 (0.001)	mg N m−2 d −1 / mg N m−2 d −1				
Kurniawan et al., 2018	Values Transition	A	C		0.999 (0.000)	mg N m−2 d −1 / mg N m−2 d −1				
Luke et al., 2017	Trend	A	T		FZSmG					
Luke et al., 2017	Values OP	A	T		0,74	mg L-1				
Luke et al., 2017	Values Transition	A	T		2.69 ± 2.63	mg L-1				
Luke et al., 2017	Trend	A	T		FZSmG					
Luke et al., 2017	Values OP	A	T		0,74	mg L-1				
Luke et al., 2017	Values Transition	A	T		0.64 ± 0.63	mg L-1				
Luke et al., 2017	Trend	A	T		FZSmG					
Luke et al., 2017	Values OP	A	T		0,74	mg L-1				
Luke et al., 2017	Values Transition	A	T		0.56 ± 0.31	mg L-1				
Chellaiah and Yule., 2018	Trend	A	T		FZSmG					
Chellaiah	Values	A	T		0.703 ±	(0.59–0.80)b				

Reference	Values type	Type	Comparation or Transition	Season	Nutrient Transport	Units	Biomass	Units	Sap Flow	Units
and Yule., 2018	OPF				0.061 (0.59–0.80)	(µg/ml)				
Chellaiah and Yule., 2018	Values OPOP	A	T		0.533 ± 0.094 (0.35–0.66)	(0.35–0.66)ab (µg/ml)				
Chellaiah and Yule., 2018	Values OPNB	A	T		0.830 ± 0.060 (0.71–0.90)	(0.71–0.90)b (µg/ml)				
Chellaiah and Yule., 2018	Values Transition NF	A	T		0.290 ± 0.066 (0.16–0.34)	(0.16–0.34)a (µg/ml)				

Table B.12 Studies addressing fluxes, trends of change, and values for the variables Soil Moisture, Groundwater, Recharge or Runoff. Table conventions can be found in Table B.3

Reference	Values type	Type	Comparation or Transition	Season	Soil Moisture	Units	Depth Average	Groundwater	Units	Recharge or Runoff	Units
Couwenberg and Hooijer., 2013	Trend	B	C	R				ECYSmX			
Couwenberg and Hooijer., 2013	Values OP	B	C	R							
Couwenberg and Hooijer., 2013	Values Transition	B	C	R							
Couwenberg and Hooijer., 2013	Trend	B	C	R				ECMSmX			
Couwenberg and Hooijer.,	Values OP	B	C	R							

Reference	Values type	Type	Comparation or Transition	Season	Soil Moisture	Units	Depth Average	Groundwater	Units	Recharge or Runoff	Units
2013											
Couwenberg and Hooijer., 2013	Values Transition	B	C	R							
Manoli et al 2018	Trend	A	T								
Manoli et al 2018	Values OP	A	T								
Manoli et al 2018	Values Transition	A	T							Pending	
Manoli et al 2018	Trend	A	T							300-2800	mm yr −1
Manoli et al 2018	Values OP	A	T								
Manoli et al 2018	Values Transition	A	T								
Algeet-Abarquero et al., 2015	Trend	A	C		ZSmG						
Algeet-Abarquero et al., 2015	Values OP	A	C								
Algeet-Abarquero et al., 2015	Values Transition	A	C								
Algeet-Abarquero et al., 2015	Trend	A	C		ZSmG						
Algeet-Abarquero et al., 2015	Values OP	A	C								
Algeet-	Values	A	C								

Reference	Values type	Type	Comparation or Transition	Season	Soil Moisture	Units	Depth Average	Groundwater	Units	Recharge or Runoff	Units
Abarquero et al., 2015	Transition										
Dufrene et al., 1992	Trend	A		D	ZPlG						
Dufrene et al., 1992	Values OP	A		D							
Dufrene et al., 1992	Values Transition	A		D							
Dufrene et al., 1992	Trend	A		R	ZPlG						
Dufrene et al., 1992	Values OP	A		R							
Dufrene et al., 1992	Values Transition	A		R							
Radersma et al., 1996	Trend	A	C	D	ZPlX						
Radersma et al., 1996	Values OP	A	C	D							
Radersma et al., 1996	Values Transition	A	C	D							
Radersma et al., 1996	Trend	A	C	R	ZSmX						
Radersma et al., 1996	Values OP	A	C	R							
Radersma et al., 1996	Values Transition	A	C	R							
Radersma et al., 1996	Trend	A	C	D	ZPlX						
Radersma et al., 1996	Values OP	A	C	D							
Radersma et al., 1996	Values Transition	A	C	D							

Reference	Values type	Type	Comparation or Transition	Season	Soil Moisture	Units	Depth Average	Groundwater	Units	Recharge or Runoff	Units
Radersma et al., 1996	Trend	A	C	R	ZSmX						
Radersma et al., 1996	Values OP	A	C	R							
Radersma et al., 1996	Values Transition	A	C	R							
Nelson et al., 2006	Trend	A			MSmG						
Nelson et al., 2006	Values OP	A									
Nelson et al., 2006	Values Transition	A									
Henson et al., 2007	Trend	A			MSmG						
Henson et al., 2007	Values OP	A									
Henson et al., 2007	Values Transition	A									
Banabas et al., 2008	Trend	A							MSmG		
Banabas et al., 2008	Values OP	A									
Banabas et al., 2008	Values Transition	A									
Carlson et al., 2013	Trend	B	S								
Carlson et al., 2013	Values OP	B	S								
Carlson et al., 2013	Values Transition	B	S								
Wösten et al., 2006	Trend	A	S					DPZReX			

Reference	Values type	Type	Comparation or Transition	Season	Soil Moisture	Units	Depth Average	Groundwater	Units	Recharge or Runoff	Units
Wösten et al., 2006	Values OP	A	S					2 to 3	m		
Wösten et al., 2006	Values Transition	A	S								
Tarigan et al., 2018	Trend	A	T							QFMMeG	
Tarigan et al., 2018	Values OP	A	T								
Tarigan et al., 2018	Values Transition	A	T								
Kurniawan et al., 2018	Trend	A	C							IFMSmG	
Kurniawan et al., 2018	Values OP	A	C							761	mm yr−1
Kurniawan et al., 2018	Values Transition	A	C							545	mm yr−1
Kurniawan et al., 2018	Trend	A	C							IFMSmG	
Kurniawan et al., 2018	Values OP	A	C							1087	mm yr−1
Kurniawan et al., 2018	Values Transition	A	C							722	mm yr−1
Sahat et al., 2016	Trend	A	S								
Sahat et al., 2016	Values OP	A	S								
Sahat et al., 2016	Values Transition	A	S							73.6 SD 4.7	%
Sahat et al., 2016	Values Transition	A								41.7 SD 5.7	%
Sahat et al., 2016	Values Transition	A								45.6 SD 18.7	%

Reference	Values type	Type	Comparation or Transition	Season	Soil Moisture	Units	Depth Average	Groundwater	Units	Recharge or Runoff	Units
Sahat et al., 2016	Values Transition	A								53.4 SD 18.8	%
Tonks et al 2017	Trend	B	C		DFMSmX	SVWC					
Tonks et al 2017	Values OP	B	C		56.56 ± 21	%					
Tonks et al 2017	Values Transition	B	C		82.3 ± 28	%					
Tonks et al 2017	Trend	B	C		DFNSmX	SVWC					
Tonks et al 2017	Values OP	B	C		33.3 ± 9	%					
Tonks et al 2017	Values Transition	B	C		82.3 ± 28	%					

Table B.13 Studies addressing fluxes, trends of change, and values for the variables Water Temperature, Overland Flow, Evaporation. Table conventions can be found in Table B.3

Reference	Values type	Type	Comparation or Transition	Season	Water Temperature	Units	Overland Flow	Units	Evaporation	Units
Carlson et al., 2015	Trend	A	C		IFYReG					
Carlson et al., 2015	Values OP	A	C		29 +- 1.8	°C				
Carlson et al., 2015	Values Transition	A	C		27 ± 1.1	°C				
Carlson et al., 2015	Trend	A	C		IFMReG					
Carlson et al., 2015	Values OP	A	C		28+-2.5	°C				

Reference	Values type	Type	Comparation or Transition	Season	Water Temperature	Units	Overland Flow	Units	Evaporation	Units
Carlson et al., 2015	Values Transition	A	C		27 ± 1.1	°C				
Algeet-Abarquero et al., 2015	Trend	A	C				IVZSmG			
Algeet-Abarquero et al., 2015	Values OP	A	C							
Algeet-Abarquero et al., 2015	Values Transition	A	C							
Algeet-Abarquero et al., 2015	Trend	A	C				IFZSmG			
Algeet-Abarquero et al., 2015	Values OP	A	C							
Algeet-Abarquero et al., 2015	Values Transition	A	C							
Kurniawan et al., 2018	Trend	A	C						IFMSmG	
Kurniawan et al., 2018	Values OP	A	C						408	mm yr−1
Kurniawan et al., 2018	Values Transition	A	C						155	mm yr−1
Kurniawan et al., 2018	Trend	A	C						IFMSmG	
Kurniawan et al., 2018	Values OP	A	C						459	mm yr−1
Kurniawan et al., 2018	Values Transition	A	C						157	mm yr−1

Table B.14 Studies addressing fluxes, trends of change, and values for the variables Baseflow, Crop Type. Table conventions can be found in Table B.3

Reference	Values type	Type	Comparation or Transition	Season	Baseflow	Units	Crop Type
Couwenberg and Hooijer., 2013	Trend	B	C	R			Acacia
Couwenberg and Hooijer., 2013	Values OP	B	C	R			
Couwenberg and Hooijer., 2013	Values Transition	B	C	R			
Couwenberg and Hooijer., 2013	Trend	B	C	R			Acacia
Couwenberg and Hooijer., 2013	Values OP	B	C	R			
Couwenberg and Hooijer., 2013	Values Transition	B	C	R			
Frazao et al., 2014	Trend	B	C				
Frazao et al., 2014	Values OP	B	C				
Frazao et al., 2014	Values Transition	B	C				
Frazao et al., 2014	Trend	B	C				Mixed secondary agroforest
Frazao et al., 2014	Values OP	B	C				
Frazao et al.,	Values	B	C				

Reference	Values type	Type	Comparation or Transition	Season	Baseflow	Units	Crop Type
2014	Transition						
Radersma et al., 1996	Trend	A	C	D			Cocoa
Radersma et al., 1996	Values OP	A	C	D			Cocoa
Radersma et al., 1996	Values Transition	A	C	D			Cocoa
Radersma et al., 1996	Trend	A	C	R			Cocoa
Radersma et al., 1996	Values OP	A	C	R			Cocoa
Radersma et al., 1996	Values Transition	A	C	R			Cocoa
Radersma et al., 1996	Trend	A	C	D			Rice, Maize
Radersma et al., 1996	Values OP	A	C	D			Rice, Maize
Radersma et al., 1996	Values Transition	A	C	D			Rice, Maize
Radersma et al., 1996	Trend	A	C	R			Rice, Maize
Radersma et al., 1996	Values OP	A	C	R			Rice, Maize
Radersma et al., 1996	Values Transition	A	C	R			Rice, Maize
Kurniawan et al., 2018	Trend	A	C				Loam Acrisol Soil
Kurniawan et al., 2018	Values OP	A	C				Loam Acrisol Soil
Kurniawan et al., 2018	Values Transition	A	C				Loam Acrisol Soil
Kurniawan et	Trend	A	C				Clay Acrisol Soil

Reference	Values type	Type	Comparation or Transition	Season	Baseflow	Units	Crop Type
al., 2018							
Kurniawan et al., 2018	Values OP	A	C				Clay Acrisol Soil
Kurniawan et al., 2018	Values Transition	A	C				Clay Acrisol Soil
Allen et al., 2015	Trend	A	T				Loam Acrisol Soil
Allen et al., 2015	Values OP	A	T				Loam Acrisol Soil
Allen et al., 2015	Values Transition	A	T				Loam Acrisol Soil
Allen et al., 2015	Trend	A	T				Clay Acrisol Soil
Allen et al., 2015	Values OP	A	T				Clay Acrisol Soil
Allen et al., 2015	Values Transition	A	T				Clay Acrisol Soil
Nainar et al., 2018	Trend	A	T		DFMReG		
Nainar et al., 2018	Values OP	A	T		38,43	%	PF (Primary forest)
Nainar et al., 2018	Values Transition	A	T		67,92	%	
Nainar et al., 2018	Trend	A	T		DFMReG		
Nainar et al., 2018	Values OP	A	T		38,43	%	VJR (Virgin jungle reserve)
Nainar et al., 2018	Values Transition	A	T		42,18	%	
Nainar et al., 2018	Trend	A	T		DFMReG		
Nainar et al.,	Values OP	A	T		38,43	%	LF2 (Twice-logged forest with 22

Reference	Values type	Type	Comparation or Transition	Season	Baseflow	Units	Crop Type
2018							years' regeneration)
Nainar et al., 2018	Values Transition	A	T		50,84	%	
Nainar et al., 2018	Trend	A	T		DFMReG		
Nainar et al., 2018	Values OP	A	T		38,43	%	LF3 (Multiple-logged forest with 8 years' regeneration)
Nainar et al., 2018	Values Transition	A	T		55,02	%	
Nainar et al., 2018	Trend	A	T				
Nainar et al., 2018	Values OP	A	T				PF (Primary forest)
Nainar et al., 2018	Values Transition	A	T				
Nainar et al., 2018	Trend	A	T				
Nainar et al., 2018	Values OP	A	T				VJR (Virgin jungle reserve)
Nainar et al., 2018	Values Transition	A	T				
Nainar et al., 2018	Trend	A	T				
Nainar et al., 2018	Values OP	A	T				LF2 (Twice-logged forest with 22 years' regeneration)
Nainar et al., 2018	Values Transition	A	T				
Nainar et al., 2018	Trend	A	T				
Nainar et al., 2018	Values OP	A	T				LF3 (Multiple-logged forest with 8 years' regeneration)
Nainar et al.,	Values	A	T				

Reference	Values type	Type	Comparation or Transition	Season	Baseflow	Units	Crop Type
2018	Transition						
Luke et al., 2017	Trend	A	T				
Luke et al., 2017	Values OP	A	T				
Luke et al., 2017	Values Transition	A	T				Oil Palm with buffer Strips (OPB)
Luke et al., 2017	Trend	A	T				
Luke et al., 2017	Values OP	A	T				
Luke et al., 2017	Values Transition	A	T				Logged forest (LF)
Luke et al., 2017	Trend	A	T				
Luke et al., 2017	Values OP	A	T				
Luke et al., 2017	Values Transition	A	T				Old.growth forest (OG)
Da Sato et al., 2017	Trend	A	S				Clay (< 2 µm)
Da Sato et al., 2017	Values OP	A	S				
Da Sato et al., 2017	Values Transition	A	S				0-20 cm
Da Sato et al., 2017	Trend	A	S				Silt (2-50 µm)
Da Sato et al., 2017	Values OP	A	S				
Da Sato et al., 2017	Values Transition	A	S				0-20 cm
Da Sato et al.,	Trend	A	S				Sand (50-200 µm)

Reference	Values type	Type	Comparation or Transition	Season	Baseflow	Units	Crop Type
2017							
Da Sato et al., 2017	Values OP	A	S				
Da Sato et al., 2017	Values Transition	A	S				0-20 cm
Meijide et al., 2017	Trend	A	T				1 yerar old
Meijide et al., 2017	Values OP	A	T				
Meijide et al., 2017	Values Transition	A	T				
Meijide et al., 2017	Trend	A	T				12 year old
Meijide et al., 2017	Values OP	A	T				
Meijide et al., 2017	Values Transition	A	T				
Sabajo et al., 2017	Trend	A	T				
Sabajo et al., 2017	Values OP	A	T				Palma Madura
Sabajo et al., 2017	Values Transition	A	T				Rubber
Sabajo et al., 2017	Values Transition	A	T				Acacia
Sabajo et al., 2017	Trend	A	T				
Sabajo et al., 2017	Values OP	A	T				Palma Joven
Sabajo et al., 2017	Values Transition	A	T				Urban
Sabajo et al.,	Values	A	T				clear cut

Reference	Values type	Type	Comparation or Transition	Season	Baseflow	Units	Crop Type
2017	Transition						
Satriawan et al., 2016	Trend	A	S				
Satriawan et al., 2016	Values OP	A	S				5-7 months/Slopes 15-25% (P1)
Satriawan et al., 2016	Values OP	A	S				
Satriawan et al., 2016	Values OP	A	S				
Satriawan et al., 2016	Values OP	A	S				7–25 months / slopes 15–25% (P2)
Satriawan et al., 2016	Values OP	A	S				
Satriawan et al., 2016	Values OP	A	S				
Satriawan et al., 2016	Values OP	A	S				5–7 months / slopes 30–40% (P3)
Satriawan et al., 2016	Values OP	A	S				
Satriawan et al., 2016	Values OP	A	S				
Satriawan et al., 2016	Values OP	A	S				7–25 months / slopes 30–40% (P4)
Satriawan et al., 2016	Values OP	A	S				
Satriawan et al., 2016	Values OP	A	S				
Satriawan et al., 2016	Values Transition	A	S				LC weeds allowed (T1)
Satriawan et al., 2016	Values Transition	A	S				Rice + soybeans (T2)
Satriawan et	Values	A	S				Rice + soybeans + strip M. bracteata

Reference	Values type	Type	Comparation or Transition	Season	Baseflow	Units	Crop Type
al., 2016	Transition						(T3)
Merten et al., 2016	Trend	A	C				
Merten et al., 2016	Values OP	A	C				Oil palm
Merten et al., 2016	Values Transition	A	C				Rubber plantation
Merten et al., 2016	Values Transition	A	C				Forest
Sahat et al., 2016	Trend	A	S				
Sahat et al., 2016	Values OP	A	S				
Sahat et al., 2016	Values Transition	A	S				Bare Soil
Sahat et al., 2016	Values Transition	A					Full Grass Cover
Sahat et al., 2016	Values Transition	A					Half Grass Cover
Sahat et al., 2016	Values Transition	A					Half Dry Frond

APPENDIX C: SUPPLEMENTAL INFORMATION TO CHAPTER 4

C.1 Range of the spectrometer bands. Arable Mark

Table C.1 Band spectrometer range in the Arable Mark I

Band	Arable Mark
1	440-510
2	515-555
3	565-595
4	620-690
5	690-740
6	780-900
7	930-960

C.2. Database design

A database was designed to storage the data collected by the stations (Figure C.1). This database helps to organize the data and facilitate search and storage of information. A data dictionary explains the meaning of each column and table in the database

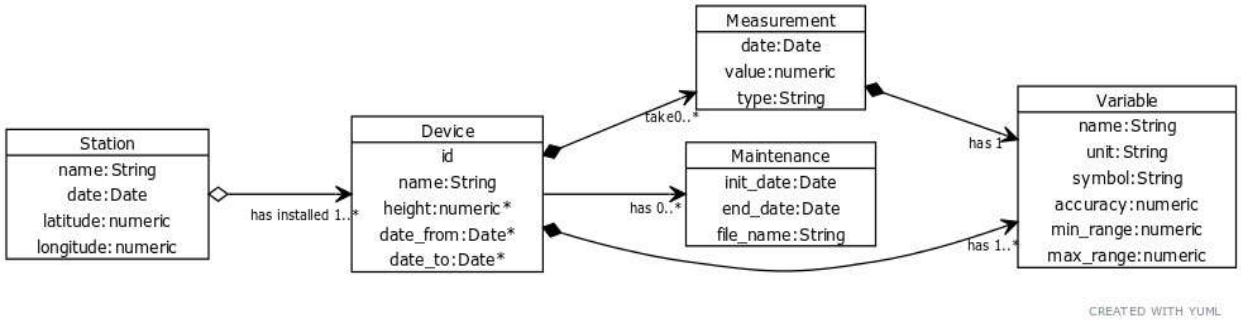

Figure C.1 Structure of the database designed to storage data from the stations. The scheme is based on the Unified Modeling Language (UML). Each box represents a table in the database. The attributes of each table are listed in each box after the title. The type of each attribute or column is described in the diagram after the semicolon (:). Connectors represent the relations among the tables that make possible retrieve the data and linked in the programming language.

Table C.2 Description of table Station

Table name: Station. Contains the list and main characteristics of each station		
Attribute or Column name	**Type of data it contains**	**Description**
name	String	Name of the station
date	Date	Date of installation
latitude	Numeric	Latitude at which the station is located
longitude	Numeric	Longitude at which the station is located

Table C.3 Description of table Device

Table name: Device. Storage information about the device		
Attribute or Column name	**Type of data it contains**	**Description**
id	String	Each sensor identification. The one assigned by the manufacture company
name	String	Name of the device
height	Numeric*	Height at which the device is placed. It can be one or many
date_from	Date*	Initial date in which the device was placed at the specific height. It can be one or many
date_to	Date*	Final date in which the device was placed at the specific height. It can be one or many

Table C.4 Description of table Measurement

Table name: Measurement. Storage data measurements		
Attribute or Column name	**Type of data it contains**	**Description**
date	date	Date in which the measurement was taken or registerd
value	Numeric	Value registered
type	String	Variable corresponding to the value measured

Table C.5 Description of table Maintenance

Table name: Maintenance. Storage the dates in which the maintenance was done at each sensor		
Attribute or Column name	**Type of data it contains**	**Description**
init_date	date	Date and time in which the maintenance started for a device
end_date	date	Date and time in which the maintenance ended for a device
filename	String	Filename in which the data was stored

Table C.6 Description of table Variable

Table name: Variable. Storage information about the variables		
Attribute or Column name	**Type of data it contains**	**Description**
name	date	Date and time in which the maintenance started for a device
unit	date	Date and time in which the maintenance ended for a device
symbol	String	Filename in which the data was stored
accuracy	Numeric	Accuracy defined for each variable and sensor
min_range	Numeric	Maximum range of the variable at a sensor
max_range	Numeric	Minimum range of the variable at a sensor

C.3. Energy balance estimates Python Code.

```
#Class EnergyBalance contain all the equations for the energy balance calculation
import sys
import os
sys.path.append(os.getcwd())
from src.resources.arablepy.physics import *
import pandas as pd
import numpy as np

class EnergyBalance:
    _J2Wm2 = 1000000
    _Ra = 461.495  # Specific gas constant for moist air in Jkg-1K-1
    _C2K_f: float = 273.15 #K
    _e = 0.622
    _Cp = 1013 #Jkg-1 K-1
    _R = 8.314462 #J/(K*mol)
    _Mv = 0.018016 #Kg/mol
    _Md = 0.028965 #Kg/mol

    # Parameters
    parameters = {'tair_fd': 'tair', 'time_fd': 'dtime', 'lat_fd': 'lat', 'long_fd': 'long',
                  'swuw_fd': 'swuw', 'swdw_fd': 'swdw', 'ea_fd':'ea_wvp','alb_fd': 'albedo'}
    def __init__(self, df=None):
        self.df = df

    """Create a data frame or a copy of the existing one to make the calculations
       The idea behind it is to use a copy of a data frame instead of the original reference to memory
       This function is only used by the methods and have no effect on the Energy Balance
calculations"""

    def _val_data_frame(self, df_local):
```

```
        if self.df is None and df_local is None:
            # Create an empty dataframe and use it for the operation
            return pd.DataFrame()  # TODO: Instead of logical error manage from the caller, use a try-catch and propagate the error
        elif df_local is not None:
            df = df_local.copy()
        else:
            df = self.df.copy()
        return df

    #TODO: Pending convert other T units. For now convert from C to K
    def convert_temperature(self, t_fd, df_local=None, inplace=False, o_unit='C', d_unit='K'):
        df = self._val_data_frame(df_local)
        if o_unit=='C' and d_unit=='K':
            f_name = t_fd + '_K'
            df[f_name] = df[t_fd] + self._C2K_f
        elif o_unit == 'K' and d_unit == 'C':
            f_name = t_fd + '_C'
            df[f_name] = df[t_fd] - self._C2K_f
        else:
            raise Exception('Working on implementing other conversions. Check o_unit and d_unit inputs')
        if inplace:
            self.df = df
        return df

# TODO: Include conversion from other units, for now, only kPa and Degree celsious
# Source: http://www.atmo.arizona.edu/students/courselinks/fall11/atmo551a/ATMO_451a_551a_files/WaterVapor.pdf

    def wvp2wvd(self, df_local, tair_fd, ea_wvp_fd, inplace=False, unit_t='C', unit_e='kPa'):
        df = self._val_data_frame(df_local)
        if unit_t == 'C' and unit_e == 'kPa':
            tair_fd_K = tair_fd + '_' + 'K'
            df[tair_fd_K] = df[tair_fd] + self._C2K_f
            ea_wvp_fd_Pa = ea_wvp_fd + '_' + 'Pa'
            df[ea_wvp_fd_Pa] = 1000 * df[ea_wvp_fd]
        df['wvd'] = df[ea_wvp_fd_Pa] / (461.5 * df[tair_fd_K])  # Units kg/m3
        if inplace:
            self.df = df
        return df
    def calc_air_density(self, pressure_fd, ea_fd, tair_fd, df_local=None, inplace=False, unit_t='C', unit_ea='kPa', unit_p='kPa'):
        df=self._val_data_frame(df_local)
        if unit_t=='C':
            tair_fd_K = tair_fd + '_' + 'K'
            df[tair_fd_K] = df[tair_fd] + self._C2K_f
        elif unit_t=='K':
            tair_fd_K = tair_fd
        if unit_p=='kPa':
            pressure_fd_Pa= pressure_fd + '_' + 'Pa'
```

```
            df[pressure_fd_Pa]= df[pressure_fd] * 1000
        elif unit_p=='Pa':
            pressure_fd_Pa = pressure_fd
        if unit_ea=='kPa':
            ea_fd_Pa=ea_fd+'_'+'Pa'
            df[ea_fd_Pa] = df[ea_fd] * 1000
        elif unit_p=='Pa':
            ea_fd_Pa = ea_fd
        df['mad'] = (df[pressure_fd_Pa]*self._Md + df[ea_fd_Pa]*(self._Mv -
self._Md))/(self._R*df[tair_fd_K])
        if inplace:
            self.df = df
        return df

    """Calc long wave radiation based on the Dong equation. Call the function for net radiation using
Dong.
        TODO: Pending to change to make an independent calculation"""
    def calc_lwdw_based_Dong(self, df_local=None, params_fd_dict=None, albedo_calc='prod',
T_untis = 'K', inplace=False):
        df = self.Rn_dong92_adapted(df_local, params_fd_dict, albedo_calc, T_untis)
        df['lwdw_fn'] = np.where(df['lwdw'].isnull(),df['lwdw_calc'],df['lwdw'])
        if inplace:
            self.df = df
        return df

    def calc_net_radiation(self, df_local=None, fields=None, inplace=False):
        """Calculate net radiation calc_net_radiation (self, df_local=None, fields=None, inplace=False):
                fields={'swdw': swdw_field, 'lwdw': lwdw_field, 'swuw': swuw_field, 'lwuw': lwuw_field}"""
        df = self._val_data_frame(df_local)
        if fields is None:
            try:
                # TODO: Create a uniform dictionary of fieldnames
                df['nr'] = df['swdw'] + df['lwdw'] + df['swuw'] + df['lwuw']
            except:
                return pd.DataFrame()
        else:
            swdw_fd=fields['swdw']
            swuw_fd=fields['swuw']
            lwdw_fd=fields['lwdw']
            lwuw_fd=fields['lwuw']
            df['nr']=df[swdw_fd] + df[lwdw_fd] + df[swuw_fd] + df[lwuw_fd]
        if inplace:
            self.df = df
        return df

    def calc_albedo(self, swdw_fd, swup_fd, df_local=None, inplace=False):

        df = self._val_data_frame(df_local)
        try:
            # TODO: Create a uniform dictionary of fieldnames
            df['albedo'] = df[swup_fd] / df[swdw_fd]
```

```
            df['albedo'] = df['albedo'].abs()
        except:
            return pd.DataFrame()
        if inplace:
            self.df = df
        return df

    """Water pressure calculation at a given height
        This function calculate the saturated water vapor pressure as well if necessary
        field_rh: field with relative humidity data
        field_air_t: field name with the air temperature
        df_local: local dataframe if not specified it uses the one in the class
        rh_percentage: Default=False, is the RH expressed as %?
        cal_swvp: if true, calculate the saturated water vapor pressure. Default: true
        equation: Implement Buck or Teten equation. Default Buck

        Output Dataframe with an additional field ea_wvp water vapor pressure

        checked 03/31/2021"""

    def calc_water_vapor_pressure(self, field_rh, field_air_t, df_local=None, rh_percentage=False,
equation='Buck_1981',
                                  cal_swvp=True, inplace=False):
        df = self._val_data_frame(df_local)
        if rh_percentage == True:
            df[field_rh] = df[field_rh] / 100
        if cal_swvp == True:
            df = self.calc_saturated_wvp(field_air_t, df, equation, inplace)
        df['ea_wvp'] = df[field_rh] * df['es_wvp']
        if inplace:
            self.df = df
        return df

    # TODO: add Buck equation when T<0
    """Units in kPa, input units T[C],
    output dataframe with additional column saturated vapor pressure: es_wvp
    checked 06/16/2021"""

    def calc_saturated_wvp(self, field_air_t, df_local=None, equation='Buck_1981', inplace=False):

        df = self._val_data_frame(df_local)

        df['es_wvp'] = 6.1121 * np.exp(
            (18.678 - df[field_air_t] / 234.5) * df[field_air_t] / (257.14 + df[field_air_t]))
        if equation == 'Teten_FAO56':
            df['es_wvp'] = 6.11 * np.exp(17.27 * df[field_air_t] / (273.3 + df[field_air_t]))
        df['es_wvp'] = df['es_wvp'] / 10  # Convert units from hPa to kPa
        if inplace:
            self.df = df
        return df
```

```
    """Calculate the VPD
        for now all the fields are by default none which means they are assumed to be calculated inside the function
        otherwise specify:
        df_local: datafame with water vapor pressure saturation and water vapor pressure. Default, inside the instance
        field_es: field name/column with saturated water vapor pressure in kPa. default name es_wvp
        field_ea: field name/column with water vapor pressure in kPa. default name ea_wvp"""

    def calc_VPD(self, df_local=None, field_es=None, field_ea=None, inplace=False):
        df = self._val_data_frame(df_local)
        f_es = 'es_wvp'
        f_ea = 'ea_wvp'
        if field_ea is not None:
            f_es = field_es
        if field_es is not None:
            f_ea = field_ea
        df['VPD'] = df[f_es]-df[f_ea]
        if inplace:
            self.df = df
        return df

    """Calculate the mixing ratio as equivalent to specific humidity
        p_fd: field name with the Pressure
        ea_wvp_fd: water vapor presure at a given height"""

    def calc_mixing_ratio(self, p_fd, ea_wvp_fd, df_local=None, suffix=None, inplace=False):
        df = self._val_data_frame(df_local)
        mr_name = 'mr'
        if suffix is not None:
            mr_name = mr_name + '_' + suffix
        # _e should be 0.622
        df[mr_name] = self._e * df[ea_wvp_fd] / df[p_fd]
        if inplace:
            self.df = df
        return df

    """Calculate virtual temperature assuming mixing ratio has been already calculated"""

    def calc_virtual_temperature(self, tair_fd, mr_fd, df_local=None, suffix=None, inplace=False):
        df = self._val_data_frame(df_local)
        tv_name = 'tv'
        if suffix is not None:
            tv_name = tv_name + '_' + suffix
        df[tv_name] = df[tair_fd] * (1 + 0.61 * df[mr_fd])
        if inplace:
            self.df = df
        return df

    """Calculate virtual potential temperature for a given height under a known virtual temperature
        p_fd has to be in KPa"""
```

```
    def calc_virtual_potential_temperature(self, p_fd, tv_fd, df_local=None, suffix=None,
inplace=False):
        df = self._val_data_frame(df_local)
        tvp_name = 'tvp'
        if suffix is not None:
            tvp_name = tvp_name + '_' + suffix
        df[tvp_name] = df[tv_fd] * (100 / df[p_fd]) ** (self._Ra / self._Cp)
        if inplace:
            self.df = df
        return df

    """Fixed to calculate at each height and have different name specified by suffix
        Output is in MJkg-1"""

    def calc_latent_heat_vaporization(self, tair_fd, df_local=None, equation='Harrison_1963',
suffix=None,
                                      inplace=False):

        df = self._val_data_frame(df_local)
        lambda_name = 'lambda'
        if suffix is not None:
            lambda_name = lambda_name + '_' + suffix
        # temperature in degree Celsius
        df[lambda_name] = 2.501 - 2.361E-3 * df[tair_fd]  # Harrison 1963. (Refs
http://www.fao.org/3/X0490E/x0490e0k.htm Gavilan y Berenguena 2007)
        if inplace:
            self.df = df
        return df

    # Reference: Brunt (1952)
    # TODO: Validate units
    def calc_psychrometric_constant(self, pressure_fd, lambda_fd, df_local=None, p_units='kPa',
suffix=None,
                                    inplace=False):

        df = self._val_data_frame(df_local)
        if p_units != 'kPa':
            raise Exception('Units different from kPa not supported yet')
        Cp = self._Cp  # Specific heat of moist air [J kg-1 C-1]
        e = self._e  # Ratio molecular weight of water vapor/dry air
        gamma_name = 'g_constant'
        if suffix is not None:
            gamma_name = gamma_name + '_' + suffix
        df[gamma_name] = Cp * df[pressure_fd] / (e * df[lambda_fd])  # kPa k-1

        if inplace:
            self.df = df
        return df

    # TODO: Validate units
```

```
    def calc_atmospheric_density(self, pressure_fd, tair_fd, ea_wvp_fd, df_local=None, tair_units='C',
                                 pressure_units='kPa', inplace=False):

        df = self._val_data_frame(df_local)

        if tair_units == 'C':
            tair_fd_K = tair_fd + '_' + 'K'
            df[tair_fd_K] = df[tair_fd] + 273.15
        elif tair_units == 'K':
            tair_fd_K = tair_fd
        # else:
        #     raise

        if pressure_units == 'kPa':
            pressure_fd_kPa = pressure_fd
            ea_wvp_fd_kPa = ea_wvp_fd
        elif pressure_units == 'Pa':
            ea_wvp_fd_kPa = ea_wvp_fd + '_' + 'kPa'
            pressure_fd_kPa = pressure_fd + '_' + 'kPa'
            df[pressure_fd_kPa] = df[pressure_fd] * 1000
            df[ea_wvp_fd_kPa] = df[ea_wvp_fd] * 1000
        # From FAO http://www.fao.org/3/X0490E/x0490e0k.htm#TopOfPage
        df['air_density'] = df[tair_fd_K] * (3.486 * df[pressure_fd_kPa] - 1.318 * df[ea_wvp_fd_kPa])

        if inplace:
            self.df = df
        return df

    def latent_heat_2s(self, wind_up_fd, wind_dw_fd, ma_up_fd, ma_dw_fd, tair_up_fd, tair_dw_fd,
mr_up_fd, mr_dw_fd,
                       # lambda_up_fd, lambda_dw_fd,
                       inplace=False, ma_type='D', unit_t='C', unit_ea='kPa', unit_p='kPa',
                       p_up_fd=None, p_dw_fd=None, df_local=None):
        """ Recieve a dataframe with date and the corresponding rows up and down values to calculate
latent heat fluxes at two co-located sites arrange in the vertical"""
        # TODO: Correct the method if is incorrect
        """ Inputs:
            df_local: Dataframe with the infomation
            wind_up_fd: Field or column with horizontal wind at point X1
            wind_dw_fd: Field or column with horizontal wind at point X2
            ma_up_fd: Field or column with moist air property at point X1. It can be density or pressure.
Specify type in wv_type
            ma_dw_fd: Field or column with moist air property at point X2
            ma_type: If P, it will convert pressure to density to calculate latent heat, if D it will use the
wv_up wv_dw columns as moist air density. Default D
            tair_up_fd: Field or Column with values of air temperature at point X1
            tair_dw_fd: Field or Column with values of air temperature at point X2
            mr_up_fd: Field or Column with values of mixing ration at point X1
            mr_dw_fd: Field or Column with values of mixing ration at point X2"""
        # TODO: Validate Null data and empty to non-existen dataframes/fields
        df = self._val_data_frame(df_local)
```

```
        if ma_type == 'P':  # Convert from air Vapor Pressure to air Pressure Density
            if p_up_fd is not None and p_dw_fd is not None:
                # if tair_up_fd is None or tair_dw_fd is None:
                #     raise Exception('Air Temperature needed to convert Water Vapor Pressure to Water
Pressure Density')
                df = self.calc_air_density(df, pressure_fd=p_up_fd, ea_fd=ma_up_fd, tair_fd=tair_up_fd,
                                           inplace=inplace, unit_t=unit_t, unit_p=unit_p, unit_ea=unit_ea)
                df.rename(columns={'mad': 'up_mad'}, inplace=True)
                mad_up_fd = 'up_mad'
                df = self.calc_air_density(df, pressure_fd=p_dw_fd, ea_fd=ma_dw_fd, tair_fd=tair_dw_fd,
                                           inplace=inplace, unit_t=unit_t, unit_p=unit_p, unit_ea=unit_ea)
                df.rename(columns={'mad': 'dw_mad'}, inplace=True)
                mad_dw_fd = 'dw_mad'
        else:
            mad_dw_fd = ma_dw_fd
            mad_up_fd  = ma_up_fd
        # Calculate delta fluxes first
        df['delta_w'] = df[wind_up_fd] - df[wind_dw_fd]
        df['delta_mr'] = df[mr_up_fd] - df[mr_dw_fd]
        df['avg_mad'] = df[[mad_up_fd, mad_dw_fd]].mean(axis=1)
        #Assume latent heat vaporization calculated
        df['tair_mean'] = df[[tair_up_fd, tair_dw_fd]].mean(axis=1)
        df = self.calc_latent_heat_vaporization('tair_mean', df, inplace=inplace)
        df['LambdaE'] = df['lambda'] * df['avg_mad']* df['delta_w'] * df['delta_mr']  # Mega joules
        df['LambdaE'] = df['LambdaE'] * self._J2Wm2  # Convert to J or W/m2
        if inplace:
            self.df = df
        return df

    def calc_sensible_heat_2s(self, psychrometric_up_fd, psychrometric_dw_fd, tvp_up_fd, tvp_dw_fd,
                              wind_up_fd, wind_dw_fd,ma_up_fd, ma_dw_fd,tair_up_fd, tair_dw_fd,
ma_type='D', unit_t='C',
                              unit_ea='kPa', unit_p='kPa', p_up_fd=None, p_dw_fd=None, df_local=None,
inplace=False):
        df = self._val_data_frame(df_local)
        if ma_type == 'P':  # Convert from air Pressure to air Density
            if p_up_fd is not None and p_dw_fd is not None:
                df = self._convert_updw_ap2ad(df, p_up_fd, p_dw_fd, ma_up_fd, ma_dw_fd, tair_up_fd,
tair_dw_fd, unit_t,
                                              unit_p, unit_ea, inplace)
                mad_up_fd = 'up_mad'
                mad_dw_fd = 'dw_mad'

        else:
            mad_dw_fd = ma_dw_fd
            mad_up_fd  = ma_up_fd
        #Calculate independent terms
        #avg air density
        df['avg_mad'] = df[[mad_up_fd, mad_dw_fd]].mean(axis=1)
        #avg phsychrometric constant
        df['mean_g_constant'] = (df[psychrometric_dw_fd] + df[psychrometric_up_fd]) / 2
```

```
        #delta virtual temperature
        df['delta_tvp'] = df[tvp_dw_fd] - df[tvp_up_fd]
        #delta wind speed
        df['delta_w'] = df[wind_dw_fd] - df[wind_up_fd]
        df['SH']=df['avg_mad']*df['mean_g_constant']*df['delta_tvp']*df['delta_w']
        if inplace==True:
            self.df = df
        return df

    def _convert_updw_ap2ad(self, df, p_up_fd,p_dw_fd,ma_up_fd, ma_dw_fd,tair_up_fd,
tair_dw_fd,unit_t='C', unit_p='kPa', unit_ea='kPa', inplace=False):
        # if tair_up_fd is None or tair_dw_fd is None:
        #     raise Exception('Air Temperature needed to convert Water Vapor Pressure to Water Pressure
Density')
        df=self._val_data_frame(df)
        df = self.calc_air_density(df, pressure_fd=p_up_fd, ea_fd=ma_up_fd, tair_fd=tair_up_fd,
                                   inplace=inplace, unit_t=unit_t, unit_p=unit_p, unit_ea=unit_ea)
        df.rename(columns={'mad': 'up_mad'}, inplace=True)

        df = self.calc_air_density(df, pressure_fd=p_dw_fd, ea_fd=ma_dw_fd, tair_fd=tair_dw_fd,
                                   inplace=inplace, unit_t=unit_t, unit_p=unit_p, unit_ea=unit_ea)
        df.rename(columns={'mad': 'dw_mad'}, inplace=True)

        if inplace:
            self.df=df
        return df
    # virtual potential Temperature must be in C
    # Presure must be in kPa
    # Psychrometric constant must be in kPaC-1
    def calc_bowen_ratio(self, psychrometric_up_fd, psychrometric_dw_fd, tvp_up_fd, tvp_dw_fd,
                         ea_wvp_up_fd, ea_wvp_dw_fd, df_local=None,
                         inplace=False):
        df = self._val_data_frame(df_local)
        df['mean_g_constant']=(df[psychrometric_dw_fd]+df[psychrometric_up_fd])/2
        df['delta_tvp'] = df[tvp_dw_fd] - df[tvp_up_fd]
        df['delta_wvp'] = df[ea_wvp_dw_fd] - df[ea_wvp_up_fd]
        df['bowen_r'] = df['mean_g_constant'] * df['delta_tvp'] / df['delta_wvp']

        if inplace:
            self.df = df
        return df

    def Rn_dong92_adapted(self,df_local=None, params_fd_dict=None, albedo_calc='prod',
T_untis='K'):
        """albedo_calc= 'prod' calc from arable
                        'done' input as a field in params in the alb_fd variable
                        'dong' calculate it with Dong, 1992 eq"""
        df = self._val_data_frame(df_local)

        if params_fd_dict is None:
            params_fd_dict = self.parameters
```

```
tair_fd=params_fd_dict['tair_fd']
time_fd=params_fd_dict['time_fd']
lat_fd = params_fd_dict['lat_fd']
long_fd = params_fd_dict['long_fd']
swuw_fd= params_fd_dict['swuw_fd']
swdw_fd= params_fd_dict['swdw_fd']
ea_fd=params_fd_dict['ea_fd']

#Calc temperatures
if T_untis=='C':
    df['tair_K']=df[tair_fd]+ self._C2K_f
    tair_fd='tair_K'
#TODO:Pending the other conversions

# Temperatures
Tk = df[tair_fd]
To = df[tair_fd]  # clear sky temp
Tc = df[tair_fd]  # cloud top temp
Ts = df[tair_fd]  # surface temp; per Dong p472 set to air temp at 1.5m

# solar angles
sza = solar_psi_(df[time_fd].dt, df[lat_fd], df[long_fd])
cossza = np.cos(sza)
theta = 90. - sza * 180. / np.pi  # solar altitude in degrees, cf Dong eqn 15

# Irradiance, Dong eqn 5
if 'SWP' not in df.columns:
    df['SWP'] = SWP_(df[time_fd].dt, df[lat_fd], df[long_fd])

I = df.SWP

# albedo, Dong eqn 6
if albedo_calc == 'prod':
    # use our swdw/swuw
    alpha = (-1.0 * df[swuw_fd]) / df[swdw_fd]
    # clip to between 0 and 0.5 based on Adam's rec
    alpha = alpha.clip(0, 0.5)
elif albedo_calc=='done':
    alpha = df[params_fd_dict['alb_fd']]
else:
    # use Dong version
    if 'Kt' not in df.columns:
        df['Kt'] = Kt_(df[swdw_fd], df[time_fd].dt, df[lat_fd], df[long_fd])
    Rs_I = df.Kt
    alpha = 0.00158 * theta + 0.386 * exp(-0.0188 * theta)
    alpha[df.Kt < 0.375] = 0.26

# emissivity
epss = 0.98  # surface emissivity. Dong assumes 0.98, but CIMIS uses
epsc = 1.  # assumed cloud emissivity of 1.0
```

```
        # clear sky emissivity, Dong eqn 10
        # ea is in mbar in this eqn
        epso = 1.08 * (1.0 - np.exp(-(df[ea_fd] * 10.) ** (Tk / 2016.)))

        # fraction of cloud cover
        Ra = (0.79 - 3.75 / theta) * I
        Ra[theta < 10] = (0.79 - 3.75 / 10.) * I  # handles low zenith angles
        c = (1.333 - 1.333 * (df[swdw_fd] / Ra)) ** 0.294
        c = np.clip(c, 0, 1)

        # Rn, equation 19 p 477
        E = 0.89

        SWdw = E * df[swdw_fd]
        SWuw = E * alpha * df[swuw_fd]
        LWdw = E * epss * (epso * (1. - c) * SBC * (To ** 4) + c * SBC * (Tc ** 4))  # why Tc if the
paper has Ta here too
        LWuw = E * epss * SBC * (Ts ** 4)
        df['lwdw_calc']=LWdw
        df['Rn_Dong'] = SWdw - SWuw + SWdw - LWdw

        return df
```

```
import pandas as pd
import os
from datetime import datetime as dt
from datetime import date, timedelta
from pytz import timezone

# from itertools import tee, izip
#Useful to call directy to modules and classes storage in different scripts (find_dotenv has to be
installed first)
#DataQuality class
import sys
from dotenv import find_dotenv
sys.path.append(os.path.dirname(find_dotenv()))

from weather_data import WeatherFile

class DataQuality:

    def filter_maintenance(self, df, date_field, st, sensor_ir=None):
        # open maintanance file
        dw = os.getcwd()
        os.chdir("..")
        dir_name = os.getcwd() + "/data/"
        file_name = 'date_maintenance.csv'
        os.chdir(dw)
        filter_dates = pd.read_csv(dir_name + file_name, sep=',')
```

```
        # filter stations that were taken off. Field name: Bajo_estacion
        # filter station that is the station in the data
        field_st_taken = 'Bajo_estacion'
        station = 'Station'
        start_date_field = 'Combined_started_date'
        end_date_field = 'Combined_end_date'
        filter_dates[field_st_taken] = filter_dates[field_st_taken].str.upper().str.strip()
        st_down = filter_dates[(filter_dates[field_st_taken] == 'SI') & (filter_dates[station].str.strip() ==
st)]

        # filter in df the dates from the file

        try:
            #if the call was done by irrometer
            if sensor_ir == True:
                df[date_field]=pd.to_datetime(df[date_field], format="%d/%m/%Y
%H:%M").dt.strftime("%m/%d/%Y %H:%M")
            df[date_field]= pd.to_datetime(df[date_field]).dt.tz_localize('America/Bogota')
        except:
            print("Field is already datetime")
            #TODO: Fix this to a more contundent actions
        tz_date=timezone('America/Bogota')
        for index, row in st_down.iterrows():

            start_date = tz_date.localize(dt.strptime(row[start_date_field], '%d/%m/%Y %H:%M:%S'))
            end_date = tz_date.localize(dt.strptime(row[end_date_field], '%d/%m/%Y %H:%M:%S'))
            df = df[(df[date_field] < start_date) | (df[date_field] > end_date)]

        return df

    def count_data(self, df, group_field):
        # Count amount of data by field
        dfsum=df.groupby(group_field, as_index=False).count()

        return dfsum

    def reshape_to_long(self, df, id_fields, fields_to_remove=None, has_time_col=True, type=None):
        if fields_to_remove is not None:
            df=df.remove(fields_to_remove)
        if has_time_col==True:
            if type is not None:
                wfdl=WeatherFile().get_time_cols('A')
            else:
                wfdl=WeatherFile().get_time_cols()
            id_fields= wfdl + id_fields

        return pd.melt(df, id_fields,
                       var_name='variable',
                       value_name='value')

    """merge_df_by_date
```

```
        Merge two dataframes by date distinguising all the fields from df_one by a prefix df_one_prefix
and
        fields in dataframe two by a prefix df_two_prefix"""
    def merge_df_by_date(self, df_one, df_two,name_date_fd,df_one_prefix,df_two_prefix):
        #TODO: It should be a way to do this easier/faster by vectorizing
        df_one=df_one.copy()
        df_two = df_two.copy()
        col_names_df1 = df_one.columns
        col_names_df2 = df_two.columns
        col_names_df1_r = []
        col_names_df2_r = []
        i = 0
        for c in col_names_df1:
            col_names_df1_r.append(df_one_prefix + '_' + c)
            i += 1
        df_one.columns = col_names_df1_r
        i = 0
        for c in col_names_df2:
            col_names_df2_r.append(df_two_prefix + '_' + c)
            i += 1

        df_two.columns = col_names_df2_r
        name_date_fd_1 = df_one_prefix + '_' + name_date_fd
        name_date_fd_2 = df_two_prefix + '_' + name_date_fd
        df_out = pd.merge(df_one, df_two, left_on=name_date_fd_1, right_on=name_date_fd_2)

        return df_out
```

Table C.7 Summary statistics Conventions values at each hour for each station and season

Column name	Meaning
Station	Name of the measurement station
Season	Refers to the tropical climatic season. I can be dry (low precipitation) and Wet (high precipitation)
Hour	Hour of the day
No records	Number of records summarized
Mean	Variable's mean value
STD	Variable's standard deviation
Min	Variable's minimum value
25%	Variable's 25% percentile
50%	Variable's 50% percentile
75%	Variable's 75% percentile
Max	Variable's maximum value

Table C.8 Summary statistics Albedo values at each hour for each station and season

Station	Season	Hour	No records	Mean	STD	Min	25%	50%	75%	Max
BA	Dry	7	101	0.08	0.02	0.06	0.07	0.07	0.08	0.19
BA	Dry	8	100	0.06	0.01	0.05	0.06	0.06	0.07	0.11
BA	Dry	9	100	0.06	0.01	0.05	0.05	0.06	0.06	0.10
BA	Dry	10	101	0.06	0.01	0.04	0.05	0.06	0.06	0.12
BA	Dry	11	101	0.06	0.01	0.04	0.05	0.05	0.06	0.11
BA	Dry	12	101	0.06	0.02	0.04	0.05	0.05	0.06	0.11
BA	Dry	13	101	0.06	0.02	0.04	0.05	0.05	0.06	0.17
BA	Dry	14	101	0.07	0.02	0.05	0.05	0.06	0.06	0.13
BA	Dry	15	102	0.08	0.04	0.05	0.06	0.07	0.07	0.21
BA	Dry	16	103	0.15	0.16	0.06	0.08	0.09	0.10	0.94
BA	Dry	17	94	0.15	0.09	0.07	0.10	0.12	0.15	0.71
BA	Wet	7	128	0.10	0.08	0.04	0.05	0.05	0.13	0.49
BA	Wet	8	128	0.09	0.07	0.03	0.04	0.05	0.10	0.33
BA	Wet	9	128	0.08	0.07	0.03	0.04	0.04	0.06	0.22
BA	Wet	10	129	0.08	0.06	0.03	0.04	0.04	0.06	0.21
BA	Wet	11	130	0.08	0.06	0.03	0.04	0.04	0.07	0.21
BA	Wet	12	130	0.08	0.06	0.04	0.04	0.04	0.06	0.22
BA	Wet	13	131	0.08	0.06	0.04	0.04	0.05	0.07	0.28
BA	Wet	14	131	0.08	0.06	0.04	0.05	0.05	0.06	0.23
BA	Wet	15	131	0.10	0.07	0.05	0.05	0.06	0.07	0.22
BA	Wet	16	131	0.11	0.07	0.05	0.06	0.07	0.11	0.30
BA	Wet	17	131	0.18	0.11	0.06	0.10	0.13	0.23	0.62
LP	Dry	7	70	0.06	0.01	0.05	0.05	0.05	0.06	0.13
LP	Dry	8	70	0.05	0.00	0.04	0.05	0.05	0.05	0.07
LP	Dry	9	70	0.05	0.00	0.04	0.04	0.05	0.05	0.06
LP	Dry	10	70	0.04	0.00	0.04	0.04	0.04	0.05	0.05
LP	Dry	11	71	0.04	0.00	0.04	0.04	0.04	0.05	0.05
LP	Dry	12	71	0.04	0.00	0.04	0.04	0.04	0.05	0.05
LP	Dry	13	71	0.05	0.03	0.04	0.04	0.04	0.05	0.24
LP	Dry	14	69	0.05	0.01	0.04	0.05	0.05	0.05	0.16
LP	Dry	15	69	0.06	0.02	0.05	0.05	0.05	0.06	0.21
LP	Dry	16	71	0.07	0.04	0.05	0.06	0.06	0.07	0.38
LP	Dry	17	71	0.14	0.10	0.07	0.09	0.11	0.13	0.64
LP	Wet	7	173	0.15	0.13	0.04	0.06	0.07	0.24	0.61
LP	Wet	8	173	0.12	0.10	0.04	0.05	0.06	0.22	0.45
LP	Wet	9	174	0.11	0.08	0.04	0.05	0.06	0.20	0.42
LP	Wet	10	176	0.10	0.07	0.04	0.05	0.06	0.18	0.25
LP	Wet	11	174	0.09	0.06	0.04	0.05	0.05	0.17	0.26

Station	Season	Hour	No records	Mean	STD	Min	25%	50%	75%	Max
LP	Wet	12	175	0.09	0.07	0.04	0.05	0.05	0.16	0.57
LP	Wet	13	175	0.09	0.07	0.04	0.05	0.05	0.16	0.35
LP	Wet	14	177	0.10	0.07	0.04	0.05	0.06	0.18	0.24
LP	Wet	15	178	0.12	0.09	0.04	0.06	0.07	0.21	0.58
LP	Wet	16	177	0.12	0.10	0.05	0.06	0.07	0.21	0.68
LP	Wet	17	172	0.21	0.20	0.06	0.08	0.11	0.28	0.99
SI	Dry	7	122	0.11	0.09	0.06	0.08	0.09	0.11	0.77
SI	Dry	8	122	0.09	0.09	0.06	0.07	0.08	0.09	0.92
SI	Dry	9	121	0.07	0.02	0.06	0.06	0.07	0.08	0.25
SI	Dry	10	120	0.07	0.01	0.06	0.06	0.07	0.08	0.10
SI	Dry	11	121	0.07	0.01	0.05	0.07	0.07	0.08	0.10
SI	Dry	12	122	0.07	0.01	0.05	0.06	0.07	0.07	0.10
SI	Dry	13	122	0.07	0.01	0.06	0.06	0.07	0.08	0.11
SI	Dry	14	122	0.08	0.01	0.06	0.07	0.08	0.08	0.10
SI	Dry	15	122	0.09	0.01	0.07	0.08	0.09	0.10	0.12
SI	Dry	16	122	0.12	0.02	0.07	0.10	0.12	0.13	0.22
SI	Dry	17	121	0.18	0.08	0.09	0.13	0.16	0.20	0.51
SI	Wet	7	213	0.09	0.06	0.06	0.07	0.08	0.09	0.73
SI	Wet	8	212	0.08	0.02	0.05	0.06	0.07	0.08	0.23
SI	Wet	9	212	0.07	0.02	0.05	0.06	0.07	0.08	0.21
SI	Wet	10	211	0.07	0.02	0.05	0.06	0.07	0.08	0.26
SI	Wet	11	210	0.07	0.01	0.05	0.06	0.07	0.07	0.11
SI	Wet	12	210	0.07	0.01	0.05	0.06	0.06	0.07	0.12
SI	Wet	13	211	0.07	0.01	0.05	0.06	0.07	0.07	0.11
SI	Wet	14	212	0.08	0.01	0.06	0.07	0.07	0.08	0.21
SI	Wet	15	212	0.09	0.05	0.06	0.08	0.09	0.09	0.66
SI	Wet	16	211	0.13	0.08	0.07	0.09	0.11	0.13	0.67
SI	Wet	17	194	0.25	0.19	0.09	0.12	0.17	0.29	0.95

Table C.9 Summary statistics WRDVI values at each hour for each station and season

Station	Season	Hour	No records	Mean	STD	Min	25%	50%	75%	Max
BA	Dry	7	99	0.25	0.10	-0.23	0.22	0.28	0.31	0.40
BA	Dry	8	98	0.34	0.06	0.16	0.32	0.35	0.37	0.51
BA	Dry	9	98	0.36	0.06	0.20	0.34	0.37	0.40	0.54
BA	Dry	10	99	0.37	0.07	0.16	0.34	0.37	0.41	0.55
BA	Dry	11	99	0.37	0.07	0.14	0.35	0.38	0.41	0.56
BA	Dry	12	99	0.36	0.08	0.14	0.34	0.37	0.41	0.55
BA	Dry	13	99	0.35	0.09	0.12	0.34	0.37	0.40	0.54
BA	Dry	14	99	0.32	0.10	0.05	0.34	0.35	0.37	0.53
BA	Dry	15	99	0.28	0.12	-0.06	0.28	0.32	0.34	0.48
BA	Dry	16	100	0.20	0.17	-0.30	0.24	0.26	0.29	0.40
BA	Dry	17	100	0.04	0.22	-0.52	0.00	0.14	0.20	0.26
BA	Wet	7	125	0.35	0.15	-0.23	0.33	0.39	0.43	0.54
BA	Wet	8	125	0.42	0.10	-0.11	0.40	0.44	0.46	0.56
BA	Wet	9	125	0.44	0.05	0.27	0.43	0.45	0.47	0.55
BA	Wet	10	126	0.46	0.06	0.28	0.44	0.46	0.47	0.61
BA	Wet	11	127	0.46	0.05	0.28	0.43	0.47	0.49	0.58
BA	Wet	12	127	0.47	0.05	0.33	0.44	0.48	0.51	0.55
BA	Wet	13	128	0.47	0.05	0.23	0.45	0.48	0.51	0.54
BA	Wet	14	128	0.46	0.05	0.28	0.43	0.47	0.49	0.53
BA	Wet	15	128	0.44	0.05	0.21	0.41	0.45	0.48	0.52
BA	Wet	16	128	0.39	0.08	0.02	0.35	0.41	0.44	0.52
BA	Wet	17	128	0.08	0.27	-0.54	-0.14	0.19	0.29	0.42
LP	Dry	7	68	0.28	0.09	0.00	0.28	0.31	0.34	0.39
LP	Dry	8	68	0.38	0.03	0.27	0.37	0.38	0.40	0.43
LP	Dry	9	68	0.42	0.02	0.38	0.41	0.42	0.43	0.46
LP	Dry	10	68	0.44	0.01	0.41	0.44	0.44	0.45	0.49
LP	Dry	11	69	0.46	0.02	0.42	0.45	0.46	0.47	0.50
LP	Dry	12	69	0.46	0.02	0.39	0.45	0.47	0.48	0.52
LP	Dry	13	69	0.45	0.06	0.03	0.45	0.47	0.48	0.50
LP	Dry	14	67	0.44	0.03	0.37	0.43	0.44	0.45	0.49
LP	Dry	15	67	0.40	0.03	0.24	0.39	0.40	0.42	0.45
LP	Dry	16	69	0.33	0.08	-0.03	0.29	0.34	0.39	0.43
LP	Dry	17	69	0.01	0.18	-0.52	-0.08	0.05	0.15	0.25
LP	Wet	7	171	0.28	0.13	-0.39	0.26	0.32	0.36	0.43
LP	Wet	8	171	0.36	0.08	-0.25	0.34	0.38	0.40	0.45
LP	Wet	9	172	0.40	0.04	0.24	0.38	0.41	0.42	0.45
LP	Wet	10	175	0.41	0.05	-0.02	0.40	0.42	0.44	0.47
LP	Wet	11	173	0.42	0.04	0.27	0.41	0.43	0.45	0.47

Station	Season	Hour	No records	Mean	STD	Min	25%	50%	75%	Max
LP	Wet	12	174	0.42	0.09	-0.70	0.41	0.43	0.46	0.49
LP	Wet	13	174	0.42	0.05	0.09	0.41	0.43	0.44	0.46
LP	Wet	14	174	0.40	0.04	0.27	0.38	0.41	0.42	0.48
LP	Wet	15	175	0.37	0.06	0.20	0.33	0.38	0.41	0.47
LP	Wet	16	174	0.36	0.11	-0.21	0.33	0.39	0.43	0.48
LP	Wet	17	174	0.12	0.27	-0.59	0.02	0.22	0.31	0.45
SI	Dry	7	119	0.09	0.10	-0.44	0.05	0.09	0.14	0.27
SI	Dry	8	119	0.16	0.08	-0.38	0.12	0.15	0.21	0.29
SI	Dry	9	118	0.19	0.05	0.10	0.16	0.18	0.22	0.31
SI	Dry	10	117	0.21	0.05	0.12	0.17	0.19	0.26	0.31
SI	Dry	11	118	0.23	0.05	0.15	0.20	0.21	0.27	0.34
SI	Dry	12	119	0.24	0.04	0.12	0.21	0.23	0.27	0.33
SI	Dry	13	119	0.25	0.05	0.15	0.22	0.25	0.29	0.34
SI	Dry	14	119	0.24	0.04	0.14	0.20	0.24	0.27	0.35
SI	Dry	15	119	0.20	0.04	0.10	0.18	0.20	0.22	0.29
SI	Dry	16	119	0.17	0.05	0.03	0.14	0.17	0.21	0.25
SI	Dry	17	119	-0.02	0.18	-0.53	-0.15	0.04	0.12	0.25
SI	Wet	7	209	0.16	0.13	-0.39	0.14	0.20	0.23	0.29
SI	Wet	8	208	0.22	0.07	-0.22	0.21	0.24	0.26	0.32
SI	Wet	9	208	0.23	0.05	0.06	0.22	0.24	0.26	0.34
SI	Wet	10	207	0.25	0.03	0.12	0.23	0.25	0.27	0.33
SI	Wet	11	206	0.26	0.04	0.16	0.24	0.26	0.28	0.35
SI	Wet	12	207	0.27	0.05	0.10	0.24	0.27	0.30	0.38
SI	Wet	13	208	0.27	0.05	0.12	0.24	0.27	0.30	0.37
SI	Wet	14	208	0.25	0.05	0.07	0.22	0.25	0.28	0.35
SI	Wet	15	208	0.20	0.09	-0.21	0.17	0.21	0.25	0.33
SI	Wet	16	208	0.09	0.16	-0.43	0.02	0.13	0.19	0.35
SI	Wet	17	208	-0.19	0.29	-0.73	-0.42	-0.18	0.07	0.32

Table C.10 Summary statistics Air Temperature (°C) values at each hour for each station and season

Station	Season	Hour	No records	Mean	STD	Min	25%	50%	75%	Max
BA	Dry	7	86	26.45	0.70	24.90	26.00	26.70	27.00	27.40
BA	Dry	8	82	27.62	0.71	26.10	27.00	27.60	28.28	28.80
BA	Dry	9	80	28.13	0.63	26.80	27.60	28.15	28.60	29.30
BA	Dry	10	83	28.41	0.73	26.90	27.90	28.40	29.00	29.70
BA	Dry	11	82	28.16	0.67	26.90	27.60	28.20	28.70	29.60
BA	Dry	12	89	28.05	0.82	26.90	27.40	28.00	28.60	29.70
BA	Dry	13	83	28.27	0.78	27.20	27.70	28.10	28.85	29.80
BA	Dry	14	83	28.33	0.64	27.40	27.80	28.20	28.80	29.60

Station	Season	Hour	No records	Mean	STD	Min	25%	50%	75%	Max
BA	Dry	15	82	28.48	0.46	27.80	28.10	28.40	28.88	29.40
BA	Dry	16	82	28.51	0.43	27.60	28.23	28.55	28.80	29.20
BA	Dry	17	83	27.90	0.39	27.20	27.55	27.90	28.20	28.60
BA	Wet	7	104	25.63	0.81	24.20	25.08	25.60	26.30	27.20
BA	Wet	8	103	26.53	0.78	25.00	25.80	26.60	27.10	28.00
BA	Wet	9	104	27.22	0.79	25.70	26.60	27.20	27.70	29.00
BA	Wet	10	105	27.95	0.87	26.20	27.40	27.90	28.50	29.80
BA	Wet	11	104	28.65	0.98	26.90	27.80	28.75	29.40	30.40
BA	Wet	12	105	29.33	0.96	27.30	28.70	29.40	30.10	30.90
BA	Wet	13	106	29.86	1.03	27.10	29.20	30.00	30.68	31.50
BA	Wet	14	105	30.15	1.13	27.30	29.50	30.40	30.90	31.90
BA	Wet	15	105	30.13	1.22	27.00	29.40	30.30	31.10	32.40
BA	Wet	16	105	29.41	1.36	26.90	28.40	29.30	30.40	32.30
BA	Wet	17	109	28.14	1.08	26.00	27.20	28.20	28.80	30.00
LP	Dry	7	57	26.08	0.54	25.10	25.70	26.00	26.50	27.00
LP	Dry	8	56	27.37	0.52	26.40	27.00	27.35	27.70	28.30
LP	Dry	9	58	27.70	0.71	26.60	27.13	27.60	28.20	29.10
LP	Dry	10	58	28.20	0.73	27.20	27.60	28.10	28.78	29.60
LP	Dry	11	59	28.87	0.91	27.60	27.95	28.70	29.70	30.40
LP	Dry	12	58	29.14	0.94	27.30	28.42	29.10	29.95	30.70
LP	Dry	13	57	29.57	0.83	27.80	29.00	29.60	30.10	30.80
LP	Dry	14	59	29.79	0.99	27.90	29.10	30.00	30.40	31.30
LP	Dry	15	56	29.69	0.77	28.30	29.15	29.60	30.33	31.40
LP	Dry	16	58	29.26	0.72	27.80	28.73	29.30	29.70	30.80
LP	Dry	17	59	28.24	0.62	26.90	27.75	28.30	28.70	29.30
LP	Wet	7	140	25.52	0.77	24.10	24.98	25.50	26.03	27.00
LP	Wet	8	143	26.68	0.94	25.00	26.10	26.60	27.30	28.60
LP	Wet	9	142	27.70	1.01	26.00	26.90	27.70	28.40	29.50
LP	Wet	10	144	28.28	1.02	26.20	27.50	28.20	29.10	30.20
LP	Wet	11	142	28.68	1.11	26.50	27.92	28.70	29.58	30.60
LP	Wet	12	143	29.15	1.14	26.80	28.50	29.20	30.10	31.00
LP	Wet	13	141	29.44	0.95	27.44	28.70	29.60	30.20	31.00
LP	Wet	14	142	29.59	0.94	27.60	29.03	29.75	30.20	31.30
LP	Wet	15	143	29.60	0.92	27.70	28.85	29.70	30.30	31.20
LP	Wet	16	143	29.34	1.29	26.60	28.40	29.50	30.31	31.40
LP	Wet	17	141	28.42	1.35	25.80	27.40	28.61	29.60	30.50
SI	Dry	7	100	25.55	0.61	24.20	25.10	25.70	26.00	26.40
SI	Dry	8	96	27.14	0.80	25.40	26.60	27.20	27.73	28.50
SI	Dry	9	98	27.52	1.01	25.60	26.70	27.60	28.40	29.20
SI	Dry	10	98	28.15	1.09	26.30	27.33	28.00	29.08	30.20

Station	Season	Hour	No records	Mean	STD	Min	25%	50%	75%	Max
SI	Dry	11	101	28.93	1.00	27.20	28.00	29.00	29.80	30.50
SI	Dry	12	100	29.38	0.82	27.70	28.80	29.60	30.00	30.50
SI	Dry	13	96	29.68	0.66	27.90	29.30	29.80	30.20	30.70
SI	Dry	14	98	29.99	0.69	28.10	29.63	30.00	30.40	31.20
SI	Dry	15	98	30.16	0.78	28.60	29.53	30.30	30.80	31.30
SI	Dry	16	98	29.79	0.98	27.80	29.10	29.80	30.68	31.40
SI	Dry	17	96	28.91	0.73	27.40	28.38	29.05	29.50	30.30
SI	Wet	7	174	25.22	0.74	23.80	24.70	25.20	25.90	26.50
SI	Wet	8	170	26.34	0.86	24.60	25.70	26.40	27.10	27.80
SI	Wet	9	169	27.08	0.94	25.20	26.40	27.10	27.70	29.00
SI	Wet	10	170	27.78	1.09	25.90	26.92	27.60	28.60	29.90
SI	Wet	11	169	28.38	1.10	26.20	27.50	28.40	29.20	30.30
SI	Wet	12	171	29.06	1.12	26.80	28.00	29.20	30.10	30.80
SI	Wet	13	168	29.49	1.03	27.40	28.60	29.70	30.30	31.10
SI	Wet	14	169	29.64	1.08	27.40	28.80	29.80	30.40	31.40
SI	Wet	15	170	29.54	1.19	27.20	28.63	29.70	30.50	31.70
SI	Wet	16	168	28.86	1.35	26.30	27.70	28.80	29.92	31.50
SI	Wet	17	169	27.72	1.33	24.90	26.70	27.90	28.80	29.90

Table C.11 Summary statistics VPD (kPa) values at each hour for each station and season

Station	Season	Hour	No records	Mean	STD	Min	25%	50%	75%	Max
BA	Dry	7	82	0.51	0.13	0.25	0.43	0.53	0.62	0.70
BA	Dry	8	80	0.74	0.16	0.37	0.67	0.78	0.85	0.99
BA	Dry	9	80	0.89	0.17	0.51	0.80	0.90	1.01	1.19
BA	Dry	10	81	0.95	0.19	0.53	0.81	0.95	1.08	1.34
BA	Dry	11	81	0.90	0.16	0.63	0.75	0.86	1.02	1.29
BA	Dry	12	81	0.86	0.16	0.63	0.72	0.83	1.02	1.16
BA	Dry	13	81	0.89	0.18	0.64	0.73	0.84	1.04	1.24
BA	Dry	14	81	0.91	0.16	0.65	0.78	0.88	1.05	1.21
BA	Dry	15	80	0.94	0.16	0.68	0.80	0.90	1.08	1.25
BA	Dry	16	81	0.94	0.16	0.69	0.82	0.91	1.08	1.23
BA	Dry	17	82	0.82	0.13	0.61	0.72	0.82	0.90	1.06
BA	Wet	7	102	0.37	0.12	0.18	0.28	0.36	0.44	0.61
BA	Wet	8	102	0.54	0.13	0.30	0.44	0.53	0.64	0.80
BA	Wet	9	102	0.67	0.15	0.39	0.57	0.67	0.77	1.06
BA	Wet	10	103	0.80	0.16	0.47	0.68	0.79	0.93	1.13
BA	Wet	11	105	0.93	0.19	0.58	0.79	0.92	1.08	1.28
BA	Wet	12	104	1.05	0.20	0.56	0.93	1.04	1.21	1.46
BA	Wet	13	106	1.18	0.26	0.67	1.00	1.16	1.39	1.65

Station	Season	Hour	No records	Mean	STD	Min	25%	50%	75%	Max
BA	Wet	14	105	1.25	0.29	0.65	1.08	1.25	1.49	1.77
BA	Wet	15	105	1.25	0.31	0.64	1.01	1.23	1.48	1.91
BA	Wet	16	105	1.07	0.30	0.57	0.85	0.98	1.30	1.81
BA	Wet	17	105	0.77	0.21	0.38	0.62	0.74	0.93	1.19
LP	Dry	7	56	0.39	0.14	0.14	0.28	0.42	0.49	0.60
LP	Dry	8	56	0.63	0.15	0.24	0.58	0.68	0.73	0.83
LP	Dry	9	56	0.77	0.16	0.39	0.70	0.79	0.83	1.12
LP	Dry	10	56	0.90	0.16	0.60	0.81	0.89	1.03	1.24
LP	Dry	11	59	1.02	0.19	0.76	0.86	0.99	1.16	1.43
LP	Dry	12	57	1.03	0.18	0.76	0.90	0.98	1.14	1.47
LP	Dry	13	57	1.09	0.19	0.72	0.97	1.08	1.19	1.53
LP	Dry	14	55	1.15	0.21	0.68	1.03	1.14	1.29	1.62
LP	Dry	15	55	1.12	0.18	0.77	1.00	1.11	1.23	1.52
LP	Dry	16	57	1.01	0.19	0.69	0.87	0.98	1.18	1.36
LP	Dry	17	57	0.80	0.16	0.43	0.70	0.77	0.90	1.06
LP	Wet	7	138	0.31	0.10	0.16	0.22	0.31	0.37	0.53
LP	Wet	8	138	0.52	0.14	0.29	0.41	0.51	0.62	0.83
LP	Wet	9	139	0.71	0.17	0.39	0.58	0.71	0.83	1.05
LP	Wet	10	142	0.83	0.19	0.47	0.68	0.83	0.98	1.22
LP	Wet	11	140	0.96	0.23	0.58	0.78	0.94	1.13	1.45
LP	Wet	12	141	1.06	0.24	0.62	0.86	1.04	1.27	1.52
LP	Wet	13	141	1.11	0.25	0.71	0.90	1.07	1.29	1.61
LP	Wet	14	141	1.15	0.26	0.70	0.93	1.13	1.35	1.72
LP	Wet	15	142	1.10	0.26	0.66	0.89	1.06	1.30	1.69
LP	Wet	16	141	0.97	0.30	0.45	0.75	0.93	1.22	1.56
LP	Wet	17	141	0.75	0.24	0.31	0.57	0.77	0.90	1.18
SI	Dry	7	96	0.49	0.13	0.25	0.38	0.50	0.61	0.72
SI	Dry	8	96	0.81	0.19	0.42	0.69	0.84	0.96	1.10
SI	Dry	9	97	0.99	0.17	0.57	0.89	1.00	1.12	1.30
SI	Dry	10	96	1.16	0.18	0.77	1.04	1.19	1.31	1.48
SI	Dry	11	97	1.35	0.21	0.93	1.20	1.35	1.50	1.69
SI	Dry	12	96	1.47	0.22	0.90	1.33	1.50	1.63	1.80
SI	Dry	13	96	1.55	0.22	1.05	1.41	1.58	1.71	1.92
SI	Dry	14	96	1.61	0.23	1.08	1.45	1.64	1.80	1.95
SI	Dry	15	96	1.60	0.26	1.07	1.38	1.65	1.83	1.96
SI	Dry	16	96	1.48	0.27	0.96	1.31	1.48	1.73	1.93
SI	Dry	17	96	1.22	0.24	0.71	1.11	1.26	1.41	1.58
SI	Wet	7	169	0.27	0.07	0.16	0.22	0.27	0.33	0.43
SI	Wet	8	169	0.49	0.14	0.27	0.37	0.47	0.59	0.79
SI	Wet	9	168	0.66	0.19	0.38	0.50	0.63	0.82	1.05

Station	Season	Hour	No records	Mean	STD	Min	25%	50%	75%	Max
SI	Wet	10	169	0.81	0.23	0.43	0.62	0.76	0.99	1.26
SI	Wet	11	168	0.94	0.26	0.49	0.70	0.93	1.11	1.43
SI	Wet	12	169	1.09	0.30	0.57	0.83	1.11	1.35	1.63
SI	Wet	13	168	1.18	0.29	0.68	0.91	1.20	1.41	1.73
SI	Wet	14	169	1.23	0.32	0.66	0.95	1.23	1.49	1.87
SI	Wet	15	170	1.18	0.37	0.60	0.86	1.19	1.48	1.92
SI	Wet	16	168	0.97	0.37	0.37	0.64	0.94	1.26	1.77
SI	Wet	17	168	0.68	0.28	0.25	0.44	0.67	0.91	1.23

Table C.12 Summary statistics Relative humidity values at each hour for each station and season

Station	Season	Hour	No records	Mean	STD	Min	25%	50%	75%	Max
BA	Dry	7	83	0.85	0.04	0.80	0.82	0.85	0.87	0.92
BA	Dry	8	83	0.80	0.04	0.74	0.77	0.80	0.82	0.89
BA	Dry	9	83	0.77	0.04	0.71	0.74	0.77	0.79	0.86
BA	Dry	10	82	0.76	0.04	0.68	0.73	0.76	0.79	0.85
BA	Dry	11	83	0.77	0.04	0.69	0.74	0.78	0.80	0.82
BA	Dry	12	81	0.77	0.04	0.71	0.74	0.78	0.81	0.83
BA	Dry	13	82	0.77	0.04	0.70	0.73	0.78	0.81	0.83
BA	Dry	14	85	0.77	0.04	0.70	0.73	0.77	0.80	0.83
BA	Dry	15	84	0.76	0.04	0.69	0.72	0.76	0.79	0.82
BA	Dry	16	82	0.76	0.04	0.70	0.73	0.76	0.79	0.82
BA	Dry	17	88	0.78	0.03	0.72	0.75	0.78	0.81	0.83
BA	Wet	7	102	0.89	0.03	0.83	0.87	0.89	0.91	0.94
BA	Wet	8	106	0.85	0.03	0.79	0.82	0.85	0.87	0.91
BA	Wet	9	108	0.82	0.04	0.74	0.79	0.82	0.84	0.89
BA	Wet	10	109	0.79	0.04	0.72	0.76	0.79	0.81	0.86
BA	Wet	11	109	0.77	0.04	0.70	0.74	0.77	0.80	0.84
BA	Wet	12	105	0.74	0.04	0.67	0.72	0.74	0.77	0.84
BA	Wet	13	110	0.72	0.05	0.64	0.68	0.72	0.76	0.81
BA	Wet	14	110	0.71	0.05	0.62	0.67	0.71	0.74	0.82
BA	Wet	15	107	0.71	0.06	0.60	0.67	0.71	0.75	0.82
BA	Wet	16	106	0.74	0.05	0.63	0.70	0.76	0.78	0.84
BA	Wet	17	112	0.80	0.05	0.71	0.76	0.80	0.84	0.89
LP	Dry	7	58	0.89	0.04	0.83	0.86	0.87	0.92	0.96
LP	Dry	8	56	0.83	0.04	0.79	0.81	0.82	0.84	0.93
LP	Dry	9	58	0.80	0.04	0.73	0.77	0.79	0.81	0.89
LP	Dry	10	58	0.76	0.04	0.70	0.74	0.76	0.79	0.84
LP	Dry	11	60	0.75	0.04	0.67	0.72	0.75	0.77	0.81
LP	Dry	12	58	0.74	0.04	0.66	0.72	0.75	0.77	0.81

Station	Season	Hour	No records	Mean	STD	Min	25%	50%	75%	Max
LP	Dry	13	60	0.74	0.04	0.65	0.72	0.74	0.76	0.82
LP	Dry	14	56	0.73	0.04	0.64	0.70	0.73	0.75	0.82
LP	Dry	15	55	0.73	0.04	0.67	0.71	0.74	0.76	0.80
LP	Dry	16	57	0.75	0.04	0.69	0.72	0.75	0.78	0.81
LP	Dry	17	57	0.79	0.04	0.74	0.76	0.80	0.82	0.88
LP	Wet	7	149	0.91	0.03	0.85	0.89	0.91	0.93	0.95
LP	Wet	8	146	0.85	0.04	0.78	0.82	0.85	0.88	0.91
LP	Wet	9	143	0.81	0.04	0.74	0.78	0.81	0.84	0.88
LP	Wet	10	145	0.79	0.04	0.71	0.76	0.78	0.82	0.87
LP	Wet	11	142	0.76	0.05	0.67	0.72	0.77	0.80	0.84
LP	Wet	12	145	0.74	0.05	0.65	0.70	0.74	0.78	0.83
LP	Wet	13	146	0.73	0.05	0.63	0.69	0.74	0.77	0.81
LP	Wet	14	147	0.72	0.05	0.62	0.68	0.73	0.77	0.82
LP	Wet	15	145	0.74	0.05	0.63	0.70	0.74	0.78	0.82
LP	Wet	16	145	0.77	0.06	0.65	0.72	0.78	0.81	0.87
LP	Wet	17	151	0.81	0.05	0.73	0.78	0.81	0.85	0.91
SI	Dry	7	103	0.86	0.04	0.79	0.82	0.85	0.89	0.92
SI	Dry	8	104	0.78	0.05	0.71	0.74	0.77	0.81	0.87
SI	Dry	9	103	0.73	0.05	0.66	0.69	0.73	0.76	0.84
SI	Dry	10	97	0.69	0.04	0.63	0.66	0.69	0.72	0.78
SI	Dry	11	98	0.66	0.04	0.60	0.63	0.66	0.69	0.75
SI	Dry	12	97	0.64	0.04	0.58	0.60	0.64	0.67	0.75
SI	Dry	13	99	0.63	0.05	0.56	0.59	0.63	0.66	0.73
SI	Dry	14	101	0.62	0.05	0.55	0.58	0.62	0.66	0.73
SI	Dry	15	100	0.62	0.05	0.55	0.59	0.62	0.66	0.74
SI	Dry	16	100	0.65	0.05	0.57	0.60	0.64	0.68	0.76
SI	Dry	17	98	0.70	0.05	0.62	0.66	0.69	0.73	0.81
SI	Wet	7	180	0.92	0.02	0.87	0.90	0.92	0.93	0.95
SI	Wet	8	171	0.86	0.03	0.79	0.83	0.87	0.89	0.91
SI	Wet	9	172	0.82	0.04	0.73	0.78	0.82	0.86	0.89
SI	Wet	10	178	0.79	0.05	0.69	0.74	0.79	0.83	0.87
SI	Wet	11	177	0.76	0.06	0.65	0.72	0.76	0.81	0.86
SI	Wet	12	175	0.74	0.06	0.63	0.68	0.73	0.79	0.84
SI	Wet	13	172	0.72	0.06	0.62	0.67	0.72	0.77	0.82
SI	Wet	14	176	0.71	0.06	0.59	0.66	0.71	0.77	0.82
SI	Wet	15	176	0.72	0.07	0.58	0.65	0.72	0.78	0.84
SI	Wet	16	170	0.76	0.08	0.62	0.70	0.77	0.83	0.89
SI	Wet	17	173	0.82	0.06	0.71	0.76	0.82	0.88	0.92

Table C.13 Summary statistics Net Radiation values at each hour for each station and season

Station	Season	Hour	No records	Mean	STD	Min	25%	50%	75%	Max
BA	Dry	7	81	31.35	26.37	-20.40	12.60	31.90	54.40	75.30
BA	Dry	8	80	176.81	58.96	52.90	131.10	172.95	232.17	270.70
BA	Dry	9	80	301.16	94.42	135.30	233.10	296.25	377.90	481.50
BA	Dry	10	81	369.27	119.12	141.40	274.10	387.10	460.90	598.30
BA	Dry	11	81	424.84	121.93	196.90	350.10	419.90	503.40	690.90
BA	Dry	12	81	502.08	158.55	202.00	357.70	519.00	633.30	744.00
BA	Dry	13	81	513.83	132.80	252.50	403.40	536.60	623.60	704.80
BA	Dry	14	81	458.70	93.37	242.90	380.60	493.40	534.10	591.30
BA	Dry	15	80	291.95	77.03	114.90	229.25	303.85	352.97	410.10
BA	Dry	16	81	114.69	56.34	-9.50	69.90	131.90	159.00	182.50
BA	Dry	17	81	-22.69	19.33	-74.20	-30.70	-16.50	-10.60	1.40
BA	Wet	7	102	82.21	60.08	-17.50	38.40	74.45	135.48	206.60
BA	Wet	8	102	214.84	97.64	52.90	124.63	221.45	290.62	407.50
BA	Wet	9	102	323.53	128.36	74.00	230.95	315.20	422.60	567.60
BA	Wet	10	103	406.05	146.28	93.00	302.40	423.60	516.05	657.70
BA	Wet	11	104	464.66	162.78	118.20	343.18	481.90	606.53	746.00
BA	Wet	12	104	483.67	145.17	189.40	386.17	497.25	603.20	715.80
BA	Wet	13	105	442.06	129.01	164.70	341.20	474.60	558.60	629.50
BA	Wet	14	105	327.06	87.63	164.80	262.80	322.20	398.30	485.80
BA	Wet	15	105	186.18	54.61	73.30	138.10	177.50	229.60	295.60
BA	Wet	16	105	50.08	36.18	-14.30	21.50	45.00	82.80	123.60
BA	Wet	17	105	-41.50	22.46	-69.10	-61.50	-48.60	-23.60	3.40
LP	Dry	7	56	51.87	45.19	-18.80	4.78	53.05	89.30	120.70
LP	Dry	8	56	226.25	107.15	34.70	142.08	247.50	319.87	358.40
LP	Dry	9	56	365.35	133.20	129.70	245.98	374.25	491.13	538.20
LP	Dry	10	56	461.11	134.33	208.00	334.82	504.05	581.65	617.70
LP	Dry	11	57	509.92	135.12	237.60	388.60	543.20	631.20	697.80
LP	Dry	12	57	530.52	145.71	167.00	452.40	547.00	662.00	740.40
LP	Dry	13	57	474.60	134.14	189.40	396.60	486.30	587.30	648.80
LP	Dry	14	55	387.03	104.40	142.40	312.10	397.50	479.75	533.70
LP	Dry	15	55	248.53	81.67	105.20	181.95	262.40	318.80	367.50
LP	Dry	16	57	90.05	44.45	-5.40	60.90	97.00	128.20	146.80
LP	Dry	17	57	-32.22	14.16	-58.70	-45.10	-27.60	-21.00	-13.70
LP	Wet	7	138	19.02	32.97	-32.80	-7.98	12.15	37.38	94.70
LP	Wet	8	138	116.90	62.52	5.00	67.30	111.65	164.47	245.00
LP	Wet	9	139	203.58	92.41	51.20	128.55	196.80	271.20	413.90
LP	Wet	10	142	266.94	101.76	82.30	186.10	268.41	335.25	509.40

Station	Season	Hour	No records	Mean	STD	Min	25%	50%	75%	Max
LP	Wet	11	140	328.16	141.00	108.10	194.32	325.53	443.68	603.60
LP	Wet	12	141	347.77	136.48	98.90	235.20	331.90	471.00	603.40
LP	Wet	13	140	313.85	125.36	83.80	214.38	311.26	411.30	538.30
LP	Wet	14	141	258.53	103.99	86.70	175.40	246.12	323.80	491.10
LP	Wet	15	142	163.00	77.45	16.90	101.65	162.23	220.23	325.70
LP	Wet	16	141	55.02	48.19	-28.10	20.80	49.30	81.20	187.10
LP	Wet	17	141	-34.66	17.63	-63.60	-48.70	-34.20	-21.50	4.10
SI	Dry	7	96	43.46	39.54	-22.40	10.28	43.00	71.40	118.80
SI	Dry	8	96	189.12	93.90	31.60	116.95	185.65	266.65	351.30
SI	Dry	9	97	318.63	138.62	99.60	197.40	323.70	436.60	539.90
SI	Dry	10	96	390.21	126.98	170.30	295.97	385.00	514.18	606.50
SI	Dry	11	97	415.41	112.80	202.00	333.20	412.10	497.50	608.20
SI	Dry	12	96	427.84	129.23	156.70	335.25	428.05	528.78	658.20
SI	Dry	13	96	412.93	113.95	225.60	300.80	424.05	497.05	594.80
SI	Dry	14	96	318.37	85.97	156.70	244.90	326.20	387.90	458.80
SI	Dry	15	96	192.76	55.28	93.50	143.00	196.45	238.25	289.90
SI	Dry	16	96	60.33	26.69	7.50	40.15	59.65	83.13	105.00
SI	Dry	17	96	-34.66	10.94	-54.40	-45.00	-34.55	-24.53	-18.70
SI	Wet	7	169	40.01	43.84	-29.30	6.00	31.70	62.60	145.20
SI	Wet	8	168	156.59	95.36	14.80	73.68	145.25	226.20	348.50
SI	Wet	9	168	266.78	130.44	58.70	171.85	239.65	374.33	539.50
SI	Wet	10	169	353.73	142.87	103.00	233.70	342.50	484.40	617.50
SI	Wet	11	168	405.61	136.91	152.10	298.60	415.50	506.13	645.10
SI	Wet	12	169	434.23	146.06	157.30	304.30	450.90	553.20	689.00
SI	Wet	13	168	408.85	117.43	168.00	319.32	410.30	513.32	618.30
SI	Wet	14	168	323.31	110.29	124.80	237.45	323.35	419.10	517.80
SI	Wet	15	168	171.29	79.52	31.30	97.62	178.00	241.07	313.30
SI	Wet	16	168	32.99	38.78	-41.90	1.90	32.60	61.18	109.00
SI	Wet	17	168	-43.36	14.34	-63.20	-55.92	-47.55	-30.65	-13.30

Table C.14 Summary statistics NDVI values at each hour for each station and season

Station	Season	Hour	No records	Mean	STD	Min	25%	50%	75%	Max
BA	Dry	7	99	0.78	0.05	0.52	0.77	0.80	0.81	0.84
BA	Dry	8	98	0.82	0.02	0.75	0.81	0.82	0.83	0.88
BA	Dry	9	98	0.83	0.02	0.76	0.82	0.83	0.84	0.89
BA	Dry	10	99	0.83	0.03	0.75	0.82	0.83	0.85	0.89
BA	Dry	11	99	0.83	0.03	0.74	0.82	0.83	0.85	0.89
BA	Dry	12	99	0.83	0.03	0.74	0.82	0.83	0.85	0.89

Station	Season	Hour	No records	Mean	STD	Min	25%	50%	75%	Max
BA	Dry	13	99	0.82	0.03	0.73	0.82	0.83	0.84	0.89
BA	Dry	14	99	0.81	0.04	0.69	0.82	0.83	0.83	0.88
BA	Dry	15	99	0.79	0.05	0.63	0.80	0.81	0.82	0.87
BA	Dry	16	100	0.76	0.09	0.45	0.78	0.79	0.80	0.84
BA	Dry	17	100	0.67	0.15	0.23	0.66	0.74	0.76	0.79
BA	Wet	7	125	0.82	0.07	0.52	0.82	0.84	0.85	0.89
BA	Wet	8	125	0.85	0.04	0.60	0.84	0.86	0.86	0.89
BA	Wet	9	125	0.86	0.02	0.80	0.85	0.86	0.86	0.89
BA	Wet	10	126	0.86	0.02	0.80	0.85	0.86	0.87	0.91
BA	Wet	11	127	0.86	0.02	0.80	0.85	0.87	0.87	0.90
BA	Wet	12	127	0.87	0.01	0.82	0.86	0.87	0.88	0.89
BA	Wet	13	128	0.87	0.02	0.78	0.86	0.87	0.88	0.89
BA	Wet	14	128	0.86	0.02	0.80	0.85	0.87	0.87	0.88
BA	Wet	15	128	0.86	0.02	0.77	0.85	0.86	0.87	0.88
BA	Wet	16	128	0.84	0.03	0.68	0.83	0.84	0.86	0.88
BA	Wet	17	128	0.68	0.16	0.20	0.58	0.76	0.80	0.85
LP	Dry	7	68	0.80	0.04	0.67	0.80	0.81	0.82	0.84
LP	Dry	8	68	0.84	0.01	0.80	0.83	0.84	0.84	0.85
LP	Dry	9	68	0.85	0.01	0.84	0.85	0.85	0.85	0.86
LP	Dry	10	68	0.86	0.00	0.85	0.85	0.86	0.86	0.87
LP	Dry	11	69	0.86	0.01	0.85	0.86	0.86	0.87	0.88
LP	Dry	12	69	0.86	0.01	0.84	0.86	0.86	0.87	0.88
LP	Dry	13	69	0.86	0.02	0.68	0.86	0.86	0.87	0.88
LP	Dry	14	67	0.86	0.01	0.83	0.85	0.86	0.86	0.87
LP	Dry	15	67	0.84	0.01	0.78	0.84	0.84	0.85	0.86
LP	Dry	16	69	0.82	0.03	0.65	0.80	0.82	0.84	0.85
LP	Dry	17	69	0.66	0.12	0.23	0.62	0.70	0.74	0.79
LP	Wet	7	171	0.79	0.07	0.38	0.79	0.81	0.83	0.85
LP	Wet	8	171	0.83	0.04	0.50	0.82	0.84	0.84	0.86
LP	Wet	9	172	0.84	0.01	0.78	0.83	0.84	0.85	0.86
LP	Wet	10	175	0.84	0.02	0.65	0.84	0.85	0.85	0.87
LP	Wet	11	173	0.85	0.01	0.80	0.84	0.85	0.86	0.87
LP	Wet	12	174	0.85	0.07	-0.06	0.85	0.85	0.86	0.87
LP	Wet	13	174	0.85	0.02	0.71	0.84	0.85	0.86	0.86
LP	Wet	14	174	0.84	0.01	0.79	0.84	0.84	0.85	0.87
LP	Wet	15	175	0.83	0.02	0.76	0.82	0.84	0.85	0.87
LP	Wet	16	174	0.83	0.05	0.53	0.82	0.84	0.85	0.87
LP	Wet	17	174	0.70	0.17	0.13	0.68	0.77	0.81	0.86
SI	Dry	7	119	0.71	0.06	0.32	0.69	0.72	0.74	0.79
SI	Dry	8	119	0.74	0.04	0.39	0.73	0.74	0.77	0.80

Station	Season	Hour	No records	Mean	STD	Min	25%	50%	75%	Max
SI	Dry	9	118	0.76	0.02	0.72	0.75	0.76	0.77	0.81
SI	Dry	10	117	0.77	0.02	0.73	0.75	0.76	0.79	0.81
SI	Dry	11	118	0.78	0.02	0.74	0.76	0.77	0.79	0.82
SI	Dry	12	119	0.78	0.02	0.73	0.77	0.78	0.80	0.82
SI	Dry	13	119	0.79	0.02	0.74	0.77	0.78	0.80	0.82
SI	Dry	14	119	0.78	0.02	0.74	0.77	0.78	0.79	0.82
SI	Dry	15	119	0.76	0.02	0.72	0.75	0.76	0.77	0.80
SI	Dry	16	119	0.75	0.03	0.68	0.74	0.75	0.77	0.79
SI	Dry	17	119	0.64	0.12	0.21	0.58	0.69	0.73	0.79
SI	Wet	7	209	0.74	0.07	0.37	0.74	0.76	0.78	0.80
SI	Wet	8	208	0.77	0.04	0.52	0.77	0.78	0.79	0.81
SI	Wet	9	208	0.78	0.02	0.70	0.77	0.78	0.79	0.82
SI	Wet	10	207	0.78	0.01	0.73	0.78	0.79	0.79	0.82
SI	Wet	11	206	0.79	0.02	0.75	0.78	0.79	0.80	0.82
SI	Wet	12	207	0.79	0.02	0.72	0.78	0.79	0.80	0.83
SI	Wet	13	208	0.79	0.02	0.73	0.78	0.79	0.81	0.83
SI	Wet	14	208	0.78	0.02	0.71	0.77	0.78	0.80	0.82
SI	Wet	15	208	0.76	0.04	0.53	0.75	0.77	0.78	0.82
SI	Wet	16	208	0.71	0.09	0.33	0.68	0.73	0.76	0.82
SI	Wet	17	208	0.50	0.24	-0.12	0.34	0.55	0.70	0.81

REFERENCES

Abood, S. A., Lee, J. S. H., Burivalova, Z., Garcia-Ulloa, J., & Koh, L. P. (2015). Relative Contributions of the Logging, Fiber, Oil Palm, and Mining Industries to Forest Loss in Indonesia. Conservation Letters, 8(1), 58–67. https://doi.org/10.1111/conl.12103

Adnan, N. A., & Atkinson, P. M. (2011). Exploring the impact of climate and land use changes on streamflow trends in a monsoon catchment. International Journal of Climatology, 31(6), 815–831. https://doi.org/10.1002/joc.2112

Akita, Y., Carter, G., & Serre, M. L. (2007). Spatiotemporal Nonattainment Assessment of Surface Water Tetrachloroethylene in New Jersey. Journal of Environmental Quality, 36(2), 508–520. https://doi.org/10.2134/jeq2005.0426

Algeet-Abarquero, N., Marchamalo, M., Bonatti, J., Fernández-Moya, J., & Moussa, R. (2015). Implications of land use change on runoff generation at the plot scale in the humid tropics of Costa Rica. CATENA, 135, 263–270. https://doi.org/10.1016/j.catena.2015.08.004

Amigun, B., Musango, J. K., & Stafford, W. (2011). Biofuels and sustainability in Africa. Renewable and Sustainable Energy Reviews, 15(2), 1360–1372. https://doi.org/10.1016/j.rser.2010.10.015

Arias, P. A., Villegas, J. C., Machado, J., Serna, A. M., Vidal, L. M., Vieira, C., … Mejía, Ó. A. (2016). Reducing Social Vulnerability to Environmental Change: Building Trust through Social Collaboration on Environmental Monitoring. Weather, Climate, and Society, 8(1), 57–66. https://doi.org/10.1175/WCAS-D-15-0049.1

Asubonteng, K., Pfeffer, K., Ros-Tonen, M., Verbesselt, J., & Baud, I. (2018). Effects of Tree-crop Farming on Land-cover Transitions in a Mosaic Landscape in the Eastern Region of Ghana. Environmental Management. https://doi.org/10.1007/s00267-018-1060-3

Assumpção, T. H., Popescu, I., Jonoski, A., & Solomatine, D. P. (2018). Citizen observations contributing to flood modelling: opportunities and challenges. Hydrology and Earth System Sciences, 22(2), 1473–1489. https://doi.org/10.5194/hess-22-1473-2018

Austin, K. G., Lee, M. E., Clark, C., Forester, B. R., Urban, D. L., White, L., Kasibhatla, P. S., & Poulsen, J. R. (2017). An assessment of high carbon stock and high conservation value approaches to sustainable oil palm cultivation in Gabon. Environmental Research Letters, 12(1), 014005. https://doi.org/10.1088/1748-9326/aa5437

Austin, K. G., Mosnier, A., Pirker, J., McCallum, I., Fritz, S., & Kasibhatla, P. S. (2017). Shifting patterns of oil palm driven deforestation in Indonesia and implications for zero-deforestation commitments. Land Use Policy, 69, 41–48. https://doi.org/10.1016/j.landusepol.2017.08.036

Babel, M. S., Shrestha, B., & Perret, S. R. (2011). Hydrological impact of biofuel production: A case study of the Khlong Phlo Watershed in Thailand. Agricultural Water Management, 101(1), 8–26. https://doi.org/10.1016/j.agwat.2011.08.019

Baldwin, C., Tan, P.-L., White, I., Hoverman, S., & Burry, K. (2012). How scientific knowledge informs community understanding of groundwater. Journal of Hydrology, 474, 74–83. https://doi.org/10.1016/j.jhydrol.2012.06.006

Banabas, M., Turner, M. A., Scotter, D. R., & Nelson, P. N. (2008). Losses of nitrogen fertiliser under oil palm in Papua New Guinea: 1. Water balance, and nitrogen in soil solution and runoff. Australian Journal of Soil Research, 46(4), 332–339. https://doi.org/10.1071/SR07171

Barcelos, E., Rios, S. de A., Cunha, R. N. V., Lopes, R., Motoike, S. Y., Babiychuk, E., Skirycz, A., & Kushnir, S. (2015). Oil palm natural diversity and the potential for yield improvement. Frontiers in Plant Science, 6, 190. https://doi.org/10.3389/fpls.2015.00190

Bayona-Rodríguez, C. J., Ochoa-Cadavid, I., & Romero, H. M. (2016). Impacts of the dry season on the gas exchange of oil palm (Elaeis guineensis) and interspecific hybrid (Elaeis oleífera x Elaeis guineensis) progenies under field conditions in eastern Colombia. Agronomía Colombiana, 34, 329–335.

Bayona-Rodríguez, C. J., & Romero, H. M. (2016). Estimation of transpiration in oil palm (Elaeis guineensis Jacq.) with the heat ratio method. Agronomía Colombiana, 34(2), 172. https://doi.org/10.15446/agron.colomb.v34n2.55649

Bayona-Rodriguez, C. J., & Romero, H. M. (2019). Physiological and agronomic behavior of commercial cultivars of oil palm (Elaeis guineensis) and OxG hybrids (Elaeis oleifera x Elaeis guineensis) at rainy and dry seasons. ResearchGate, 13(3), 424–432. https://doi.org/10.21475/ajcs.19.13.03.p1354

Becker, A. (1987). Macroscale hydrologic models in support to climate research. Proceedings of the Vancouver Symposium, 16.

Benami, E., Curran, L. M., Cochrane, M., Venturieri, A., Franco, R., Kneipp, J., & Swartos, A. (2018). Oil palm land conversion in Para, Brazil, from 2006-2014: Evaluating the 2010 Brazilian Sustainable Palm Oil Production Program. Environmental Research Letters, 13(3), 034037. https://doi.org/10.1088/1748-9326/aaa270

Bessou, C., Verwilghen, A., Beaudoin-Ollivier, L., Marichal, R., Ollivier, J., Baron, V., Bonneau, X., Carron, M.-P., Snoeck, D., Naim, M., Aryawan, A. A. K., Raoul, F., Giraudoux, P., Surya, E., Sihombing, E., & Caliman, J.-P. (2017). Agroecological practices in oil palm plantations: Examples from the field. Ocl-Oilseeds and Fats Crops and Lipids, 24(3), D305. https://doi.org/10.1051/ocl/2017024

Betancur-Vargas, T., García-Giraldo, D. A., Vélez-Duque, A. J., Gómez, A. M., Flórez-Ayala, C., Patiño, J., & Ortiz-Tamayo, J. Á. (2017). Aguas subterráneas, humedales y servicios ecosistémicos en Colombia. Biota Colombiana, 18(1), 1–28. https://doi.org/10.21068/c2017.v18n01a1

Betancur, T. (2008). Una aproximación al conocimiento de un sistema acuífero tropical. Caso de estudio: Bajo Cauca antioqueño, 1–227. Retrieved from http://scholar.google.com/scholar?hl=en&btnG=Search&q=intitle:Una+aproximación+al+conocimiento+de+un+sistema+acuífero+tropical.+caso+de+estudio:+el+bajo+cauca+antioqueño.#0%5Cnhttp://scholar.google.com/scholar?hl=en&btnG=Search&q=intitle:Una+aproximación+

Betancur, T. (2014). Aguas Subterraneas en el Bajo Cauca Antioqueño. Medellin: Universidad de Antioquia.

Betancur, T., Palacio, C., & Escobar, J. (2012). Conceptual Models in Hydrogeology, Methodology and Results. In Hydrogeology. A global perspective (pp. 203–222). https://doi.org/10.5772/28155

Bicalho, T., Bessou, C., & Pacca, S. A. (2016). Land use change within EU sustainability criteria for biofuels: The case of oil palm expansion in the Brazilian Amazon. Renewable Energy, 89, 588–597. https://doi.org/10.1016/j.renene.2015.12.017

Bonan, G. B. (2008). Forests and Climate Change: Forcings, Feedbacks, and the Climate Benefits of Forests. Science, 320(5882), 1444–1449. https://doi.org/10.1126/science.1155121

Brum, M., Oliveira, R. S., López, J. G., Licata, J., Pypker, T., Chia, G. S., Tinôco, R. S., & Asbjornsen, H. (2021). Effects of irrigation on oil palm transpiration during ENSO-induced drought in the Brazilian Eastern Amazon. Agricultural Water Management, 245, 106569. https://doi.org/10.1016/j.agwat.2020.106569

Bruun, T. B., Egay, K., Mertz, O., & Magid, J. (2013). Improved sampling methods document decline in soil organic carbon stocks and concentrations of permanganate oxidizable carbon after transition from swidden to oil palm cultivation. Agriculture Ecosystems & Environment, 178, 127–134. https://doi.org/10.1016/j.agee.2013.06.018

Buytaert, W., Zulkafli, Z., Grainger, S., Acosta, L., Alemie, T. C., Bastiaensen, J., … Zhumanova, M. (2014). Citizen science in hydrology and water resources: opportunities for knowledge generation, ecosystem service management, and sustainable development. Frontiers in Earth Science, 2(October), 1–21. https://doi.org/10.3389/feart.2014.00026

Burton, M. E. H., Poulsen, J. R., Lee, M. E., Medjibe, V. P., Stewart, C. G., Venkataraman, A., & White, L. J. T. (2017). Reducing Carbon Emissions from Forest Conversion for Oil Palm Agriculture in Gabon. Conservation Letters, 10(3), 297–307. https://doi.org/10.1111/conl.12265

Castro, J. E. (2008). Water struggles, citizenship and governance in Latin America. Development, 51(1), 72–76. https://doi.org/10.1057/palgrave.development.1100440

Carlson, K. M., Curran, L. M., Ponette-González, A. G., Ratnasari, D., Ruspita, Lisnawati, N., Purwanto, Y., Brauman, K. A., & Raymond, P. A. (2014). Influence of watershed-climate interactions on stream temperature, sediment yield, and metabolism along a land use intensity gradient in Indonesian Borneo. Journal of Geophysical Research: Biogeosciences, 119(6), 1110–1128. https://doi.org/10.1002/2013JG002516

Carlson, K. M., Curran, L. M., Ponette-González, A. G., Ratnasari, D., Ruspita, Lisnawati, N., Purwanto, Y., Brauman, K. A., & Raymond, P. A. (2015). Consistent results in stream hydrology across multiple watersheds: A reply to Chew and Goh. Journal of Geophysical Research: Biogeosciences, 120(4), 812–817. https://doi.org/10.1002/2014JG002834

Carr, M. K. V. (2011). The water relations and irrigation requirements of oil palm (Elaeis guineensis): A review. Experimental Agriculture, 47(04), 629–652. https://doi.org/10.1017/S0014479711000494

Castiblanco, C., Etter, A., & Aide, T. M. (2013). Oil palm plantations in Colombia: A model of future expansion. Environmental Science & Policy, 27, 172–183. https://doi.org/10.1016/j.envsci.2013.01.003

Chellaiah, D., & Yule, C. M. (2018a). Effect of riparian management on stream morphometry and water quality in oil palm plantations in Borneo. Limnologica, 69, 72–80. https://doi.org/10.1016/j.limno.2017.11.007

Chellaiah, D., & Yule, C. M. (2018b). Litter decomposition is driven by microbes and is more influenced by litter quality than environmental conditions in oil palm streams with different riparian types. Aquatic Sciences, 80(4), UNSP 43. https://doi.org/10.1007/s00027-018-0595-y

Christakos, G. (1990). A Bayesian/maximum-entropy view to the spatial estimation problem. Mathematical Geology, 22(7), 763–777. https://doi.org/10.1007/BF00890661

Christakos, G., Bogaert, P., & Serre, M. (2001). Temporal GIS: Advanced Functions for Field-Based Applications. https://doi.org/10.1007/978-3-642-56540-3

Chong, K. S., Abdullah, K., Jafri, M. Z. M., & Hwee, S. L. (2013). Combination of radar and optical remote sensing data for land cover/use mapping. 2013 IEEE International Conference on Space Science and Communication (IconSpace), 224–227. https://doi.org/10.1109/IconSpace.2013.6599469

Comte, I., Colin, F., Whalen, J. K., Gruenberger, O., & Caliman, J.-P. (2012). Agricultural practices in oil palm plantations and their impact on hydrological changes, nutrient fluxes and water quality in Indonesia: A review. In D. L. Sparks (Ed.), Advances in Agronomy (Vol. 116, pp. 71–124).

Cooper, C. B., Dickinson, J., Phillips, T., & Bonney, R. (2007). Citizen science as a tool for conservation in residential ecosystems. Ecology and Society, 12(2). https://doi.org/11

CORANTIOQUIA, & Universidad de Antioquia. (2003). Evaluación hidrogeológica entre los municipios de Caucasia y Cáceres. Medellin.

Corley, R. H. V., & Tinker, P. B. (2015). The Oil Palm. Chichester, UK: John Wiley & Sons, Ltd. https://doi.org/10.1002/9781118953297

Cuartas, M. E., Giraldo, L., Maya, M., & Bejarano, O. (2000). Bajo Cauca Desarrollo regional: una tarea común universidad-región. (Insitituto de Estudios Regionals, Ed.). Medellin, Colombia: Universidad de Antioquia. Retrieved from http://www.udea.edu.co/wps/wcm/connect/udea/c3957be6-8230-4d1f-9e41-845154328ce5/caracterizacion-bajo-cauca.pdf?MOD=AJPERES

Custodio, E., & Llamas, R. (1996). Hidrología Subterránea. Tomo I (Second). Spain: Ediciones Omega, S.A.

Culman, M., de Farias, C. M., Bayona, C., & Cabrera Cruz, J. D. (2019). Using agrometeorological data to assist irrigation management in oil palm crops: A decision support method and results from crop model simulation. Agricultural Water Management, 213, 1047–1062. https://doi.org/10.1016/j.agwat.2018.09.052

da Sato Michel Keisuke, L. H. V. de F. R. L. da C. R. S. S. Á. P. (2017). Least limiting water range for oil palm production in Amazon region, Brazil. Scientia Agricola, 74, 148–156.

Departamento Administrativo Nacional de Estadística, D. (2012). Reporte de indice de pobreza multidimensional - 2011. Retrieved May 12, 2019, from https://www.dane.gov.co/index.php/estadisticas-por-tema/pobreza-y-condiciones-de-vida/pobreza-y-desigualdad/pobreza-y-desigualdad-2011

Descals, A., Wich, S., Meijaard, E., Gaveau, D. L. A., Peedell, S., & Szantoi, Z. (2021). High-resolution global map of smallholder and industrial closed-canopy oil palm plantations. Earth System Science Data, 13(3), 1211–1231. https://doi.org/10.5194/essd-13-1211-2021

Dislich, C., Keyel, A. C., Salecker, J., Kisel, Y., Meyer, K. M., Auliya, M., Barnes, A. D., Corre, M. D., Darras, K., Faust, H., Hess, B., Klasen, S., Knohl, A., Kreft, H., Meijide, A., Nurdiansyah, F., Otten, F., Pe'er, G., Steinebach, S., Wiegand, K. (2017). A review of the ecosystem functions in oil palm plantations, using forests as a reference system. Biological Reviews, 92(3), 1539–1569. https://doi.org/10.1111/brv.12295

D'Odorico, P., Laio, F., Porporato, A., Ridolfi, L., Rinaldo, A., & Rodriguez-Iturbe, I. (2010). Ecohydrology of Terrestrial Ecosystems. BioScience, 60(11), 898–907. https://doi.org/10.1525/bio.2010.60.11.6

Dufrene, E., Dubos, B., Rey, H., Quencez, P., & Saugier, B. (1992). Changes in evapotranspiration from an oil palm stand (Elaeis guineensis Jacq.) exposed to seasonal soil water deficits. Acta Œcologica, 13(3), 299–314.

Dufrêne, E., & Saugier, B. (1993). Gas Exchange of Oil Palm in Relation to Light, Vapour Pressure Deficit, Temperature and Leaf Age. Functional Ecology, 7. https://doi.org/10.2307/2389872

Erniwati, Zuhud, E. A. M., Anas, I., Sunkar, A., & Santosa, Y. (2017). Independent Smallholder Oil Palm Expansion and Its Impact on Deforestation: Case Study in Kampar District, Riau Province, Indonesia. Manajemen Hutan Tropika, 23(3), 119–127. https://doi.org/10.7226/jtfm.23.3.119

Fan, Y., Li, H., & Miguez-Macho. (2013). Global Patterns of Groundwater Table Depth. Sicence, 13626(February), 940–944.

Fan, Y., A. Meijide, D.M. Lawrence, O. Roupsard, K.M. Carlson, H.-Y. Chen, A. Röll, F. Niu, and A. Knohl. "Reconciling Canopy Interception Parameterization and Rainfall Forcing Frequency in the Community Land Model for Simulating Evapotranspiration of Rainforests and Oil Palm Plantations in Indonesia." Journal of Advances in Modeling Earth Systems 11, no. 3 (2019): 732–51. https://doi.org/10.1029/2018MS001490.

Fitzherbert, E. B., Struebig, M. J., Morel, A., Danielsen, F., Bruhl, C. A., Donald, P. F., & Phalan, B. (2008). How will oil palm expansion affect biodiversity? Trends in Ecology & Evolution, 23(10), 538–545. https://doi.org/10.1016/j.tree.2008.06.012

Fowler, D., Nemitz, E., Misztal, P., Di Marco, C., Skiba, U., Ryder, J., Helfter, C., Cape, J. N., Owen, S., Dorsey, J., Gallagher, M. W., Coyle, M., Phillips, G., Davison, B., Langford, B., MacKenzie, R., Muller, J., Siong, J., Dari-Salisburgo, C., … Hewitt, C. N. (2011). Effects of land use on surface-atmosphere exchanges of trace gases and energy in Borneo: Comparing fluxes over oil palm

plantations and a rainforest. Philosophical Transactions of the Royal Society B-Biological Sciences, 366(1582), 3196–3209. https://doi.org/10.1098/rstb.2011.0055

Frazao, L. A., Paustian, K., Pellegrino Cern, C. E., & Cerri, C. C. (2014). Soil carbon stocks under oil palm plantations in Bahia State, Brazil. Biomass & Bioenergy, 62, 1–7. https://doi.org/10.1016/j.biombioe.2014.01.031

Furumo, R. P., & Aide, M. T. (2017). Characterizing commercial oil palm expansion in Latin America: Land use change and trade. Environmental Research Letters, 12(2), 024008. https://doi.org/10.1088/1748-9326/aa5892

Gamon, J. A., Field, C. B., Goulden, M. L., Griffin, K. L., Hartley, A. E., Joel, G., Peñuelas, J., & Valentini, R. (1995). Relationships Between NDVI, Canopy Structure, and Photosynthesis in Three Californian Vegetation Types. Ecological Applications, 5(1), 28–41. https://doi.org/10.2307/1942049

Garcia-Ulloa, J., Sloan, S., Pacheco, P., Ghazoul, J., & Koh, L. P. (2012). Lowering environmental costs of oil-palm expansion in Colombia. Conservation Letters, 5(5), 366–375. https://doi.org/10.1111/j.1755-263X.2012.00254.x

Gharibreza, M., Raj, J. K., Yusoff, I., Othman, Z., Tahir, W. Z. W. M., & Ashraf, M. A. (2013). Land use changes and soil redistribution estimation using 137Cs in the tropical Bera Lake catchment, Malaysia. Soil and Tillage Research, 131, 1–10. https://doi.org/10.1016/j.still.2013.02.010

Gitelson, A. A. (2004). Wide Dynamic Range Vegetation Index for Remote Quantification of Biophysical Characteristics of Vegetation. Journal of Plant Physiology, 161(2), 165–173. https://doi.org/10.1078/0176-1617-01176

Gleeson, T., Befus, K. M., Jasechko, S., Luijendijk, E., & Cardenas, M. B. (2016). The global volume and distribution of modern groundwater. Nature Geoscience, 9(2), 161–164. https://doi.org/10.1038/ngeo2590

Goodrick, I., Nelson, P. N., Banabas, M., Wurster, C. M., & Bird, M. I. (2015). Soil carbon balance following conversion of grassland to oil palm. Global Change Biology Bioenergy, 7(2), 263–272. https://doi.org/10.1111/gcbb.12138

Grieef, L. A., & Hayashi, M. (2007). Establishing a Rural Groundwater Monitoring Network Using Existing Wells: West Nose Creek Pilot Study, Alberta. Canadian Water Resources Journal, 32(4), 303–314. https://doi.org/10.4296/cwrj3204303

Guillaume, T., Damris, M., & Kuzyakov, Y. (2015). Losses of soil carbon by converting tropical forest to plantations: Erosion and decomposition estimated by δ13C. Global Change Biology, 21(9), 3548–3560. https://doi.org/10.1111/gcb.12907

Gutierrez-Velez, V. H., DeFries, R., Pinedo-Vasquez, M., Uriarte, M., Padoch, C., Baethgen, W., Fernandes, K., & Lim, Y. (2011). High-yield oil palm expansion spares land at the expense of forests in the Peruvian Amazon. Environmental Research Letters, 6(4), 044029. https://doi.org/10.1088/1748-9326/6/4/044029

Haitjema, H. M., & Mitchell-Bruker, S. (2005). Are water tables a subdued replica of the topography? Ground Water, 43(6), 781–786. https://doi.org/10.1111/j.1745-6584.2005.00090.x

Haklay, M. (2013). Citizen Science and Volunteered Geographic Information – overview and typology of participation. In D. Sui, S. Elwood, & M. Goodchild (Eds.), Crowdsourcing Geographic Knowledge: Volunteered Geographic Information (VGI) in Theory and Practice (Vol. 9789400745, pp. 105–122). Springer Berlin Heidelberg. https://doi.org/10.1007/978-94-007-4587-2

Hardwick, S. R., Toumi, R., Pfeifer, M., Turner, E. C., Nilus, R., & Ewers, R. M. (2015). The relationship between leaf area index and microclimate in tropical forest and oil palm plantation: Forest disturbance drives changes in microclimate. Agricultural and Forest Meteorology, 201, 187–195. https://doi.org/10.1016/j.agrformet.2014.11.010

Hernandez-Rojas, D. A., Lopez-Barrera, F., & Bonilla-Moheno, M. (2018). Preliminary analysis of the land use dynamic associated with oil palm (Elaeis guineensis) Plantations in México. Agrociencia, 52(6), 875–893.

He, J., & Kolovos, A. (2018). Bayesian maximum entropy approach and its applications: a review. Stochastic Environmental Research and Risk Assessment, 32(4), 859–877. https://doi.org/10.1007/s00477-017-1419-7

Horton, A. J., Lazarus, E. D., Hales, T. C., Constantine, J. A., Bruford, M. W., & Goossens, B. (2018). Can Riparian Forest Buffers Increase Yields From Oil Palm Plantations? Earth's Future, 6(8), 1082–1096. https://doi.org/10.1029/2018EF000874

Hosseini, M., & Kerachian, R. (2017). A Bayesian maximum entropy-based methodology for optimal spatiotemporal design of groundwater monitoring networks. Environmental Monitoring and Assessment, 189(9), 433. https://doi.org/10.1007/s10661-017-6129-6

Instituto Geográfico Agustín Codazzi, I. (2007a). Estudio semidetallado de suelos de las áreas potencialmente agrícolas: Bajo Cauca departamento de Antioquia. (I. Instituto GeogrÃ¡fico AgustÃn Codazzi & GobernaciÃ3n, Eds.), Estudio Integral de Suelos y Coberturas Terrestres Departamento de Antioquia. MedellÃn: IGAC : Gobernación de Antioquia.

Instituto Geográfico Agustín Codazzi, I. (2007b). Levantamiento semidetallado de las coberturas terrestres: departamento de Antioquia. (I. G. A. C. IGAC, Ed.). Bogotá, Colombia : IGAC,.

Koh, L. P., Miettinen, J., Liew, S. C., & Ghazoul, J. (2011). Remotely sensed evidence of tropical peatland conversion to oil palm. Proceedings of the National Academy of Sciences of the United States of America, 108(12), 5127–5132. https://doi.org/10.1073/pnas.1018776108

Koh, L. P., & Wilcove, D. S. (2008). Is oil palm agriculture really destroying tropical biodiversity? Conservation Letters, 1(2), 60–64. https://doi.org/10.1111/j.1755-263X.2008.00011.x

Kurniawan, S., Corre, M. D., Matson, A. L., Schulte-Bisping, H., Utami, R., van Straaten, O., & Veldkamp, E. (2018). Conversion of tropical forests to smallholder rubber and oil palm plantations impacts nutrient leaching losses and nutrient retention efficiency in highly weathered soils. Biogeosciences, 15(16), 5131–5154. https://doi.org/10.5194/bg-15-5131-2018

Larsen, R. K., Jiwan, N., Rompas, A., Jenito, J., Osbeck, M., & Tarigan, A. (2014). Towards "hybrid accountability" in EU biofuels policy? Community grievances and competing water claims in the Central Kalimantan oil palm sector. Geoforum, 54, 295–305. https://doi.org/10.1016/j.geoforum.2013.09.010

Lasso, C., Guiérrez, F., & Morales-B, D. (2014). Humedales interiores de Colombia: identificación, caracterización y establecimiento de límites según criterios biológicos y ecológicos. X. Serie Editorial Recursos Hidrobiológicos y Pesqueros Continentales de Colombia. Instituto de Investigación de Recurs. Bogotá D.C., Colombia : Instituto de Investigación de Recursos Biológicos Alexander von Humboldt (IAvH). Retrieved from http://hdl.handle.net/20.500.11761/9280

Le Coz, J., Patalano, A., Collins, D., Guillén, N. F., García, C. M., Smart, G. M., … Braud, I. (2016). Crowdsourced data for flood hydrology: Feedback from recent citizen science projects in Argentina, France and New Zealand. https://doi.org/10.1016/j.jhydrol.2016.07.036

Lewandowski, J., Arnon, S., Banks, E., Batelaan, O., Betterle, A., Broecker, T., … Wu, L. (2019). Is the hyporheic zone relevant beyond the scientific community? Water (Switzerland), 11(11). https://doi.org/10.3390/w11112230

Little, K. E., Hayashi, M., & Liang, S. (2016). Community-Based Groundwater Monitoring Network Using a Citizen-Science Approach, 54(3), 317–324. https://doi.org/10.1111/gwat.12336

Lowry, C. S., Fienen, M. N., Hall, D. M., & Stepenuck, K. F. (2019). Growing pains of crowdsourced stream stage monitoring using mobile phones: The development of crowdhydrology. Frontiers in Earth Science, 7(May), 1–10. https://doi.org/10.3389/feart.2019.00128

Luke, S. H., Barclay, H., Bidin, K., Chey, V. K., Ewers, R. M., Foster, W. A., Nainar, A., Pfeifer, M., Reynolds, G., Turner, E. C., Walsh, R. P. D., & Aldridge, D. C. (2017). The effects of catchment and riparian forest quality on stream environmental conditions across a tropical rainforest and oil palm landscape in Malaysian Borneo. Ecohydrology, 10(4), UNSP e1827. https://doi.org/10.1002/eco.1827

Manoli, G., Meijide, A., Huth, N., Knohl, A., Kosugi, Y., Burlando, P., Ghazoul, J., & Fatichi, S. (2018). Ecohydrological changes after tropical forest conversion to oil palm. Environmental Research Letters, 13(6), 064035. https://doi.org/10.1088/1748-9326/aac54e

Marchetti, Z. Y., & Carrillo-Rivera, J. J. (2014). Tracing Groundwater Discharge in the floodplain of the Parana River, Argentina: Implications for its biological communities. River Research and Applications, 30(2), 166–179. https://doi.org/10.1002/rra.2629

Margat, J., & van der Gun, J. (2013). Groundwater around the world. A greographic synopsis. (C. P. (Taylor & F. G. Francis, Ed.). Boca Raton, FL.

Martorano, L. G., de Moraes, J. R. S. C., Lisboa, L. S. S., Junior, R. A. G., do Amaral, V. P., & Aparecido, L. E. O. (2017). Expansion of palm oil (Elaeis guineensis Jacq.) in the state of Maranhão and soil water deficit limitations in the Brazilian Amazon. Australian Journal of Crop Science, 11(11), 1386–1391. https://doi.org/10.21475/ajcs.17.11.11.pne439

Matysek, M., Evers, S., Samuel, M. K., & Sjogersten, S. (2018). High heterotrophic CO2 emissions from a Malaysian oil palm plantations during dry-season. Wetlands Ecology and Management, 26(3), 415–424. https://doi.org/10.1007/s11273-017-9583-6

Meijide, A., Badu, C. S., Moyano, F., Tiralla, N., Gunawan, D., & Knohl, A. (2018). Impact of forest conversion to oil palm and rubber plantations on microclimate and the role of the 2015 ENSO event. *Agricultural and Forest Meteorology*, *252*, 208–219. https://doi.org/10.1016/j.agrformet.2018.01.013

Meijide, A., Röll, A., Fan, Y., Herbst, M., Niu, F., Tiedemann, F., June, T., Rauf, A., Hölscher, D., & Knohl, A. (2017). Controls of water and energy fluxes in oil palm plantations: Environmental variables and oil palm age. Agricultural and Forest Meteorology, 239, 71–85. https://doi.org/10.1016/j.agrformet.2017.02.034

Merten, J., Röll, A., Guillaume, T., Meijide, A., Tarigan, S., Agusta, H., Dislich, C., Dittrich, C., Faust, H., Gunawan, D., Hein, J., Hendrayanto, Knohl, A., Kuzyakov, Y., Wiegand, K., & Hölscher, D. (2016). Water scarcity and oil palm expansion: Social views and environmental processes. Ecology and Society, 21(2), 21. https://doi.org/10.5751/ES-08214-210205

Messier, K. P., Kane, E., Bolich, R., & Serre, M. L. (2014). Nitrate variability in groundwater of North Carolina using monitoring and private well data models. Environmental Science and Technology, 48(18), 10804–10812. https://doi.org/10.1021/es502725f

Miettinen, J., Shi, C., & Liew, S. C. (2016). Land cover distribution in the peatlands of Peninsular Malaysia, Sumatra and Borneo in 2015 with changes since 1990. Global Ecology and Conservation, 6, 67–78. https://doi.org/10.1016/j.gecco.2016.02.004

Minasny, B., & Mcbratney, A. B. (2018). Limited effect of organic matter on soil available water capacity. European Journal of Soil Science, 69(1), 39–47. https://doi.org/doi: 10.1111/ejss.12475

Mozzon, M., Foligni, R., & Mannozzi, C. (2020). Current Knowledge on Interspecific Hybrid Palm Oils as Food and Food Ingredient. Foods, 9(5). https://doi.org/10.3390/foods9050631

Nelson, P. N., Banabas, M., Nake, S., Goodrick, I., Webb, M. J., & Gabriel, E. (2014). Soil fertility changes following conversion of grassland to oil palm. Soil Research, 52(7), 698–705. https://doi.org/10.1071/SR14049

Njue, N., Stenfert Kroese, J., Gräf, J., Jacobs, S. R., Weeser, B., Breuer, L., & Rufino, M. C. (2019). Citizen science in hydrological monitoring and ecosystem services management: State of the art and future prospects. Science of the Total Environment, 693. https://doi.org/10.1016/j.scitotenv.2019.07.337

Niu, F., Roll, A., Hardanto, A., Meijide, A., Kohler, M., Hendrayanto, & Holscher, D. (2015). Oil palm water use: Calibration of a sap flux method and a field measurement scheme. Tree Physiology, 35(5), 563–573. https://doi.org/10.1093/treephys/tpv013

Nurulita, Y., Adetutu, E. M., Kadali, K. K., Zul, D., Mansur, A. A., & Ball, A. S. (2015). The assessment of the impact of oil palm and rubber plantations on the biotic and abiotic properties of tropical peat swamp soil in Indonesia. International Journal of Agricultural Sustainability, 13(2), 150–166. https://doi.org/10.1080/14735903.2014.986321

Organization World Health. (1999). Guidelines for drinking-water quality: volume 3: drinking-water quality control in small-community supplies. Geneva PP - Geneva: World Health Organization. Retrieved from https://apps.who.int/iris/handle/10665/252074

Palacio, P. (2014). Modelo Hidrológico Conceptual para la Cuenca del Río Man a partir de Técnicas Hidrológicas, Hidrogeoquímicas e Isotópicas. Universidad de Antioquia.

Palacio, P., & Betancur, T. (2007). Identificación de fuentes y zonas de recarga a partir de isotopos estables del agua (caso de estudio Bajo Cauca antioqueño). Gestion y Ambiente, 10(4), 93p.

Palacio, P., Dapena, C., & Betancur, T. (2013). Use of Isotopic Techniques for the Assessment of Hydrological Interactions Between Ground and Surface Waters - Rio Man, Cienaga Colombia. In Isotopes in Hydrology , Marine Ecosystems and Climate Change Studies. International Atomic Energy Agency (IAEA): IAEA.

Pardon, L., Bessou, C., Nelson, P. N., Dubos, B., Ollivier, J., Marichal, R., Caliman, J.-P., & Gabrielle, B. (2016). Key unknowns in nitrogen budget for oil palm plantations. A review. Agronomy for Sustainable Development, 36(1), 1–21. https://doi.org/10.1007/s13593-016-0353-2

Pardon, L., Bessou, C., Saint-Geours, N., Gabrielle, B., Khasanah, N., Caliman, J.-P., & Nelson, P. N. (2016). Quantifying nitrogen losses in oil palm plantations: Models and challenges. Biogeosciences, 13(19), 5433–5452. https://doi.org/10.5194/bg-13-5433-2016

Paterson, R. R. M., Kumar, L., Shabani, F., & Lima, N. (2016). World climate suitability projections to 2050 and 2100 for growing oil palm. Journal of Agricultural Science, 155(5), 689–702. https://doi.org/10.1017/S0021859616000605

Peng, X., Heitman, J., Horton, R., & Ren, T. (2017). Determining Near-Surface Soil Heat Flux Density Using the Gradient Method: A Thermal Conductivity Model–Based Approach. Journal of Hydrometeorology, 18(8), 2285–2295. https://doi.org/10.1175/JHM-D-16-0290.1

Pirker, J., Mosnier, A., Kraxner, F., Havlík, P., & Obersteiner, M. (2016). What are the limits to oil palm expansion? Global Environmental Change, 40, 73–81. https://doi.org/10.1016/j.gloenvcha.2016.06.007

Pongratz, J., Bounoua, L., DeFries, R. S., Morton, D. C., Anderson, L. O., Mauser, W., & Klink, C. A. (2006). The Impact of Land Cover Change on Surface Energy and Water Balance in Mato Grosso, Brazil. Earth Interactions, 10(19), 1–17. https://doi.org/10.1175/EI176.1

Quezada, J. C., Etter, A., Ghazoul, J., Buttler, A., & Guillaume, T. (2019). Carbon neutral expansion of oil palm plantations in the Neotropics. Science Advances, 5(11), eaaw4418. https://doi.org/10.1126/sciadv.aaw4418

Radersma, S., & de Ridder, N. (1996). Computed evapotranspiration of annual and perennial crops at different temporal and spatial scales using published parameter values. Agricultural Water Management, 31(1–2), 17–34. https://doi.org/10.1016/0378-3774(95)01235-4

Ramdani, F., Moffiet, T., & Hino, M. (2014). Local surface temperature change due to expansion of oil palm plantation in Indonesia. Climatic Change, 123(2), 189–200. https://doi.org/10.1007/s10584-013-1045-4

Re, V. (2015). Incorporating the social dimension into hydrogeochemical investigations for rural development: the Bir Al-Nas approach for socio-hydrogeology. Hydrogeology Journal, 23(7), 1293–1304. https://doi.org/10.1007/s10040-015-1284-8

Reyes, J. M., Xu, Y., Vizuete, W., & Serre, M. L. (2017). Regionalized PM2 . 5 Community Multiscale Air Quality model performance evaluation across a continuous spatiotemporal domain. Atmospheric Environment, 148, 258–265. https://doi.org/10.1016/j.atmosenv.2016.10.048

Rhebergen, T., Fairhurst, T., Zingore, S., Fisher, M., Oberthür, T., & Whitbread, A. (2016). Climate, soil and land-use based land suitability evaluation for oil palm production in Ghana. European Journal of Agronomy, 81, 1–14. https://doi.org/10.1016/j.eja.2016.08.004

Rivera-Mendes, Y. D., Cuenca, J. C., & Romero, H. M. (2016). Physiological responses of oil palm (Elaeis guineensis Jacq.) seedlings under different water soil conditions. Agronomía Colombiana, 34(2), 163–171.

Rodriguez-Iturbe, I. (2000). Ecohydrology: A hydrologic perspective of climate-soil-vegetation dynamies. Water Resources Research, 36(1), 3–9. https://doi.org/10.1029/1999WR900210

Röll, A., Niu, F., A. Meijide, Hardanto, A., Hendrayanto, Knohl, A., & Holscher, D. (2015). Transpiration in an oil palm landscape: Effects of palm age. Biogeosciences, 12(19), 5619–5633. https://doi.org/10.5194/bg-12-5619-2015

Romero-Ruiz, M. H., Flantua, S. G. A., Tansey, K., & Berrio, J. C. (2012). Landscape transformations in savannas of northern South America: Land use/cover changes since 1987 in the Llanos Orientales of Colombia. Applied Geography, 32(2), 766–776. https://doi.org/10.1016/j.apgeog.2011.08.010

Rudnitskaya, A. (2018). Calibration Update and Drift Correction for Electronic Noses and Tongues. Frontiers in Chemistry, 0. https://doi.org/10.3389/fchem.2018.00433

Saadun, N., Lim, E. A. L., Esa, S. M., Ngu, F., Awang, F., Gimin, A., Johari, I. H., Firdaus, M. A., Wagimin, N. I., & Azhar, B. (2018). Socio-ecological perspectives of engaging smallholders in environmental-friendly palm oil certification schemes. Land Use Policy, 72, 333–340. https://doi.org/10.1016/j.landusepol.2017.12.057

Sabajo, C. R., le Maire, G., June, T., Meijide, A., Roupsard, O., & Knohl, A. (2017). Expansion of oil palm and other cash crops causes an increase of the land surface temperature in the Jambi province in Indonesia. Biogeosciences, 14(20), 4619–4635. https://doi.org/10.5194/bg-14-4619-2017

Sanders, A. P., Messier, K. P., Shehee, M., Rudo, K., Serre, M. L., & Fry, R. C. (2012). Arsenic in North Carolina: Public Health Implications. Environment International, 38(1), 10–16. https://doi.org/10.1016/j.envint.2011.08.005

Sandoval, R. (2004). A participatory approach to integrated aquifer management: The case of Guanajuato State, Mexico. Hydrogeology Journal, 12(1), 6–13. https://doi.org/10.1007/s10040-003-0311-3

Santa-Arango, D., Martinez, C., & Betancur-Vargas, T. (2010). Uso De Hidroquímica E Isótopos Ambientales Para La Evaluación De La Conexión Hidrológica Entre El Agua Subterránea Y El Humedal Ciénaga Colombia. (Un Primer Acercamiento). Gestión y Ambiente, 11(2).

Serre, M. L., & Christakos, G. (1999). Modern geostatistics: Computational BME analysis in the light of uncertain physical knowledge - The Equus Beds study. Stochastic Environmental Research and Risk Assessment, 13(1–2), 1–26. https://doi.org/10.1007/s004770050029

Serre, M. L., Christakos, G., Li, H., & Miller, C. T. (2003). A BME solution of the inverse problem for saturated groundwater flow. Stochastic Environmental Research and Risk Assessment, 17(6), 354–369. https://doi.org/10.1007/s00477-003-0156-2

Sheaves, M., Johnston, R., Miller, K., & Nelson, P. N. (2018). Impact of oil palm development on the integrity of riparian vegetation of a tropical coastal landscape. Agriculture Ecosystems & Environment, 262, 1–10. https://doi.org/10.1016/j.agee.2018.04.011

Smit, H. H., Meijaard, E., van der Laan, C., Mantel, S., Budiman, A., & Verweij, P. (2013). Breaking the Link between Environmental Degradation and Oil Palm Expansion: A Method for Enabling Sustainable Oil Palm Expansion. PLoS ONE, 8(9), e68610. https://doi.org/10.1371/journal.pone.0068610

Snyder, D. . (2008). Estimated Depth to Ground Water and Configuration of the Water Table in the Portland , Oregon Area Scientific Investigations Report 2008 – 5059. Retrieved from http://pubs.usgs.gov/ sir/2008/5059/

Sophocleous, M. (2002). Interactions between groundwater and surface water: the state of the science. Hydrogeology Journal, 10(1), 52–67. https://doi.org/10.1007/s10040-001-0170-8

Spracklen, D. V., Baker, J. C. A., Garcia-Carreras, L., & Marsham, J. H. (2018). The Effects of Tropical Vegetation on Rainfall. Annual Review of Environment and Resources, 43(1), 193–218. https://doi.org/10.1146/annurev-environ-102017-030136

Sun, G., Hallema, D., & Asbjornsen, H. (2017). Ecohydrological processes and ecosystem services in the Anthropocene: A review. Ecological Processes, 6(1), 35. https://doi.org/10.1186/s13717-017-0104-6

Tarigan, S. D., Sunarti, Wiegand, K., Dislich, C., Slamet, B., Heinonen, J., & Meyer, K. (2016). Mitigation options for improving the ecosystem function of water flow regulation in a watershed with rapid expansion of oil palm plantations. Sustainability of Water Quality and Ecology, 8, 4–13. https://doi.org/10.1016/j.swaqe.2016.05.001

Tittor, A. (2017). Documenting the social and environmental consequences of oil palm plantations in Nicaragua. Future of Food-Journal on Food Agriculture and Society, 5(3), 46–61.

Tonks, A. J., Aplin, P., Beriro, D. J., Cooper, H., Evers, S., Vane, C. H., & Sjogersten, S. (2017). Impacts of conversion of tropical peat swamp forest to oil palm plantation on peat organic chemistry, physical properties and carbon stocks. Geoderma, 289, 36–45. https://doi.org/10.1016/j.geoderma.2016.11.018

Tsujino, R., Yumoto, T., Kitamura, S., Djamaluddin, I., & Darnaedi, D. (2016). History of forest loss and degradation in Indonesia. Land Use Policy, 57, 335–347. https://doi.org/10.1016/j.landusepol.2016.05.034

UNESCO & UN-Water. (2017). Wastewater: The Untapped Resource. UN World Water Development Report 2017.

Urrea, V., Ochoa, A., & Mesa, O. (2019). Seasonality of Rainfall in Colombia. Water Resources Research, 55(5), 4149–4162. https://doi.org/10.1029/2018WR023316

Vijay, V., Pimm, S. L., Jenkins, C. N., & Smith, S. J. (2016). The Impacts of Oil Palm on Recent Deforestation and Biodiversity Loss. PloS One, 11(7), e0159668. https://doi.org/10.1371/journal.pone.0159668

von Geibler, J. (2013). Market-based governance for sustainability in value chains: Conditions for successful standard setting in the palm oil sector. Journal of Cleaner Production, 56, 39–53. https://doi.org/10.1016/j.jclepro.2012.08.027

Wösten, H., Hooijer, A., Siderius, C., Rais, D. S., Idris, A., & Rieley, J. (2006). Tropical peatland water management modelling of the air hitam laut catchment in indonesia. International Journal of River Basin Management, 4(4), 233–244. https://doi.org/10.1080/15715124.2006.9635293

Wang, B., Luo, X., Yang, Y. M., Sun, W., Cane, M. A., Cai, W., … Liu, J. (2019). Historical change of El Niño properties sheds light on future changes of extreme El Niño. Proceedings of the National Academy of Sciences of the United States of America, 116(45), 22512–22517. https://doi.org/10.1073/pnas.1911130116

Weeser, B., Stenfert Kroese, J., Jacobs, S. R., Njue, N., Kemboi, Z., Ran, A., … Breuer, L. (2018). Citizen science pioneers in Kenya – A crowdsourced approach for hydrological monitoring. Science of the Total Environment, 631–632, 1590–1599. https://doi.org/10.1016/j.scitotenv.2018.03.130

Wiggins, A., & Crowston, K. (2011). From Conservation to Crowdsourcing: A Typology of Citizen Science. In 2011 44th Hawaii International Conference on System Sciences (pp. 1–10). Koloa, HI: IEEE. https://doi.org/10.1109/HICSS.2011.207

Wijnen, M., Augeard, B., Hiller, B., Ward, C., & Huntjens, P. (2012). Managing the Invisible: Understanding and Improving groundwater governance. Washington, DC. Retrieved from https://openknowledge.worldbank.org/handle/10986/17228

Winter, T. C., Harvey, J. W., Franke, O. L., & Alley, W. M. (1998). Groundwater and surface water: A single resource. USGS Circular 1139, U.S. Government Printing Office. Denver, CO.

Wright, C., Kagawa-Viviani, A., Gerlein-Safdi, C., Mosquera, G. M., Poca, M., Tseng, H., & Chun, K. P. (2018). Advancing ecohydrology in the changing tropics: Perspectives from early career scientists. Ecohydrology, 11(3), e1918. https://doi.org/10.1002/eco.1918

Villegas, J. C., Law, D. J., Stark, S. C., Minor, D. M., Breshears, D. D., Saleska, S. R., Swann, A. L. S., Garcia, E. S., Bella, E. M., Morton, J. M., Cobb, N. S., Barron-Gafford, G. A., Litvak, M. E., &

Kolb, T. E. (2017). Prototype campaign assessment of disturbance-induced tree loss effects on surface properties for atmospheric modeling. Ecosphere, 8(3), e01698. https://doi.org/10.1002/ecs2.1698